THE
PHYSICAL REVIEW
*A journal of experimental and theoretical physics established by E. L. Nichols in 1893*

SECOND SERIES, VOL. 69, NOS. 5 AND 6 MARCH 1 AND 15, 1946

# On the Variation along Range of the Hρ-Distribution and the Charge of the Fission Fragments of the Light Group

N. O. LASSEN
*Universitetets Institut for Teoretisk Fysik, Copenhagen, Denmark*
(Received December 14, 1945)

AS mentioned in earlier papers[1,2] the Hρ-distribution of fission fragments has been determined by deflecting the fragments in the magnetic field of the cyclotron. By using the apparatus described in the first paper,[1] the Hρ-distribution has now been determined for fragments of the light group having traversed mica foils of various thicknesses; the foils were placed close to the uranium layer and the fragments were deflected in the magnetic field after their passage through the foils. Both these absorber foils and the mica window of the ionization chamber were examined for homogenity by means of monochromatic light.

Figure 1 gives the result of the measurements. The curve with the highest Hρ-values is the one obtained with no mica foil covering the uranium; then, by moving in the direction of decreasing Hρ-values, follow the curves corresponding to absorber foils of thicknesses 0.63, 1.0, and 1.3 mg/cm²; the curves are drawn in such scales as to correspond to the same total number of fragments. The vertical lines indicating the statistical errors show that the curve obtained with an absorber of thickness 1.3 mg/cm² is not determined with the same degree of accuracy as are the other curves; this is due partly to the fact that smaller doses of neutrons were used, but the reliability of this curve is also somewhat smaller than of the other ones, because the pulses in the ionization chamber produced by fission particles having traversed the absorber and the mica window and aluminium foil of the chamber (1.3+0.79+0.25 mg/cm²) are not much greater than the background pulses and, in fact, about half of the pulses due to fragments of the light group disappear in the background. When no

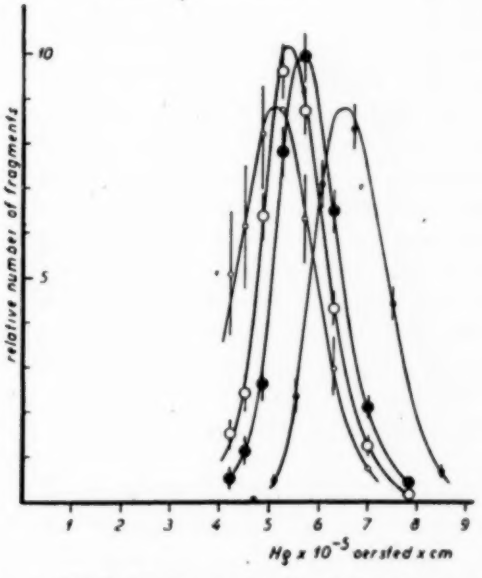


FIG. 1. Hρ-distribution-curves for fission fragments of the light group having traversed mica foils of various thicknesses. 1. Small black points: thickness of absorber 0 mg/cm²; 2. Big black points: thickness of absorber 0.63 mg/cm²; 3. Big white points: thickness of absorber 1.0 mg/cm²; 4. Small white points: thickness of absorber 1.3 mg/cm².

[1] N. O. Lassen, Kgl. Danske Vid. Sels. Math.-Fys. Medd. **23**, No. 2 (1945).
[2] N. O. Lassen, Phys. Rev. **68**, 142 (1945).

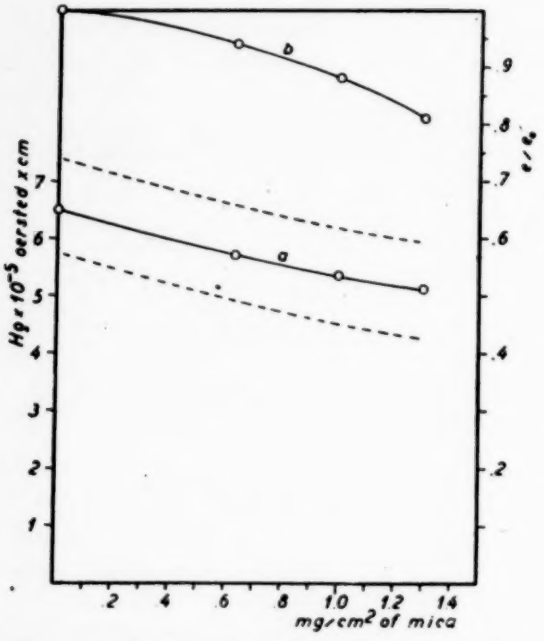


FIG. 2. (a) Most probable value of Hρ for fission fragments of the light group. Scale of ordinates to the left-hand side. (b) Most probable value of the ratio $e/e_0$ for fission fragments of the light group. Scale of ordinates to the right-hand side.

absorber is used, a rather good separation is obtained among the background pulses, the pulses due to fragments of the heavy group, and the pulses due to fragments of the light group[2]; when the absorber thickness is 0.63 or 1.0 mg/cm², the light group can still be clearly identified, while for an absorber of 1.3 mg/cm² no distinct separation can be made between background pulses and fission pulses. The heavy group cannot be seen for absorber thicknesses greater than 0.63 mg/cm², and when this absorber is used, about half of the group disappears in the background; the Hρ-distribution curve obtained for the rest of the group indicates that the fission fragments of the heavy group behave in almost the same manner as those of the light group.

Figure 2(a) gives Hρ for the light group as a function of the absorber thickness; the full drawn curve represents the most probable value while the two dotted curves give almost the limits of Hρ.

In Fig. 3 the most probable energy of the light group is plotted against the thickness of the traversed mica foils; except for the first one, the points are obtained in the way described in the papers referred to. As the mica window of the ionization chamber could not be avoided, the initial energy of the fragments could not be measured by means of the present arrangement, but the figure was taken from the paper of Flammersfeld, Jensen, and Gentner,[3] although this is perhaps not strictly permissible, since Flammersfeld *et al.* used slow neutrons while fast neutrons were used in these experiments; nevertheless, this is expected to cause no serious errors. The curve in Fig. 3 is in rather close agreement with the velocity-range-curve obtained by Bøggild, Brostrøm, and Lauritzen,[4] the two curves in all points giving within five percent the same value for the ratio of the velocity $V$ to the initial velocity $V_0$.

Combining the most probable values of the energy $E$ and of Hρ and denoting with indices 0 the initial values we get for the most probable value of the total fragment charge

$$\frac{e}{e_0}=\frac{(H\rho)_0}{H\rho}\cdot\left(\frac{E}{E_0}\right)^{\frac{1}{2}}.$$

Using this equation we get the curve Fig. 2(b); as seen, the decrease in charge is nearly 20

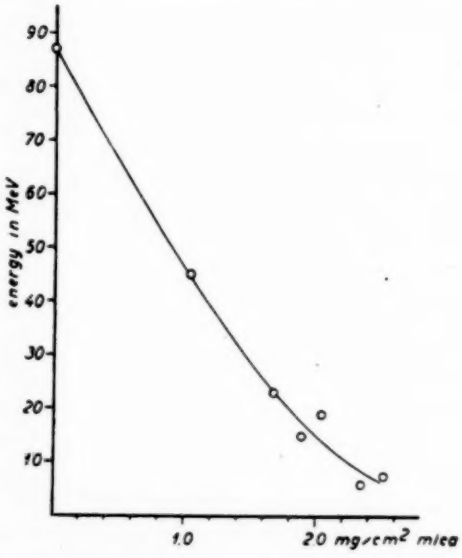


FIG. 3. Most probable value of energy $E$ for fission fragments of the light group.

[3] Flammersfeld, Jensen, and Gentner, Zeits. f. Physik 120, 450 (1943).

[4] Bøggild, Brostrøm, and Lauritzen, Kgl. Danske Vid. Sels. Math.-Fys. Medd. 18, 4 (1940).

percent for an absorber of thickness 1.3 mg/cm² of mica ~9 mm of air.

In Table I is shown the value of the ratio $e/e_0$ for the various absorber thicknesses. The third and fourth columns give the corresponding values for $(V/V_0)^{\frac{1}{2}}$ as derived from Fig. 3 and from the velocity-range-curve of Bøggild *et al.*, respectively.

It will be seen that in the velocity interval considered $e$ is closely proportional to $V^{\frac{1}{2}}$.

In a preliminary theoretical discussion of the stopping of fission fragments, Bohr[5] has, for the effective charge of the fragments, given the estimate

$$Z^{eff}=Z^{\frac{1}{2}}\cdot(V/V_H),$$

where $Z$ is the atomic number and $V_H$ the electron velocity in the hydrogen atom $(=e^2/\hbar)$. As seen, this simple formula cannot account for the experimentally found variation of the fragment charge for the considered velocities; as mentioned in the previous papers,[1,2] it neither accounts for the fact that the heavy group of the fission fragments has the higher initial $e$ value and the light group the lower $e$ value. As pointed out to me by Professor Bohr, the insufficiency of the formula is probably due to the relatively high value of the ratio $Z^{eff}/Z$ which, in particular for the lighter fragments, makes the estimate of the electron binding used for the deduction of the formula somewhat too small. This point will be more closely discussed in a forthcoming paper by Bohr containing a general theoretical discussion of the stopping problems.

TABLE I.

| Thickness of absorber mg/cm² of mica | $e/e_0$ | $(V/V_0)^{\frac{1}{2}}$ this work | $(V/V_0)^{\frac{1}{2}}$ Bøggild *et al.* |
|---|---|---|---|
| 0.63 | 0.94 | 0.92 | 0.90 |
| 1.00 | 0.88 | 0.85 | 0.84 |
| 1.29 | 0.81 | 0.80 | 0.79 |

The present experiments were carried out at the Institute of Theoretical Physics in Copenhagen, and I wish to express my heartiest thanks to the Director of the Institute, Professor Niels Bohr, and to Professor J. C. Jacobsen, for their continued interest in this work.

[5] N. Bohr, Phys. Rev. **59**, 270 (1941).

# Radioactive Te from Sb Bombardment

J. E. EDWARDS AND M. L. POOL
*Mendenhall Laboratory, Ohio State University, Columbus, Ohio*

(Received November 10, 1945)

A radioactive isomer has been found in $Te^{121}$ with the help of a curved crystal x-ray spectrograph. The pair consists of a new 17±1-day activity produced by the reactions Sb $(d, 2n)$ and Sb $(p, n)$ and a previously assigned activity evaluated here as 143±5 days. Sb and Te x-rays, a 0.61-Mev gamma-ray, a 0.223-Mev gamma-ray, and conversion electrons are associated with the long period. Sb x-rays and a 0.61-Mev gamma-ray are associated with the short period. The observations are simply explained by the isomeric transition. No evidence of the "fast" gamma-transition was found.

## INTRODUCTION

TWO activities have been found in the Te chemical fraction after deuteron bombardment of antimony. An activity of half-life 30 days consisting of several gamma-ray energies was reported,[1] two of which, 0.082 Mev and 0.0882 Mev, are internally converted with *K-L-M* conversion electron energy differences characteristic of Te. Other gamma-ray energies of 0.136, 0.1573, 0.2108, and 0.615 Mev were also found[1] in the Te fraction. A 125-day Te activity has been produced by the reactions[2] Sb $(d, 2n)$, Sb $(p, n)$, and Sn $(\alpha, n)$ and has been assigned to $Te^{121}$. There is evidence of shorter half-lives in the activity resulting from the Sn $(\alpha, n)$ reaction.[2]

The radiations from the long period $Te^{121}$ are very complex consisting of x-rays, internal conversion electrons, and gamma-rays. Two gamma-ray energies, 0.23 Mev and 0.61 Mev, are associated with this activity.[1,3] The 0.23-Mev gamma-ray is strongly internally converted[3,4] and there is some evidence that the 0.61-Mev gamma-ray is partially internally converted.[4] X-rays characteristic of Sb and shorter wave-length "tellurium-like" x-rays were detected[5] in the Te fraction after deuteron bombardment of Sb. The two x-ray wave-lengths were distinguished by critical absorption and fluorescent measurements.[5] Coincidence counter observations[3] have shown that the "tellurium-like" x-ray is associated with the 0.23-Mev gamma-ray but chemical tests[5] for an isomeric transition in Te failed to show a daughter product. The "tellurium-like" x-ray has been interpreted[3,5,6] as caused by *K*-capture in $Te^{121}$ followed immediately by internal conversion of the 0.23-Mev gamma-ray in the singly-ionized *K*-shell. The x-ray is then emitted by the Sb atom having both *K*-electrons missing. The x-ray wave-length emitted by this process would differ slightly from that of Te.

It is the purpose of this paper to report the results of a study of the radiations from $Te^{121}$ obtained with the aid of a curved crystal spectrograph.[7]

## $Te^{121}$ DECAY CHARACTERISTICS

Hilger Sb metal lab. no. 11707 was activated by 10 Mev deuterons. The sample was dissolved with a Te carrier in *aqua regia* then evaporated to dryness. The residue was taken up by hot dilute HCl and an excess of tartaric acid. The Te metal was then precipitated from this solution with hydrazine dihydrochloride. Sb was precipitated from the filtrate by $H_2S$.

Figure 1 shows the decay of the Te fraction starting 40 days after bombardment. An activity of half-life 17±1 days is observed in addition to the longer half-life of 143±5 days. The branching ratio of the long period activity to the short period is approximately 3. The 17-day activity was also observed in the Te fraction after bombardment of Sb with 5-Mev protons. The 17-day

[1] C. V. Kent and J. M. Cork, Phys. Rev. 62, 297 (1942).
[2] G. T. Seaborg, J. J. Livingood, and J. W. Kennedy, Phys. Rev. 57, 363 (1940).
[3] Rosalyn S. Yalow and M. Goldhaber, Phys. Rev. 67, 59 (1945).
[4] E. B. Hales and E. B. Jordon, Phys. Rev. 64, 202 (1943).
[5] R. D. O'Neal and Gertrud Scharff-Goldhaber, Phys. Rev. 62, 83 (1942).
[6] Rosalyn S. Yalow and M. Goldhaber, Phys. Rev. 66, 36 (1944).
[7] J. E. Edwards, M. L. Pool, and F. C. Blake, Phys. Rev. 67, 150 (1945).

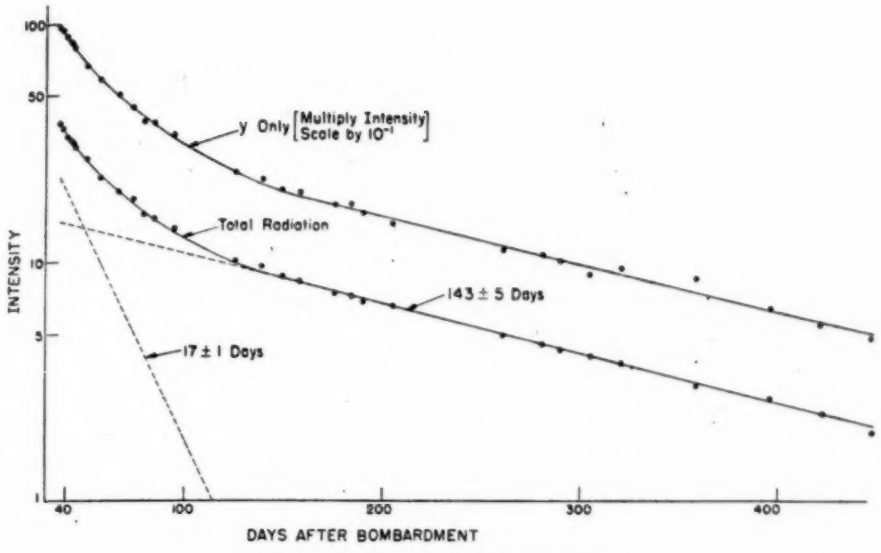


FIG. 1. Decay curve of $Te^{121}$ from Sb+$d$.

half-life is a new activity produced by the reactions Sb ($d$, $2n$) and Sb ($p$, $n$) and is assigned to $Te^{121}$. This assignment will be discussed later in the paper. The long period activity is undoubtedly the same as the 125±5-day activity assigned earlier[2] to $Te^{121}$. Re-evaluation of this period by the authors has yielded a half-life of 143±5 days.

The Sb fraction from Sb+$d$ activation contains 2.5-day and 60-day half-lives confirming other observations.[8, 9]

### $Te^{121}$ RADIATION ENERGIES BY ABSORPTION

Aluminum absorption curves obtained in the early part of the decay while the 17-day activity was still strong showed x-rays characteristic of the Sb-Te region and conversion electrons. At the same time two gamma-ray energies, 0.61 Mev and a lower energy 0.22 Mev, were determined by lead absorption.

About 125 days after bombardment when the 17-day activity had dropped to less than $\frac{1}{10}$ the intensity of the 143-day activity additional absorption curves were obtained. These curves are shown in Figs. 2–4. Both gamma-rays of energies 0.61 Mev and 0.223 Mev are observed in the long

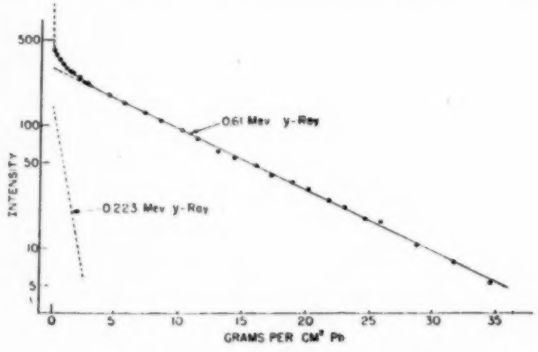


FIG. 2. Pb absorption curve of $Te^{121}$.

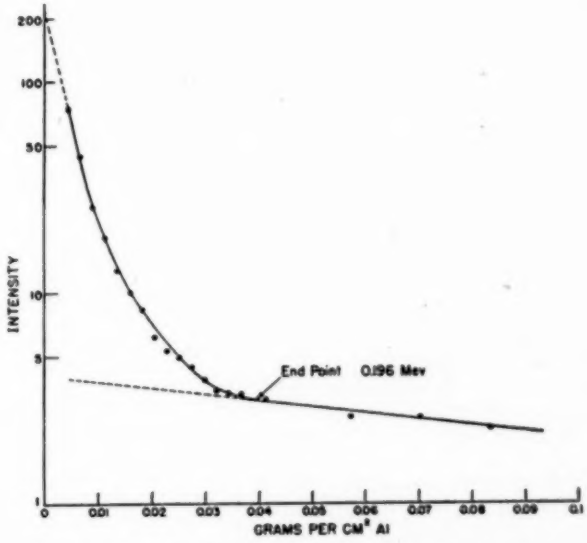


FIG. 3. Thin Al absorption curve showing conversion electrons from $Te^{121}$.

[8] J. J. Livingood and G. T. Seaborg, Phys. Rev. **52**, 135 (1937).
[9] J. J. Livingood and G. T. Seaborg, Phys. Rev. **55**, 414 (1939).

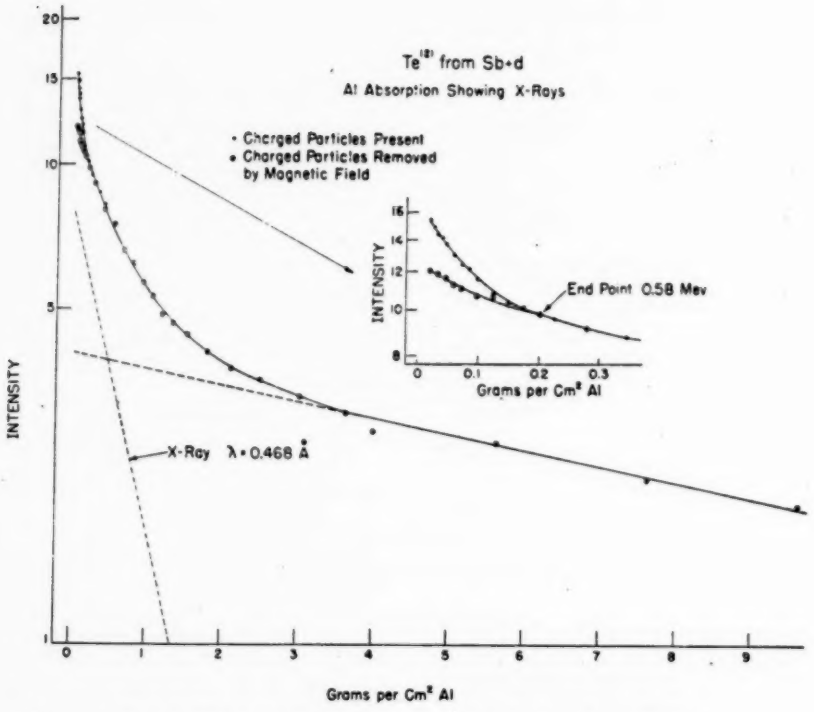
Te[121] from Sb+d
Al Absorption Showing X-Rays
• Charged Particles Present
• Charged Particles Removed by Magnetic Field
INTENSITY
End Point 0.58 Mev
Grams per Cm² Al
X-Ray λ = 0.468 Å
Grams per Cm² Al

FIG. 4. Thick Al absorption curve of radiations from $Te^{121}$.

period activity as shown by Fig. 2. The intensity of the 0.61-Mev gamma-ray relative to the 0.223-Mev gamma-ray decreases somewhat with the decay of the 17-day activity. This indicates that the 0.61-Mev gamma-ray must be associated with both the 17-day and the 143-day activities. The aluminum absorption curve in Fig. 3 shows electrons of maximum energy 0.196 Mev indi-

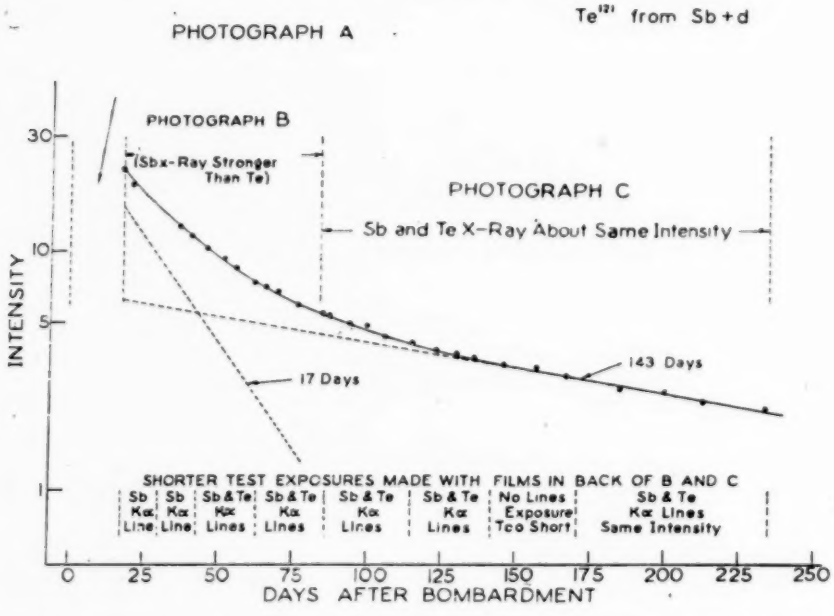
PHOTOGRAPH A
Te[121] from Sb+d
PHOTOGRAPH B
(Sb x-Ray Stronger Than Te)
PHOTOGRAPH C
Sb and Te X-Ray About Same Intensity
INTENSITY
17 Days
143 Days
SHORTER TEST EXPOSURES MADE WITH FILMS IN BACK OF B AND C
Sb Kα Line
Sb Kα Line
Sb & Te Kβ Lines
Sb & Te Kα Lines
Sb & Te Kα Lines
Sb & Te Kα Lines
No Lines Exposure Too Short
Sb & Te Kα Lines Same Intensity
DAYS AFTER BOMBARDMENT

FIG. 5. Procedure of photographic analysis of x-rays from $Te^{121}$ using a curved crystal spectrograph.

cating considerable internal conversion of the 0.223-Mev gamma-ray in the $K$-shell of Te or Sb. The principal curve in Fig. 4 shows aluminum absorption of the radiation after the charged particles were removed by magnetic deflection. Intensities with and without the magnetic field were obtained on the upper portion of the curve extending to the region where the readings coincided. X-rays characteristic of the Sb-Te region are shown and there is some evidence that the 0.61-Mev gamma-ray is internally converted to a slight exfent.

A search for x-rays in the Sb fraction by absorption of the radiation in Al after removal of the charged particles magnetically failed to reveal any x-radiation. The possible existence of $K$-capture in $Sb^{124}$ as reported[10] is not confirmed by these observations.

### $Te^{121}$ PHOTOGRAPHIC ANALYSIS OF X-RAYS

A curved crystal spectrograph employing a mica crystal curved to a radius of 15 inches[7] was used in photographing the x-rays emitted by $Te^{121}$ during various phases of its decay. Figure 5 illustrates the photographic procedure. After deuteron bombardment the Sb sample was first photographed for 18 days before the chemical separation was made. The spectrograph was aligned so that $K\alpha$-radiation in the Sn, Sb, Te, I region would form lines on the film. The result of this exposure is shown in photograph $A$, Fig. 6. Sb $K\alpha$, Sb $K\beta$, and very weak Te $K\alpha$ lines are visible. Sb and Te calibration lines are shown in the lower half of each photograph in Fig. 6. During the exposure of photograph $A$, other films were placed just off the focal circle of the spectrograph in back of the main film. Each of these test films remained in position for a few days, then it was removed and replaced by a new film. In this way the progress of the main exposure could be determined and any change in the relative intensity of lines could be noted. Four such films exposed while photograph $A$ was being made showed clearly the Sb lines, but the Te lines were not visible.

After chemical separation the Te fraction was photographed for a total of 217 days according to the procedure shown in Fig. 5. The same spectrograph was used for photographs $A$, $B$, and $C$. The Sb fraction was also photographed. A single exposure of the Sb fraction was made in a

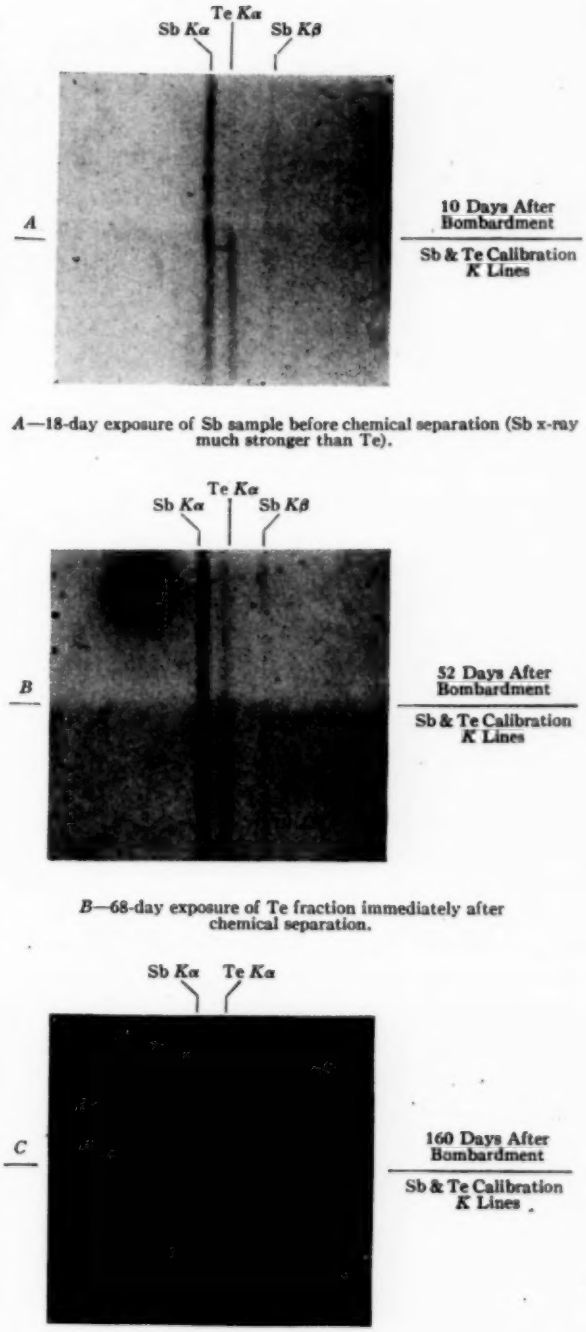
Te Kα
Sb Kα
Sb Kβ
A
10 Days After Bombardment
Sb & Te Calibration K Lines
A—18-day exposure of Sb sample before chemical separation (Sb x-ray much stronger than Te).
Te Kα
Sb Kα
Sb Kβ
B
52 Days After Bombardment
Sb & Te Calibration K Lines
B—68-day exposure of Te fraction immediately after chemical separation.
Sb Kα
Te Kα
C
160 Days After Bombardment
Sb & Te Calibration K Lines
C—149-day exposure of Te fraction following exposure B.

FIG. 6. X-ray photographs of $Te^{121}$ taken with a curved crystal spectrograph.

[10] Allan C. G. Mitchell, Lawrence M. Langer, and Paul W. McDaniel, Phys. Rev. **57**, 1107 (1940).

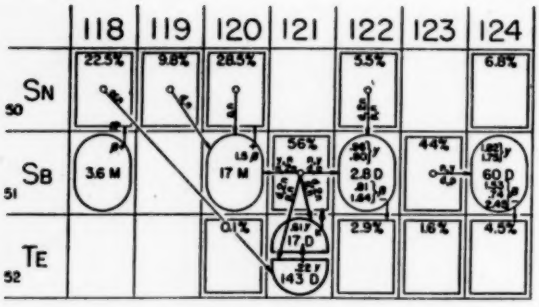


FIG. 7. Region of atomic chart showing decay process of $Te^{121}$.

similar spectrograph extending over a period of 120 days but no x-rays were found. Therefore, it can be assumed that the x-ray lines appearing in photograph *A* were associated with the Te fraction. The upper half of photograph *B* (Fig. 6) is the result of a 68-day exposure of the Te fraction starting immediately after chemical separation. The Sb lines are still strong but the intensity of the Te $K\alpha$ line relative to the Sb $K\alpha$ line is considerably greater than in photograph *A*. It is evident from photographs *A* and *B* that the source of Sb x-rays must be decaying more rapidly than the source of Te x-rays. The four test films obtained during the 68-day exposure also show a decrease in the intensity of Sb x-rays with respect to the Te x-rays. It may be observed from Fig. 5 that the 17-day and the 143-day activities had approximately the same average intensity during the 68-day exposure.

Photograph *C* (Fig. 6) was exposed for 149 days starting immediately after exposure *B*. The Sb and Te lines are about the same intensity and it can be seen from the decay curves of Fig. 5 that the average intensity of the 17-day activity is very small compared to the intensity of the 143-day activity during this exposure. The four test films obtained during this exposure show conclusively that Sb and Te x-rays of approximately the same intensity are associated with the 143-day activity.

## DISCUSSION

The existence of a 143-day Te activity which emits x-rays characteristic of Te and Sb can be readily explained by a genetically related isomeric pair as indicated in Fig. 7. Since Sb x-rays and a 0.61-Mev gamma-ray appear to be associated with the 17-day activity as well as with the 143-day activity, these two activities logically form the isomeric pair. The highly converted 0.223-Mev gamma-ray is emitted in the isomeric transition accounting for the relatively high intensity of the Te x-rays. The 0.61-Mev gamma-ray being associated with both periods must be emitted with the return of the $Sb^*$ nucleus to the ground state following *K*-capture.

No evidence of the "fast" gamma-transition type of decay was found. If such "fast" transitions occur in the Te-Sb decay their number must be small compared to the isomeric transitions since no satellite x-ray lines were observed near the strong characteristic $K\alpha$ lines.

The authors are grateful for the support received from Mr. Julius F. Stone, The Ohio State University Development Fund, The Ohio State University Research Foundation and the Graduate School.

# The Scattering of Slow Neutrons by Ortho- and Paradeuterium*

M. HAMERMESH, *New York University, University Heights, New York, New York***

AND

JULIAN SCHWINGER, *Harvard University, Cambridge, Massachusetts****

(Received December 16, 1945)

Information relating to the spin dependence of the neutron-deuteron interaction can be obtained from slow neutron scattering experiments in ortho- and paradeuterium. Theoretical formulae have been derived for the cross sections of the various transitions among the molecular rotational levels, which involve the scattering amplitudes $a_{3/2}$ and $a_{1/2}$ for the two spin states of the neutron-deuteron system. In particular, numerical results are given for the first few transitions originating from the ground levels of the ortho- and para-systems with neutron energies not exceeding 0.05 ev. The influence of the thermal motion of the molecule is described, and explicit formulae are given for the important transitions occurring at small neutron energies, on the assumption that the $D_2$ is in gaseous form at low temperature. The ratio of the ortho- and para-cross sections, under these conditions, is examined in its dependence upon the ratio of the scattering amplitudes. If the scattering amplitudes are of the same sign, the cross-section ratio is never greater than 1.31 and attains this magnitude only for small values of $a_{3/2}$ relative to $a_{1/2}$. If, however, the amplitudes are of opposite sign, this ratio can be as large as 1.75 and always exceeds 1.11. This experiment measures only the magnitudes of the amplitude combinations $(2a_{3/2}+a_{1/2})$ and $(a_{3/2}-a_{1/2})$, but not their signs, and thus leaves a fourfold ambiguity in interpretation. The possibility is discussed of determining the sign of $(2a_{3/2}+a_{1/2})$ by scattering experiments in HD. It is pointed out that the sign of $(a_{3/2}-a_{1/2})$ cannot be fixed by any experiment in which the deuteron spin is unoriented in space. An alternative experimental method, involving the depolarization of neutrons, is mentioned.

EXPERIMENTS on slow neutron scattering in ortho- and parahydrogen[1] have provided decisive information concerning the spin of the neutron[2] and the spin dependence of the neutron-proton interaction.[3] With improvements in technique, these experiments will yield data on the range of the neutron-proton interaction, and facilitate accurate measurements of the slow neutron cross sections for scattering and capture by protons.[4] It is evident that analogous investigations with ortho- and paradeuterium can be of value in supplying further information relating to the spin dependence and exchange character of the forces between elementary particles. It is the purpose of this note to analyze the scattering of slow neutrons by ortho- and paradeuterium in order that the values of the fundamental nuclear quantities may be readily extracted from the results of such an experiment. The basic ideas underlying the problem are essentially identical with those relating to ortho- and parahydrogen, and we shall therefore be content to indicate the necessary modifications in mathematical detail, together with some improvements in the treatment.[5]

The scattering of a slow neutron by a nucleus of mass number $A$ and spin $S$ can be described by an effective interaction operator to be employed in conjunction with the Born approximation:

$$U=-\frac{2\pi\hbar^2}{M}\frac{A+1}{A}\left[\frac{S+1}{2S+1}a_{S+\frac{1}{2}}+\frac{S}{2S+1}a_{S-\frac{1}{2}}+(a_{S+\frac{1}{2}}-a_{S-\frac{1}{2}})\frac{\boldsymbol{\sigma}\cdot\mathbf{S}}{2S+1}\right]\delta(\mathbf{r}-\mathbf{R}). \quad (1)$$

Here, $M$ is the mass of the neutron; $\frac{1}{2}\boldsymbol{\sigma}$ and $\mathbf{S}$ are the spin operators of the neutron and nucleus,

* This work was completed in 1939, and reported at the New York meeting of the American Physical Society (Phys. Rev. 55, 679 (1939)).

** On leave at the Radio Research Laboratory, Harvard University, Cambridge, Massachusetts.

*** On leave at the Radiation Laboratory, Massachusetts Institute of Technology, Cambridge, Massachusetts.

[1] J. Halpern, I. Estermann, O. C. Simpson, and O. Stern, Phys. Rev. 52, 142 (1937); F. G. Brickwedde, J. R. Dunning, H. J. Hoge, and J. H. Manley, Phys. Rev. 54, 266 (1938); W. F. Libby and E. A. Long, Phys. Rev. 55, 339 (1939); L. W. Alvarez and K. S. Pitzer, Phys. Rev. 58, 1003 (1940).

[2] J. Schwinger, Phys. Rev. 52, 1250 (1937).

[3] J. Schwinger and E. Teller, Phys. Rev. 52, 286 (1937).

[4] J. Schwinger, Phys. Rev. 58, 1004 (1940).

[5] The notation used here conforms to that in reference 3. References to equations in that paper will be indicated by the prefix ST.

respectively; $\delta(\mathbf{r}-\mathbf{R})$ represents a delta-function of the distance between the position of the neutron, $\mathbf{r}$, and the position of the nucleus, $\mathbf{R}$; and $a_{S\pm\frac{1}{2}}$ are the amplitudes of the scattered waves for the two total spin states of the system. The amplitudes are related to the corresponding cross sections for each spin state by

$$\sigma_{S\pm\frac{1}{2}}=4\pi a^2_{S\pm\frac{1}{2}}. \tag{2}$$

The total scattering cross section for a free nucleus is an appropriately weighted average of the cross sections for the two states of spin:

$$\sigma=\frac{S+1}{2S+1}\sigma_{S+\frac{1}{2}}+\frac{S}{2S+1}\sigma_{S-\frac{1}{2}}. \tag{3}$$

For the deuteron, the effective interaction operator becomes

$$U=-\frac{\pi\hbar^2}{M}[2a_{3/2}+a_{1/2}+(a_{3/2}-a_{1/2})\boldsymbol{\sigma}\cdot\mathbf{S}]\delta(\mathbf{r}-\mathbf{R}), \tag{4}$$

and the scattering cross section for a free deuteron is

$$\sigma=\tfrac{2}{3}\sigma_{3/2}+\tfrac{1}{3}\sigma_{1/2}. \tag{5}$$

The effective interaction between a neutron and the two deuterons in the $D_2$ molecule is conveniently expressed as

$$U=-\frac{\pi\hbar^2}{M}[2a_{3/2}+a_{1/2}+\tfrac{1}{2}(a_{3/2}-a_{1/2})\boldsymbol{\sigma}\cdot\mathbf{S}][\delta(\mathbf{r}_n-\mathbf{r}_1)+\delta(\mathbf{r}_n-\mathbf{r}_2)]$$
$$-\frac{\pi\hbar^2}{M}(a_{3/2}-a_{1/2})\boldsymbol{\sigma}\cdot\frac{\mathbf{S}_1-\mathbf{S}_2}{2}[\delta(\mathbf{r}_n-\mathbf{r}_1)-\delta(\mathbf{r}_n-\mathbf{r}_2)], \tag{6}$$

where now

$$\mathbf{S}=\mathbf{S}_1+\mathbf{S}_2 \tag{7}$$

represents the total spin of the molecule. The states of a deuterium molecule are divided into ortho-levels, those possessing even total spin and rotational angular momenta ($S=0,\ 2;\ J=0,\ 2,\ \cdots$), and para-levels, those with odd quantum numbers ($S=1;\ J=1,\ 3,\ \cdots$). The symmetrical part of the neutron-molecule interaction produces transitions in which the total molecular spin does not change, that is, ortho→ortho- and para→para-transitions. The antisymmetrical part of the interaction induces transitions accompanied by a spin change of unity; ortho→para- and para→ortho-transitions.

We wish to calculate the differential cross section for a scattering process in which a neutron with momentum $\mathbf{p}^0$ collides with a $D_2$ molecule with momentum $-\mathbf{p}^0$ in the internal state specified by the vibrational, rotational, and spin quantum numbers $v$, $J$, $S$, thereby producing a neutron with momentum $\mathbf{p}$ which has been scattered through the angle $\Theta$ into the solid angle $d\Omega$, leaving the molecule in the state characterized by $-\mathbf{p}$, $v'$, $J'$, $S'$. The differential cross section, as computed by the Born approximation, is

$$\sigma_{J',v',S';\,J,v,S}(\Theta)d\Omega=\frac{16}{25}\frac{p}{p^0}\frac{1}{2(2S+1)(2J+1)}\sum_{m',m_{J'},m_{S'}}\sum_{m,m_J,m_S}\left|\left(\Psi_f,\frac{MV}{2\pi\hbar^2}U\Psi_i\right)\right|^2 d\Omega, \tag{8}$$

which differs formally from the corresponding $H_2$ molecule cross section (ST (21)) only by the replacement of the numerical factor 4/9, the square of the reduced mass of the neutron $-H_2$ molecule system, by 16/25, the square of the reduced mass of the neutron $-D_2$ molecule system. These reduced mass factors arise in calculating the number of final neutron states per unit range of the total energy, and in the value of the neutron flux relative to the molecule. The differential cross section for those transitions in which the molecular spin is unchanged can be immediately obtained

from the corresponding $H_2$ cross section (ST (28)) by suitable changes in the scattering amplitudes and the numerical replacement just discussed. The result is

$$\sigma_{J',v',S';\,J,v,S}(\Theta)d\Omega=\frac{16}{25}\frac{p}{p^0}[(2a_{3/2}+a_{1/2})^2+\tfrac{1}{4}(a_{3/2}-a_{1/2})^2S(S+1)]$$
$$\cdot\frac{1}{2J+1}\sum_{m_J,\,m_{J'}}\left|\int\cos\frac{\mathbf{p}^0-\mathbf{p}}{2\hbar}\cdot\mathbf{r}\phi^*_{v',\,J',\,m_{J'}}(\mathbf{r})\phi_{v,\,J,\,m_J}(\mathbf{r})d\tau\right|^2 d\Omega. \quad (9)$$

The analog of (ST (30)), the cross section for transitions in which the molecular spin changes, is

$$\sum_{S'\neq S}\sigma_{J',v',S';\,J,v,S}(\Theta)d\Omega=\frac{16}{25}\frac{p}{p^0}(a_{3/2}-a_{1/2})^2\frac{8-S(S+1)}{4}$$
$$\cdot\frac{1}{2J+1}\sum_{m_J,\,m_{J'}}\left|\int\sin\frac{\mathbf{p}^0-\mathbf{p}}{2\hbar}\cdot\mathbf{r}\phi^*_{v',\,J',\,m_{J'}}(\mathbf{r})\phi_{v,\,J,\,m_J}(\mathbf{r})d\tau\right|^2 d\Omega. \quad (10)$$

In these formulae, the magnitude of the neutron momentum after collision is obtained from energy conservation (cf. ST (17)):

$$\frac{5}{8M}p^{0^2}+E_{J,v}=\frac{5}{8M}p^2+E_{J',v'}, \quad (11)$$

and $\mathbf{p}^0$ is related to $\mathbf{p}_0$, the initial neutron momentum in a coordinate system in which the molecule is initially at rest, by

$$\mathbf{p}^0=\tfrac{4}{5}\mathbf{p}_0. \quad (12)$$

Further calculations will be restricted to molecules in the lowest vibrational state, $v=0$, and the rotational wave functions employed will be those of a rigid rotator with internuclear separation $r_e$:

$$\phi_{0,\,J,\,m_J}(\mathbf{r})=P_J^{m_J}(\mathbf{r})\frac{(\delta(r-r_e))^{\frac{1}{2}}}{r_e}. \quad (13)$$

Here, $P_J^{m_J}$ is a spherical harmonic of the angular coordinates associated with the vector $\mathbf{r}$, normalized in accordance with

$$\int|P_J^{m_J}(\mathbf{r})|^2d\omega=1. \quad (14)$$

The cross-section formulae for both types of spin transitions ($S'=S$, $S'\neq S$) involve summations of the type

$$\frac{1}{2J+1}\sum_{m_J,\,m_{J'}}\left|\int\exp(i\mathbf{k}\cdot\mathbf{r})\phi^*_{0,\,J',\,m_{J'}}(\mathbf{r})\phi_{0,\,J,\,m_J}(\mathbf{r})d\tau\right|^2$$
$$=\frac{1}{2J+1}\sum_{m_J,\,m_{J'}}\left|\int\exp(i\mathbf{k}\cdot\mathbf{r})P_{J'}^{m_{J'}*}(\mathbf{r})P_J^{m_J}(\mathbf{r})d\omega\right|^2\equiv\sum, \quad (15)$$

with

$$\mathbf{k}=(\mathbf{p}^0-\mathbf{p})/2\hbar \quad (16)$$

for the symmetry properties of the rotational functions will automatically select the real or imaginary part of $\exp(i\mathbf{k}\cdot\mathbf{r})$. To evaluate this sum, we regard the square of the absolute value of the integral as a double integral and perform the summations with respect to $m_J$ and $m_{J'}$, employing the spherical harmonic addition theorem:

$$\sum_{m_J}P_J^{m_J*}(\mathbf{r})P_J^{m_J}(\mathbf{r}')=\frac{2J+1}{4\pi}P_J(\cos\theta), \quad (17)$$

where $P_J(\cos\theta)$ is a Legendre polynomial of the cosine of the angle between the vectors $\mathbf{r}$ and $\mathbf{r}'$.

Hence

$$\sum=(2J'+1)\int \exp\left[i\mathbf{k}\cdot(\mathbf{r}-\mathbf{r}')\right]P_J(\cos\theta)P_{J'}(\cos\theta)\frac{d\omega}{4\pi}\frac{d\omega'}{4\pi}. \tag{18}$$

Now it is evident that the scattering cross section cannot depend upon the absolute direction of the initial neutron momentum, but involves only the angle $\Theta$ between $\mathbf{p}^0$ and $\mathbf{p}$. Hence the above integral is unaffected on replacing $\exp\left[i\mathbf{k}\cdot(\mathbf{r}-\mathbf{r}')\right]$ by its average over all directions of the vector $\mathbf{k}$, namely $\sin k|\mathbf{r}-\mathbf{r}'|/k|\mathbf{r}-\mathbf{r}'|$. With the aid of the expansion[6]

$$\frac{\sin k|\mathbf{r}-\mathbf{r}'|}{k|\mathbf{r}-\mathbf{r}'|}=\frac{\sin(2kr_e\sin\frac{1}{2}\theta)}{2kr_e\sin\frac{1}{2}\theta}=\sum_{L=0}^{\infty}(2L+1)j_L^2(kr_e)P_L(\cos\theta), \tag{19}$$

where

$$j_L(x)=\left(\frac{\pi}{2x}\right)^{\frac{1}{2}}J_{L+\frac{1}{2}}(x) \tag{20}$$

the quantity $\sum$ can be cast into the form

$$\sum=(2J'+1)\sum_L(2L+1)C_{LJJ'}j_L^2(kr_e), \tag{21}$$

with

$$C_{LJJ'}=\int_0^{\pi}P_L(\cos\theta)P_J(\cos\theta)P_{J'}(\cos\theta)\frac{\sin\theta d\theta}{2}. \tag{22}$$

Hence, the various differential cross sections can be expressed as

$$\sigma_{J',S;J,S}(\Theta)d\Omega=\frac{16}{25}\frac{p}{p^0}\left[(2a_{3/2}+a_{1/2})^2+\tfrac{1}{4}(a_{3/2}-a_{1/2})^2S(S+1)\right]$$
$$\cdot(2J'+1)\sum_L(2L+1)C_{LJJ'}j_L^2\left[\frac{r_e}{2\hbar}(p^{02}+p^2-2p^0p\cos\Theta)^{\frac{1}{2}}\right]d\Omega, \tag{23}$$

$$\sum_{S'\neq S}\sigma_{J',S';J,S}(\Theta)d\Omega=\frac{16}{25}\frac{p}{p^0}(a_{3/2}-a_{1/2})^2\frac{8-S(S+1)}{4}$$
$$\cdot(2J'+1)\sum_L(2L+1)C_{LJJ'}j_L^2\left[\frac{r_e}{2\hbar}(p^{02}+p^2-2p^0p\cos\Theta)^{\frac{1}{2}}\right]d\Omega.$$

The constants $C_{LJJ'}$ are zero unless $L$ has one of the values

$$L=J+J',\ J+J'-2,\ \cdots|J-J'|. \tag{24}$$

Some important and useful properties can be obtained from the defining Eq. (22), rewritten as

$$\sum_L(2L+1)C_{LJJ'}P_L(z)=P_J(z)P_{J'}(z). \tag{25}$$

On placing $z=1$, and recalling that $P_J(1)=1$, we obtain the sum formula

$$\sum_L(2L+1)C_{LJJ'}=1. \tag{26}$$

If Eq. (25) is multiplied by $z$, and use is made of the relation

$$zP_L(z)=\frac{L+1}{2L+1}P_{L+1}(z)+\frac{L}{2L+1}P_{L-1}(z), \tag{27}$$

a recurrence relation is obtained for the $C_{LJJ'}$ as a function of $L$

$$\frac{L+1}{2L+1}C_{L+1,J,J'}+\frac{L}{2L+1}C_{L-1,J,J'}=\frac{J+1}{2J+1}C_{L,J+1,J'}+\frac{J}{2J+1}C_{L,J-1,J'}. \tag{28}$$

[6] J. A. Stratton, *Electromagnetic Theory* (McGraw-Hill Book Company, Inc., New York, 1941), p. 413.

Thus, starting with the orthogonality integral

$$C_{0JJ'}=\frac{\delta_{JJ'}}{2J+1}, \tag{29}$$

where $\delta_{JJ'}$ is the customary Kronecker symbol, one obtains, successively

$$\begin{aligned} C_{1JJ'}&=\frac{1}{(2J+1)(2J'+1)}[J\delta_{J,J'+1}+J'\delta_{J',J+1}],\\ C_{2JJ'}&=\frac{J(J+1)}{(2J-1)(2J+1)(2J+3)}\delta_{JJ'}+\frac{3}{2}\frac{1}{(2J+1)(2J'+1)}\left[\frac{J(J'+1)}{2J-1}\delta_{J,J'+2}+\frac{J'(J+1)}{2J'-1}\delta_{J',J+2}\right] \end{aligned} \tag{30}$$

and so on. The recurrence relation combined with the sum formula and the symmetry of $C_{LJJ'}$, enables one to obtain the required values with little effort. Alternatively, the values of $C_{LJJ'}$ can be computed directly from the explicit formula:[7]

$$C_{LJJ'}=\frac{(J+L-J')!(J'+L-J)!(J+J'-L)!}{(J+J'+L+1)!}\left[\left(\frac{J+J'+L}{2}\right)!\Big/\left(\frac{J+L-J'}{2}\right)!\left(\frac{J'+L-J}{2}\right)!\left(\frac{J+J'-L}{2}\right)!\right]^2. \tag{31}$$

To evaluate the total scattering cross section for a given transition, we integrate Eq. (23) with respect to the scattering angle $\Theta$ and obtain:

$$\sigma_{J'S;\,JS}=\frac{16}{25}\pi\left[(2a_{3/2}+a_{1/2})^2+\frac{1}{4}(a_{3/2}-a_{1/2})^2S(S+1)\right](2J'+1)\left(\frac{2\hbar}{p^0r_e}\right)^2A_{JJ'}, \tag{32}$$

$$\sum_{S'\neq S}\sigma_{J'S';\,JS}=\frac{16}{25}\pi(a_{3/2}-a_{1/2})^2\frac{8-S(S+1)}{4}(2J'+1)\left(\frac{2\hbar}{p^0r_e}\right)^2A_{JJ'},$$

where

$$A_{JJ'}=2\sum_L(2L+1)C_{LJJ'}\int_{(r_e/2\hbar)|p^0-p|}^{(r_e/2\hbar)(p^0+p)}j^2_L(x)x\,dx. \tag{33}$$

A relation between the Bessel function integrals for successive values of $L$ can be established with the aid of the recurrence formulae:[8]

$$j_{L-1}(x)=\frac{d}{dx}j_L(x)+\frac{L+1}{x}j_L(x),\quad j_L(x)=-\frac{d}{dx}j_{L-1}(x)+\frac{L-1}{x}j_{L-1}(x). \tag{34}$$

On multiplying the first equation by $x^2j_L(x)$, the second equation by $x^2j_{L-1}(x)$, and comparing the resultant expressions, we find that

$$xj^2_L-xj^2_{L-1}=-\frac{1}{2L}\frac{d}{dx}[x^2(j^2_{L-1}+j^2_L)], \tag{35}$$

or

$$\int_0^x xj^2_L\,dx-\int_0^x xj^2_{L-1}\,dx=-\frac{1}{2L}x^2(j^2_{L-1}(x)+j^2_L(x)). \tag{36}$$

Hence

$$\int_0^x xj^2_1\,dx=\int_0^x xj^2_0\,dx-\tfrac{1}{2}x^2(j^2_0(x)+j^2_1(x)), \tag{37}$$

and, in general,

$$\int_0^x xj^2_L\,dx=\int_0^x xj^2_0\,dx-\tfrac{1}{2}x^2\left[j^2_0(x)+\sum_{K=1}^{L-1}\frac{2K+1}{K(K+1)}j^2_K(x)+\frac{1}{L}j^2_L(x)\right]. \tag{38}$$

[7] E. T. Whittaker and G. N. Watson, *Modern Analysis* (The MacMillan Company, New York, 1944), p. 331.
[8] Reference 6, p. 406.

Thus, all such Bessel function integrals are reduced to that for $L=0$:

$$\int_0^x xj^2_0 dx = \int_0^x \frac{\sin^2 x}{x} dx = \tfrac{1}{2}\int_0^{2x} \frac{1-\cos t}{t} dt = \tfrac{1}{2} Cin 2x. \tag{39}$$

The function *Cinx* is related to the more customary cosine integral

$$Cix = -\int_x^\infty \frac{\cos t}{t} dt, \tag{40}$$

by

$$Cinx = \log x + C - Cix, \tag{41}$$

where $C=0.5772$ is the Eulerian constant. Finally, then, the quantity $A_{JJ'}$ can be expressed as

$$A_{JJ'} = [Cin 2x - \textstyle\sum_L (2L+1) C_{LJJ'} f_L(x)]^{(r_e/2\hbar)(p^0+p)}_{(r_e/2\hbar)|p^0-p|}, \tag{42}$$

where use has been made of the sum formula (26), and

$$\begin{aligned} f_L(x) &= 0, \quad L=0 \\ &= x^2(j^2_0 + j^2_1), \quad L=1, \\ &= x^2\left(j^2_0 + \sum_{K=1}^{L-1} \frac{2K+1}{K(K+1)} j^2_K + \frac{1}{L} j^2_L\right), \quad L>1. \end{aligned} \tag{43}$$

The cross section for any transition originating from an ortho-level must be averaged over the two ortho-spin states, $S=0, 2$ with the statistical weights $\frac{1}{3}$ and $\frac{5}{3}$, respectively. Therefore, the final cross-section formulae for ortho→ortho- and ortho→para-transitions are:

$$\begin{aligned} &\text{ortho}\rightarrow\text{ortho}: \quad \sigma_{J'\leftarrow J} = \frac{16}{25}\pi\left[(2a_{3/2}+a_{1/2})^2 + \frac{5}{4}(a_{3/2}-a_{1/2})^2\right]\left(\frac{2\hbar}{p^0 r_e}\right)^2 (2J'+1) A_{JJ'}, \\ &\text{ortho}\rightarrow\text{para}: \quad \sigma_{J'\leftarrow J} = \frac{12}{25}\pi(a_{3/2}-a_{1/2})^2\left(\frac{2\hbar}{p^0 r_e}\right)^2 (2J'+1) A_{JJ'}. \end{aligned} \tag{44}$$

To obtain the cross sections for transitions originating in a para-level, we need merely place $S=1$, whence

$$\begin{aligned} &\text{para}\rightarrow\text{para}: \quad \sigma_{J'\leftarrow J} = \frac{16}{25}\pi\left[(2a_{3/2}+a_{1/2})^2 + \tfrac{1}{2}(a_{3/2}-a_{1/2})^2\right]\left(\frac{2\hbar}{p^0 r_e}\right)^2 (2J'+1) A_{JJ'}, \\ &\text{para}\rightarrow\text{ortho}: \quad \sigma_{J'\leftarrow J} = \frac{24}{25}\pi(a_{3/2}-a_{1/2})^2\left(\frac{2\hbar}{p^0 r_e}\right)^2 (2J'+1) A_{JJ'}. \end{aligned} \tag{45}$$

The energy levels of the deuterium molecule, considered as a rigid rotator, are

$$E_J = \frac{\hbar^2}{2Mr_e^2} J(J+1), \tag{46}$$

and, in particular,

$$E_1 = \hbar^2/Mr_e^2. \tag{47}$$

The initial neutron momentum $p^0$, expressed in terms of the neutron energy in the rest system of the molecule before collision, is

$$p^0 = \tfrac{1}{2}(2ME)^{\frac{1}{2}} \tag{48}$$

whence

$$\frac{p^0 r_e}{\hbar} = \frac{4}{5}\left(\frac{2E}{E_1}\right)^{\frac{1}{2}} \equiv \xi. \tag{49}$$

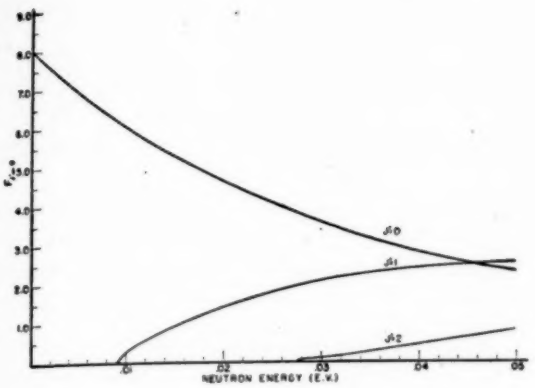


FIG. 1. Cross sections for transitions originating from the orthodeuterium ground state, omitting amplitude factors (cf. Eq. (52)).

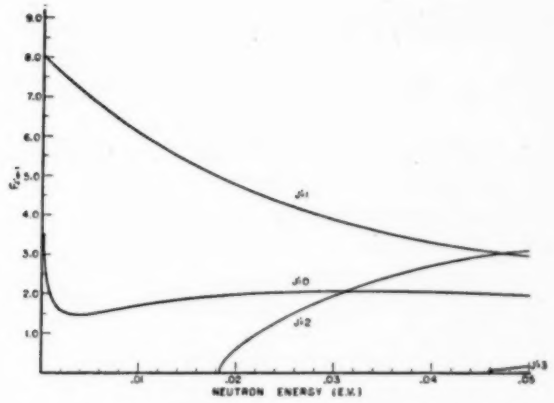


FIG. 2. Cross sections for transitions originating from the paradeuterium ground state, omitting amplitude factors (cf. Eq. (52)).

The neutron momentum $p$ after a rotational transition $J\rightarrow J'$ is determined by (cf. Eq. (11))

$$p^2=p^{0^2}+\frac{4}{5}\frac{\hbar^2}{r_e^2}[J(J+1)-J'(J'+1)], \tag{50}$$

or

$$\frac{pr_e}{\hbar}=\{\xi^2+\tfrac{4}{5}[J(J+1)-J'(J'+1)]\}^{\frac{1}{2}}. \tag{51}$$

Hence the neutron energy is effectively measured in units of the energy of the first rotational level, $E_1=0.0074$ ev.[9]

Explicit expressions for the cross sections describing the first few transitions originating from the ground levels of the ortho- and para-systems are:

$$\sigma_{0\leftarrow 0}=[(2a_{3/2}+a_{1/2})^2+(5/4)(a_{3/2}-a_{1/2})^2]F_{0\leftarrow 0}(E),$$

$$F_{0\leftarrow 0}(E)=\frac{64}{25}\pi\frac{1}{\xi^2}Cin2\xi,$$

$$\sigma_{1\leftarrow 0}=(a_{3/2}-a_{1/2})^2F_{1\leftarrow 0}(E),$$

$$F_{1\leftarrow 0}(E)=\frac{144}{25}\pi\frac{1}{\xi^2}[Cin2x-x^2(j^2{}_0(x)+j^2{}_1(x))]_{\frac{1}{2}[\xi-(\xi^2-(8/5))^{\frac{1}{2}}]}^{\frac{1}{2}[\xi+(\xi^2-(8/5))^{\frac{1}{2}}]},$$

$$\sigma_{2\leftarrow 0}=[(2a_{3/2}+a_{1/2})^2+(5/4)(a_{3/2}-a_{1/2})^2]F_{2\leftarrow 0}(E),$$

$$F_{2\leftarrow 0}(E)=\frac{64}{5}\pi\frac{1}{\xi^2}[Cin2x-x^2(j^2{}_0(x)+\tfrac{3}{2}j^2{}_1(x)+\tfrac{1}{2}j^2{}_2(x))]_{\frac{1}{2}[\xi-(\xi^2-(24/5))^{\frac{1}{2}}]}^{\frac{1}{2}[\xi+(\xi^2-(24/5))^{\frac{1}{2}}]},$$

$$\sigma_{0\leftarrow 1}=(a_{3/2}-a_{1/2})^2F_{0\leftarrow 1}(E),$$

$$F_{0\leftarrow 1}(E)=\frac{96}{25}\pi\frac{1}{\xi^2}[Cin2x-x^2(j^2{}_0(x)+j^2{}_1(x))]_{\frac{1}{2}[(\xi^2+(8/5))^{\frac{1}{2}}-\xi]}^{\frac{1}{2}[(\xi^2+(8/5))^{\frac{1}{2}}+\xi]}, \tag{52}$$

$$\sigma_{1\leftarrow 1}=[(2a_{3/2}+a_{1/2})^2+\tfrac{1}{2}(a_{3/2}-a_{1/2})^2]F_{1\leftarrow 1}(E),$$

$$F_{1\leftarrow 1}(E)=\frac{192}{25}\pi\frac{1}{\xi^2}[Cin2\xi-\xi^2(\tfrac{2}{3}j^2{}_0(\xi)+j^2{}_1(\xi)+\tfrac{1}{3}j^2{}_2(\xi))],$$

$$\sigma_{2\leftarrow 1}=(a_{3/2}-a_{1/2})^2F_{2\leftarrow 1}(E),$$

$$F_{2\leftarrow 1}(E)=\frac{96}{5}\pi\frac{1}{\xi^2}\left[Cin2x-x^2\left(j^2{}_0(x)+\frac{13}{10}j^2{}_1(x)+\frac{1}{2}j^2{}_2(x)+\frac{1}{5}j^2{}_3(x)\right)\right]_{\frac{1}{2}[\xi-(\xi^2-(16/5))^{\frac{1}{2}}]}^{\frac{1}{2}[\xi+(\xi^2-(16/5))^{\frac{1}{2}}]},$$

[9] A. Farkas, *Orthohydrogen, Parahydrogen, and Heavy Hydrogen* (Cambridge University Press, New York, 1935).

$$\sigma_{3\leftarrow 1}=[(2a_{3/2}+a_{1/2})^2+\tfrac{1}{2}(a_{3/2}-a_{1/2})^2]F_{3\leftarrow 1}(E),$$

$$F_{3\leftarrow 1}(E)=\frac{448}{25}\pi\frac{1}{\xi^2}\left[Cin2x-x^2\left(j^2_0(x)+\frac{3}{2}j^2_1(x)+\frac{29}{42}j^2_2(x)+\frac{1}{3}j^2_3(x)+\frac{1}{7}j^2_4(x)\right)\right]_{\frac{1}{2}[\xi-(\xi^2-8)^{\frac{1}{2}}]}^{\frac{1}{2}[\xi+(\xi^2-8)^{\frac{1}{2}}]}.$$

The functions $F_{J'\rightarrow J}(E)$ for these seven transitions are plotted in Figs. 1 and 2 over the neutron energy range: $E=0-0.05$ ev.

The minimum neutron energy required for an excitation process is $E=(5/4)E_1=0.0093$ ev, corresponding to the 0→1 transition. If the neutron energy does not exceed this threshold, and the deuterium temperature is sufficiently low, insuring that the $J=0$ and 1 rotational levels alone are occupied, the only transitions that can occur are 0→0, 1→1, 1→0. Approximate expressions for the energy dependence of these cross sections, accurate to within a few percent for $E\lesssim E_1$, are

$$F_{0\leftarrow 0}(E)=F_{1\leftarrow 1}(E)=\frac{64}{25}\pi\left(1-\frac{16}{75}\frac{E}{E_1}\right),\quad F_{0\leftarrow 1}(E)=\frac{24}{25}\pi\left(\frac{E_1}{E}\right)^{\frac{1}{2}}\left(0.1833+0.3276\frac{E}{E_1}\right). \tag{53}$$

Under the conditions thus contemplated—neutron and molecular velocities of comparable magnitudes—the thermal agitation of the molecules must be considered before a comparison with experiment is possible.

The effective scattering cross section for a neutron of velocity $\mathbf{v}$, $\bar{\sigma}(v)$, is related to the true cross section, $\sigma(v)$, by

$$v\bar{\sigma}(v)=\int|\mathbf{v}-\mathbf{u}|\sigma(|\mathbf{v}-\mathbf{u}|)N(\mathbf{u})(d\mathbf{u})=\int w\sigma(w)N(\mathbf{v}+\mathbf{w})(d\mathbf{w}), \tag{54}$$

where $N(\mathbf{u})$ is the velocity distribution function of the target molecules, which is subject to the normalization condition

$$\int N(\mathbf{u})(d\mathbf{u})=1. \tag{55}$$

In order that the effect of thermal agitation be analyzable with precision, we shall suppose the deuterium to be in the gaseous phase at the temperature $T$, whence

$$N(\mathbf{u})=\left(\frac{2M}{\pi kT}\right)^{\frac{3}{2}}\exp\left(-2Mu^2/kT\right) \tag{56}$$

and

$$\bar{\sigma}(v)=\frac{2}{v^2}\left(\frac{2M}{\pi kT}\right)^{\frac{1}{2}}\exp\left(-2Mv^2/kT\right)\int_0^\infty\exp\left(-2Mw^2/kT\right)\sinh\frac{4Mvw}{kT}w^2\sigma(w)dw. \tag{57}$$

The effective cross sections for the three transitions under consideration, as described by Eq. (53), can be written as:

$$\begin{aligned}\bar{\sigma}_{0\leftarrow 0}(E)&=\frac{64}{25}\pi[(2a_{3/2}+a_{1/2})^2+(5/4)(a_{3/2}-a_{1/2})^2]G_{0\leftarrow 0}(E),\\ \bar{\sigma}_{1\leftarrow 1}(E)&=\frac{64}{25}\pi[(2a_{3/2}+a_{1/2})^2+\tfrac{1}{2}(a_{3/2}-a_{1/2})^2]G_{1\leftarrow 1}(E),\\ \bar{\sigma}_{0\leftarrow 1}(E)&=\frac{24}{25}\pi(a_{3/2}-a_{1/2})^2G_{0\leftarrow 1}(E),\end{aligned} \tag{58}$$

with

$$\begin{aligned}G_{0\leftarrow 0}(E)=G_{1\leftarrow 1}(E)=&\left[\frac{1}{(\pi)^{\frac{1}{2}}}\frac{\exp(-x^2)}{x}+\left(1+\frac{1}{2x^2}\right)\Phi(x)\right]\\ &-\frac{16}{75}\frac{E}{E_1}\left[\frac{1}{(\pi)^{\frac{1}{2}}}\left(1+\frac{5}{2x^2}\right)\frac{\exp(-x^2)}{x}+\left(1+\frac{3}{x^2}+\frac{3}{4x^4}\right)\Phi(x)\right],\end{aligned} \tag{59}$$

$$G_{0\leftarrow 1}(E)=0.1833\left(\frac{E_1}{E}\right)^{\frac{1}{2}}+0.3276\left(\frac{E}{E_1}\right)^{\frac{1}{2}}\left(1+\frac{3}{8}\frac{kT}{E}\right).$$

Here,

$$x^2=\frac{2Mv^2}{kT}=\frac{4E}{kT}, \tag{60}$$

and

$$\Phi(x)=\frac{2}{(\pi)^{\frac{1}{2}}}\int_0^x \exp(-t^2)dt. \tag{61}$$

An approximate expression for $G_{0\leftarrow 0}(E)$, which is accurate within one percent for $x>1$, or $E>\frac{1}{4}kT$, is

$$G_{0\leftarrow 0}(E)=1+\frac{kT}{E}-\frac{16}{75}\frac{E}{E_1}\left(1+\frac{3}{4}\frac{kT}{E}+\frac{3}{64}\left(\frac{kT}{E}\right)^2\right). \tag{62}$$

As a numerical illustration of these results, we shall assume that $E=kT=0.233E_1$, corresponding to a temperature $T=20°\text{K}$. Under these conditions,

$$G_{0\leftarrow 0}=G_{1\leftarrow 1}=1.036, \quad G_{0\leftarrow 1}=0.5971, \tag{63}$$

and

$$\begin{aligned}\bar{\sigma}_{0\leftarrow 0}&=8.33[(2a_{3/2}+a_{1/2})^2+(5/4)(a_{3/2}-a_{1/2})^2],\\ \bar{\sigma}_{1\leftarrow 1}&=8.33[(2a_{3/2}+a_{1/2})^2+\tfrac{1}{2}(a_{3/2}-a_{1/2})^2],\\ \bar{\sigma}_{0\leftarrow 1}&=1.80(a_{3/2}-a_{1/2})^2.\end{aligned} \tag{64}$$

Hence

$$\begin{aligned}\bar{\sigma}_{\text{para}}&=\bar{\sigma}_{1\leftarrow 1}+\bar{\sigma}_{0\leftarrow 1}=8.33(2a_{3/2}+a_{1/2})^2+5.97(a_{3/2}-a_{1/2})^2,\\ \bar{\sigma}_{\text{ortho}}&=\bar{\sigma}_{0\leftarrow 0}=8.33(2a_{3/2}+a_{1/2})^2+10.42(a_{3/2}-a_{1/2})^2.\end{aligned} \tag{65}$$

The cross section for neutron scattering by free deuterons

$$\sigma_0=\frac{4\pi}{9}[(2a_{3/2}+a_{1/2})^2+2(a_{3/2}-a_{1/2})^2] \tag{66}$$

is related to the ortho- and para-cross sections by

$$\sigma_0=0.403\bar{\sigma}_{\text{ortho}}-0.235\bar{\sigma}_{\text{para}} \tag{67}$$

which provides a useful check on the measurements.

It is apparent that the ortho-cross section always exceeds the para-cross section. A consideration of the ratio of the cross sections in its dependence upon the ratio of the unknown scattering amplitudes is of importance in indicating the degree of precision with which the experiment must be performed in order to yield useful information. The ratio

$$\frac{\bar{\sigma}_{\text{ortho}}}{\bar{\sigma}_{\text{para}}}=\frac{1+1.25\rho}{1+0.716\rho}, \quad \rho=\left(\frac{a_{3/2}-a_{1/2}}{2a_{3/2}+a_{1/2}}\right)^2 \tag{68}$$

is plotted as a function of $a_{3/2}/a_{1/2}$ in Fig. 3. If the scattering amplitudes possess the same sign, the cross-section ratio never exceeds 1.31 and attains this order of magnitude only for very small values of $a_{3/2}$ relative to $a_{1/2}$. If, however, the amplitudes are of opposite sign, the cross-section ratio is always greater than 1.11, but never exceeds 1.75. The latter value corresponds to $a_{3/2}/a_{1/2}=-\frac{1}{2}$. It is clear that if the experiment is to provide significant data, one must be prepared to measure the ortho- and para-cross

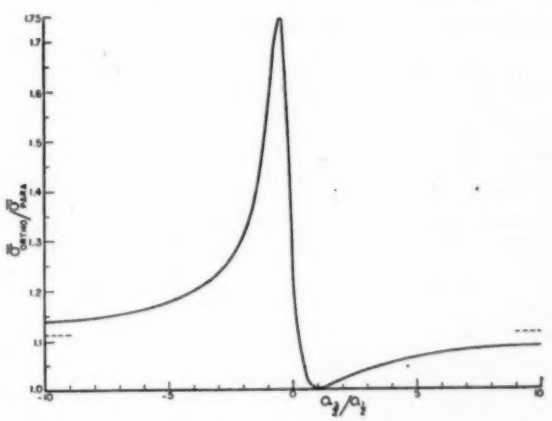


FIG. 3. Ratio of ortho- to para-scattering cross section as a function of $a_{3/2}/a_{1/2}$ (cf. Eq. (68)).

sections with an accuracy of a few percent.[10] It should also be noted that a given ortho-para-scattering ratio may correspond to either of two amplitude ratios, and the experiment can in no way distinguish between them. The amplitudes are further undetermined to the extent of a common sign factor. This fourfold ambiguity obviously stems from the fact that the ortho- and para-cross sections fix only the magnitudes of the amplitude factors $2a_{3/2}+a_{1/2}$ and $a_{3/2}-a_{1/2}$, but not their signs. The same situation arises, of course, in ortho-para-$H_2$ experiments, but with hydrogen our theoretical knowledge of the sign and order of magnitude of the triplet amplitude permits a unique determination.

In order to reduce this ambiguity in the interpretation of the ortho-para-measurements, it is necessary to measure the deuterium scattering amplitudes relative to the known values of some other nucleus. Since hydrogen is the only substance with well-known scattering properties, this suggests a consideration of scattering by the HD molecule. We give, without derivation, the total cross section for neutron scattering by HD molecules in the $J=0$ rotational level, in the limit of zero neutron energy:

$$\sigma_{HD}=\frac{9\pi}{16}[(3a_1+a_0+2a_{3/2}+a_{1/2})^2 +3(a_1-a_0)^2+2(a_{3/2}-a_{1/2})^2], \quad (69)$$

$$=\frac{9}{4}\sigma_H+\frac{81}{64}\sigma_D+\frac{9\pi}{8}(3a_1+a_0)(2a_{3/2}+a_{1/2}).$$

In this formula, $a_1$ and $a_0$ are the hydrogen scattering amplitudes for the triplet and singlet spin states; $\sigma_H$ and $\sigma_D$ are the total cross sections for scattering by a free proton and deuteron, respectively. It is clear that an absolute measurement of the HD cross section, combined with the information supplied by ortho-parahydrogen and deuterium experiments, namely the numerical magnitudes of all the quantities appearing in Eq. (69), together with the theoretically known sign of $a_1$, in principle determines the sign of the amplitude combination $2a_{3/2}+a_{1/2}$. Unfortunately, the influence of the interference term on $\sigma_{HD}$ is slight, since the hydrogen amplitude factor $3a_1+a_0$ is small, as evidenced by the very low parahydrogen elastic cross section. If one inserts the theoretically known hydrogen amplitudes and a free deuteron cross section $\sigma_D=4\times10^{-24}$ cm$^2$, the contribution of the interference term to $\sigma_{HD}$ is found to be less than 7 percent, and attains this magnitude only if $a_{3/2}\cong a_{1/2}$. Thus, in order that this experiment be successful, the large cross sections $\sigma_H$ and $\sigma_{HD}$ must be measured with high precision, and the corrections for the finite neutron energy and molecular motion must be accurately incorporated into the theory.

It may be remarked that the sign of the amplitude combination $a_{3/2}-a_{1/2}$ can never be determined by any experiment in which the deuteron spin remains arbitrarily oriented in space.

In the event that the scattering amplitudes $a_{3/2}$ and $a_{1/2}$ are not such as to produce an observable difference between the ortho- and para-$D_2$ cross sections, information may still be obtained by studies on the depolarization of polarized neutrons diffusing through substances containing deuterium. The cumulative effect of a large number of slightly depolarizing collisions can produce easily measurable effects in much the same way that diffusion experiments allow the determination of small capture cross sections. A paper dealing with this subject is being prepared for publication.

[10] From the experimental viewpoint, it would be desirable to use liquid, rather than gaseous, deuterium. If the scattering cross sections are to be unaffected by the intermolecular forces in the liquid phase, the neutron energy must exceed, say, 0.01 ev. An inspection of the data contained in Figs. 1 and 2, which are now directly applicable to the experimental results, indicates that effects comparable with those discussed in the text are obtained if the neutron energy is insufficient to excite the $1\rightarrow2$ transition, that is, $E<0.018$ ev.

# The Energy Distribution and Number of Cosmic-Ray Neutrons in the Free Atmosphere

S. A. KORFF AND B. HAMERMESH
*New York University, New York, New York*

(Received October 27, 1945)

A balloon flight to determine the energy distribution and the number of neutrons in the free atmosphere, produced by the cosmic radiation, is described. It is found that there are practically no thermal neutrons in the free atmosphere, in contrast to the fact that near the surface of the ground most of the neutrons are thermal. The number and the rate of production of the neutrons increases rapidly with elevation, in good agreement with previous measurements.

## INTRODUCTION

IT is well known that, among other effects, the cosmic radiation produces neutrons in the atmosphere. These neutrons are presumably evaporated out of nuclei by high energy constituents of the radiation, and originally have comparatively high energies, of the order of a few Mev or so. The neutrons then experience elastic and inelastic collisions with the nitrogen and other nuclei in the atmosphere. Finally they become slow, and are absorbed. On the basis of such a picture, Bethe, Korff, and Placzek[1] calculated the energy distribution which was to be expected of these neutrons. These authors (to be referred to subsequently as BKP) concluded that as a consequence of capture of slow neutrons by nitrogen, there should be comparatively few slow or thermal neutrons in equilibrium in the free atmosphere. Thus the neutrons would be in a "diffusion equilibrium," in which they would be continuously being produced, slowed down, and captured, with few ever attaining thermal velocities. They (BKP) also concluded that near the surface of the earth or near the surface of water the energy distribution would be primarily determined by the water in the vicinity. Some neutrons which had been produced in the water and slowed down in the water, or which had been produced in the air and had diffused down into the water, would diffuse back up from the surface into the air and most of these would have thermal velocities. That the neutrons near the ground are largely thermal is known, because it has been found by Korff and Clarke[2] that cadmium shields cut out most of the neutrons at the surface of the ground at various elevations, e.g., sea level and Mt. Evans. The purpose of the present experiment was to study experimentally, in the free atmosphere, the energy distribution and number of the neutrons produced by the cosmic radiation.

## EXPERIMENTAL PROCEDURE AND APPARATUS

In order to study the energy distribution of the neutrons, a flight employing a neutron counter was carried out. This neutron counter was carried to high elevations in a free balloon experiment in which techniques[3] which have been previously described were used. The counter used in this experiment was 100 cm long and 4.9 cm in diameter. It had a volume of 1850 cc and was filled to a pressure of 28 cm of boron trifluoride to which xenon was added to increase the pressure by two cm. It was operated at about 2000 volts. The counter was arranged in a vertical position and two shields, one made of cadmium, $\frac{1}{2}$-mm thick, the other of boron (6 mm of boron carbide), were so disposed that they would automatically at prearranged intervals slip over the counter. The entire arrangement was cyclical and was driven by a small electric motor. In the cycle used, first the boron shield would be in place around the counter for two minutes, then would follow a period of two minutes with no shield, then the cadmium shield would be in place for two minutes and then again no shield. About twelve seconds was required to change shields. The counts occurring during the interval

[1] H. A. Bethe, S. A. Korff, and G. Placzek, Phys. Rev. 57, 573 (1940).
[2] S. A. Korff and E. T. Clarke, Phys. Rev. 61, 422 (1942).
[3] E. T. Clarke and S. A. Korff, J. Frank. Inst. 232, 217 (1941).

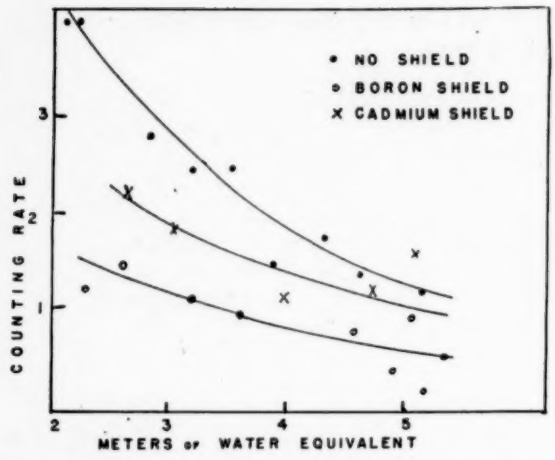


FIG. 1. Counting rate, in arbitrary units, observed with no shield and with boron shield, as a function of altitude.

while the shields were in motion were disregarded. A sliding contact caused emission of a signal which informed the observer which shield was in place. The counting rates in each of the three positions, that is, with no shield, with the cadmium shield and with the boron shield could be determined. These counting rates represented the number of counts occurring during the interval of approximately two minutes. Since the altitude of the instrument was known from the barograph which accompanied it, it was, therefore, possible to obtain the counting rate with each of the two shields separately and with no shield, as a function of elevation.

## RESULTS

The counting rates obtained with and without the boron shield were plotted as a function of position in the atmosphere expressed in meters of water equivalent below the top and are shown in Fig. 1. The solid points represent the counting rate with no shield, and the circles represent the counting rate with the boron shield in place. A smooth curve has been drawn (by inspection) through the experimental points. The differences between the two smooth curves, i.e., the difference between the counting rates with and without the boron shield is presented in Fig. 2. We shall call this curve the "boron difference." The difference curve represents the effect produced by the shield and indicates the amount of the radiation which was cut out by that shield. Each point in Fig. 1 is based on the number of counts which occurred during an interval of approximately two minutes. In computing the number of counts occurring in each interval, a correction was made for the length of time during which the instrument was not sensitive to the cosmic radiation because it was recording the temperature or the pressure or the shield position, or the shield was in motion. The approximate accuracy may be judged from the statistical scatter of the points in Figs. 1 and 2.

## DISCUSSION

Consider the quantities measured by the counter with the shields as described above. The counter employs a boron gas and a count occurs each time a neutron is captured by $B^{10}$ nucleus. Since the boron capture cross section for neutrons follows the $(1/v)$ law, the counter will detect neutrons of all energies, from thermal up to hundreds of volts. At still greater energies the detector continues to be sensitive but the cross-section decreases to so small a value that competing processes, e.g., recoils, become the predominating factor. The counter thus measures neutrons of all energies, efficiently by capture in the low energy region, inefficiently by capture in the intermediate energy region, and inefficiently by recoil at high energies. Most of the counts, in a neutron diffusion equilibrium such as exists in the atmosphere, will be produced by neutrons

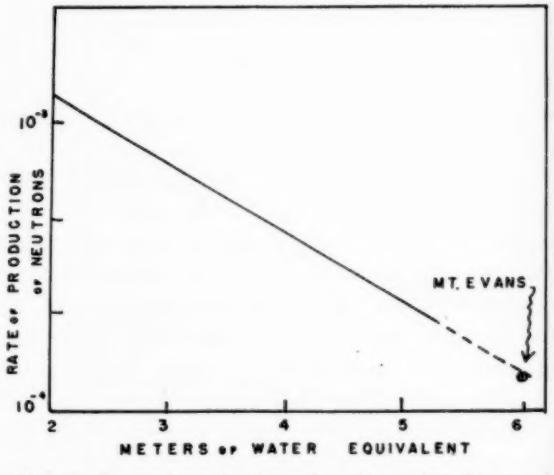


FIG. 2. Rate of production of neutrons by the cosmic radiation in the atmosphere, $q$, per gram per second, derived from Fig. 1, as a function of altitude. Point at 6 meters previously observed on Mt. Evans, for comparison.

in the lower energy ranges, and by thermal neutrons if such exist.

A cadmium shield, by virtue of the extremely large capture cross section of cadmium for thermal neutrons, will exclude thermal neutrons. Since, however, cadmium absorption does not follow the $(1/v)$ law, such a shield will not obstruct the passage of neutrons whose energy is a volt or more. The difference in the counting rate of a boron-trifluoride counter, with and without a cadmium shield, serves to determine the number of thermal or very slow (say below 0.3 volt) neutrons. On the other hand, the boron shield has the same dependence of efficiency on energy as has the detector. Hence the fraction of the neutrons which get through the absorber and are detected by the detector is independent of the energy.

At any given velocity the intensity (or number of neutrons per second) getting through the absorber, $I$, is related to the number $I_0$ incident in the absorber, through the equation

$$I = I_0 e^{-\alpha x}, \tag{1}$$

where $x$ is the thickness of the absorber and $\alpha$ is the absorption coefficient, which is defined by

$$\alpha = Nd\sigma/w, \tag{2}$$

where $N$ is Avogadro's number, $d$ the density of the absorber, $\sigma$ the capture cross section of the absorber for neutrons of the velocity under discussion, and $w$ the atomic weight of the absorber. In this case $x$ was about 0.6 cm, $d$ was about unity, and $w$ about 56. Assuming four boron atoms per molecule and taking $\sigma$ as $550\times10^{-24}$ sq. cm for thermal neutrons (a figure which already includes the $B^{10}$:$B^{11}$ isotope ratio) we find that no detectible number of neutrons will get through the boron shield at thermal velocities. Indeed, applying the $(1/v)$ law to the value of $\sigma$ in Eq. (2), we find that not one percent of incident neutrons will get through the boron shield unless their energies are nearly ten times thermal.* At this energy the sensitivity of the detector is one-tenth of what it is for a thermal neutron, and hence the number detected is correspondingly less. At high energies, when, because of the $(1/v)$ law, $\sigma$ in Eq. (2) becomes small, the exponential in Eq. (1) may be expanded and written in terms of its first two series members. The number of neutrons detected, $N$, will be related to the number $N_0$ incident in the absorber by

$$N = N_0 E_d(v) E_a(v), \tag{3}$$

where $E_d(v)$ and $E_a(v)$ are the efficiencies of the detector and absorber, each a function of the velocity. The efficiency of a detector is the fraction of the neutrons incident upon it which are detected, and the efficiency of an absorber we define as the fraction of the number of neutrons incident upon it, which penetrate it. These two efficiencies are, as we have pointed out, reciprocal functions of the velocity and hence $N/N_0$ is independent of the velocity. In these experiments, $N/N_0$ is small. The boron may be thought of as excluding neutrons of all energies. Thus the cadmium difference should be a measure of the number of thermal neutrons, while the boron difference should be a measure of all the neutrons.

Now the BKP calculations predicted that in the free atmosphere there should be practically no thermal neutrons: while near the ground many of those present might be thermal. Hence we might expect the boron difference to be determined by the total number of neutrons, a quantity known to increase rapidly with elevation, while the cadmium difference should be small after the instrument had left the ground. Inspection of Fig. 1 shows that this expectation was admirably fulfilled. The experiment may, therefore, be regarded as a verification of the BKP postulates.

The BKP energy distribution also checks with that found near the surface of the ground. It will be recalled that Korff and Kupferberg[4] operated a large neutron counter near sea level with a boron and a cadmium shield. The boron difference was found to be only about ten percent greater than the cadmium difference, indicating that almost all the neutrons were thermal. The counter used in the flight discussed in the present paper was much smaller, and operation at sea level gave so low a neutron counting rate (boron difference) that the measurement at sea level

* The exponent in Eq. (1) becomes unity in this experiment for a neutron energy of about 33 electron volts.

[4] S. A. Korff and M. Kupferberg, Phys. Rev. 65, 253(A) (1944).

with the flight set had small statistical accuracy. On the other hand the larger counter could not be flown for reasons of weight.

It will be seen in Fig. 1 that the counting rate when the boron shield is in place is not zero. There is always a background present, which is produced by several agencies, namely (a) natural contamination alpha-particles, (b) cores of giant showers, (c) protons and nuclear explosion processes and stars, and (d) neutrons which got in through those areas which the shield did not cover, e.g., the ends. This background increases slowly with elevation. This is to be expected, since, while (a) should be independent of altitude, the remaining agencies will show an altitude dependence.

The question has been raised as to whether there is any appreciable "mass effect" in the flight experiment. By this is meant that if a mass, such as the shield, surrounds the counter, the various components of the cosmic radiation might (a) produce any secondary effects in such a mass which would actuate the counter or (b) such a mass might exclude from the counter some heavily ionizing events which might cause it to count. In other words, would a proportional counter, not sensitive to neutrons, have its counting rate altered appreciably by the presence around it of a mass equivalent to half a millimeter of cadmium? The fact that the cadmium difference is so very nearly zero indicates that the mass effect is negligible, unless one makes the improbable assumption that the mass effect is exactly equal and opposite to the number of thermal neutrons at each elevation.

The counting rate of the counter may be expressed in terms of the rate of production $q$ of neutrons per gram per second in the atmosphere. It was shown in the BKP calculations that the relation between these quantities was given by the equation:

$$q=22.4\times10^{3}n\sigma_A/VP\sigma_B w, \qquad (4)$$

where $n$ is the number of counts per second (the boron difference), $V$ is the volume of the counter, $p$ the pressure in atmospheres of $BF_3$, $w$ the average atomic weight of the surrounding substance in which the production takes place, $\sigma_A$ and $\sigma_B$ are the cross sections for capture of the air and of the detector, respectively. Taking $w$ as 29, and $\sigma_A$ and $\sigma_B$ as 1.5 and 550 each $\times10^{-24}$ sq. cm, respectively, and the dimensions of the counter as stated above, the value for $q$ at the highest elevation reached in this flight, two meters of water equivalent, was about $1{,}75\times10^{-4}$ neutrons per gram per second. A scale of values of $q$ is shown on Fig. 2.

In order to compare this with the values of $q$ obtained in other experiments, the point determined on Mt. Evans[2] is also shown on Fig. 2. Satisfactory agreement is found with the number of neutrons obtained in a different experiment and with another counter.

The density of neutrons $\rho$ per cc is related to the rate of production $q$ by the equation

$$\rho=qtd, \qquad (5)$$

where $t$ is the average lifetime of the neutrons, i.e., the time-interval between their production and absorption. If we take $t$ as between 0.1 and 0.2 second,[5] and the density of air $d$ as $10^{-4}$ gram/cc at this elevation, $\rho$ at two meters of water equivalent will be between 3.5 and $7\times10^{-8}$ neutron per cc. It should be noted that this value is independent of velocity and refers to neutrons of all velocities.

The increase of the rate of production of neutrons with elevation is a factor of about seven in the 4-meter interval from 6 to 2 meters of water equivalent. This corresponds to an average factor of about 1.55 per meter of water in this interval.

## ACKNOWLEDGMENTS

The flight described was launched from the grounds of the University of Chicago. The authors wish to extend their especial thanks to Professor Schein and to all of his staff for the most effective, extensive, and pleasant cooperation it has been our pleasure to experience. Financial support was received from the Carnegie Institution of Washington. The instrument, and especially the automatic shield-positioning mechanism, was built by L. G. Collyer; and S. Friedland of New York University assisted with various operations.

*Note added in proof by* H. A. BETHE,* S. A. KORFF, AND G. PLACZEK.** The question has

[5] S. A. Korff, Rev. Mod. Phys. 11, 211 (1939).

been raised as to just how much the cadmium shield may be expected to cut out. Now the equilibrium energy of neutrons in nitrogen may be defined as that energy at which the capture and scattering cross sections are equal. Taking the values cited in previous work, this energy is about 0.1 ev. If we take the cadmium cutoff as about 0.3 or 0.4 ev, the reduction effected by the cadmium shield ought to be about in the ratio of the square roots of the energies, i.e., between 1.7 and 2 for the cadmium values mentioned. Inspection of Fig. 1 shows that the cadmium curve lies approximately half-way between the boron curve and the unshielded one.

* Cornell University, Ithaca, New York.
** Los Alamos, New Mexico.

PHYSICAL REVIEW VOLUME 69, NUMBERS 5 AND 6 MARCH 1 AND 15, 1946

# The Structure of Cosmic-Ray Air Showers

KONRAD L. KINGSHILL AND LLOYD G. LEWIS
*Ryerson Physical Laboratory, The University of Chicago, Chicago, Illinois*

(September 27, 1945)

Bursts of ionization occurring in each of two thin-walled unshielded ionization chambers were measured at Chicago (elevation 190 meters), with the same apparatus used at Echo Lake (elevation 3100 meters). A comparison of the size-frequency distribution curve for bursts occurring in a single chamber at Chicago with the corresponding curve observed at Echo Lake shows that the altitude dependence for bursts containing more than 50 particles is similar to the altitude dependence of large air showers measured with Geiger-Müller counters. In contrast to this, the altitude dependence for the largest bursts is much greater. The ratio of the coincident burst rate to the single chamber burst rate is as low at Chicago as at Echo Lake. If one assumes the validity of the cascade theory of showers and of the theory of multiple scattering of electrons in air, one must conclude from these data that showers exhibiting these narrow regions of high particle density cannot originate close to the top of the atmosphere. The data presented in this paper, together with the data of Lapp and of Carmichael, show that the slope of the size-frequency distribution curve for bursts in a single chamber is dependent upon the chamber wall.

MEASUREMENTS with two thin-walled unshielded ionization chambers at Echo Lake, Colorado,[1] revealed the presence of many relatively narrow cosmic-ray air showers. These showers were more numerous and had a much smaller lateral extension of their high particle density region than is anticipated[2,3] on the basis of cascade theory applied to primary electrons. This result at Echo Lake makes the sea-level rates for the single bursts and for coincident bursts of particular interest, since the comparison of the two sets of data might give a clue to the vertical structure of air showers.

## APPARATUS

The ionization chambers and the associated d.c. amplifiers[1] were used under exactly the same conditions as at Echo Lake. The galvanometers, however, were adjusted for a higher current sensitivity, so that bursts containing more than 30 particles could be measured. This higher sensitivity could be used at Chicago since the accidental coincidence rate is negligible for bursts considerably smaller than 80 particles. The precision with which the occurrence of a coincidence could be determined was increased by changing the rate of travel of the galvanometer film from 75 mm/hr. to 300 mm/hr. This made it possible to determine a burst coincidence to within 0.1 second (the collection time of the ions was 0.4 second).[1]

The whole apparatus was placed in the same portable houses used in the burst investigations at Echo Lake. It should be pointed out here that, in addition to the thin roof described previously, the walls and the floors of these

[1] L. G. Lewis, Phys. Rev. **67**, 228 (1945).
[2] L. Wolfenstein, Phys. Rev. **67**, 238 (1945).
[3] H. Euler, Zeits. f. Physik **116**, 73 (1940).

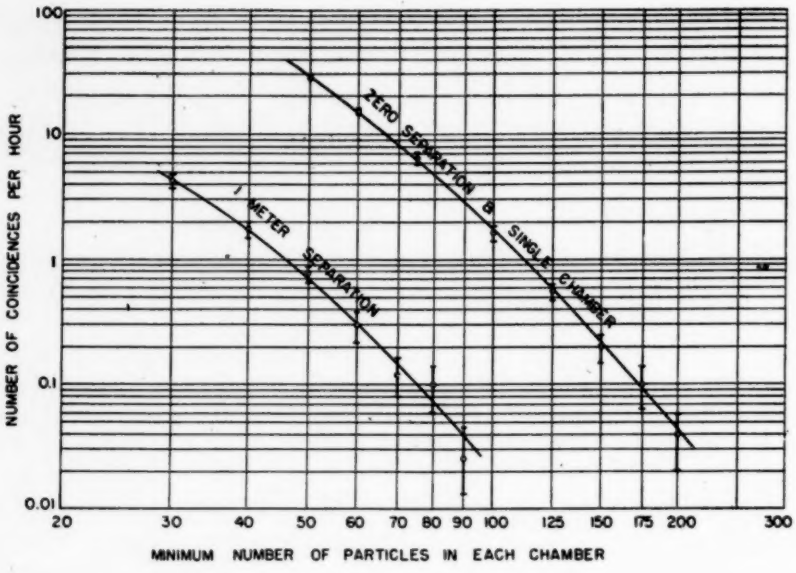


FIG. 1. The frequency of coincident bursts of more than a given number of particles in each chamber is plotted as a function of that number of particles (in a double logarithmic scale), for zero separation and for one meter separation of the ionization chambers. The zero-separation frequency is numerically equal to the single chamber rate.

portable houses consisted of sheets of plywood. The walls had an outer sheet of three-eighths of an inch and an inner sheet of one-quarter of an inch. The three-inch space between the inner and outer sheets was filled with loosely packed shredded redwood bark. This provided good heat insulation without bringing any heavy atoms or much total mass in the vicinity of the chambers. In order to avoid mesotron initiated showers or multiplication of electrons, the portable houses were located on an open space of the campus of the University of Chicago, with no buildings in the immediate neighborhood. The mechanical thermostats used at Echo Lake for controlling the temperature in the houses were replaced by vacuum tube thermostats capable of holding the inside temperature within 0.1°C. Each thermostat consisted essentially of a Wheatstone bridge. Two of the resistors were tungsten filament wires and the other two were Advance wires. An a.c. potential of low voltage was put across the bridge: when the bridge unbalance was changed due to a change in temperature the resulting signal change was amplified and actuated a relay controlling the current to the electrical heaters.

The calibration of the burst apparatus was carried out in the same way as at Echo Lake. The number of particles per burst was computed by using the value of 100 ion pairs per centimeter path for a pressure of argon of one atmosphere, determined for Echo Lake.[1] Test runs with the galvanometers disconnected from the ionization chamber circuits showed only very small fluctuations, probably caused by external vibrations or by Brownian motion. A run was performed with chamber *I* filled with argon as usual and with chamber *II* evacuated to a pressure of a few mm Hg. Bursts were recorded in chamber *I* unaccompanied by any fluctuations in chamber *II*, demonstrating that there was no coupling between the amplifiers of the two chambers. To make certain that the bursts recorded on the film were caused by particles entering from the outside, one chamber was covered with $1\frac{1}{2}$ inches of lead and the other was left unshielded. The shielded chamber recorded more than twice as many bursts containing more than 50 particles.

## RESULTS AND DISCUSSION

A total of 2000 cosmic-ray bursts was recorded at Chicago. Over the entire period of time the absolute burst rates for the two chambers were the same within statistical error. For this reason it was possible to include data from both chambers in the cumulative size-frequency distribution curve of Fig. 1, labeled "zero separation and single chamber rate." This curve shows that the size-frequency distribution at Chicago for single bursts does not follow a power law with a constant exponent. This is in contrast to the computation of Wolfenstein,[2] who concluded

that, if the showers are originated at the top of the atmosphere by primary electrons which have a power law spectrum, the size-frequency distribution curve for bursts must also be a power law with exponent smaller than that of the primary spectrum. The average slope of the curve given in Fig. 1 is approximately 4.6, which cannot be explained by a primary power law spectrum with exponent 1.8. It will be pointed out later in this paper that the slope of the size-frequency distribution curve is dependent on the ionization chamber construction.

The ratio of the single chamber burst rates at Echo Lake to those at Chicago is given in Fig. 2. In this graph the ratio of the frequency of bursts greater than a given size at Echo Lake to the frequency of the corresponding bursts at Chicago is plotted as a function of the burst size. Logarithmic scales are used on both coordinates. The points can be approximated by a straight line giving a power law relation between the ratio of the frequencies ($R$) and the minimum number of particles per burst ($N$).

$$R=KN^{\beta},$$

where $K$ is a constant and $\beta=2.7\pm0.3$. The point at $N>50$ was obtained by extrapolating the Echo Lake data. This point, therefore, cannot be considered as accurate as the other points.

The theoretical results computed by Wolfenstein gave an increase of burst frequency of 5.7 for densities greater than 1000 per square meter (97 particle bursts) and an increase of 4 for densities greater than 2000 per square meter (193 particle bursts). These values are very much smaller than those given in Fig. 2. In addition, the slope of the calculated curve is negative whereas the slope of the observed curve is positive.

The altitude dependence of extensive cosmic-ray air showers was investigated by Hilberry,[4] who used a set of counters in fourfold coincidence. He found that the counting rate at Echo Lake was ten times higher than that at Chicago. The ratio computed from the cascade theory for his counter geometry was 15. In more recent experiments, Rogozinski[5] observed 7 as the ratio of the counting rates of coincidence counters for these two stations. All these results seem to show general agreement with the value given in Fig. 2 for the smallest size bursts. The slope of the curve in Fig. 2 is sufficient to explain why a relatively small variation in the counter geometry or in the counter shielding would result in the relatively large variation in the observed altitude dependence, because the geometry and the shielding of the counter arrangement select that particular size of shower which produces the majority of the counter coincidences.

The data on burst coincidences were taken only with a chamber separation of 1 meter. Present circumstances do not permit a more extensive investigation. The curve of Fig. 1 labeled "one meter separation" represents the frequency of coincident bursts of more than a given number of particles in each chamber as a function of that number of particles, for a chamber separation of one meter. The small percentage of coincident bursts in comparison with the single bursts is shown by a comparison of this curve with the "zero separation" curve,

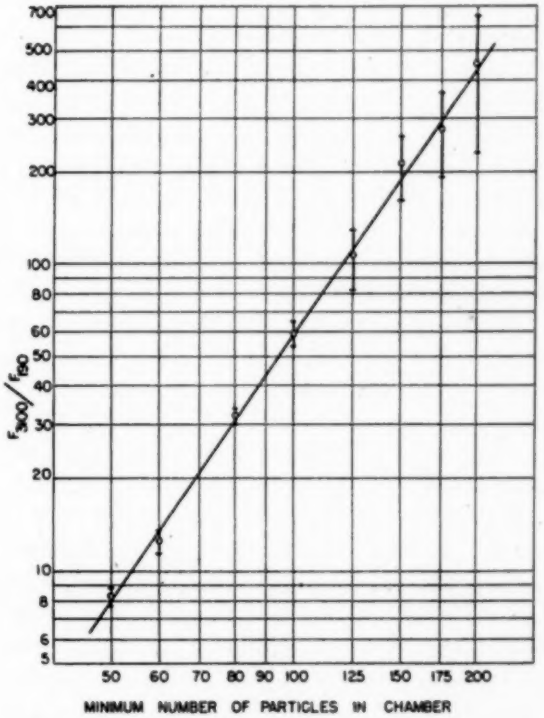


FIG. 2. The ratio of the frequency of occurrence of bursts with more than a given number of particles at Echo Lake ($F_{200}$), to the frequency of occurrence of the corresponding bursts at Chicago ($F_{100}$), is plotted as a function of that number of particles.

[4] N. Hilberry, Phys. Rev. 60, 1 (1941).
[5] A. Rogozinski, Phys. Rev. 65, 291 (1944).

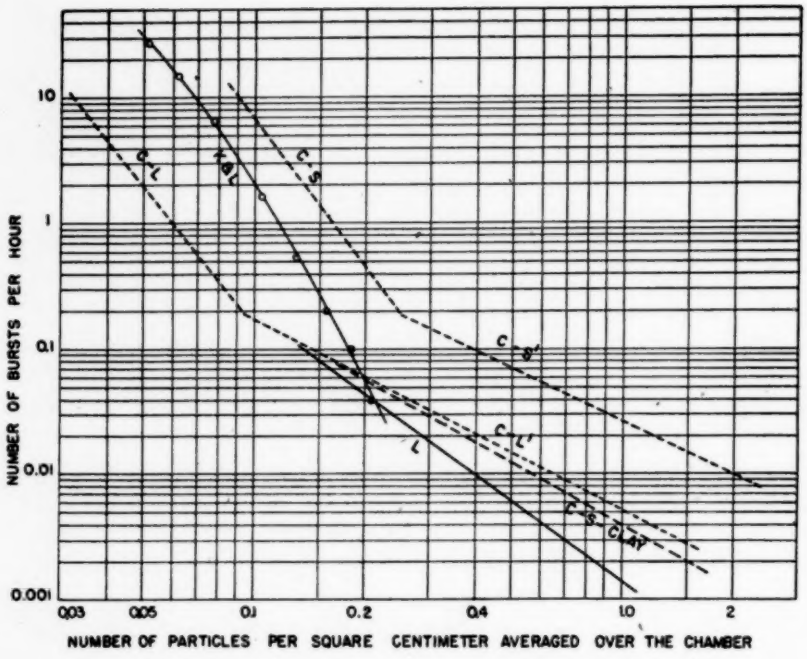


FIG. 3. Size-frequency distribution curves for various chambers are replotted on this graph to show the frequency of occurrence of bursts with greater than a given average particle density as a function of the particle density. All the data are reduced to a specific ionization of 100 ion pairs per cm. path length in argon of atmospheric pressure. The curve $C-S$ represents Carmichael's results taken with his small ionization chamber described in Table I; the curve $C-L$ represents those taken with Carmichael's large chamber; the curve $L$ represents Lapp's data; and the curve $K\&L$, the data presented in this paper. The curve $C-S$-clay represents the results obtained with Carmichael's small chamber shielded by 30 meters of clay. Carmichael's original curves differ slightly from the straight lines used in this figure.

Fig. 1. It is indicated that the ratio of coincident burst frequency to single burst frequency decreases with increasing burst size. This is similar to the result found at Echo Lake. Deflections on the photographic trace corresponding to 10 particles could be measured but were difficult to distinguish from statistical fluctuations: hence burst coincidence measurements were not extended below 30 particles. The measured frequency of the 30-particle burst coincidences is probably slightly too high because of the statistical fluctuations.[6]

A comparison of burst coincidence rates at the two altitudes was possible only for bursts of more than 80 particles in each chamber. At Echo Lake the coincidence rate was 14.5 per hour and at Chicago 0.1. The ratio of 145:1 between the two elevations is similar to that observed for single bursts of more than 120 particles (cf. Fig. 2), suggesting that single bursts of 120 particles and coincident bursts of 80 particles are caused by a similar type of air shower. The lack of burst coincidences, for a chamber separation of one meter, shown in Fig. 1, demonstrates that at Chicago the majority of the bursts of more than 50 particles must originate from showers having a small lateral spread of their high density region.

It is possible that one or more heavily ionizing particles with sufficient energy may traverse the chamber, giving rise to a burst of ionization comparable to that produced by more than 50 cosmic-ray particles. The nature of the present experiment, however, excludes the possibility that any appreciable fraction of the large bursts and burst coincidences in the unshielded ionization chambers can originate from such heavily ionizing particles. This is supported by the following facts: only protons of a relatively narrow energy range (about $10^7$ ev) would be capable of traversing our chamber and still have velocities sufficiently small to produce a number of ion-pairs equivalent to a burst of more than 50 particles. Such protons could possibly enter the

TABLE I. Comparison of ionization chambers.

| | Carmichael large chamber | Carmichael small chamber | Carnegie Model C | Kingshill and Lewis |
|---|---|---|---|---|
| Shape | cylinder | cylinder | sphere | sphere |
| Volume | 175 liters | 1 liter | 19.7 liters | 22.4 liters |
| Cross-sectional area | 1960 cm² | ~65 cm² | 1000 cm² | 965 cm² |
| Filling | 115 cm Hg. argon | not specified | 50 atmos. argon | 100 cm Hg argon |
| Wall thickness: | 3 mm steel | 1.2 cm Al | 1.25 cm steel | 0.03 cm steel |
| in radiation units | 0.167 | 0.12 | 0.69 | 0.017 |

[6] L. G. Lewis and R. Hayden, Phys. Rev. 65, 346A (1944).

ionization chambers from the air, but this is an extremely rare event at elevations close to sea level. Protons may also be ejected from the walls of the chamber in a process of nuclear evaporation. This possibility is ruled out in the case of large bursts by the direct experiment of Lapp,[7] who measured bursts in a high pressure chamber of 1.25-cm wall thickness in coincidence with distant Geiger-Müller counters, and found that whenever a burst of more than 100 particles occurred in the ionization chamber the distant counters were tripped simultaneously. Most of the protons produced in nuclear evaporations would not possess enough energy to penetrate deep into Lapp's chamber, which was filled with 50 atmospheres of argon. On the other hand, the fact that Lapp's data can be correlated satisfactorily with the results of the present experiment is strong additional evidence that most of the large bursts in unshielded ionization chambers are not caused by the passage of nuclear particles through the chamber.

Lapp[7] and Carmichael[8,9] have reported size-frequency distribution curves for bursts occurring in single unshielded ionization chambers. Lapp used a Carnegie Model C chamber in coincidence with several sets of Geiger-Müller counters. This chamber was spherical and had about the same volume as the chambers used in the present investigation. Carmichael used two cylindrical chambers, one with a volume of 1 liter and the other with a volume of 175 liters. The specifications of the several chambers mentioned in this discussion are given in Table I.

The data of Lapp[7] and of Carmichael[8,9] are replotted on the graph of Fig. 3. In all the curves of Fig. 3 a specific ionization of 100 ion-pairs per cm path length per atmosphere of argon was used. The ordinate used in Fig. 3 is the frequency of occurrence of bursts with more than a given average particle density, and the abscissa the average particle density in the ionization chamber. These coordinates were chosen for burst data on air showers, since the information desired is the rate of occurrence of a shower of a given total number of particles.

[7] R. E. Lapp, Phys. Rev. **64**, 129 (1943).
[8] H. Carmichael and Chang-Ning Chan, Nature **144**, 325 (1939).
[9] H. Carmichael, Proc. Roy. Soc. **A154**, 223 (1936).

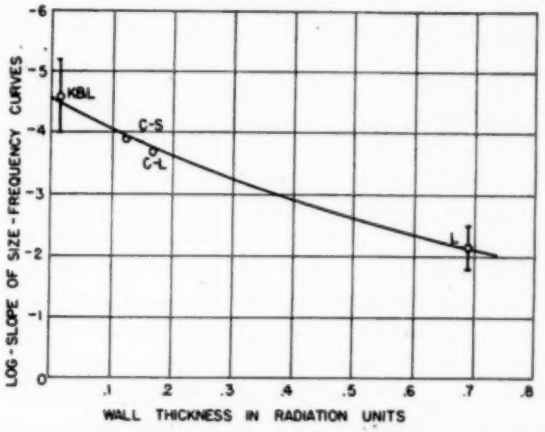


FIG. 4. This graph represents the logarithmic slope of the size-frequency distribution curves taken with the various ionization chambers described in Table I as a function of the wall thickness of the chambers measured in radiation units. The point $C-S$ gives the slope for Carmichael's small chamber; $C-L$ for Carmichael's large chamber; $L$ for Lapp's chamber; and $K\&L$ for the chamber used in this experiment. It was not possible to determine the error limits for Carmichael's data.

Two facts concerning Carmichael's data should be mentioned before drawing any conclusions from the curves of Fig. 3. (1) Carmichael himself draws attention to the fact that the bursts of less than 100 ionizing rays were difficult to distinguish from the normal statistical fluctuations. This obviously means that his curves are not very accurate for the smaller size bursts. (2) The location of Carmichael's chambers was not very favorable for measuring particle densities in large air showers. His description of this location is as follows: "Above the ionization chamber, as shown in Fig. 1, is a strong wooden platform on which heavy material can be placed. The roof of the building is 8 feet above this platform, flat, made of concrete and supported by heavy iron girders. Directly above the ionization chamber, however, is a skylight, 6 feet wide." The walls of the building were probably in keeping with the roof and, therefore, were also heavy.

The portions $C-S'$ and $C-L'$ of Carmichael's size-frequency distribution curves given in Fig. 3 are very nearly parallel to the size-frequency distribution curve for bursts occurring under 30 meters of clay (Fig. 3, curve $C-S$-clay). Bursts occurring under this much shielding are caused by mesotron initiated showers. Therefore, the similarity in slope of these curves, and the

TABLE II.

| | Wall thickness in radiation units | Slope of size-frequency distribution curves of Fig. 3 |
|---|---|---|
| Kingshill and Lewis | 0.017 | −4.6 (approx.) |
| Carmichael (small) | 0.12 | −3.9 (approx.) |
| Carmichael (large) | 0.167 | −3.7 (approx.) |
| Lapp | 0.69 | −2.15±0.35 |

amounts of heavy material in the neighborhood of the supposedly unshielded ionization chambers, makes it probable that the portions of Carmichael's curves labeled $C-S'$ and $C-L'$ do not represent bursts due only to air showers, but represent bursts caused predominantly by mesotron initiated showers. This conclusion is strengthened by the data given in curve $K\&L$. This curve covers a range of frequencies which includes the one corresponding to the discontinuities in the slopes of Carmichael's curves $C-L$ and $C-S$, yet does not exhibit such a discontinuity. For these reasons, we limit our discussion to those parts of Carmichael's curves ($C-S$ and $C-L$) which are most probably due to air showers alone.

Lapp's size-frequency distribution curve in Fig. 4 is not subject to the above criticism, since his chamber was located under the thin glass roof of the greenhouse on top of the Botany Building at Chicago. In addition, four Geiger-Müller counter coincidence sets were used in order to make sure that the recorded bursts of ionization were caused by air showers.

In spite of the fact that it is extremely difficult to make quantitative comparisons between bursts measured in cylindrical and in spherical ionization chambers, certain relations can be found between the various curves of Fig. 3. The most noticeable is that Carmichael's small chamber recorded the highest average particle density for bursts of a given frequency ($C-S$), whereas his large chamber recorded the lowest ($C-L$). The chambers used in this investigation had a cross-sectional area intermediate between Carmichael's small and large chambers, and recorded an intermediate value of the average particle density at a given frequency ($K\&L$). This is precisely what one should expect from the comparison of single and coincident bursts represented in Fig. 1.

A second relation can be described as follows: Lapp's size-frequency distribution curve of Fig. 3, which has been shown to be due to large air showers, has a very different slope from that of the curve found in this experiment. This difference is presumably due to the fact that Lapp's chamber had a considerably heavier wall. It follows, then, since his chamber and the one used in this experiment were both spherical and had substantially the same diameter, that the average energy of the electrons in the showers producing the bursts at the point of intersection of the two curves $K\&L$ and $L$ is such that the increase in the number of shower particles by multiplication in the wall of Lapp's chamber is approximately compensated for by a decrease of their number through absorption. For bursts of particle density less than at this point of intersection, the absorption effect apparently predominates, whereas, for bursts of particle density greater than that at the intersection point, the opposite is the case. The four curves in Fig. 3 seem to be in agreement with such an explanation, since their slopes are such that the curve corresponding to the chamber with the thinnest wall has the steepest slope ($K\&L$); the curve for the next thinnest wall has the next steepest slope ($C-S$); and so on. This is demonstrated clearly by the figures given in Table II, and by the graph in Fig. 4. An exponential curve is drawn through the points of Fig. 4 (however, a linear curve could be drawn as well).

These comparisons of the three sets of experimental data lead to the following two conclusions: First, the density distribution function for air showers near sea level is such that measurements near the center of the showers should be made with very small ionization chambers (of the order of a few liters volume); second, that a wall thickness of even 0.1 of a radiation unit may alter the size-frequency distribution curve of bursts originating from air showers. Wall thicknesses usually described as "thin" are therefore not sufficiently thin for such measurements. Spherical chambers in general are much more suitable for burst investigations since a comparison between experiment and theory is possible.

The authors wish to thank Dr. Marcel Schein for suggesting the problem and for his help in the preparation of the discussion.

# The Zeeman Effect in the Spectrum of Chlorine I

J. B. GREEN* AND J. T. LYNN**
*Mendenhall Laboratory of Physics, Ohio State University, Columbus, Ohio*
(Received November 20, 1945)

Zeeman effects of about two hundred lines have been measured in the spectrum of chlorine I and have led to the discovery of 12 new lines and about 50 new classifications. Seventeen new levels have been found, completing parts of configurations given by Kiess. A striking example of the sharing of $g$-values by two configurations is demonstrated.

THE present paper is the report of work done during the years 1941–2 on the 21-ft. concave grating set-up at the Mendenhall Laboratory, the preliminary results of which have already been reported.[1]

The arc spectrum of chlorine has been described and classified in great detail by Kiess[2] from λ3944 to λ10428. In the present work, the discovery of several new lines has extended the spectrum to λ3694, and has led to the classification of about 50 more lines and the determination of 17 new energy levels. Thus, about three-fourths of the known lines of the arc spectrum of chlorine have now yielded to classification.

The spectrum was excited by an electrodeless discharge in a capillary tube set at right angles to the magnetic field, by means of an oscillator with a frequency of about 40 megacycles. The experimental arrangement has been described elsewhere.[3] The capillary was evacuated, and then with the voltage applied, chlorine vapor from a reservoir was admitted until the discharge, which starts in the bulbs at the ends of the capillary, broke through the magnetic field. No air-cooling was required for the capillary. In fact, when air-cooling was used, it tended to "blow out" the discharge, probably because the chlorine would condense and reduce the vapor pressure below that required to maintain the discharge through the magnetic field.

Except in the region below λ5000, Eastman spectroscopic plates, hypersensitized in a 4 per-cent ammonia bath, were employed. Exposure of 120 hours was usually made. The period of hypersensitivity probably does not last beyond this time, and lines which are not sufficiently intense to be recorded in this time are probably below or at least close to the lower threshold of intensity required to produce a photographic image.

All of the lines included in the present investigation are caused by transitions between excited levels, transitions to the normal state ($p^5$) being in the Schumann region. These excited states tend to three series limits of Cl II ($^3P$, $^1D$, and $^1S$) but levels with series limits $^3P$ and $^1D$ are the only ones that have been found up to the present, and in only the $3p^4 4s$ and $3p^4 4p$ for the latter limit.

Table I gives a list of the Zeeman effects of the well-authenticated lines in the spectrum of Cl I. Parentheses in columns (1) or (3) indicate new lines or new classifications. Table II is a list of lines involving one well-established level and one level that seems to be definite, with the $g$-value of the latter. Table III is a list of resolved or partially resolved lines with tentative transitions and $g$-values given.

Table IV gives a list of new levels determined by the present investigation. Of these, 4290.7 and 4257.6 are in about the correct position to supply the $^2P$ pair missing from Kiess's list for $3p^4 5d$. There can be no doubt about the classification of 4049.1 and 3949.4 and $6d\,^4D_{1/2}$ and $6d\,^4D_{3/2}$, respectively. The lines resulting from transitions involving the latter and lines arising from $6d\,^4D_{5/2}$ (3942.5) show beginning Paschen-Back effects.

Table V is a summary of the $g$-values gleaned in the investigation, together with $g$-sums. The $4s$ configuration shows $LS$ values within limits

* Now at Naval Ordnance Laboratory, Washington, D. C.
** Now at North Carolina State College, Raleigh, North Carolina.
[1] J. B. Green and T. J. Lynn, Phys. Rev. **62**, 179 (1942).
[2] C. C. Kiess, Bur. Stand. J. Research **10**, 827 (1933).
[3] J. B. Green and J. A. Peoples, Jr., Phys. Rev. **54**, 602 (1938).

TABLE I. Zeeman effects in the spectrum of chlorine I.

| λ | ν | Classification | Pattern | $g_a$ | $g_b$ |
|---|---|---|---|---|---|
| (3691.58) | 27,080.99 | $4s^4P_{3/2}-5425°_{3/2}$ | (−), (**0.583**), 1.134, **1.523**, 1.917 | 1.718 | 1.328 |
| (3694.15) | 27,062.15 | $4s^4P_{5/2}-5975°_{3/2}$ | 1.962 g | 1.599* | 1.358 |
| (3703.03) | 26,997.26 | $4s^4P_{1/2}-5171°_{3/2}$ | (−), 0.613, f | 2.652* | 1.295 |
| (3768.05) | 26,513.42 | $4s^4P_{3/2}-5975°_{3/2}$ | (−), (**0.596**), 1.127, **1.511**, 1.918 | 1.710 | 1.313 |
| 3944.79 | 25,342.74 | $(4s^2P_{3/2}-5425°_{3/2})$ | 1.324 h | 1.340* | 1.309 |
| (4005.51) | 24,958.58 | $4s^2P_{1/2}-5171°_{3/2}$ | (0.332), 0.968, **1.595** | 0.625 | 1.274 |
| 4032.14 | 24,973.75 | $(4s^2P_{3/2}-5975°_{1/2})$ | 1.333 h | 1.340* | 1.325 |
| 4104.78 | 24,354.99 | $4s^4P_{5/2}-5p^2P°_{3/2}$ | (**0.159**), (0.508), ----, 1.391, 1.740, **2.050** c | 1.582 | 1.269 |
| 4139.00 | 24,153.64 | $(4s^2P_{1/2}-5975°_{3/2})$ | (0.314), 0.978, **1.633** | 0.680 | 1.316 |
| 4209.68 | 23,748.11 | $4s^4P_{5/2}-5p^2D°_{3/2}$ | (**0.139**), (0.414), 1.161 1.443, 1.728, **2.020** | 1.601 | 1.321 |
| 4226.44 | 23,653.94 | $4s^4P_{5/2}-5p^4S°_{3/2}$ | 1.654 h | 1.599* | 1.526 |
| 4264.59 | 23,442.34 | $4s^4P_{5/2}-5p^2D°_{5/2}$ | (−), (0.371), (**0.620**), 0.963, 1.221, **1.457**, 1.727, 1.980 | 1.599 | 1.350 |
| 4280.43 | 23,355.59 | $4s^4P_{5/2}-5p^4D°_{3/2}$ | (**0.224**), (0.670), 1.369, 1.823, **2.276** | 1.602 | 1.152 |
| 4323.35 | 23,123.73 | $4s^4P_{3/2}-5p^4S°_{3/2}$ | (−), (**0.301**), 1.408, **1.630**, 1.842 | 1.734 | 1.527 |
| (4326.12) | 23,108.93 | $4s^4P_{3/2}-5p^2S°_{1/2}$ | (0.523), 1.419, **2.251** | 1.732 | 0.692 |
| 4337.80 | 23,046.70 | $4s^4P_{3/2}-5p^4D°_{1/2}$ | (**0.183**), 1.532, **1.893** | 1.711 | 1.348 |
| 4363.30 | 22,912.02 | $4s^4P_{5/2}-5p^2D°_{5/2}$ | (**0.187**), (0.549), **0.807**, 1.165, 1.541, 1.902 | 1.727 | 1.356 |
| 4369.52 | 22,879.40 | $4s^4P_{1/2}-5p^2D°_{3/2}$ | (−), 1.986 f | 2.652* | 1.320 |
| 4371.55 | 22,868.78 | $4s^4P_{5/2}-5p^4D°_{5/2}$ | (−), (−), (−), ----, 1.782, 2.124, ----, a | 1.586 | 1.236 |
| 4379.90 | 22,825.18 | $4s^4P_{3/2}-5p^4D°_{3/2}$ | (0.282), (−), ----, 1.434, 2.018 f | 1.722 | 1.147 |
| 4387.55 | 22,785.38 | $4s^4P_{1/2}-5p^4S°_{3/2}$ | (0.563), **0.969**, ---- | 2.656 | 1.531 |
| 4389.76 | 22,773.91 | $4s^4P_{3/2}-5p^4D°_{7/2}$ | (**0.092**), (0.267), (0.452), **0.961**, 1.169, 1.342, 1.517, 1.685, ---- | 1.614 | 1.420 |
| 4390.38 | 22,770.70 | $4s^4P_{1/2}-5p^2S°_{1/2}$ | b | — | 0.700 |
| 4402.58 | 22,707.60 | $4s^4P_{1/2}-5p^4D°_{1/2}$ | (0.625), 2.033 | 2.647 | 1.418 |
| 4403.03 | 22,705.27 | $4s^4P_{5/2}-5p^4P°_{3/2}$ | (−), (0.206), **1.383**, ----, ----, ---- | 1.589 | 1.727 |
| 4438.48 | 22,523.93 | $4s^4P_{3/2}-5p^4P°_{5/2}$ | 1.579 h | 1.599* | 1.558 |
| 4445.83 | 22,486.70 | $4s^4P_{1/2}-5p^4D°_{3/2}$ | (0.743), **0.399**, 1.895 | 2.642 | 1.148 |
| 4446.11 | 22,485.28 | $4s^4P_{3/2}-5p^4P°_{1/2}$ | (0.289), ----, 2.012 | 1.726 | 2.305 |
| 4469.37 | 22,368.26 | $4s^2P_{3/2}-5p^2P°_{1/2}$ | (0.321), 1.021, **1.662** | 1.341 | 0.699 |
| 4475.31 | 22,338.57 | $4s^4P_{3/2}-5p^4D°_{5/2}$ | (**0.230**), (0.713), **0.537**, 1.005, 1.481 | 1.713 | 1.248 |
| 4491.05 | 22,260.29 | $4s^2P_{3/2}-4p^2D°_{3/2}(^1P^1D)$ | (0.228), (−), ----, **1.105**, **1.581** f | 1.341 | 0.869 |
| 4526.20 | 22,087.42 | $4s^2P_{3/2}-5p^2P°_{3/2}$ | 1.314 h | 1.340* | 1.288 |
| (4548.26) | 21,980.29 | $4s^2P_{3/2}-4p^2P°_{1/2}(^1P^1D)$ | (0.434), 1.292, **2.144** | 1.716 | 0.861 |
| 4578.17 | 21,836.69 | $4s^4P_{1/2}-5p^4P°_{3/2}$ | (0.463), **1.258**, 2.187 | 2.646 | 1.721 |
| 4580.47 | 21,825.72 | $4s^4P_{3/2}-4p^2P°_{3/2}(^1P^1D)$ | (−), (**0.599**), 1.106, **1.518**, 1.942 | 1.716 | 1.318 |
| 4601.00 | 21,728.34 | $4s^2P_{1/2}-5p^2P°_{1/2}$ | 0.697 i | 0.663* | 0.731 |
| 4623.96 | 21,620.45 | $4s^2P_{1/2}-4p^2D°_{3/2}(^1P^1D)$ | (0.106), 0.759, **0.966** | 0.638 | 0.860 |
| 4654.05 | 21,480.67 | $4s^2P_{3/2}-5p^2D°_{3/2}$ | 1.331 h | 1.340* | 1.322 |
| 4661.22 | 21,447.63 | $4s^2P_{1/2}-5p^2P°_{3/2}$ | (0.309), 0.978, **1.590** | 0.667 | 1.283 |
| 4674.40 | 21,387.15 | $4s^2P_{3/2}-5p^4S°_{3/2}$ | (−), (0.292), 1.442 j | 1.345 | 1.539 |
| 4677.76 | 21,371.79 | $4s^2P_{3/2}-5p^2S°_{1/2}$ | (0.322), 1.019, **1.662** | 1.341 | 0.697 |
| 4691.73 | 21,309.07 | $4s^2P_{3/2}-5p^4D°_{1/2}$ | 1.323 h | 1.340* | 1.411 |
| 4721.24 | 21,174.97 | $4s^2P_{3/2}-5p^2D°_{5/2}$ | 1.355 h | 1.340* | 1.349 |
| 4740.71 | 21,088.01 | $4s^2P_{3/2}-5p^4D°_{3/2}$ | (−), (**0.291**), 1.035, **1.240**, 1.445 | 1.339 | 1.142 |
| 4852.70 | 20,601.35 | $4s^2P_{3/2}-5p^4D°_{5/2}$ | 1.028 h | 1.340* | 1.162 |
| (4891.52) | 20,437.85 | $4s^2P_{3/2}-5p^4P°_{3/2}$ | (−), (**0.567**), 1.129, **1.528**, 1.920 | 1.335 | 1.722 |
| (4938.59) | 20,243.06 | $4s^2P_{3/2}-4p^2P°_{1/2}(^1P^1D)$ | (0.233), 1.083, **1.577** | 1.337 | 0.857 |
| (4971.77) | 20,107.97 | $4s^2P_{1/2}-5p^4P°_{1/2}$ | (0.825), 1.499 | 0.677 | 2.322 |
| 4976.62 | 20,088.37 | $4s^2P_{3/2}-4p^2P°_{3/2}(^1P^1D)$ | 1.337 h | 1.340* | 1.361 |
| 5099.80 | 19,603.16 | $4s^2P_{1/2}-4p^2P°_{1/2}(^1P^1D)$ | (0.102), 0.769 | 0.667 | 0.872 |
| 5140.35 | 19,448.52 | $4s^2P_{1/2}-4p^2P°_{3/2}(^1P^1D)$ | (0.338), 1.001, **1.664** | 0.657 | 1.328 |
| 5532.13 | 18,071.21 | $4p^4P°_{5/2}-6d^4D_{7/2}$ | (**0.105**), (0.310), (0.527), **0.867**, 1.074, 1.286, 1.484, 1.693, ---- | 1.593 | 1.383 |
| 5578.13 | 17,922.16 | $4p^4P°_{3/2}-6d^4D_{5/2}$ | (**0.184**), (0.539), **0.816**, 1.186, 1.547, ---- | 1.727 | 1.363 |
| 5580.45 | 17,914.74 | $(4p^4P°_{5/2}-6d^4D_{3/2})$ | (unsymmetrical) | 1.723 | 1.168 |
| 5620.72 | 17,786.39 | $(4p^4P°_{5/2}-4290_{3/2})$ | 1.542 h | 1.591* | 1.657 |
| 5654.20 | 17,681.07 | $(4p^4P°_{1/2}-6d^4D_{3/2})$ | (0.731), **0.437**, 1.910 | 2.629 | 1.168 |
| 5686.26 | 17,581.32 | $(4p^4P°_{1/2}-6d^4D_{1/2})$ | (0.801), 1.811 | 2.613 | 1.010 |
| 5765.55 | 17,339.60 | $(4p^4P°_{1/2}-4290_{3/2})$ | (0.485), **1.155**, 2.138 | 2.621 | 1.644 |
| 5772.58 | 17,318.48 | $4p^4P°_{5/2}-5d^4P_{3/2}$ | 0.993 h | 1.591* | 2.391 |
| 5802.84 | 17,228.17 | $4p^4P°_{3/2}-6d^2F°_{7/2}$ | (−), (−), (−), ----, 1.385, ----, ----, f | 1.578 | 1.192 |
| 5826.24 | 17,158.98 | $4p^4D°_{7/2}-6d^4D_{5/2}$ | 1.527 h | 1.422* | 1.385 |
| 5847.68 | 17,096.07 | $4p^4D°_{7/2}-6d^4D_{7/2}$ | (0.140), 1.397 j | 1.422 | 1.373 |
| 5856.70 | 17,069.74 | $4p^4P°_{5/2}-5d^4D_{5/2}$ | 1.585 h | 1.591* | 1.595 |
| 5908.22 | 16,920.89 | $4p^4D°_{5/2}-6d^4D_{5/2}$ | (0.137), 1.325 j | 1.230 | 1.353 |
| 5910.75 | 16,913.65 | $(4p^4D°_{5/2}-6d^4D_{3/2})$ | (unsymmetrical) | 1.308* | 1.168 |
| 5930.35 | 16,857.75 | $4p^4P°_{3/2}-5d^4P_{5/2}$ | (**0.068**), (0.205), **1.386**, 1.521, ----, ---- | 1.734 | 1.593 |
| 5948.40 | 16,806.60 | $4p^4P°_{1/2}-5d^4P_{1/2}$ | (0.555), 2.026 | 2.583 | 1.470 |
| 5991.42 | 16,685.92 | $(4p^4P°_{1/2}-4944_{3/2})$ | (0.589), **0.823**, 2.006 | 2.595 | 1.414 |
| 6019.71 | 16,607.51 | $(4p^4P°_{1/2}-5023_{1/2})$ | (0.707), 1.918 | 2.625 | 1.212 |
| 6082.53 | 16,435.99 | $4p^4P°_{5/2}-5d^4D_{3/2}$ | (**0.174**), (0.525), 1.071, 1.412, 1.767, **2.118** | 1.593 | 1.243 |
| 6114.37 | 16,350.77 | $4p^4P°_{5/2}-5d^4D_{5/2}$ | (0.120), (0.327), (**0.581**), 1.002, 1.243, **1.476**, 1.710, 1.942 | 1.593 | 1.359 |
| 6140.21 | 16,281.59 | $4p^4P°_{5/2}-5d^4D_{7/2}$ | (**0.099**), (0.296), (0.506), **0.888**, 1.124, 1.317, 1.509, 1.687 | 1.586 | 1.387 |
| 6141.79 | 16,277.40 | $4p^4P°_{3/2}-5d^4D_{1/2}$ | (0.674), 1.040, **2.401** c | 1.726 | 0.375 |
| (6151.22) | 16,252.45 | $(4p^4D°_{3/2}-4257_{1/2})$ | (0.207), **0.956**, 1.357 | 1.165 | 1.579 |
| 6162.05 | 16,223.89 | $4p^4P°_{3/2}-5d^4D_{3/2}$ | (0.241), (**0.710**), 1.009, **1.479**, 1.965 | 1.717 | 1.241 |
| 6194.72 | 16,138.32 | $4p^4P°_{3/2}-5d^4D_{5/2}$ | (**0.179**), (0.529), **0.835**, 1.183, 1.539, 1.894 | 1.722 | 1.368 |
| 6211.55 | 16,094.60 | $4p^4D°_{7/2}-5d^4P_{5/2}$ | (**0.084**), (0.253), (0.423), 1.010, 1.180, 1.344, ----, ----, ---- | 1.424 | 1.592 |
| 6226.39 | 16,056.24 | $(4p^2D°_{5/2}-4291_{3/2})$ | (**0.185**), (0.543), **0.731**, 1.085, 1.454, 1.844 | 1.270 | 1.640 |
| 6231.48 | 16,043.12 | $4p^4P°_{1/2}-5d^4D_{1/2}$ | (1.127), 1.487 | 2.615 | 0.360 |

TABLE I.—(*Continued*).

TABLE I.—(*Continued*).

| λ | ν | Classification | Pattern | $g_a$ | $g_b$ |
|---|---|---|---|---|---|
| 6242.54 | 16,014.70 | $4p^4D^\circ_{5/2}-5d^2F_{7/2}$ | (−), (0.194) i, 1.012 g | 1.284 | 1.206 |
| 6252.26 | 15,989.80 | $4p^4D^\circ_{1/2}-5d^4D_{3/2}$ | (0.702), **0.543**, 1.926 | 2.626 | 1.231 |
| 6280.20 | 15,918.67 | $(4p^4D^\circ_{5/2}-4944_{3/2})$ | (0.185), 1.134 | 1.317 | 1.441 |
| 6326.74 | 15,801.57 | $(4p^2S^\circ_{1/2}-6d^4D_{3/2})$ | 1.139 h | 1.284 | 1.168* |
| 6394.75 | 15,633.52 | $4p^4D^\circ_{5/2}-5d^4F_{5/2}$ | (0.392) i, 1.222 h | 1.301 | 1.146 |
| 6398.63 | 15,624.04 | $4p^4D^\circ_{7/2}-5d^4F_{9/2}$ | ----, 0.923 g | 1.420 | 1.310 |
| 6434.79 | 15,536.24 | $4p^4D^\circ_{5/2}-5d^4F_{7/2}$ | ----, 0.818 g | 1.181 | 1.326 |
| 6450.30 | 15,498.88 | $4p^2D^\circ_{5/2}-5d^2F_{7/2}$ | ----, 1.150 h | 1.274 | 1.218 |
| 6502.21 | 15,375.15 | $4p^4D^\circ_{7/2}-5d^4D_{5/2}$ | 1.549 h | 1.422* | 1.321 |
| 6531.39 | 15,306.45 | $4p^4D^\circ_{7/2}-5d^4D_{7/2}$ | (0.131) i, 1.416 h | 1.436 | 1.401 |
| 6536.10 | 15,295.43 | $(4p^4P^\circ_{5/2}-4258_{1/2})$ | (0.136), **1.197**, 1.473 | 1.334 | 1.608 |
| 6542.40 | 15,280.70 | $4p^4D^\circ_{3/2}-5d^4F_{5/2}$ | 1.139 h | 1.163* | 1.149 |
| 6567.35 | 15,222.64 | $4p^4D^\circ_{3/2}-5d^4D_{3/2}$ | 1.382 h | 1.321 | 1.240 |
| 6604.57 | 15,136.86 | $4p^4D^\circ_{5/2}-5d^4D_{5/2}$ | (0.144) i, 1.338 h | 1.308 | 1.369 |
| 6609.26 | 15,126.12 | $4p^4P^\circ_{5/2}-4d^4P_{3/2}$ | 1.558 h | 1.591* | 1.636 |
| 6865.36 | 14,561.87 | $4p^4P^\circ_{5/2}-6s^4P_{3/2}$ | (0.112), (0.327), ----, ----, ----, **1.912** | 1.584 | 1.364 |
| 6872.85 | 14,546.00 | $4p^2D^\circ_{3/2}-4d^2P_{3/2}$ | (0.483) i | 0.986* | 1.305 |
| 6910.32 | 14,467.02 | $4p^2S^\circ_{1/2}-4d^2P_{1/2}$ | 1.285 h | 1.280* | 1.289 |
| 6932.90 | 14,420.00 | $4p^4P^\circ_{5/2}-4d^4P_{5/2}$ | (−), (0.571), (**0.873**), ----, 1.068, **1.415**, 1.764, 2.109 | 1.589 | 1.241 |
| 6966.80 | 14,349.84 | $4p^4P^\circ_{3/2}-6s^4P_{3/2}$ | (−), (**0.506**), 1.234, **1.559**, 1.903 | 1.727 | 1.391 |
| 6981.85 | 14,318.91 | $4p^4P^\circ_{5/2}-6s^4P_{5/2}$ | (0.223) i, 1.548 h | 1.594 | 1.505 |
| 6995.88 | 14,290.19 | $4p^2S^\circ_{1/2}-4d^2P_{3/2}$ | (0.357), ----, **1.632** | 0.560 | 1.275 |
| 7086.80 | 14,106.86 | $4p^4P^\circ_{3/2}-6s^4P_{5/2}$ | (**0.113**), (0.347), 1.149, 1.380, 1.609, ---- | 1.723 | 1.493 |
| 7256.63 | 13,776.71 | $4s^4P^\circ_{5/2}-4p^4S_{3/2}$ | (**0.137**), (0.418), **1.181**, 1.463, 1.738, 2.011 | 1.599 | 1.876 |
| 7329.33 | 13,640.06 | $4p^4D^\circ_{7/2}-4d^2D_{5/2}$ | 1.507 h | 1.422* | 1.346 |
| 7342.74 | 13,615.15 | $4p^4D^\circ_{3/2}-6s^4P_{1/2}$ | (0.399), **0.765**, 1.564 | 1.165 | 1.964 |
| 7372.65 | 13,559.91 | $4p^4D^\circ_{3/2}-4d^4P_{3/2}$ | (−), (0.707), ----, ----, ---- | 1.163* | 1.634 |
| 7414.10 | 13,484.10 | $4s^4P_{5/2}-4p^2P^\circ_{3/2}$ | (**0.134**), (0.407), 1.187, 1.458, 1.727, **2.004** | 1.597 | 1.326 |
| 7435.71 | 13,444.91 | $4p^4D^\circ_{1/2}-4d^4P_{3/2}$ | (**0.095**), (0.293), (−), ----, ----, ----, ----, ----, 1.919 | 1.434 | 1.240 |
| 7454.08 | 13,410.49 | $4p^4D^\circ_{1/2}-6s^4P_{1/2}$ | 0.979 f | (0)? | 1.959 |
| 7462.40 | 13,396.83 | $4p^2D^\circ_{5/2}-4d^4P_{3/2}$ | (**0.174**), (0.512), **0.755**, 1.087, 1.450, ---- | 1.265 | 1.607 |
| 7489.46 | 13,348.43 | $4p^4D^\circ_{5/2}-6s^4P_{3/2}$ | 1.215 h | 1.308* | 1.425 |
| 7492.12 | 13,343.69 | $4p^4D^\circ_{7/2}-6s^4P_{5/2}$ | 1.303 h | 1.422* | 1.518 |
| 7547.06 | 13,246.55 | $4s^4P_{3/2}-4p^4S^\circ_{3/2}$ | (0.067), (**0.235**), 1.614, **1.800**, 1.983 | 1.715 | 1.886 |
| 7672.44 | 13,030.08 | $4s^4P_{5/2}-4p^2D^\circ_{3/2}$ | (**0.307**), (0.935), 0.648, 1.294, 1.911, **2.532** | 1.604 | 0.985 |
| 7717.57 | 12,953.89 | $4s^4P_{3/2}-4p^2P^\circ_{3/2}$ | (0.195), (**0.596**), 1.132, **1.530**, 1.926 | 1.729 | 1.331 |
| 7744.94 | 12,908.11 | $4s^4P_{1/2}-4p^4S^\circ_{3/2}$ | (0.395), **1.482**, 2.260 | 2.655 | 1.869 |
| 7821.35 | 12,782.01 | $4p^4P^\circ_{1/2}-4d^4D_{1/2}$ | (**0.088**), (0.262), (0.447), **0.976**, 1.108, 1.334, 1.507, 1.681, ---- | 1.592 | 1.416 |
| 7830.76 | 12,766.64 | $4p^4P^\circ_{3/2}-4d^4D_{3/2}$ | (0.262), (**0.758**), 9.961, **1.464**, 1.981 | 1.718 | 1.210 |
| 7839.42 | 12,752.54 | $4p^4D^\circ_{3/2}-6s^4P_{5/2}$ | (**0.179**), (0.481), ----, ----, 1.676, **1.990** | 1.163 | 1.494 |
| 7878.22 | 12,689.74 | $4s^4P_{5/2}-4p^2D^\circ_{5/2}$ | (0.169), (0.492), (−), ----, 1.107, 1.433, 1.761, 2.086 f | 1.597 | 1.270 |
| 7899.28 | 12,655.90 | $4p^4P^\circ_{3/2}-4d^4D_{5/2}$ | (**0.178**), (0.531), **0.834**, 1.189, 1.535, 1.881 | 1.721 | 1.367 |
| 7915.09 | 12,630.62 | $4p^4P^\circ_{1/2}-4d^4D_{1/2}$ | **1.324** f | 2.648 | (0)? |
| 7924.62 | 12,615.44 | $4s^4P_{1/2}-4p^2P^\circ_{3/2}$ | (−), ----, 1.987 f | **2.652*** | 1.324 |
| 7952.49 | 12,571.22 | $4p^4D^\circ_{1/2}-4d^4F_{3/2}$ | (−), ----, 1.480 f | **0.059*** | 0.987 |
| 7976.95 | 12,532.58 | $4p^4P^\circ_{1/2}-4d^4D_{3/2}$ | (0.710), **0.498**, ---- | 2.629 | 1.209 |
| 7997.80 | 12,500.01 | $4s^4P_{3/2}-4p^2D^\circ_{3/2}$ | (−), (1.113), 0.605, **1.353**, 2.094 | 1.725 | 0.982 |
| 8015.57 | 12,472.31 | $4s^2D_{3/2}-5p^2P^\circ_{1/2}(^1D^2P)$ | | | |
| 8023.30 | 12,460.28 | $4p^4D^\circ_{3/2}-4d^4F_{5/2}$ | **1.000** g | **1.163*** | 1.097 |
| 8194.35 | 12,200.18 | $4s^4P_{3/2}-4p^4D^\circ_{1/2}$ | (−), ----, 2.555 f | **1.722*** | 0.059 |
| 8199.02 | 12,193.23 | $4s^2D_{5/2}-5p^2P^\circ_{3/2}(^1D^2P)$ | P.B. | | |
| 8200.20 | 12,191.48 | $4s^2D_{3/2}-5p^2P^\circ_{3/2}(^1D^2P)$ | P.B. | | |
| 8212.00 | 12,173.96 | $4s^4P_{5/2}-4p^4D^\circ_{5/2}$ | (0.153), (0.437), (**0.724**), 0.844, 1.151, **1.451**, 1.741, 2.038 | 1.598 | 1.304 |
| 8333.29 | 11,996.77 | $4s^4P_{3/2}-4p^4D^\circ_{3/2}$ | (0.281), (**0.792**), 0.903, **1.439**, 1.998 | 1.719 | 1.159 |
| 8375.95 | 11,935.66 | $4s^4P_{5/2}-4p^4D^\circ_{7/2}$ | (**0.087**), (0.264), (0.450), **0.978**, 1.171, 1.346, 1.519, 1.688, 1.860 | 1.592 | 1.417 |
| 8428.25 | 11,861.60 | $4s^4P_{1/2}-4p^4D^\circ_{1/2}$ | 1.321 f | 2.643 | (0)? |
| 8550.46 | 11,692.07 | $4s^2P_{3/2}-4p^2P^\circ_{1/2}$ | 1.328 h | **1.340*** | 1.391 |
| 8575.25 | 11,658.27 | $4s^4P_{1/2}-4p^4D^\circ_{3/2}$ | (0.749), **0.412**, 1.914 | 2.665 | 1.164 |
| 8585.96 | 11,643.72 | $4s^4P_{3/2}-4p^4D^\circ_{5/2}$ | (**0.210**), (−), ----, **1.096**, 1.516, 1.935, ----, f | 1.725 | 1.306 |
| 8686.28 | 11,509.25 | $4s^2P_{3/2}-4p^4S^\circ_{3/2}$ | (−), (**0.802**), 1.067, **1.607**, 2.142 | 1.339 | 1.875 |
| 8912.88 | 11,216.79 | $4s^2P_{3/2}-4p^2P^\circ_{3/2}$ | 1.327 h | **1.340*** | 1.315 |
| 9045.40 | 11,052.31 | $4s^2P_{1/2}-4p^2P^\circ_{1/2}$ | (0.352), ----, d | 0.663 | 1.367 |
| 9073.15 | 11,018.50 | $4s^2P_{3/2}-4p^2S^\circ_{1/2}$ | 1.374 h | **1.340*** | 1.270 |
| 9121.10 | 10,960.58 | $4s^4P_{5/2}-4p^4P^\circ_{5/2}$ | 1.596 h | **1.599*** | 1.595 |
| 9191.67 | 10,876.44 | $4s^4P_{3/2}-4p^4P^\circ_{1/2}$ | (0.448), **1.276**, ---- | 1.725 | 2.622 |

( ) New line or new classification.
* Assumed from other measurements; used in calculation of second $g$-factor.
c Long λσ comp. hidden by other lines. Pattern found from meas. on π comp. and short λσ comp.
d Long λσ comp. hidden by another line.
e Long λσ comp. hidden by other lines. Pattern found from meas. on π comp. and short λσ comp.
f Overlapping of π and σ comp.
g pattern unresolved; separation is half that between strongest σ-comp.
h Pattern unresolved; separation is half that between centers of gravity of σ groups.
i π comp. unresolved; separation is half that across π group.
j π comp. unresolved.
a All but 5 comp. covered by other lines.
b Short λ half of pattern hidden by other lines.

TABLE II. Tentative classifications of some lines in chlorine I.

| λ | ν | Classification | g |
|---|---|---|---|
| (3735.85) | 26760.09 | $4s^4P_{1/2}-5408.3^\circ_{1/2}$ | 0.49 |
| 3992.81 | 25037.96 | $4s^2P_{1/2}-5091.8^\circ_{1/2}$ | 0.81 |
| (4049.05) | 24690.20 | $4s^2P_{3/2}-6079.4^\circ_{1/2}$ | 1.91 |
| 5338.00 | 18728.41 | $4p^4P^\circ_{3/2}-3136.0_{5/2}$ | 1.45 |
| 5401.65 | 18507.73 | $4p^4P^\circ_{5/2}-3568.6_{5/2}$ | 1.60 |
| 5464.31 | 18295.50 | $4p^4P^\circ_{3/2}-3568.6_{5/2}$ | 1.61 |
| 5484.60 | 18227.82 | $4p^4P^\circ_{1/2}-3403.6_{1/2}$ | 0.69 |
| 5702.02 | 17532.79 | $4p^4D^\circ_{7/2}-3568.6_{5/2}$ | 1.60 |
| 5808.59 | 17211.12 | $4p^2D^\circ_{5/2}-3136.0_{5/2}$ | — |
| 5844.15 | 17106.40 | $(4p^4D^\circ_{3/2}-3403.6_{1/2})$? | — |
| 5936.20 | 16841.14 | $4p^4P^\circ_{3/2}-5022.9_{1/2}$ | — |
| 5972.75 | 16738.08 | $4p^4D^\circ_{3/2}-3772.0_{3/2}$? | 1.20 |
| 6040.43 | 16550.51 | $4p^4P^\circ_{3/2}-5313.9_{3/2}$ | 1.73 |
| 6073.39 | 16460.72 | $4p^4D^\circ_{1/2}-4049.4_{1/2}$ | — |
| 6127.00 | 16316.70 | $4p^4P^\circ_{1/2}-5313.9_{3/2}$? | — |
| 6157.85 | 16234.95 | $4p^2D^\circ_{3/2}-3772.0_{3/2}$? | — |
| 6334.96 | 15781.06 | $4s^2D_{3/2}-5091.8^\circ_{1/2}$ | 0.82 |
| 6366.83 | 15702.07 | $4p^2S^\circ_{1/2}-4049.4_{1/2}$ | — |
| 6452.75 | 15492.99 | $4p^2S^\circ_{1/2}-4257.6_{1/2}$ | — |
| 6455.24 | 15487.02 | $4p^4D^\circ_{3/2}-5022.9_{1/2}$ | — |
| 6471.45 | 15448.23 | $4s^2D-5426.3^\circ_{3/2}$ | — |
| 6637.15 | 15062.55 | $4p^2D^\circ_{3/2}-4944.5_{3/2}$ | — |
| 6709.90 | 14899.25 | $4s^2D_{5/2}-5975.9^\circ_{3/2}$ | — |
| 6757.75 | 14793.75 | $4s^2D_{3/2}-6079.4^\circ_{1/2}$ | — |
| 6924.40 | 14437.71 | $4p^2P^\circ_{3/2}-5313.9_{3/2}$ | — |

TABLE III. Additional lines in the spectrum of chlorine I.

| λ | ν | Transition | $g_1$ | $g_2$ |
|---|---|---|---|---|
| 5231.41 | 19110.00 | 5/2→3/2 | 1.15 | 1.40 |
| 5307.55 | 18835.86 | 3/2→3/2 | 0.94 | 0.64 |
| 5376.22 | 18594.93 | 3/2→3/2? | — | — |
| 5541.00 | 18042.28 | 3/2→3/2 | 1.71 | 1.41 |
| | | | $(4p^4P^\circ_{3/2}?)$ | |
| 5549.21 | 18015.59 | 3/2→1/2 | 1.07 | 1.57 |
| 5774.72 | 17312.07 | 1/2→3/2 | 0.00 | 0.57 |
| | | | $(4p^4D^\circ_{1/2}?)$ | |
| 5796.26 | 17247.73 | 5/2→3/2 | 1.16 | 1.45 |
| 6321.59 | 15814.44 | 1/2→1/2 | 1.45 | 0.74 |
| 6425.61 | 15558.43 | 1/2→1/2 | 1.46 | 0.75 |
| 7146.38 | 13989.25 | 1/2→1/2 | 1.00 | 0.62 |
| 7561.19 | 13221.80 | 5/2→3/2 | 1.33 | 1.03 |
| | | | $(4p^4D^\circ_{5/2}?)$ | $(6s^2P^\circ_{3/2}?)$ |

TABLE IV. New terms in the spectrum of chlorine I.

| Level | j | g | Tentative classification |
|---|---|---|---|
| 5313.9 | 3/2 | 1.73 | 7s ? |
| 5022.9 | 1/2 | 1.21 | 7s ? |
| 4944.5 | 3/2 | 1.42 | 7s ? |
| 4290.7 | 3/2 | 1.65 | $5d^2P_{3/2}$ |
| 4257.6 | 1/2 | 1.59 | $5d^2P_{1/2}$ |
| 4049.1 | 1/2 | 1.01 | $6d^4D_{1/2}$ |
| 3949.4 | 3/2 | 1.17 | $6d^4D_{3/2}$ |
| 3772.0 | 3/2? | 1.20 | 6d |
| 3568.6 | 5/2 | 1.60 | 6d |
| 3403.6 | 1/2 | 0.69 | 6d |
| 3136.0 | 5/2 | 1.45 | 6d |
| 6079.4° | 1/2 | 1.91 | $6p^4P^\circ_{1/2}$ |
| 5975.9° | 3/2 | 1.32 | $6p^4D^\circ_{3/2}$ |
| 5426.3° | 3/2 | 1.32 | 6p |
| 5408.3° | 1/2 | 0.49 | 6p |
| 5171.2° | 3/2 | 1.28 | $6p^2P^\circ_{3/2}$ |
| 5091.8° | 1/2 | 0.81 | $6p^2P^\circ_{1/2}$ |

TABLE V. g-values and g-sums in the spectrum of chlorine I.

| Level | | g(LS) | g(Exp.) | g(Exp.) | g(Exp.) |
|---|---|---|---|---|---|
| | | | 4s | 6s | 7s |
| $^2P_{1/2}$ | | 0.667 | 0.663 | — | (1.21) |
| $^4P_{1/2}$ | | 2.667 | 2.652 | 1.962 | — |
| | Sum | 3.333 | 3.315 | | |
| $^2P_{3/2}$ | | 1.333 | 1.340 | — | (1.42) |
| $^4P_{3/2}$ | | 1.733 | 1.722 | 1.393 | (1.73) |
| | Sum | 3.067 | 3.062 | | 3.15 |
| $^4P_{5/2}$ | | 1.600 | 1.599 | 1.500 | — |
| | | | 4p | 5p | 6p |
| $^4P^\circ_{1/2}$ | | 2.667 | 2.617 | 2.309 | (1.91) |
| $^4D^\circ_{1/2}$ | | 0.000 | 0.059 | 1.409 | (0.49) |
| $^2S^\circ_{1/2}$ | | 2.000 | 1.280 | 0.699 | — |
| $^2P^\circ_{1/2}$ | | 0.667 | 1.379 | 0.712 | (0.81) |
| | Sum | 5.333 | 5.335 | 5.129 | |
| $^2P^\circ_{1/2}(^1D)$ | | 0.667 | 0.872 | — | — |
| $^4P^\circ_{3/2}$ | | 1.733 | 1.723 | 1.722 | |
| $^4D^\circ_{3/2}$ | | 1.200 | 1.163 | 1.147 | (1.32) |
| $^2D^\circ_{3/2}$ | | 0.800 | 0.986 | 1.321 | (1.32) |
| $^2D^\circ_{3/2}$ | | 1.333 | 1.327 | 1.286 | (1.28) |
| $^4S^\circ_{3/2}$ | | 2.000 | 1.877 | 1.531 | — |
| | Sum | 7.067 | 7.076 | 7.007 | |
| $^2P^\circ_{3/2}(^1D)$ | | 1.333 | 1.328 | — | — |
| $^2D^\circ_{3/2}(^1D)$ | | 0.800 | 0.867 | — | — |
| | Sum | 2.133 | 2.195 | | |
| $^4P^\circ_{5/2}$ | | 1.600 | 1.591 | 1.559 | — |
| $^4D^\circ_{5/2}$ | | 1.371 | 1.308 | 1.247 | — |
| $^2D^\circ_{5/2}$ | | 1.200 | 1.269 | 1.352 | — |
| | Sum | 4.171 | 4.168 | 4.158 | |
| $^4D^\circ_{7/2}$ | | 1.429 | 1.422 | 1.420 | — |
| | | | 4d | 5d | 6d |
| $^4D_{1/2}$ | | 0.000 | 0.00 | 0.363 | (1.010) |
| $^4P_{1/2}$ | | 2.667 | — | 1.470 | — |
| $^2P_{1/2}$ | | 0.667 | 1.289 | (1.59) | — |
| | Sum | 3.333 | | 3.42 | |
| $^4F_{3/2}$ | | 0.400 | 0.967 | 1.240 | (1.20) |
| $^4D_{3/2}$ | | 1.200 | 1.209 | — | (1.168) |
| $^4P_{3/2}$ | | 1.733 | 1.620 | — | — |
| $^2D_{3/2}$ | | 0.800 | — | — | — |
| $^2P_{3/2}$ | | 1.333 | 1.306 | (1.65) | — |
| | Sum | 5.467 | | | |
| $^4F_{5/2}$ | | 1.029 | 1.097 | 1.149 | — |
| $^4D_{5/2}$ | | 1.371 | 1.367 | 1.358 | 1.364 |
| $^4P_{5/2}$ | | 1.600 | 1.241 | 1.589 | (1.60) |
| $^2F_{5/2}$ | | 0.857 | — | 1.069 | (1.45) |
| $^2D_{5/2}$ | | 1.200 | 1.355 | — | — |
| | Sum | 6.057 | | | |
| $^4F_{7/2}$ | | 1.238 | — | 1.181 | — |
| $^4D_{7/2}$ | | 1.429 | — | 1.392 | 1.377 |
| $^2F_{7/2}$ | | 1.143 | — | 1.210 | — |
| | Sum | 3.810 | | 3.783 | |
| $^4F_{9/2}$ | | 1.333 | — | 1.310 | — |

of error. Of the other configurations, only the $4p$ and $5p$ are sufficiently complete to yield interesting results.

The g-sum of the $4p(^3P)$ levels for $j=\frac{1}{2}$ is normal. But that of the $5p(^3P)$ is 0.204 too low.

On the other hand, $4p(^1D)^2P_{1/2}$ is 0.215 too high. A similar situation exists for the $j=\frac{3}{2}$ levels. For $4p(^3P)$ the $g$-sum is normal within experimental limits. For $5p(^3P)$ the sum is 0.059 too small. But the $5p(^1D)$ sum is 0.062 too large. Here is striking evidence of the sharing of $g$-values by two configurations.

It is worth noting that perturbations of $g$-values caused by configuration interaction seem to be greater the smaller the $j$-value concerned. This is in general agreement with theory.

*Note added in proof:* The $g$-values in Table V indicate that the chlorine atom, like those of the rare gases, exhibits a type of coupling (in the limit) which is represented when the electrostatic interaction is weak compared with the spin-orbit interaction, but strong compared with the spin coupling of the external electron. We have called this type of coupling $[(j_1l_1)s_1]$.

PHYSICAL REVIEW VOLUME 69, NUMBERS 5 AND 6 MARCH 1 AND 15, 1946

# Forbidden Lines of Bismuth BiI

S. MROZOWSKI*
*Department of Physics, University of Chicago, Chicago, Illinois*
(Received September 16, 1945)

A group of forbidden lines of bismuth BiI, namely λ8755, 6476, 5640, 4615, 4597, and 3014, all belonging to transitions between levels of the configuration $6p^3$ (Fig. 1) was investigated with a spectrograph of high resolving power. The hyperfine structures observed are collected in Table I and the photographs obtained are reproduced in Fig. 2. Predicted patterns with components corresponding only to the change of the quantum number $F$ by 0 or $\pm1$ and intensities calculated on basis of usual formulas for electric dipole radiation are in best agreement with the observed ones (Fig. 3). The absence of components corresponding to $\Delta F=\pm2$ shows the predominantly magnetic dipole character of the radiation. All observed separations of components and wave-lengths of the forbidden lines found are in very good agreement with the values predicted on basis of the highly accurate level scheme of the bismuth atom previously determined by the author.

IN a series of papers[1] the author succeeded in showing that the investigation of the isotopic and hyperfine structures of a forbidden line furnishes an easy method for determination of the type of the forbidden radiation, a method which is usually more convenient than the investigation of the Zeeman effect. Not many systematic investigations have been carried out on the electric quadrupole and magnetic dipole lines (the second order radiation) and until now only the case of a $p^2$ configuration has been more closely studied.[2] Since the lines of a mixed character present a considerable interest in view of a recently discovered interference effect,[3] an extension of the investigations to forbidden multiplets of the $p^3$ configuration seemed to be worth while. In this paper the author is presenting the results of corresponding experiments carried out with bismuth vapor. The experiments had to be interrupted before intensity measurements could be done. Since, however, there seems to be no hope they will be performed in the near future, it seemed appropriate to report the results now obtained, that is of the hyperfine structure investigations.

The experimental arrangement was the same as that used in the work on the analysis[4] of the spectrum of bismuth BiI. A quartz tube with outside electrodes, permanently connected to the pumping system and containing a piece of metal, was filled with helium at about 5-mm pressure and excited by short electric waves (3–4 meter wave-length). For an intense production of forbidden lines, however, higher temperatures of

* Now at the Research and Development Division, Great Lakes Carbon Corporation, Morton Grove, Illinois.

[1] For references see the general reports: S. Mrozowski, Bull. Polish Inst. Arts and Sciences America 2, 200 (1943); or S. Mrozowski, Rev. Mod. Phys. 16, 153 (1944).

[2] S. Mrozowski, Phys. Rev. 58, 1086 (1940).

[3] F. A. Jenkins and S. Mrozowski, Phys. Rev. 60, 225 (1941).

[4] S. Mrozowski, Phys. Rev. 62, 526 (1942).

the furnace (higher pressure of bismuth vapor) and a decreased power of the high frequency oscillator were required. The optimum conditions for excitation of forbidden lines of metals in such an arrangement were previously studied in the case of the spectrum of lead,[2] and it was shown that such a discharge is a very intense source of forbidden lines. The increase of the partial pressure of bismuth vapor is followed by the appearance of the well-known rich band spectrum of $Bi_2$ in the region 5000–7000A. The conditions of excitation of this band spectrum are the same as of the forbidden lines—the power delivered by the oscillator must not be too high, otherwise the molecules are dissociated by the high current and only an atomic spectrum of BiI is emitted. This band spectrum was photographed some time ago by the author in collaboration with Dr. F. Bueso-Sanllehi in the first order of the big Chicago grating No. 3 and it was found that the bands are quite nicely resolved into a multitude of lines. Long series of lines (branches) can be easily picked out; however all bands overlap strongly with each other and this creates such a mixup that no analysis was attempted. The presence of the band spectrum is of some inconvenience only in the case of the line λ5640, which is quite weak and therefore requires long exposures. Fortunately this line originates in the highest metastable level $^2P_{3/2}$ and, therefore, has its maximum intensity at relatively lower vapor densities of bismuth. The other line in the region of the band spectrum, namely λ6476, is so intense that no traces of the band lines appear even for strongly overexposed photographs of this line.

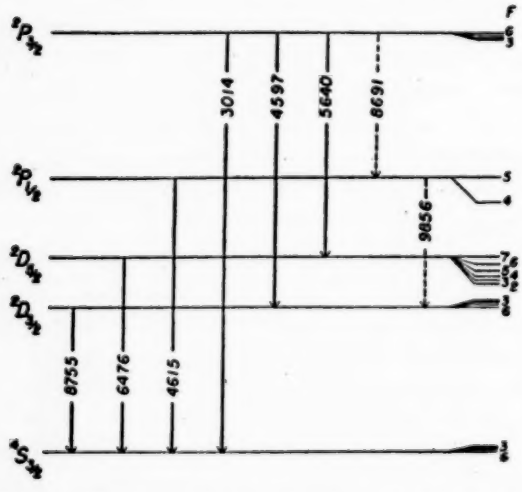


FIG. 1. The lowest levels all belong to the $6p^3$ electronic configuration and the forbidden lines of bismuth BiI. On the right the hyperfine separations of levels, but on a 1000 times larger scale, are given.

The level scheme of the lowest group of levels of BiI ($6p^3$ configuration) is represented in Fig. 1. Six forbidden lines observed and two other transitions, the presence of which was not but probably could be easily checked with a medium spectrograph (dashed lines), are inserted in this graph. No photograph of the line λ8691 could be obtained with the big grating, although exposures were extended over 60 hours. Evidently this line is much weaker than the neighboring line λ8755. The three strongest forbidden lines, namely λ8755, λ6476, and λ4615, were found in the spectrum of a discharge tube by other investigators some time ago.[5] In this work at the optimum excitation conditions these lines are belonging to prominent lines of the spectrum. All lines were photographed in the first order of the big grating No. 3, with exception of the lines λ4615 and λ3014 which could be obtained also in the second order. The exposure time ranged from a few hours (λ6476) to 48 hours (λ8755 and λ5640). The infra-red line λ8755 was photographed on Eastman-Kodak M-I plates, and λ5640 on Ilford panchromatic plates.

The photographs obtained are reproduced in Fig. 2. It is easily noticeable that the lines λ4597 and λ3014 are far from being resolved. In case of the line λ8755 a very wide slit had to be used and therefore the structure is obliterated revealing only a diffuse doublet. The results of the measurements of the hyperfine structures are collected in Table I. Since the separations of the levels involved are well known from the analysis of other lines of bismuth,[4] a comparison of observed and predicted pattern can be made. In Fig. 3 the predicted structures are inserted for the case of pure magnetic dipole radiation, that is, only components for which $\Delta F=0, \pm 1$ are included with intensities calculated on basis of the usual formulas for hyperfine structure. The applicability of these rules for the electric dipole radiation to the magnetic dipole case of hyperfine structure was demonstrated experi-

[5] G. R. Toshniwal, Phil. Mag. 4, 774 (1927).

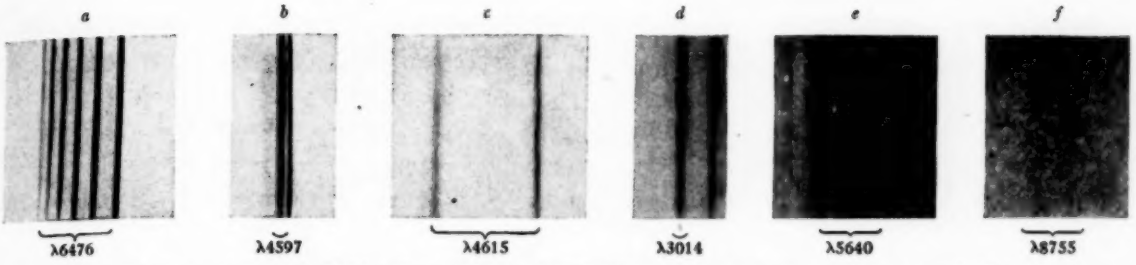


FIG. 2. Hyperfine structure of forbidden lines of bismuth BiI. Photographs *a*, *b*, *e*, and *f* were obtained in the first and *c* and *d* in the second order of a 30-foot grating spectrograph.

mentally by the author[2] and explained theoretically by Gerjuoy.[6] The observed structures are represented by curves and the measured positions of the peaks are inserted below in the form of shaded circles. The positions of weak components not quite resolved from neighboring strong ones (λ4615 and λ6476) were determined visually with the comparator. As it was observed in a similar case by the author,[7] the results are surprisingly good, our vision being sensitive rather to the rate of the change in density on the plate than to the change of the density itself. For the line λ5640 the intensity of the second component on the left seems smaller than (or equal to) that of the third; this is probably because of the partial resolution of the doublet which causes the easily visible widening of the second component and lowers at the same time its peak intensity. The measured total splitting of the line λ5640 is a little greater than the predicted value and this seems to indicate that the total splitting of the $^2P_{3/2}$ level reported in the paper[4] on BiI was a little too high and should probably be around 0.23 $cm^{-1}$ instead of 0.25 $cm^{-1}$. The separation for the ground level $^4S_{3/2}$, which was found[4] to be almost three times larger than the value estimated previously by Zeeman, Back, and Goudsmit,[8] is confirmed by the structures observed for the lines λ6476 and λ4615.

In Table II the exact wave-lengths and wave numbers for the components corresponding to transitions with highest $F$ quantum numbers are compared with the values expected on basis of the term values previously reported.[4] Very good agreement is obtained, except in the case of the weak and diffuse line λ3014; the discrepancy in the case of the line λ8755 does not have to be taken seriously, since the line is very diffuse and the wave-length was determined relative to the second-order iron lines introducing a correction

TABLE I. Hyperfine structure. Components in $10^{-3}$ $cm^{-1}$ (approx. relative intensity 1—strongest, 2—next strongest, and so on).

| | |
|---|---|
| 8755 | 0 (1), +380 (1) |
| 6476 | −2300 (6), −2030 (5), −1660 (4), −1200 (3), −676 (2), −580 (7), 0 (1) |
| 5640 | 0 (1), +520 (2), +940 (2), +1310 (3), +1640 (4), +1870 (4) |
| 4615 | −2090 (2), −1990 (4), −90 (3), 0 (1) |
| 4597 | −760 (2), −502 (2), −255 (3), 0 (1) |
| 3014 | −300 (1), 0 (2) |

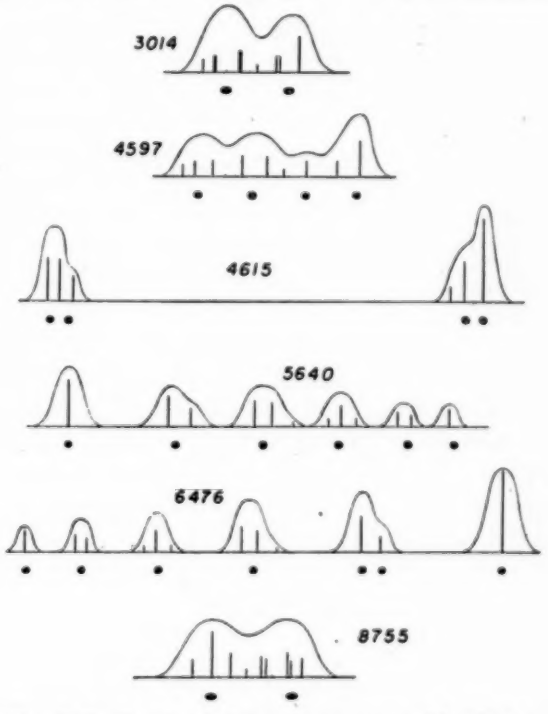


FIG. 3. Predicted and observed structures of forbidden lines of bismuth BiI.

[6] E. Gerjuoy, Phys. Rev. **60**, 233 (1941).
[7] S. Mrozowski, Zeits. f. Physik **112**, 223 (1939).
[8] P. Zeeman, E. Back, and S. Goudsmit, Zeits. f. Physik **66**, 1 (1930).

TABLE II. Measured wave numbers of components with highest $F$ quantum numbers for the forbidden lines of BiI. Deviations from predicted values in parenthesis.

| Final level \ Upper level | $^2D_{3/2}$ 11418.77 | $^2D_{5/2}$ 15438.42 | $^2P_{1/2}$ 21661.81 | $^2P_{3/2}$ 33165.01 |
|---|---|---|---|---|
| $^4S_{3/2}$ 0 | λ8754.90 11419.03 (+.26) | λ6475.535 15438.46 (+.04) | λ4615.122 21661.85 (+.04) | λ3014.343 33165.09 (+.08) |
| $^2D_{3/2}$ 11418.77 | | | | λ4597.216 21746.22 (−.02) |
| $^2D_{5/2}$ 15438.42 | | | | λ5639.702 11726.53 (−.06) |

for the dispersion of the air at the given temperature—a procedure which hardly can give a highly accurate result.

The very good agreement between the predicted and observed structures and the failure to observe any components for which $\Delta F = \pm 2$ are a good evidence for the predominantly magnetic dipole character of the radiation of the whole group of forbidden transitions studied. It is hard to estimate how high the possible admixture of an electric quadrupole radiation may be without performing intensity measurements. However from the appearance of the best resolved line λ6476 I would expect for this line the admixture to be not higher than 15 percent. Theoretically this percentage could be easily determined by use of tables published not long ago by Shortley, Aller, Baker, and Menzel,[9] if only an integral involving radial factors of the $p$-orbital would be known. From the same tables the relative intensities of lines originating from the same upper level can be obtained as functions of the unknown integral. A measurement of the relative intensities of the lines λ3014, 4597, 5640, and 8691 would therefore lead to a determination of the percentage of the electric quadrupole radiation and would at the same time present a good opportunity for a check of the theoretical predictions (since a ratio for two lines would be sufficient for determination of the percentage). On the other hand the same percentage could be determined from an observation of the interference effect in the magnetic field[3] furnishing an additional check on the theoretical relations. In the past the effort was made to get such a double check for the case of the spectrum of lead,[2,3,6] but unfortunately the agreement is not good. (See the discussion of this point in the article in Reviews of Modern Physics, reference 1.) It seems, therefore, necessary to perform measurements of relative intensities of lines in forbidden spectra with a higher accuracy, preferably for a whole group of spectra like Pb, Bi, Se, Te,[10] and maybe some others, in order to secure more reliable data for comparison with theoretical predictions. At the same time valuable information could be collected about the concentration of metastable atoms in different states and its dependence on different factors. Further experiments with the interference effect in the line λ7330 of Pb should be repeated[3] and extended to the longitudinal Zeeman effect, and also the same effect in lines of mixed character for other elements should be investigated.

[9] G. H. Shortley, L. H. Aller, Y. G. Baker, and D. H. Menzel, Astrophys. J. 93, 178 (1941).

[10] H. Niewodniczanski and F. Lipinski, Nature 142, 1160 (1938).

PHYSICAL REVIEW VOLUME 69, NUMBERS 5 AND 6 MARCH 1 AND 15, 1946

# The Elastic, Piezoelectric, and Dielectric Constants of Potassium Dihydrogen Phosphate and Ammonium Dihydrogen Phosphate

W. P. MASON
*Bell Telephone Laboratories, Murray Hill, New Jersey*
(Received October 27, 1945)

Measurements have been made of all the elastic, piezoelectric, and dielectric constants of KDP and ADP crystals through temperature ranges down to the Curie temperatures. The piezoelectric properties agree well with Mueller's phenomenological theory of piezoelectricity provided the fundamental piezoelectric constant is taken as the ratio of the piezoelectric stress to that part of the polarization due to the hydrogen bonds. It is found that the dielectric properties of KDP agree well with the theory presented by Slater based on the interaction of the hydrogen bonds with the $PO_4$ ions. ADP undergoes a transition at $-125°C$ which results in fracturing the crystal. This transition cannot be connected with the $H_2PO_4$ hydrogen bond system which controls the dielectric and piezoelectric properties, for these lie on smooth curves that do not change slope as the transition temperature is approached. It is suggested that two separate and independent hydrogen bond systems are involved in ADP. The transition temperature and specific heat anomaly appear to be connected with hydrogen bonds between the nitrogens and the oxygens of the $PO_4$ ions, while the dielectric and piezoelectric properties are controlled by the $H_2PO_4$ hydrogen bonds.

## I. INTRODUCTION

IT was first shown by Busch[1] that potassium dihydrogen phosphate $KH_2PO_4$ and several isomorphous salts, potassium dihydrogen arsenate $KH_2AsO_4$, ammonium dihydrogen phosphate $NH_4H_2PO_4$, and ammonium dihydrogen arsenate $NH_4H_2AsO_4$ exhibited phase changes at low temperatures. These crystals all exhibit phase changes at temperatures ranging from 91° absolute to 220° absolute temperature. It was established for potassium dihydrogen phosphate (which will be designated by the letters KDP) and potassium dihydrogen arsenate (KDA) by measuring the dielectric constants and the associated charge potential loops that these phase changes were of the ferroelectric type. Similar measurements of ammonium dihydrogen phosphate (ADP) and ammonium dihydrogen arsenate (ADA) failed to show ferroelectric properties on account of the sudden fracture of these crystals at temperatures above the ferroelectric Curie temperatures.

Measurements have been reported on the elastic properties of KDP,[2] and the piezoelectric constant of KDP,[3] over a temperature range, and some of the piezoelectric and elastic constants for all four crystals at room temperature,[4] but no complete measurements have been published of the properties of these crystals over temperature ranges down to the Curie temperatures. Such measurements, for small field strengths, are presented in the paper for two of these crystals KDP and ADP. The measurements for the dielectric constant of KDP are found to agree well with Slater's theory[5] based on the temperature variation of the position of the dipoles formed by the interaction of the hydrogens with $PO_4$ ions. However, the transformation occurring in ADP does not appear to be the ferroelectric type as envisaged by Slater for KDP. The measured piezoelectric relations agree with Mueller's[6] phenomenological theory of ferroelectricity if the fundamental piezoelectric constant is taken as the ratio of the piezoelectric stress to that part of the polarization due to hydrogen bonds.

[1] Georg Busch, "Neue Seignette Elektrika," Helv. Phys. Acta **11**, No. 3 (1938).
[2] W. Lüdy, "Der Einfluss der Temperature auf das Dynamisch Elastische Verhalten von Seignetteelektrika," Helv. Phys. Acta **20**, No. 8 (1942).
[3] W. Lüdy, "Piezoelectrizität von Kalium Phosphate," Zeits. f. Physik **113**, 302 (1939).
[4] H. Jaffe, "Piezoelectric studies of primary phosphates and arsenates," Abstract **D.3**, Bull. Am. Phys. Soc. (January 19, 1945).
[5] J. C. Slater, "Theory of the transition in $KH_2PO_4$," J. Chem. Phys. **9**, 16–33 (1941).
[6] H. Mueller, "Properties of Rochelle salt," Phys. Rev. **57**, 829–839 (1940).

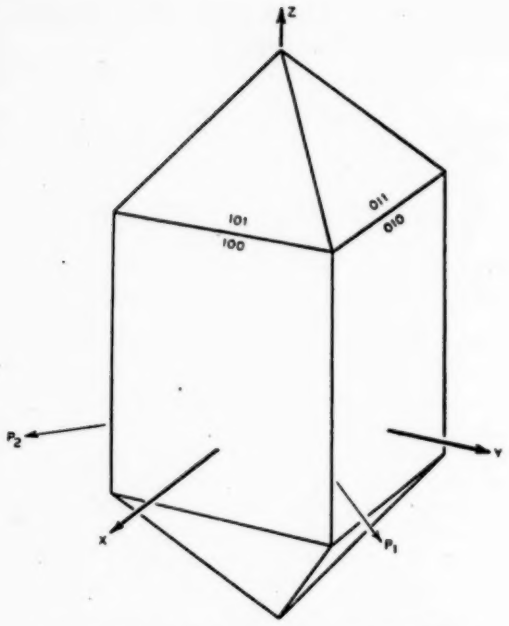


FIG. 1. Growth habit for ADP and KDP.

## II. EXPRESSIONS FOR THE ELASTIC, DIELECTRIC, AND PIEZOELECTRIC EQUATIONS FOR ADP AND KDP CRYSTALS

All of the crystals of the isomorphous group, ADP, KDP, ADA, and KDA, crystallize in the tetragonal scalenohedral class with the habit shown by Fig. 1. The $c$ or $Z$ axis lies along the long direction of the crystal. This is an axis of fourfold alternating symmetry. The $X$ and $Y$ axes lie normal to the prism faces. These are axes of twofold symmetry. Since the properties of crystals cut normal to these two surfaces are identical except for sign, it is a matter of convention which axis is called $X$ and which $Y$. The two diagonal axes, labelled $P_1$ and $P_2$ can be distinguished by piezoelectric tests, and $P_1$ has been taken as that axis along which a positive stress (tension) produces a positive charge at the positive (i.e., the upper) end of the $Z$ axis. With the $Z$ axis vertical and the $P_1$ axis toward the observer's right hand, the $X$ axis has been taken as the axis which runs from front to back of the crystal and the $Y$ axis from left to right (see Fig. 1). Etching studies by Dr. E. J. Armstrong show that an etch figure can be developed on the top surface as shown by Fig. 2 and the direction of the $P_2$ axis is in the line of the two spots.

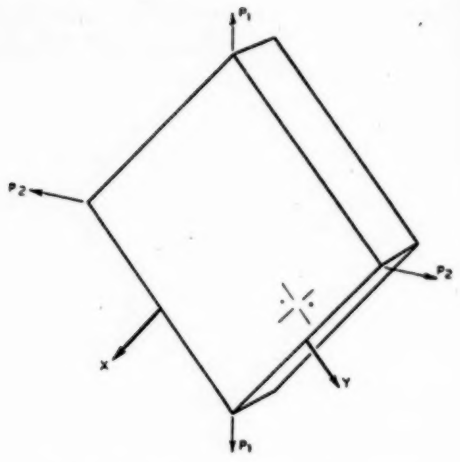


FIG. 2. Etch figures developed on ADP.

For a crystal having this symmetry Voigt[7] has shown that there will be six elastic compliances $s_{11}$, $s_{12}$, $s_{13}$, $s_{33}$, $s_{44}$, and $s_{66}$, two piezoelectric constants $d_{14}=d_{25}$ and $d_{36}$, and two dielectric constants $K_x=K_y$ and $K_z$. Voigt's method of writing the elastic and piezoelectric relations is

$$
\begin{aligned}
-x_x &= s_{11}X_x+s_{12}Y_y+s_{13}Z_z;\\
-y_y &= s_{12}X_x+s_{11}Y_y+s_{13}Z_z;\\
-z_z &= s_{13}X_x+s_{13}Y_y+s_{33}Z_z;\\
-y_z &= s_{44}{}^{E}Y_z-d_{14}E_x;\\
-z_x &= s_{44}{}^{E}Z_x-d_{14}E_y;\\
-x_y &= s_{66}{}^{E}X_y-d_{36}E_z;\\
P_x &= \kappa_1{}^{F}E_x-d_{14}Y_z;\\
P_y &= \kappa_1{}^{F}E_y-d_{14}Z_x;\\
P_z &= \kappa_3{}^{F}E_z-d_{36}X_y;\\
\sigma_x &= P_x+E_x/4\pi;\\
\sigma_y &= P_y+E_y/4\pi;\\
\sigma_z &= P_z+E_z/4\pi;
\end{aligned}
\qquad (1)
$$

where $x_x$, $\cdots$, $x_y$ are the six strain components, $X_x$, $\cdots$, $X_y$ the six stress components, $E_x$, $\cdots$, $E_z$ the three field strengths along the three axes, $P_x$, $\cdots$, $P_z$ the three polarizations along the three axes, and $\sigma_x$, $\cdots$, $\sigma_z$ the surface charges normal to the three axes. $s_{11}$ to $s_{66}$ are the six

[7] Voigt, *Lehrbuch der Kristall Physik* (B. G. Teubner, Leipzig, 1910).

elastic compliances, $d_{14}$, $d_{36}$ the two piezoelectric constants, $\kappa_1^F$, $\kappa_3^F$ the two dielectric susceptibilities of the crystal free to move (i.e., with the stresses equal to zero). The compliances $s_{44}^E$, $s_{66}^E$ are shown with a superscript $E$ to indicate that they should be measured with the applied field constant or zero. By eliminating the polarizations, the last six equations can be written

$$\begin{aligned}\sigma_x &= K_1^F E_x/4\pi - d_{14} Y_x,\\ \sigma_y &= K_1^F E_y/4\pi - d_{14} Z_x,\\ \sigma_z &= K_3^F E_z/4\pi - d_{36} X_y,\end{aligned} \tag{2}$$

where $K_1^F$, $K_3^F$ are the "free" dielectric constants which can be measured with the crystals unconstrained.

Voigt's relations can also be written by expressing the stresses in terms of the strains. These are obtained by solving the first six equations simultaneously, giving

$$\begin{aligned}&-X_x = c_{11}x_x + c_{12}y_y + c_{12}z_z; \quad -Y_x = c_{44}^E y_z - e_{14}E_x; \quad \sigma_x = K_1^C E_x/4\pi + e_{14}y_z;\\ &-Y_y = c_{12}x_x + c_{11}y_y + c_{13}z_z; \quad -Z_x = c_{44}^E z_x - e_{14}E_y; \quad \sigma_y = K_1^C E_y/4\pi + e_{14}z_x;\\ &-Z_z = c_{12}x_x + c_{13}y_y + c_{33}z_z; \quad -X_y = c_{66}^E x_y - e_{36}E_z; \quad \sigma_z = K_3^C E_z/4\pi + e_{36}x_y;\end{aligned} \tag{3}$$

where

$$c_{11} = \frac{\Delta^{11}}{\Delta}; \quad \cdots; \quad c_{33} = \frac{\Delta^{33}}{\Delta}; \quad \Delta = \begin{vmatrix} c_{11} & c_{12} & c_{13} \\ c_{12} & c_{22} & c_{13} \\ c_{13} & c_{13} & c_{33} \end{vmatrix};$$

$\Delta^{11}$ the determinant obtained by suppressing the first row and first column of $\Delta$, etc.,

$$c_{44}^E = 1/s_{44}^E; \quad c_{66}^E = 1/s_{66}^E; \quad e_{14} = d_{14}/s_{44}^E = d_{14}c_{44}^E; \quad e_{36} = d_{36}/s_{66}^E = d_{36}c_{66}^E;$$
$$K_1^C = K_1^F - 4\pi(d_{14}e_{14}); \quad K_3^C = K_3^F - 4\pi(d_{36}e_{36});$$

$K_1^C$, $K_3^C$ are the clamped dielectric constants of the crystal which are measured when the crystal is free from strain.

Voigt's relations express the stress, strain, and charge densities in terms of the applied field. It has been shown[8] that for a ferroelectric type crystal, the Voigt type parameters go through very wide changes when the crystal goes from a non-ferroelectric state to a ferroelectric state. However, if instead of the field strength, the polarization $P$ or the charge density $\sigma$ is used to relate the elastic terms to the piezoelectric terms it has been shown[6,8] for Rochelle salt that the elastic and piezoelectric constants are normal while the clamped dielectric constant shows a continuous variation with temperature. It is found advantageous to use a similar formulation for the constants of ADP and KDP.

For measuring purposes the formulation in terms of the surface charges is more advantageous since all the constants are directly determined by frequency and impedance measurements. Thus expressed the elastic constants correspond to the electrically open circuited condition while the Voigt constants correspond to the electrically short circuit condition. To obtain a piezoelectric constant that is independent of temperature requires relating the stress to that part of the polarization which depends on the temperature as will be shown later. The polarization constants are easily calculated from the charge constants by simple algebraic relations as will be discussed.

The two forms of the equations involving charge constants can be derived from Eqs. (1) and (3) by replacing $E$ by $\sigma$. The form corresponding to Eq. (1) is

$$\begin{aligned}&-x_x = s_{11}X_x + s_{12}Y_y + s_{13}Z_z; \quad -y_z = s_{44}^\sigma Y_z - g_{14}\sigma_x; \quad E_x = \frac{4\pi\sigma_x}{K_1^F} + g_{14}Y_z;\\ &-y_y = s_{12}X_x + s_{11}Y_y + s_{13}Z_z; \quad -z_x = s_{44}^\sigma Z_x - g_{14}\sigma_y; \quad E_y = \frac{4\pi\sigma_y}{K_1^F} + g_{14}Z_z;\\ &-z_z = s_{13}X_x + s_{13}Y_y + s_{33}Z_z; \quad -x_y = s_{66}^\sigma X_y - g_{36}\sigma_z; \quad E_z = \frac{4\pi\sigma_z}{K_3^F} + g_{36}X_y;\end{aligned} \tag{4}$$

[8] W. P. Mason, "A dynamic measurement of the elastic, electric, and piezoelectric constants of Rochelle salt," Phys. Rev. 55, 775–789 (1939).

where

$$s_{44}^{\sigma}=s_{44}^{E}-d_{14}g_{14};\quad s_{66}^{\sigma}=s_{66}^{E}-d_{36}g_{36};\quad g_{14}=4\pi d_{14}/K_1^{F};\quad g_{36}=4\pi d_{36}/K_3^{F}.$$

The superscript $\sigma$ over the elastic compliances $s_{44}$ and $s_{66}$ indicates that they are to be measured with the surface charge equal to zero. This is the value of the elastic constant measured mechanically or piezoelectrically in an air gap holder with a wide air gap. Similarly the form corresponding to Eq. (3) can be written,

$$\begin{aligned}
&-X_x=c_{11}x_x+c_{12}y_y+c_{13}z_z;\quad -Y_z=c_{44}^{\sigma}y_z-f_{14}\sigma_x;\quad E_x=\frac{4\pi\sigma_x}{K_1^{C}}-f_{14}y_z;\\
&-Y_y=c_{12}x_x+c_{22}y_y+c_{13}z_z;\quad -Z_x=c_{44}^{\sigma}z_x-f_{14}\sigma_y;\quad E_y=\frac{4\pi\sigma_y}{K_1^{C}}-f_{14}z_x;\\
&-Z_z=c_{13}x_x+c_{13}y_y+c_{33}z_z;\quad -X_y=c_{66}^{\sigma}x_y-f_{36}\sigma_z;\quad E_z=\frac{4\pi\sigma_z}{K_3^{C}}-f_{36}x_y;
\end{aligned}\tag{5}$$

where

$$c_{44}^{\sigma}=c_{44}^{E}+e_{14}f_{14};\quad c_{66}^{\sigma}=c_{66}^{E}+e_{36}f_{36};\quad f_{14}=4\pi e_{14}/K_1^{C}=g_{14}c_{44}^{\sigma};\quad f_{36}=4\pi e_{36}/K_3^{C}=g_{36}c_{66}^{\sigma}.$$

Other relations of interest that follow from Eqs. (4) and (5) are

$$g_{14}=f_{14}s_{44}^{\sigma};\quad g_{36}=f_{36}s_{66}^{\sigma};\quad \frac{4\pi}{K_1^{F}}=\frac{4\pi}{K_1^{C}}-g_{14}f_{14};\quad \frac{4\pi}{K_3^{F}}=\frac{4\pi}{K_3^{C}}-g_{36}f_{36}.\tag{6}$$

With all these interrelationships, all the different forms of expressing the piezoelectric relationships can be evaluated from one set of measurements.

If we wish to test whether the piezoelectric stress is proportional to the part of the polarization which varies with temperature and stress we can make use of the 6th and 9th equations of Eqs. (5), for example

$$-X_y=c_{66}^{\sigma}x_y-f_{36}\sigma_z,\quad E_z=\frac{4\pi\sigma_z}{K_3^{C}}-f_{36}x_y.\tag{7}$$

We can write that the total polarization is equal to a part $Pz_0$ which is independent of the temperature and strain and a part $P_z'$ which varies with temperature and strain. Then the charge density $\sigma_z$ is equal to

$$\sigma_z=\frac{E_z}{4\pi}+Pz_0+P_z'=\frac{E_z}{4\pi}(1+4\pi K_{30})+P_z'=\frac{E_zK_{30}}{4\pi}+P_z',\tag{8}$$

where $K_{30}$ is the temperature and strain independent part of the dielectric constant. Introducing this value into Eq. (7), the equations for the piezoelectric effect become

$$-X_y=c_{66}^{\sigma}x_y-f_{36}\left[\frac{E_zK_{30}}{4\pi}+P_z'\right],\tag{9}$$

$$E_z=\frac{4\pi}{K_3^{C}}\left(\frac{E_zK_{30}}{4\pi}+P_z'\right)-f_{36}x_y\quad\text{or}\quad E_z=\frac{4\pi}{(K_3^{C}-K_{30})}P_z'-\frac{f_{36}K_3^{C}}{K_3^{C}-K_{30}}x_y.\tag{10}$$

Introducing this value back in Eq. (9) the two piezoelectric equations become

$$E_z=\frac{4\pi P_z'}{K_3^{C}-K_{30}}-f_{36}^{*}x_y;\quad -X_y=\left(c_{66}^{\sigma}+\frac{f_{36}^{2}K_{30}K_3^{C}}{4\pi(K_3^{C}-K_{30})}\right)x_y-f_{36}^{*}P_z',\tag{11}$$

where $f_{36}^{*}$ is a constant relating the piezoelectric stress $X_y$ to the temperature variable portion of the polarization $P_z'$. Since we cannot suppress one portion of the polarization, these equations are not useful for measuring purposes, but if we have evaluated the charge constants, the proportionality of the piezoelectric stress to the polarization component $P_z'$ can be tested by determining the ratio

$$f_{36}^{*}=\frac{X_y}{P_z'}=\frac{f_{36}K_3^{C}}{K_3^{C}-K_{30}}.\tag{12}$$

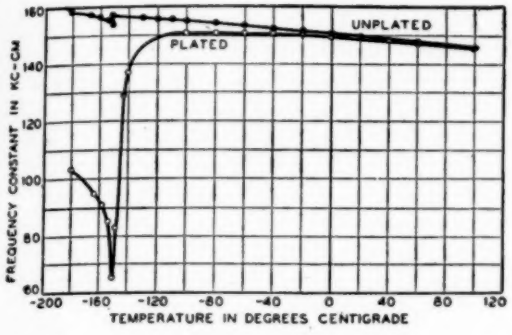


FIG. 3. Frequency constants of plated and bare 45° $Z$-cut KDP crystals.

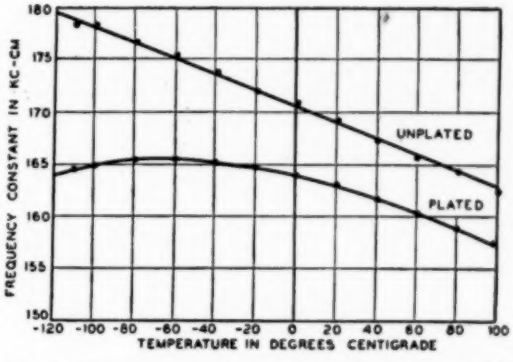


FIG. 4. Frequency constants of plated and bare 45° $Z$-cut ADP crystals.

### III. MEASUREMENTS OF THE ELASTIC CONSTANTS OF ADP AND KDP OVER A WIDE TEMPERATURE RANGE

In order to measure the elastic constants of these crystals, seven oriented cuts of each type of crystal are used. When the crystals are plated and their resonant frequencies are measured, the short circuited elastic compliances $s_{ij}^{E}$ are obtained as discussed in Appendix I. On the other hand, if the plating is removed and the crystals measured in an air gap holder with a large air gap, the open circuited constants $s_{ij}^{\sigma}$ are obtained. Near the Curie point, there is a large difference between these constants, as can be seen from Fig. 3 which shows a measurement of the frequency constant of a KDP crystal cut normal to the $Z$ axis, with its length at 45° from the $X$ and $Y$ axes. This crystal vibrates longitudinally. As can be seen the frequency constant of the plated crystal varies from 150 kilocycle-centimeters to 65 kilocycle-centimeters in the neighborhood of the Curie temperature (−151°C or +122°K). The frequency constant of the unplated crystal is a straight-line function of the temperature until the Curie temperature is reached. At that temperature a sudden discontinuity of the resonant frequency occurs larger than that occurring in Rochelle salt. This is caused by what Mueller[9] has called a "morphic" effect caused by a slight transformation of the crystal lattice.

Similar curves for a 45° $Z$-cut ADP crystal are shown by Fig. 4. At the temperature of −125°C (148°K) the crystal suddenly shatters into very small fragments. Even though the temperature was taken very slowly through this region it was not possible to prevent this shattering. Since the dielectric constant and the elastic compliance of the plated crystal do not increase sharply to a maximum, we conclude that the phase change is not one which involves the dipoles contributing to the dielectric and piezoelectric effect. It is a phase change of the first kind while that for KDP is a transition occurring over a range of temperatures.

Since it is simpler to measure the properties of a plated crystal, this has been done for the various cuts of ADP crystals and KDP crystals. In order to supplement such data near the Curie point of KDP, some measurements were made of the elastic constants of the unplated crystals cut normal to the $Z$ axis.

Five of the crystals of each set were longitudinal crystals with their lengths 6 to 8 times their width and 12.5 times their thickness. Crystals of these dimensions have been found experimentally to be free of other modes of motion and to have a very small width correction to the frequency of the longitudinal mode. Hence the elastic constants are the values of Young's modulus appropriate for the plated crystal. The other two crystals of each set are $X$-cut and $Z$-cut crystals with one dimension long compared to the width and thickness. It is shown in the Appendix that such crystals produce shear modes of motion coupled to flexure modes. By properly dimensioning the crystals, the effect of the flexure can be eliminated and pure shear modes result. This allows one to measure the $c_{44}$

[9] H. Mueller, "Properties of Rochelle salt IV," Phys. Rev. **58**, 805–811 (1940).

TABLE I. Resonant frequencies of ADP.

| Temperature in degrees cent. | X cut, L=22.5° from Z axis L=20.015 mm W= 2.985 mm T= 0.9 mm plated resonant freq. | X cut, L=45° from Z axis L=20.00 mm W= 2.96 mm T= 0.97 mm plated resonant freq. | X cut, L=67.5° from Z axis L=10.00 mm W= 2.97 mm T= 0.97 mm plated resonant freq. | Z cut, L=22.5° from X axis L=19.69 mm W= 2.94 mm T=20.96 mm plated resonant freq. | Z cut, L=45° from X axis L=19.74 mm W= 2.95 mm T= 0.96 mm plated resonant freq. | Z cut, L=45° from X axis L=19.74 mm W= 2.95 mm T= 0.96 mm unplated resonant freq. |
|---|---|---|---|---|---|---|
| 100 | —— | —— | —— | 98,248 | 79,720 | 82,200 |
| 90 | —— | —— | —— | 98,794 | 80,110 | 82,680 |
| 80 | —— | —— | —— | 99,256 | 80,560 | 83,220 |
| 70 | 88,900 | 94,400 | 116,000 | 99,784 | 80,880 | 83,720 |
| 60 | 88,980 | 94,590 | 116,320 | 100,200 | 81,300 | 84,250 |
| 50 | 89,020 | 94,780 | 116,910 | 100,626 | 81,640 | 84,730 |
| 40 | 89,100 | 94,930 | 117,420 | 101,047 | 81,980 | 85,210 |
| 30 | 89,150 | 95,110 | 117,600 | 101,421 | 82,260 | 85,700 |
| 25 | 89,190 | 95,200 | 118,090 | 101,630 | 82,420 | 85,910 |
| 20 | 89,210 | 95,300 | 118,160 | 101,908 | 82,570 | 86,140 |
| 10 | 89,300 | 95,490 | 118,360 | 102,208 | 82,820 | 86,590 |
| 0 | 89,380 | 95,640 | 118,900 | 102,667 | 83,110 | 87,050 |
| −10 | 89,450 | 95,810 | 119,290 | 102,817 | 83,280 | 87,420 |
| −20 | 89,510 | 96,000 | 119,750 | 103,112 | 83,470 | 87,840 |
| −30 | 89,590 | 96,200 | 119,910 | 103,366 | 83,620 | 88,190 |
| −40 | 89,670 | 96,380 | 120,340 | 103,591 | 83,740 | 88,520 |
| −50 | 89,720 | 96,555 | 120,890 | 103,800 | 83,850 | 88,890 |
| −60 | 89,800 | 96,700 | 121,120 | 103,936 | 83,890 | 89,220 |
| −70 | 89,880 | 96,900 | 121,320 | 104,040 | 83,900 | 89,510 |
| −80 | 89,940 | 97,100 | 121,840 | 104,078 | 83,860 | 89,910 |
| −90 | 90,010 | 97,290 | 122,250 | 104,063 | 83,730 | 90,220 |
| −100 | 90,100 | 97,460 | 122,350 | 103,946 | 83,520 | 90,590 |
| −110 | 90,190 | 97,620 | 122,750 | 103,771 | 83,340 | 90,950 |
| −120 | 90,230 | 97,780 | 123,150 | 103,475 | 83,040 | 91,300 |

and $c_{66}$ shear elastic constants directly. An alternate method used previously with Rochelle salt[8] was to use a thickness vibrating crystal dimensioned to eliminate extraneous modes of motion. However the dimensioning necessary for the face shear mode is less complicated and moreover the $c_{44}$ and $c_{66}$ constants are evaluated directly without allowing for the orientation necessary to drive the high frequency shear modes. By measuring high harmonics of the face shear mode, a frequency corresponding to a crystal very long compared with its width is obtained, and this provides a measurement free of width corrections for the shear modes.

Two of the length vibrating crystals are cut normal to the $Z$ axis of the crystal with their lengths 22.5° and 45° from the $X$ axis, respectively. The value of $s_{11}^{E'}$ (the inverse of Young's modulus) along the length of the crystal is given in the equation[8]

$$s_{11}^{E'} = s_{11}(\sin^4\varphi + \cos^4\varphi) + (2s_{12} + s_{66}^{E})\sin^2\varphi\cos^2\varphi. \quad (13)$$

Hence the two values of the frequency for these

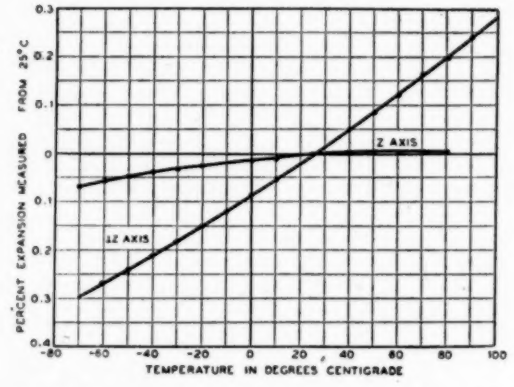


FIG. 5. Thermal expansion measurements for ADP.

TABLE II. Elastic compliances of ADP crystal cuts.

| Temperature in °C | X cut, L=22.5° from Z axis $s_{22}'^{E}$ | X cut, L=45° from Z axis $s_{22}'^{E}$ | X cut, L=67.5° from Z axis $s_{22}'^{E}$ | Z cut, L=22.5° from X axis $s_{22}'^{E}$ | Z cut, L=45° from X axis $s_{22}'^{E}$ | Z cut, L=45° from X axis $s_{22}'^{D}$ |
|---|---|---|---|---|---|---|
| 100 | — | — | — | $3.70\times10^{-12}$ | $5.59\times10^{-12}$ | 5.26 |
| 90 | — | — | — | 3.67 | 5.50 | 5.20 |
| 80 | — | — | — | 3.63 | 5.49 | 5.12 |
| 70 | $4.40\times10^{-12}$ | $3.895\times10^{-12}$ | $2.575\times10^{-12}$ | 3.57 | 5.40 | 5.06 |
| 60 | 4.39 | 3.875 | 2.550 | 3.545 | 5.42 | 5.00 |
| 50 | 4.38 | 3.86 | 2.535 | 3.52 | 5.35 | 4.93 |
| 40 | 4.37 | 3.855 | 2.52 | 3.50 | 5.29 | 4.88 |
| 30 | 4.36 | 3.840 | 2.503 | 3.47 | 5.27 | 4.83 |
| 25 | 4.355 | 3.828 | 2.496 | 3.44 | 5.25 | 4.79 |
| 20 | 4.35 | 3.815 | 2.486 | 3.425 | 5.23 | 4.76 |
| 10 | 4.34 | 3.795 | 2.472 | 3.41 | 5.20 | 4.70 |
| 0 | 4.33 | 3.775 | 2.45 | 3.40 | 5.16 | 4.65 |
| −10 | 4.315 | 3.765 | 2.43 | 3.36 | 5.13 | 4.60 |
| −20 | 4.31 | 3.75 | 2.415 | 3.34 | 5.09 | 4.55 |
| −30 | 4.305 | 3.73 | 2.404 | 3.335 | 5.07 | 4.53 |
| −40 | 4.295 | 3.72 | 2.39 | 3.33 | 5.06 | 4.51 |
| −50 | 4.29 | 3.715 | 2.37 | 3.32 | 5.05 | 4.47 |
| −60 | 4.28 | 3.70 | 2.36 | 3.305 | 5.04 | 4.42 |
| −70 | 4.275 | 3.685 | 2.35 | 3.295 | 5.045 | 4.41 |
| −80 | 4.26 | 3.67 | 2.33 | 3.29 | 5.05 | 4.40 |
| −90 | 4.25 | 3.655 | 2.32 | 3.295 | 5.06 | 4.37 |
| −100 | 4.24 | 3.64 | 2.31 | 3.30 | 5.07 | 4.34 |
| −110 | 4.23 | 3.625 | 2.29 | 3.31 | 5.12 | 4.33 |
| −120 | 4.22 | 3.61 | 2.28 | 3.34 | 5.14 | 4.32 |

two crystals determine the $s_{11}$ and $(2s_{12}+s_{66}^{E})$ constants. The next three crystals had their major surfaces normal to the $X$ axis and their lengths at approximately 22.5°, 45°, and 67.5° from the $Y$ axis. The values of their Young's moduli are given by the equation[10]

$$s_{22}^{E'}=s_{11}\cos^4\psi+(2s_{13}+s_{44}^{E})\sin^2\psi\cos^2\psi+s_{33}\cos^4\psi, \quad (14)$$

where $\psi$ is the angle of the length measured from the $Y$ axis.

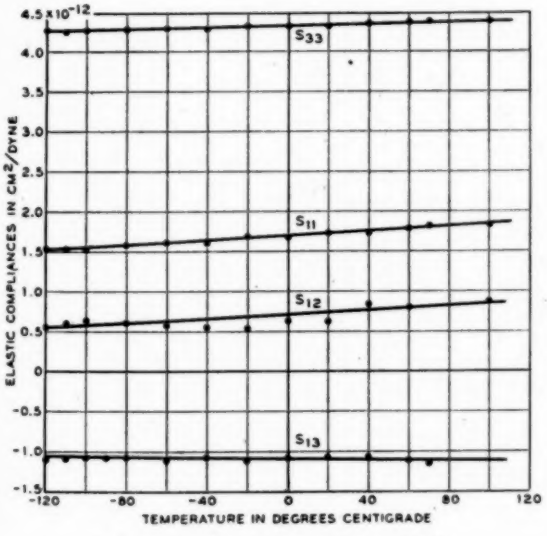


FIG. 6. Elastic compliances for ADP.

All of the crystals were lightly gold plated by the evaporation process and were held at their nodal point by a spring clamp. Five such crystals were put in one chamber[11] for which the temperature and humidity could be accurately controlled. For temperatures higher than room temperature, a heater in the central chamber was used to increase the temperature of the air. This air was circulated through the measuring chamber by means of a blower system and the

[10] This is proved for Rochelle salt in reference (8), Appendix I. The same proof holds for ADP if we let $s_{23}=s_{13}$; $s_{22}=s_{11}$.

[11] This chamber was designed and built by T. G. Kinsley and all the measurements over a wide temperature range have been taken by Kinsley and Mrs. J. Darr.

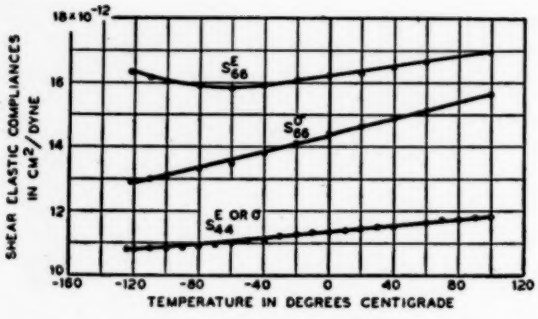


FIG. 7. Shear compliances for ADP crystals.

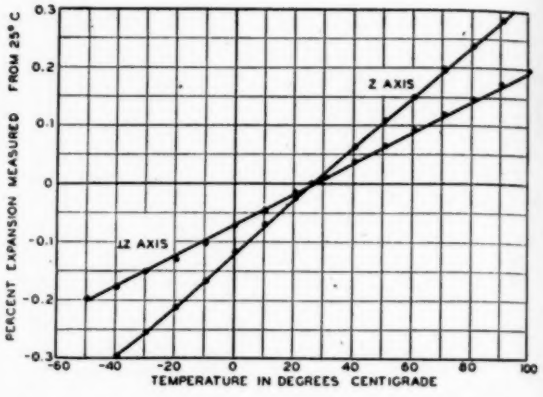


FIG. 8. Thermal expansion measurements for KDP.

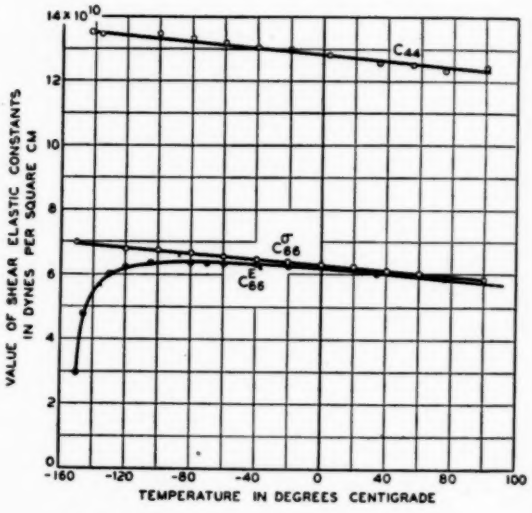


FIG. 9. Shear elastic constants of KDP.

temperature could be controlled by a thermostat on the heater system or on the blower system. For temperatures below the normal room temperature, dry ice or liquid nitrogen were placed in containers in the central chamber. The temperature in the measuring chamber was controlled by a thermostat on the blower system, and was measured by a mechanical thermometer or a thermocouple inserted near the crystal plates. With this arrangement temperatures from $-165$°C to $+250$°C can be maintained in the chamber. The humidity is kept low by the use of calcium chloride.

Table I shows the experimental data obtained for six vibrating ADP crystals. From these data, and the frequency equation

$$f=(1/2l)(1/\rho s_{22}')^{\frac{1}{2}}, \qquad (15)$$

it is possible to calculate the value of the elastic compliance $s_{22}'$ (inverse of Young's modulus) at the temperatures given. To determine the true values however, it is necessary to know the temperature expansion along the two axes $X=Y$ and $Z$ since this affects the values of $l$ and $\rho$. The value of $\rho$ has been found to be 1.804 by pycnometer methods.[12] The percentage expansions measured[13] from 25°C, for the two axes, are shown by Fig. 5. The expansion along the $Z$ axis is considerably smaller and reaches a zero slope at temperatures of about 60° to 80°C. Table II gives values of elastic compliances for the six ADP crystal cuts over the temperature range measured. From these values and Eqs. (13) and (14), the value of $s_{11}$, $s_{33}$, $(2s_{12}+s_{66}^E)$ and $(2s_{12}+s_{44}^E)$ can be calculated. The values of $s_{11}$ and $s_{33}$ are shown by Fig. 6.

To obtain the values of the two shear constants $s_{44}^E$ and $s_{66}^E$, two crystals were cut normal to the $X$ and $Z$ axes, respectively. These were dimensioned so that the shear resonance was obtained free from the other modes of motion (mostly flexural modes). For the 0° $X$ cut, having the dimensions $L$ (along $Z$) $=29.39$ mm; $W$ (along $Y$) $=5.76$ mm; $T=1.025$ mm, there was a first resonance of 203,475 cycles, a third harmonic of 572,020 cycles, and a fifth harmonic of 953,500. These give an assymptotic frequency constant of 109.8 kilocycle centimeters, which results in a shear elastic compliance of $s_{44}^E=11.50\times10^{-12}$. Since the piezoelectric coupling is very small along the $X$ axis, this is also within experi-

[12] This measurement was made by W. L. Bond.
[13] The expansion measurements have been made by Miss E. A. Baar.

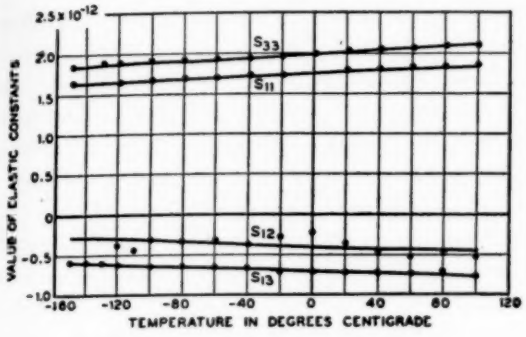


FIG. 10. Elastic compliances for KDP.

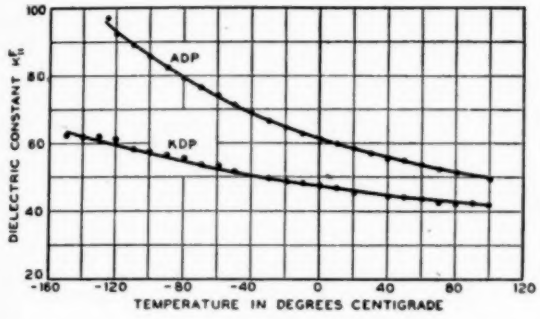


FIG. 11. Dielectric constants of ADP and KDP cut normal to the $X$ axis.

mental error the value of the $s_{44}^{\sigma}$ constant. By measuring the fifth harmonic over a temperature range, the variation of the $s_{44}$ constant was obtained as a function of temperature and is shown plotted by Fig. 7. In a similar manner a 0° $Z$-cut crystal having the dimensions $L=19.82$ mm along $X$, $W=2.96$ mm along $Y$ and $T=1.11$ mm was found to have the first, fifth, and seventh harmonics of 321,260 cycles, 1,575,298 cycles, and 2,179,250 cycles, giving a frequency constant of 92.0 kilocycle centimeters for the shear mode. Over a temperature range, the corresponding values of $s_{66}^{E}$ are shown plotted in Fig. 7. By removing the plating another resonance curve was obtained and the corresponding elastic constant $s_{66}^{\sigma}$ is shown plotted by the full line of Fig. 7. It will be noted that the charge or "open circuited" elastic compliance is a linear function of the temperature while the potential or "short circuited" elastic compliance shows the effect of the variability of the electromechanical coupling with temperature. By using these values of the shear elastic compliances and the previously determined values of $(2s_{13}+s_{44}^{E})$ and $(2s_{12}+s_{66}^{E})$,

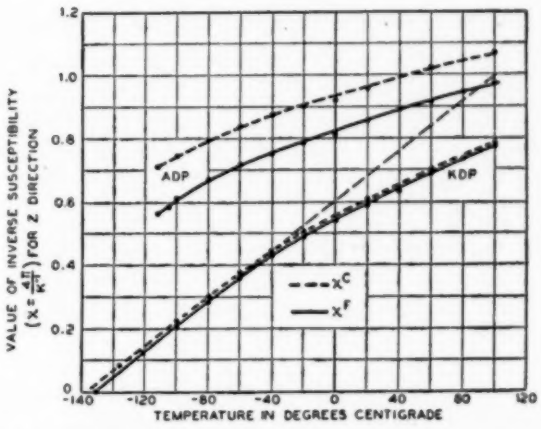


FIG. 12. Inverse of dielectric susceptibility for ADP and KDP cut normal to the $Z$ axis.

the values of $s_{12}$ and $s_{13}$ can be evaluated and are shown plotted in Fig. 6. It will be noted that all of the open circuited elastic constants show a very regular variation with temperature. The direction in which the least temperature variation is to be expected for a longitudinal mode is along the $Z$ axis. However, since no piezoelectric constant exists for driving such a vibration, this cannot be put to practical use.

A similar set of measurements has been made for all of the constants of potassium dihydrogen phosphate. In order not to burden the paper with too much detailed data, only the results are given. The changes in length of the two axes with temperature are shown by Fig. 8. The shear elastic constants of KDP, down to the Curie temperature, are shown by Fig. 9. On account of the large variation in the $c_{66}^{E}$ elastic constant this is plotted rather than its reciprocal $s_{66}^{E}$. As in ADP the coupling for an $X$-cut crystal is so small that no appreciable difference occurs between $c_{44}^{E}$ and $c_{44}^{\sigma}$. The remaining elastic constants of KDP are shown by Fig. 10. These are somewhat less than previous values of Lüdy,[2] who found values of $1.9\times10^{-12}$ for $s_{11}$ and $2.2\times10^{-12}$ for $s_{33}$ at room temperature. Other measurements of shear elastic constants $s_{44}^{E}$ and $s_{66}^{E}$ have recently been published by Jaffe.[4] For KDP he finds $s_{66}^{E}=15.5\times10^{-12}$ cm²/dyne at room temperature which is slightly less than the value of $16.4\times10^{-12}$ found here. His values for ADP of $s_{44}=11.6\times10^{-12}$ and $s_{66}^{E}=16.6\times10^{-12}$ check well with the values found here for room temperature.

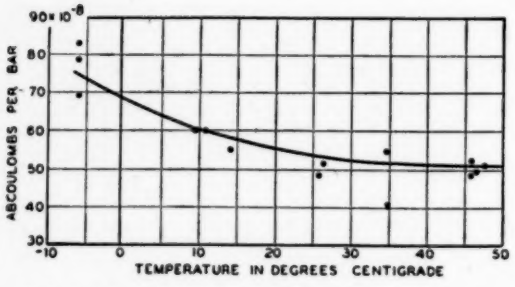


FIG. 13. Static measurements of the piezoelectric constant of KDP.

## IV. DIELECTRIC AND PIEZOELECTRIC CONSTANTS OF ADP AND KDP

The dielectric constants of ADP and KDP have been measured by measuring the capacitances of the free crystals in a capacitance bridge at 1000 cycles. The results agree well with the original measurements of Busch.[1] The results for the two crystals normal to the $X$ axis are shown by Fig. 11. On account of the high dielectric constants near the Curie point for KDP cut normal to the $Z$ axis, the reciprocal susceptibility

$$\chi_3^F = 4\pi/(K_3^F - 1) \tag{16}$$

is plotted in Fig. 12. According to the theory discussed in the next section, this inverse susceptibility should be proportional to the difference in temperature between the actual temperature and the Curie temperature. This proportionality exists for about 100° above the Curie temperature, −151°C, but above this a bending off occurs which would be accounted for if we assume a temperature independent dielectric constant of value 4.5. This gives a "free" dielectric constant of

$$K_3^F = 4.5 + 3122/(T+151) \tag{17}$$

at any temperature above the Curie temperature of −151°C, and indicates that the dielectric constant is made up of a part which varies only slightly with temperature, and another part, due presumably to the hydrogen bonds, which varies inversely as the temperature difference. A similar equation fitting ADP is

$$K_3^F = 7.0 + 2670/(T+287), \tag{18}$$

indicating that the Curie temperature due to the hydrogen bonds is in the neighborhood of absolute zero. The clamped inverse susceptibilities are calculated from the piezoelectric constants and Eq. (3).

The piezoelectric constant of KDP was measured by W. L. Bond of these Laboratories in 1937. His method was a static one of suddenly removing a weight on a lever placed on both a quartz crystal and a KDP crystal and adjusting the position of the fulcrum until the voltage generated by one crystal balanced that from the other. From the piezoelectric equations given in section II, the constant of KDP can be compared with that of quartz, which is known quite precisely. Bond's results are given in Fig. 13. Because of the fact that KDP has a volume leakage much greater than that of quartz, this is not an accurate method and Bond's results are somewhat lower than those presented here which were measured by dynamic methods.

It is shown in the appendix that the separation of the resonant and anti-resonant frequencies of a longitudinally vibrating crystal is related to the electromechanical coupling in a crystal which depends on the ratio

$$k = d(4\pi/K^F s^E)^{\frac{1}{2}}, \tag{19}$$

where $d$ is the piezoelectric constant for the longitudinal mode, $K^F$ the "free" dielectric constant appropriate to the crystal, and $s^E$ the inverse of Young's modulus for the crystal. For a 45° $Z$ cut this becomes

$$k = \frac{d_{36}}{2}(4\pi/K_3^F s_{11}^{E'})^{\frac{1}{2}}$$

$$= \frac{d_{36}}{2}\left[4\pi \Big/ K_3^F\left(\frac{s_{11}+s_{12}}{2}+\frac{s_{66}^E}{4}\right)\right]^{\frac{1}{2}}, \tag{20}$$

where $s_{11}^{E'}$ is the inverse of the short circuited

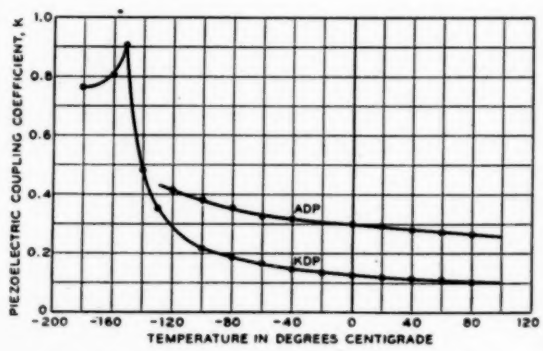


FIG. 14. Coupling constants of ADP and KDP.

value of Young's modulus. The frequency of a plated crystal is controlled by

$$f_p=(1/2l)(1/\rho s_{11}^{E'})^{\frac{1}{2}}, \tag{21}$$

while that of a bare crystal is controlled by

$$f_b=(1/2l)(1/\rho s_{11}^{\sigma})^{\frac{1}{2}}. \tag{22}$$

Hence, taking the ratio and introducing the results of Eq. (3)

$$\left(\frac{f_p}{f_b}\right)^2=\frac{s_{11}^{\sigma'}}{s_{11}^{E'}}=\frac{\frac{s_{11}+s_{12}}{2}+\frac{1}{4}\frac{1}{s_{66}^{\sigma}}}{\frac{s_{11}+s_{12}}{2}+\frac{1}{4}\frac{1}{s_{66}^{E}}}$$

$$=\frac{\frac{s_{11}+s_{12}}{2}+\frac{1}{4}(s_{66}^{E}-d_{36}g_{36})}{\frac{s_{11}+s_{12}}{2}+\frac{1}{4}\frac{1}{s_{66}^{E}}}=1-\frac{d_{36}g_{36}}{4s_{11}^{E'}}. \tag{23}$$

But since $g_{36}=4\pi d_{36}/K_3^F$, we have

$$1-\frac{d_{36}g_{36}}{4\pi s_{11}^{E'}}=1-\frac{d_{36}^2}{4}\left(\frac{4\pi}{K_3^F s_{11}^{E'}}\right)$$

$$=1-k^2=\left(\frac{f_p}{f_b}\right)^2. \tag{24}$$

Hence, the piezoelectric coupling $k$ can be evaluated from the data of the last two crystals of Table I and is shown plotted in Fig. 14 for ADP. Similarly the data of Fig. 3 gave the coupling for KDP, which is also shown on Fig. 14. It will be noted that the coupling rises to 92 percent at the

TABLE III. Piezoelectric constants of ADP.

| Temperature in °C | $d_{36}\times10^8$ | $e_{36}\times10^{-4}$ | $g_{36}\times10^3$ | $f_{36}\times10^{-4}$ | $K_3^C$ | $f_{36}^*\times10^{-4}$ |
|---|---|---|---|---|---|---|
| 100 | 129.5 | 7.62 | 117 | 7.47 | 12.9 | 16.3 |
| 80 | 132.5 | 7.82 | 116 | 7.55 | 13.0 | 16.3 |
| 60 | 136.0 | 8.14 | 116 | 7.67 | 13.3 | 16.2 |
| 40 | 142.0 | 8.61 | 117.5 | 7.87 | 13.6 | 16.2 |
| 20 | 148 | 9.04 | 118.5 | 8.09 | 14.0 | 16.2 |
| 0 | 155 | 9.54 | 120 | 8.37 | 14.4 | 16.3 |
| −20 | 161 | 10.0 | 119 | 8.44 | 14.9 | 16.0 |
| −40 | 170 | 10.65 | 121 | 8.75 | 15.4 | 16.1 |
| −60 | 180 | 11.32 | 122 | 8.94 | 16.0 | 15.9 |
| −80 | 198 | 12.4 | 125 | 9.35 | 16.7 | 16.1 |
| −100 | 207 | 12.9 | 126 | 9.6 | 17.3 | 16.1 |
| −110 | 242 | 14.9 | 130 | 10.0 | 18.2 | 16.3 |
| −120 | 261 | 15.4 | 132 | 10.2 | 18.6 | 16.3 |
| −122 | 270 | 15.6 | 132 | 10.3 | 19.0 | 16.3 |

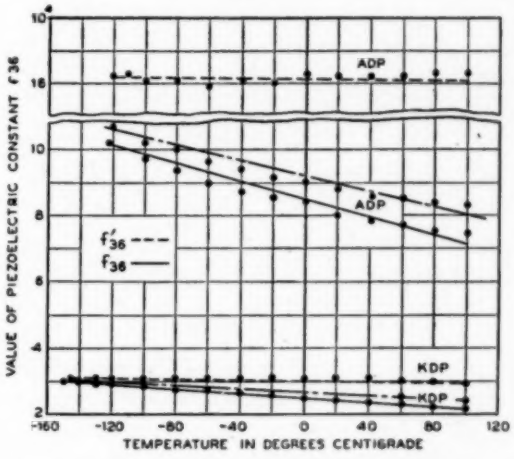


FIG. 15. Values of piezoelectric constant $f_{36}$ for KDP and ADP.

—— Ratio of piezoelectric stress to surface charge $\sigma$.
—·— Ratio of piezoelectric stress to polarization $P$.
------ Ratio of piezoelectric stress to dipole polarization $P_D$.

Curie temperature and remains high in the ferroelectric region for small applied fields.

Since the "free" dielectric constant may be obtained from Fig. 12, and the short circuited compliance modulus is given in the last column of Table II for ADP, all the necessary data are given for determining the piezoelectric constant $d_{36}$. This is shown tabulated in Table III. From the relations

$$e_{36}=d_{36}/s_{66}^{E};\quad g_{36}=4\pi d_{36}/K_3^F;$$
$$f_{36}=g_{36}c_{66}^{\sigma}, \tag{25}$$

TABLE IV. Piezoelectric constants of KDP.

| Temperature in °C | $d_{36}\times10^8$ | $e_{36}\times10^{-4}$ | $g_{36}\times10^3$ | $f_{36}\times10^{-4}$ | $K_{33}^C$ | $f_{36}^*\times10^{-4}$ |
|---|---|---|---|---|---|---|
| 100 | 50.4 | 2.91 | 36.8 | 2.16 | 17.0 | 2.93 |
| 80 | 54.0 | 3.17 | 37.2 | 2.21 | 18.0 | 2.96 |
| 60 | 59.0 | 3.5 | 38.6 | 2.32 | 18.9 | 3.05 |
| 40 | 63.2 | 3.8 | 38.8 | 2.35 | 20.3 | 3.02 |
| 20 | 69.6 | 4.26 | 39.4 | 2.44 | 21.8 | 3.09 |
| 0 | 76.2 | 4.73 | 39.6 | 2.50 | 23.75 | 3.09 |
| −20 | 85.9 | 5.39 | 40.4 | 2.58 | 26.0 | 3.13 |
| −40 | 98.6 | 6.24 | 41.0 | 2.66 | 29.4 | 3.12 |
| −60 | 119.0 | 7.55 | 41.5 | 2.73 | 34.9 | 3.12 |
| −80 | 153.0 | 9.75 | 42.0 | 2.79 | 43.9 | 3.10 |
| −100 | 202 | 12.8 | 42.2 | 2.81 | 57.6 | 3.02 |
| −120 | 334 | 20.8 | 43.0 | 2.93 | 89.8 | 3.06 |
| −130 | 480 | 29.0 | 43.2 | 2.97 | 123.0 | 3.07 |
| −140 | 875 | 47.3 | 43.4 | 2.98 | 200.0 | 3.03 |
| −145 | 1465 | 70.0 | 43.6 | 3.02 | 291.0 | 3.06 |
| −150 | 4400 | 130.0 | 44.0 | 3.07 | 542.0 | 3.03 |

TABLE V.

| Frequency | 102,250 | 102,270 | 102,280 | 102,290 | 102,300 | 102,310 | 102,320 | 102,330 |
|---|---|---|---|---|---|---|---|---|
| Equivalent shunt resistance in ohms | 1,200,000 | 680,000 | 570,000 | 500,000 | 550,000 | 700,000 | 900,000 | 1,180,000 |

all the forms of the piezoelectric constants are determined and are listed in Table III. The clamped dielectric constants $K_3^C$ can be calculated from this data by means of the formula

$$K_3^C = K_3^F - 4\pi e_{36} d_{36}. \quad (26)$$

This is given in the next to the last column and is shown plotted as the inverse susceptibility in Fig. 12. The corresponding data for KDP are given in Table IV. The inverse susceptibilities of the clamped dielectric constant are plotted by the full lines of Fig. 12. For KDP the values lie on a curve determined by the equation

$$K_3^C = 4.5 + 3100/(T+154.5), \quad (27)$$

indicating that the Curie temperature for the clamped crystal is about 3.5°C lower than for the free crystal. For ADP the equivalent formula is

$$K_3^C = 7.0 + 2560/(T+342). \quad (28)$$

The value of the indicated Curie temperature of −342°C is below absolute zero and indicates that ADP would not be ferroelectric at any temperature.

We note from Tables III and IV that the piezoelectric constant $f_{36}$, which relates the piezoelectric stress to the charge $\sigma_s$, is not a constant independent of temperature. This is shown by the curves of Fig. 15 which show a plot of the constants for ADP and KDP. To test out the supposition that the stress is proportional to that part of the polarization that is temperature variable, use is made of Eq. (12)

$$f_{36}^* = f_{36} K_3^C/(K_3^C - K_{30}). \quad (12)$$

The last column in each table shows a calculation of $f_{36}^*$ and the values for ADP and KDP are plotted by the dotted lines of Fig. 15. For ADP and KDP this supposition appears to be borne out.

Measurements were also made for $d_{14}$ for both ADP and KDP at room temperature. On account of the very small coupling for these modes, the separations of resonant and anti-resonant frequencies of 45° X-cut crystals do not become a very reliable method for measuring the constants. This follows from the fact that the maximum and minimum points for the current through the crystal become more widely separated than they should be if the crystal had no mechanical resistance. In order to determine this constant, a KDP crystal was placed in an impedance bridge and the equivalent shunt resistance was measured as a function of frequency near resonance. The result is shown by Table V for a KDP crystal having the dimension $L = 19.56$ mm; $W = 6.10$ mm; $T = 0.90$ mm. The shunt capacity of the crystal was measured and was found to be 54 $\mu\mu$f agreeing with the dielectric constant of 46 shown in Fig. 11. By considering the equivalent circuit of the crystal given in Fig. 16, it can be shown that the equivalent shunt resistance of the crystal is given by the formula

$$R_S = R_1\left[1+\left(\frac{r}{2\pi f_R R_1 C_0}\right)^2\left(\frac{f_R}{f}-\frac{f}{f_R}\right)^2\right], \quad (29)$$

where $R_1$ is the shunt resistance at resonance, i.e., the $R_1$ of Fig. 16, $C_0$ the shunt capacity of the crystal, $r$ the ratio of $C_0$ to $C_1$, and $f_R$ the resonant frequency of the crystal. From the above measurements $R_1 = 500{,}000$ ohms; $f_R = 102{,}290$ cycles; $C_0 = 54\times10^{-12}$ farad. At 40 cycles from resonance the ratio of $R_s/R_1 = 2.4$. This gives enough data to solve for $r$, which we find to be 26,400. From the appendix, we find that the electromechanical coupling factor is

$$k = \left(1\Big/1+\frac{8}{\pi^2 r}\right)^{\frac{1}{2}} = 0.00685. \quad (30)$$

From the resonant frequency and the length, $s_{22}'$

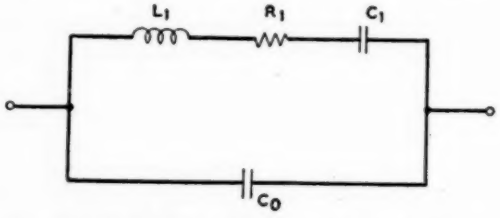


FIG. 16. Equivalent electrical circuit of a crystal.

is found to be $2.56\times10^{-12}$ cm²/dyne. Hence

$$d_{14}=2\times k(K_1^F s_{22}'/4\pi)^{\frac{1}{2}}=4.2\times10^{-8}(\text{KDP}). \quad (31)$$

A similar measurement for a 45°-, X-cut ADP crystal gives

$$d_{14}=5.0\times10^{-8}(\text{ADP}). \quad (32)$$

Hence, although the dielectric constants normal to the $X$ direction are very large, the piezoelectric constants for this direction are very small.

One other effect common to ADP and KDP not previously pointed out is that they have a volume conductance much larger than that for Rochelle salt. For crystals grown from Baker's C.P. grade salt, volume resistivities were measured by H. B. Briggs and J. B. Johnson with the results shown by Fig. 17. By comparing the conductivities between central electrodes compared to conductivities measured between guard rings on the edges, it was established that the surface leakage was negligible compared to the volume leakage provided the crystals were placed in a dry atmosphere. Certain impurities introduced into the crystal lattice have a marked effect in increasing this conductivity as will be discussed in a paper by Holden and Murphy.

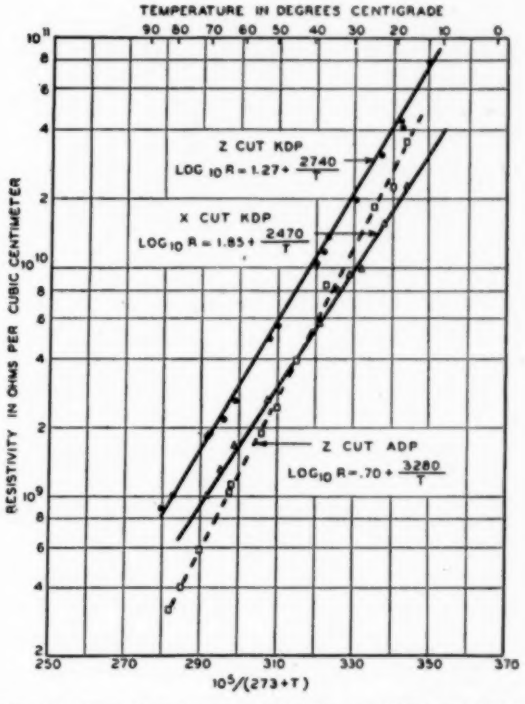
TEMPERATURE IN DEGREES CENTIGRADE
90 80 70 60 50 40 30 20 10 0
RESISTIVITY IN OHMS PER CUBIC CENTIMETER
Z CUT KDP
LOG 10 R = 1.27 + 2740/T
X CUT KDP
LOG 10 R = 1.85 + 2470/T
Z CUT ADP
LOG10 R = .70 + 3280/T
250 270 290 310 330 350 370
10⁵/(273+T)

FIG. 17. Specific volume resistivities of ADP and KDP.

## V. COMPARISON OF EXPERIMENTAL RESULTS WITH THEORY

The crystal structure of KDP has been worked out by West[14] and is shown by Fig. 18, taken from a paper by Slater,[5] which presents a theory for explaining the ferroelectric properties of KDP. The phosphate groups, $PO_4$, consist of a phosphorus tetrahedrally surrounded by four oxygens, and are shown by the tetragons. Each phosphate group is surrounded tetrahedrally by four other phosphate groups. The positions of the potassiums in the crystal are shown by the circles. The positions of the hydrogen ions are not shown by x-ray analysis, but according to Slater's model one is located somewhere on the connecting line between each pair of phosphate groups as shown in the figure. The position of these hydrogen ions varies with temperature but most of the time two and only two ions will be near each phosphate group.

Each $H_2PO_4$ group forms not only an ion but a dipole, and the dielectric behavior shows that the orientation of these dipoles along the $+c$ (or $Z$) axis or $-c$ axis must have a lower energy than at right angles to it. Hence at very low temperatures, all the dipoles must lie along the $Z$ axis. All the dipoles in one region or "domain" are lined up along the positive $Z$ axis while neighboring domains may have the direction of the dipoles reversed, and thus each domain becomes spontaneously polarized. As the temperature rises the hydrogen ions will acquire a kinetic energy and some of the dipoles will be forced into directions normal to the $Z$ axis. When this condition occurs, the crystal loses its spontaneous polarization. By calculating the number of arrangements of hydrogen when there are $N_+$, $N_0$, $N_-$ dipoles pointing along $+Z$, perpendicular to $Z$ and along $-Z$, Slater arrived at an expression for the entropy of the crystal. Combining this with the energy terms, curves for the "free" energy of the crystal are obtained as shown in Fig. 19, where $X$ is a coordinate which measures the net dipole moment of a single domain along the $Z$ axis. It gives directly the dipole moment as a fraction of the maximum or saturation value in the absence of an external

[14] J. West, Zeits. f. Krist. **74**, 306 (1930).

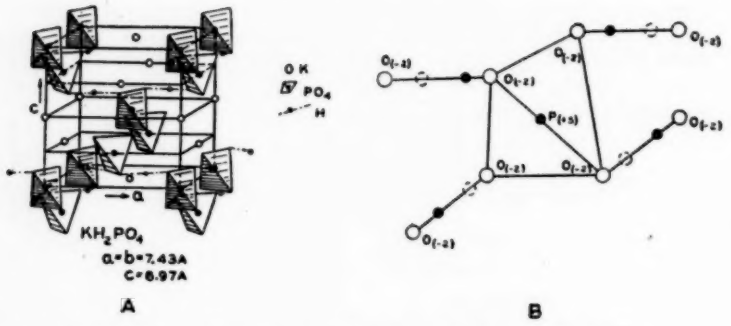


FIG. 18. Crystal structure as determined by x-rays for KDP.

field. The curves of Fig. 19 show that there is one temperature $T=\theta$, the Curie temperature, where the free energy is a straight-line function of $X$; above this temperature the value of 0 for $X$ has the least free energy, and this corresponds to the condition that the most probable states of the crystal are those arrangements of hydrogens giving a zero net dipole moment and the crystal is unpolarized. Below this temperature, the values of $X=\pm 1$ have the least free energy and the crystal becomes spontaneously polarized in one of the $Z$ directions. When a field is applied in one direction along the $Z$ axis, the equilibrium position shifts from $X=0$ as shown by the dotted lines of Fig. 19, and a polarization results. Slater finds the polarization above the Curie point to be given by the equation

$$P_z=N\mu X=\frac{N\mu^2}{kln2}\frac{E_z}{T-\theta}, \tag{33}$$

where $N$ is the number of molecules per cc, $\mu$ the dipole moment of the molecule, $k$ Boltzmann's constant, $E_z$ the applied field, $T$ the temperature, and $\theta$ the Curie temperature. Since the dipole moment has been determined from the measurements of Busch[1] to be $\mu=1.25\times10^{-18}$, the susceptibility can be calculated to be

$$\kappa_3=170/(T-\theta). \tag{34}$$

In addition to the susceptibility due to the hydrogen bonds, there is also a susceptibility independent of temperature arising from the polarizability of the other parts of the lattice, principally the oxygens in the phosphate groups. Slater's theory should apply to a single domain below the Curie point and should be applicable to the free dielectric constant above the Curie temperature. From Eq. (17) the free susceptibility

$$\kappa_3^F=\frac{K_3^F-1}{4\pi}=0.279+\frac{249}{T-\theta}, \tag{35}$$

where $\theta=-151$°C for the free crystal. The factor 249 is 1.46 times that calculated, which has been explained by Slater as being due to the extra field produced at the dipoles by the polarizability of the oxygens or other elements. The value of 4.5 for the dielectric constant for these elements alone is not out of line with that obtained for similar crystals.

Slater explains the temperature broadening of the transition (which theoretically should occur at a single temperature) as resulting from stresses set up in the various domains due to the fact that one is polarized and hence sheared in one direction while an adjacent one is polarized in the opposite direction. Hence since different domains are stressed by different amounts, they will have different Curie temperatures, and a continuous transition takes place over a definite temperature range. The maximum theoretical broadening can be calculated from the elastic and piezoelectric data obtained for this paper. One

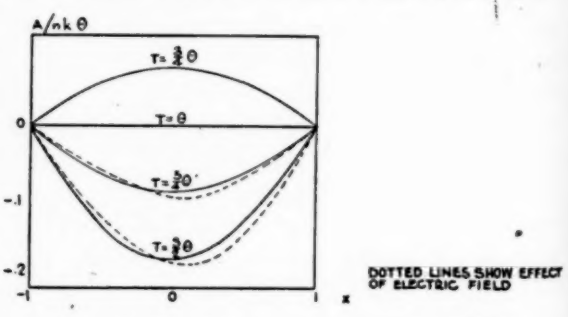


FIG. 19. Slater's free energy curves for KDP.

can show that the temperature shift should be

$$\Delta T = 2(\Delta E/N)/kln2 = 2\Delta E/Nkln2, \quad (36)$$

where $\Delta E$ is the increment of free energy per cc and $N$ the number of molecules per cubic centimeter. The change in free energy per cc due to a spontaneous polarization $P_z^0$ is according to Mueller's theory

$$\Delta E = \tfrac{1}{2}c_{66}^{\sigma}(x_y^0)^2 - f_{36}x_y^0 P_z^0 + \tfrac{1}{2}\chi_3^C(P_z^0)^2 + \tfrac{1}{4}B(P_z^0)^4, \quad (37)$$

where the last term is a non-linear term which for Rochelle salt is small compared to the linear terms. Since the spontaneous polarization ($P_z^0$) has been measured by Busch to be $4.3\times10^{-6}$ Coulomb per cc $=1.29\times10^4$ c.g.s. units per cc, and $g_{36}$ has been determined to be $44\times10^{-3}$, a spontaneous shearing strain ($x_y^0$) should occur for any one domain equal to

$$x_y^0 = g_{36}P_z^0 = 5.65\times10^{-3}. \quad (38)$$

The change in free energy then due to the linear terms in going from a clamped to a free crystal below the curie temperature is

$$\Delta E = \tfrac{1}{2}c_{66}^{\sigma}(x_y^0)^2 - f_{36}(x_y^0)P_z = -1.13\times10^6 \text{ erg per cc.}$$

Hence the temperature range of the transformation should be about

$$\Delta T = 2.29°\text{C},$$

which is somewhat less than the specific heat data[15] and the indicated change of 3.5°C between the clamped and free dielectric constants.

For ADP it appears that two separate systems of hydrogen bonds are involved. Stephenson and Zettlemoyer's[16] measurements on "The Heat Capacity of Ammonium Dihydrogen Phosphate from 15° to 300°K. The Anomaly at the Curie Temperature" indicate that the transition occuring at 148°K (−125°C) is in the nature of a rearrangement of hydrogen bonds. This is confirmed by the fact that a substitution of deuterium for hydrogen raises the transition temperature. On the other hand, the bond system controlling the transition temperature cannot be the same as the $H_2PO_4$ bond system controlling the dielectric and piezoelectric constants for the data of Figs. 12 and 15 show that there is no deviation from smooth curves as the transition temperature of −125°C is approached. Hence we conclude that the bond system causing the transition temperature is probably due to the four hydrogens in the ammonium ion. These are probably shared with the oxygens in the nearest $PO_4$ groups, raising the most probable number of hydrogen bonds for each $PO_4$ group. The sudden shattering of the crystal at −125°C is probably due to a first-order change in crystal structure connected with the ammonium hydrogen bond system. This is indicated by the fact that shattering occurs for ammonium dihydrogen phosphate and ammonium dihydrogen arsenate, but does not occur for potassium dihydrogen phosphate or potassium dihydrogen arsenate. Examples for which the hydrogens of ammonia form bonds affecting the crystal structure are furnished by the crystals ammonium hydrogen fluoride, ammonium azide, and ammonium fluoride.[17]

This ammonium hydrogen bond system may explain why the piezoelectric constant $f_{36}^*$ is five times as large in ADP as in KDP, for with the close coupling between all the $PO_4$ ions that occur through the ammonium hydrogen bonds one would expect a larger change in the lattice positions would be caused by a change in the $H_2PO_4$ dipoles than would occur in the $KH_2PO_4$ case, where the $PO_4$ ions are coupled to the K ions by central electrostatic forces.

By extrapolating the piezoelectric and dielectric constant data to low temperatures, it appears that the piezoelectric Curie temperature should come below absolute zero so that no ferroelectric properties would be expected. This may well be connected with the size of the unit cell which is 7.53A along the $a$ or $X$ axis and 7.542A along the $c$ or $Z$ axis. For KDP, as shown by Fig. 18, the values are 7.43A along $X$ and 6.97A along $Z$ which is associated with the lower energy of the hydrogen bonding system along $Z$ than along $X$. For ADP, the two are very nearly equal and ferroelectric properties, if any, might be expected to occur along $X$ rather than $Z$.

[15] C. C. Stephenson and J. G. Hooley, "The heat capacity of potassium dihydrogen phosphate from 15° to 300°K. The anomaly at the Curie temperature," J. Am. Chem. Soc. 66, 1397 (1944).

[16] Stephenson and Zettlemoyer, J. Am. Chem. Soc. 66, 1405–1408 (1944).

[17] See L. Pauling, *Nature of the Chemical Bond* (Cornell University Press, New York, 1944), pp. 299 and 300.

So far, no atomic theories have been developed which allow one to calculate the piezoelectric properties of such crystals as KDP and ADP. Several phenomenological theories have been developed, the most recent of which is the interaction theory of Mueller.[18] The formulation of the theory for small applied fields is similar to that given in Eqs. (4) and (5), except that the polarization $P$ is used in place of the total charge

$$\sigma = P + E/4\pi. \tag{39}$$

For Rochelle salt the conclusion is reached that the open circuited elastic constants show a constant variation with temperature, the piezoelectric constant $f_{14}^*$ (for the ferroelectric axis) is independent of temperature, while the only anomaly occurs in the clamped dielectric constant. The same conclusions appear justified for ADP and KDP except that to get an independence of temperature for the piezoelectric constant $f_{36}^*$, we have to take only that part of the polarization which is associated with the dipoles, i.e., the temperature variable part of the dielectric constant. This indicates that it is the shift of the positions of the hydrogen ions which causes the change in the lattice structure and hence the piezoelectric effect. The temperature independence of $f_{36}^*$ is shown by Fig. 15. The dielectric constant then provides the only anomaly.

Since no high field measurements have been made, an evaluation of the non-linear terms of Mueller's theory cannot be made.

*Note Added in Proof:* Recent unpublished measurements by W. A. Yager of this laboratory show that the dielectric constant of ADP remains substantially unchanged from the clamped value up to a frequency of $2.5\times10^{10}$ cycles/sec. (1.2 cm). This result is markedly different from that for ice, which shows marked dispersion at low frequencies, although the mechanism of polarization has been supposed to be similar in both cases (cf. W. Kauzmann, Rev. Mod. Phys. **14**, 12 (1942)). The extremely short relaxation time of ADP is difficult to understand. The mechanism of polarization by motion along hydrogen bonds from one equilibrium position to another seems to be ruled out.

## APPENDIX

### A-1 Longitudinal Vibrations

In Section IV of the paper use is made of the difference in the resonance frequencies of a plated crystal and a bare crystal to evaluate the piezoelectric coupling factor $k$ of a crystal. An alternate method is to use the frequency separation between resonance and anti-resonance. It is the purpose of this appendix to evaluate these separations as a function of the fundamental constants of an ADP or KDP crystal.

For a plated crystal, the piezoelectric relations of Eqs. (1) are the most useful form. Since only shear piezoelectric constants exist, it is necessary to cut crystals normal to the $X$ or $Z$ axis with their lengths at an angle from the other two axes, in order to generate longitudinal vibrations. Longitudinal vibrations are more advantageous for measuring piezoelectric constants for it is possible to get single modes of motion free from other couplings by using this type of vibration.

To obtain the piezoelectric relations for a 45° $Z$-cut crystal, for example, it can be shown by tensor transformation, that the equations for a crystal cut normal to $Z$ with its length at an angle $\theta$ with the $X$ axis will be

$$\begin{aligned}
-x_x' = {} & X_x'[s_{11}(\sin^4\theta+\cos^4\theta)+(2s_{12}+s_{66}^E)\sin^2\theta\cos^2\theta] \\
& + Y_y'\left[(2s_{11}-s_{66}^E)\sin^2\theta\cos^2\theta+s_{12}(\sin^4\theta+\cos^4\theta)+\frac{s_{66}^E}{2}\sin 4\theta\right]+Z_z's_{13} \\
& + X_y'\left[\frac{s_{66}^E+2s_{12}-2s_{11}}{2}\sin 4\theta\right]+E_z\frac{d_{36}}{2}\sin 2\theta, \qquad (1) \\
\sigma_z = {} & \frac{K_3^F}{4\pi}E_z-\frac{d_{36}}{2}[(X_x'-Y_y')\sin 2\theta+X_y'\cos 2\theta],
\end{aligned}$$

where the primes refer to the stresses and strains expressed with respects to the rotated axes.

[18] Reference 6 and H. Mueller, "Properties of Rochelle salt III," Phys. Rev. **58**, 565–573 (1940).

When $\theta=45°$, these equations reduce to

$$-x_x'=X_x'\left[\frac{s_{11}+s_{12}}{2}+\frac{s_{66}^E}{4}\right]+Y_y'\left[\frac{s_{11}+s_{12}}{2}-\frac{s_{66}^E}{4}\right]+Z_z's_{13}+\frac{d_{36}}{2}E_z, \quad (2)$$

$$\sigma_z=\frac{K_3^F}{4\pi}E_z-\frac{d_{36}}{2}(X_x'-Y_y').$$

A pure longitudinal vibration is obtained when the length of the crystal is much greater than the width and thickness dimensions. The stress boundary conditions to be satisfied for a freely vibrating crystal are that all stresses vanish over the surface of the crystal. Since the thickness and width are taken very small and all of the stresses are zero on the surfaces, it follows that no stress can differ appreciably from zero except the stress along the length, $X_x'$. Hence for such a crystal Eqs. (2) reduce to

$$\begin{aligned}-x_x'&=X_x's_{11}^{E'}+\frac{d_{36}}{2}E_z,\\ \sigma_z&=\frac{K_3^F}{4\pi}E_z-\frac{d_{36}}{2}X_x',\end{aligned} \quad (3)$$

where

$$s_{11}^{E'}=\frac{s_{11}+s_{12}}{2}+\frac{s_{66}^E}{4}.$$

The equations of motion can be derived from these equations and Newton's law of motion.

$$F_x=Ma=(\rho\, dxdydz)\frac{d^2\xi}{dt^2}, \quad (4)$$

where $M$ is the mass of an elementary volume $dxdydz$, $a$ the acceleration, and $\xi$ is the displacement of the element in the $X'$ direction.

Let us next consider a small cross section of the crystal with a dimension $dx'$ along the crystal length. The total force on the section is a resultant of the difference in stresses on the two faces or equal to

$$l_wl_t[X_{x_1}'-X_{x_2}']=-l_wl_t\frac{\partial X_x'}{\partial x'}dx'=F_x, \quad (5)$$

where $X_x'$ the stress is considered as a compressional stress acting on the faces of the element. By Newton's law of motion (4) we have

$$-l_wl_tdx'\frac{\partial X_x'}{\partial x'}=l_wl_tdx'\rho\frac{d^2\xi}{dt^2}$$

or

$$\frac{\partial X_x'}{\partial x'}=-\rho\frac{d^2\xi}{dt^2}. \quad (6)$$

For a completely plated crystal such as we are considering, the potential gradient $E_z$ will be independent of the $x'$ direction, since any charge distribution will be equalized with the speed of light which is much higher than the speed of sound in a crystal. Then Eq. (3) when differentiated with respect to $x'$ becomes

$$-\frac{\partial X_x'}{\partial x'}=\frac{1}{s_{11}^{E'}}\frac{\partial x_x'}{\partial x}=\frac{1}{s_{11}^{E'}}\frac{\partial^2\xi}{\partial x'^2}, \quad (7)$$

by the equation of the longitudinal stress $X_x'$. Introducing this equation into (6), the equation of motion for a plated crystal becomes

$$\frac{\partial^2\xi}{\partial x'^2}=s_{11}^{E'}\rho\frac{d^2\xi}{dt^2}. \quad (8)$$

For simple harmonic motion the variation of $\xi$ with time can be written in the usual form

$$\xi=\xi e^{j\omega t}, \quad (9)$$

so that the simple harmonic motion Eq. (8) becomes

$$\frac{d^2\xi}{dx'^2}-\omega^2\rho s_{11}^{E'}\xi=\frac{d^2\xi}{dx'^2}-\frac{\omega^2}{v^2}\xi=0, \quad (10)$$

where $v$ the velocity of a plated crystal is given by the formula

$$v^2=1/\rho s_{11}^{E'}. \quad (11)$$

A solution of Eq. (10) with two arbitrary boundary conditions is

$$\xi=A\cos\frac{\omega x'}{v}+B\sin\frac{\omega x'}{v}. \quad (12)$$

To determine the constants $A$ and $B$, use is

made of Eqs. (3). Differentiating (12)

$$-\frac{d\xi}{dx'}=-x_x'=\frac{\omega}{v}\left[A\sin\frac{\omega x'}{v}-B\cos\frac{\omega x'}{v}\right]$$

$$=s_{11}^{E'}X_x'+\frac{d_{36}}{2}E_z. \quad (13)$$

When $x'=0$ and $x'=l$ the bar length, for a free crystal the stress

$$X_x'=0 \text{ when } x'=0 \text{ and } x'=l. \quad (14)$$

Under these conditions

$$-\frac{\omega}{v}B=\frac{d_{36}}{2}E_z$$

and

$$\frac{\omega}{v}\left[A\sin\frac{\omega l}{v}-B\cos\frac{\omega l}{v}\right]=\frac{d_{36}}{2}E_z. \quad (15)$$

Solving these equations for $A$ and $B$ and substituting in (13), we have

$$-x_x'=\frac{d_{36}}{2}E_z\left[\tan\frac{\omega l}{2v}\sin\frac{\omega x'}{v}+\cos\frac{\omega x'}{v}\right]$$

$$=s_{11}^{E'}X_x'+\frac{d_{36}}{2}E_z$$

or

$$x_x'=\frac{-d_{36}E_z}{2s_{11}^{E'}}\left[1-\frac{\cos\dfrac{\omega(x'-l/2)}{v}}{\cos\dfrac{\omega l}{2v}}\right]. \quad (16)$$

The electrical impedance measured at the terminals of a plated crystal is then determined by substituting the value of $x_x'$ in the last of Eqs. (3) and integrating the charge $\sigma$ over the whole surface. The current into the crystal is then

$$i=j\omega\int\sigma_z dS=j\omega l_w\int_0^l E_z\left[\frac{K_3^F}{4\pi}-\frac{d_{36}^2}{4s_{11}^{E'}}\left(1-\frac{\cos\dfrac{\omega(x'-l/2)}{v}}{\cos\dfrac{\omega l}{2v}}\right)\right]dx'$$

$$=j\omega E_z l_w l\left[\frac{K_3^F}{4\pi}-\frac{d_{36}^2}{4s_{11}^{E'}}\left(1-\frac{\tan\dfrac{\omega l}{2v}}{\dfrac{\omega l}{2v}}\right)\right]=j\omega E_z l_w l\left[\frac{K_3^{LC}}{4\pi}+\frac{d_{36}^2}{4s_{11}^{E'}}\frac{\tan\dfrac{\omega l}{2v}}{\dfrac{\omega l}{2v}}\right], \quad (17)$$

where $K_3^{LC}=K_3^F-\pi d_{36}^2/s_{11}^{E'}$ is called the longitudinally clamped dielectric constant, i.e., the dielectric constant that would be measured if we suppress the longitudinal strain along the $x'$ axis but not the other strains. The admittance of the crystal then is

$$\frac{i}{E}=\frac{i}{E_z l_t}=\frac{j\omega l_w l}{l_t}\left[\frac{K_3^{LC}}{4\pi}+\frac{d_{36}^2}{4s_{11}^{E'}}\frac{\tan\dfrac{\omega l}{2v}}{\dfrac{\omega l}{2v}}\right]. \quad (18)$$

This consists of two terms which represent parallel branches in the equivalent circuit. One of these is the capacitance

$$C_0=\frac{l_w l K_3^{LC}}{4\pi l_t}\text{c.g.s. units}=\frac{l_w l K_3^{LC}}{4\pi l_t(9\times10^{11})}\text{farads.} \quad (19)$$

The other branch contains the impedance

$$\frac{-jlt}{\omega l_w l}\left[\frac{4s_{11}^{E'}}{d_{36}^2}\frac{\dfrac{\omega l}{2v}}{\tan\dfrac{\omega l}{2v}}\right]\text{c.g.s. units}$$

$$=\frac{-jl_t 4s_{11}^{E'}\dfrac{\omega l}{2v}\times9\times10^{11}}{\omega l_w l d_{36}^2\tan\dfrac{\omega l}{2v}}\text{ ohms.} \quad (20)$$

This branch will have a zero impedance or will resonate when the tangent is infinite or when

$$\frac{2\pi f_R l}{2v}=\frac{\pi}{2} \quad \text{or} \quad f_R=\frac{v}{2l}=\frac{1}{2l(\rho s_{11}^{E'})^{\frac{1}{2}}}. \quad (21)$$

Hence for the fully plated crystal it is the zero field elastic constant that determines the resonant frequency.

The anti-resonant frequency (the frequency of highest impedance) is determined by setting Eq. (18) equal to zero and solving for the resultant frequency. This is given by the equation

$$\tan\frac{\omega l}{2v}=-\frac{\omega l}{2v}\left(\frac{4s_{11}^{E'}K_3^{LC}}{4\pi d_{36}^2}\right). \tag{22}$$

Now since

$$K_3^{LC}=K_3^{F}-\pi d_{36}^2/s_{11}^{E'},$$

this can be written

$$\tan\frac{\omega l}{2v}=-\frac{\omega l}{2v}\left[\frac{4s_{11}^{E'}K_3^{F}}{4\pi d_{36}^2}\left(1-\frac{4\pi d_{36}^2}{4s_{11}^{E'}K_3^{F}}\right)\right]=-\frac{\omega l}{2v}\left(\frac{1-k^2}{k^2}\right), \tag{23}$$

by the definition of the coupling.

If the coupling is small, the impedance of Eq. (20) can be represented near the resonant frequency by a series capacitance and inductance having the values

$$C_1=\frac{l_w l}{l_t}\frac{8}{\pi^2}\frac{d_{36}^2}{4s_{11}^{E'}\times 9\times 10^{11}}\text{ farads};$$
$$L_1=4\frac{\rho s_{11}^{E'} l l_t\times 9\times 10^{11}}{8 l_w d_{36}^2}\text{ henries}. \tag{24}$$

Taking the ratio of $C_0$ to $C_1$, we have

$$\frac{C_0}{C_1}=r=\frac{\pi^2}{8}\left(\frac{K_3^{LC}s_{11}^{E'}}{\pi d_{36}^2}\right)=\frac{\pi^2}{8}\left(\frac{1-k_2}{k^2}\right). \tag{25}$$

When $k$ is large, this representation is not accurate. Fig. 20 shows a calculation of the ratio of the resonant frequency and anti-resonant frequency to the resonant frequency of an unplated crystal expressed as a function of the coupling $k$. Hence if the ratio of anti-resonant to resonant frequency is known, the coupling can be evaluated. Similarly if the ratio of the resonant frequency of a plated crystal to the resonant frequency of an unplated crystal is known, the coupling can be evaluated. Care must be taken, however, that the weight of the plating is not sufficient of itself to lower the frequency of the plated crystal. This precaution has been followed in the data given in this paper.

To determine the frequency of an unplated crystal measured mechanically, or electrically in an air gap holder with a large air gap, use can be made of the equations expressed as in Eq. (4) of the body of the paper. For an unplated crystal with all driving plates a long distance away, the electrical boundary conditions are that the surface charges are equal to zero. The effect of any polarization produced by a motion of the crystal is annulled by a depolarizing field

$$E_z=-4\pi P_z. \tag{26}$$

Hence the elastic constants operative are the charge or "open circuited" elastic constants. By tensor transformations, the equations for a 45° $Z$-cut crystal become

$$-x_x'=X_x'\left[\frac{s_{11}+s_{12}}{2}+\frac{s_{66}^{\sigma}}{4}\right]+Y_y'\left[\frac{s_{11}+s_{12}}{2}-\frac{s_{66}^{\sigma}}{4}\right]+Z_z's_{13}+\frac{g_{36}}{2}\sigma_z, \tag{27}$$
$$E_z=\frac{4\pi\sigma_z}{K_3^{F}}+\frac{g_{36}}{2}(X_x'-Y_y').$$

For a longitudinal crystal, isolated electrically,

$$Y_y'=Z_z'=\sigma_z=0. \tag{28}$$

Then the equation of motion becomes

$$\frac{\partial^2\xi}{\partial x'^2}=\left(\frac{s_{11}+s_{12}}{2}+\frac{s_{66}^{\sigma}}{4}\right)\rho\frac{d^2\xi}{dt^2}=s_{11}^{\sigma'}\rho\frac{d^2\xi}{dt^2}, \tag{29}$$

and the resonant frequency is determined by the "open circuited" elastic constant $s_{11}'^{\sigma}$. By Eqs. (3) this is related to the short circuited elastic constant

$$s_{11}^{\sigma'}=\frac{s_{11}+s_{12}}{2}+\frac{s_{66}^{\sigma}}{4}=\frac{s_{11}+s_{12}}{2}+\frac{s_{66}^{E}-d_{36}g_{36}}{4}$$
$$=\left(\frac{s_{11}+s_{12}}{2}+\frac{s_{66}^{E}}{4}\right)\left[1-\frac{4\pi d_{36}^2}{4K_3^{F}\left(\frac{s_{11}+s_{12}}{2}+\frac{s_{66}^{E}}{4}\right)}\right]=s_{11}^{E'}\left[1-\frac{4\pi d_{36}^2}{4K_3^{F}s_{11}^{E'}}\right]=s_{11}^{E'}(1-k^2). \tag{30}$$

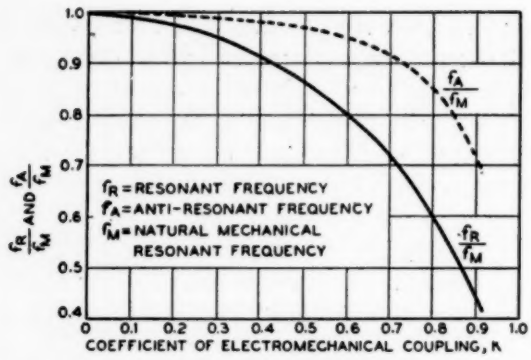


FIG. 20. Ratios of resonant and anti-resonant frequencies to the natural mechanical resonant frequency plotted as a function of the coupling coefficient $k$.

Hence the ratios of the open circuited to the short circuited frequencies is given by

$$f_0/f_s=1/(1-k^2)^{\frac{1}{2}} \tag{31}$$

as shown plotted in Fig. 20.

### A-2 Face Shear Vibrations

In measuring the shear elastic constants of ADP and KDP, a crystal was used cut normal to the $Z$ or $X$ axes, with its length large compared to its width and very large compared to its thickness. The elastic shear constant was measured by dimensioning the crystal so that no coupling occurred to adjacent flexure modes or by measuring high harmonics of the shear mode. We wish to show that this measurement determines the $c_{66}^E$ or $c_{44}^E$ elastic constants.

This is a more general contour mode than the longitudinal one considered and involves satisfying boundary conditions along four edges. We consider a $Z$-cut crystal and assume that the thickness is so small that the stresses determined by the $Z$ direction can be set equal to zero. Hence

$$Z_z=X_z;\quad Z_y=Y_z;\quad Z_z \tag{32}$$

can all be set equal to zero. The remaining stresses

$$X_z,\ X_y,\ Y_y \tag{33}$$

are all finite throughout the crystal but vanish at the edges. The vanishing of the stresses of Eq. (32) simplifies the equations of motion for it results in only three independent strains $x_z$, $x_y$, $y_y$. This is readily seen from Eq. (3) of the body of the paper by setting $Z_z=Y_z=Z_z=E_z=E_y=0$. Then $y_z=z_z=0$ and

$$z_z=(c_{13}x_z+c_{13}y_y)/c_{33}.$$

Hence the piezoelectric equations become

$$\begin{aligned}
-X_z&=c_{11}^*x_z+c_{12}^*y_y,\quad c_{11}^*=c_{11}-c_{13}^2/c_{33},\\
-Y_y&=c_{12}^*x_z+c_{11}^*y_y,\quad c_{12}^*=c_{12}-c_{13}^2/c_{33},\\
-X_y&=c_{66}^Ex_y-e_{36}E_z,\\
\sigma_z&=\frac{K_3^C}{4\pi}E_z+e_{36}x_y.
\end{aligned} \tag{34}$$

Newton's equations of motion for a two-dimension crystal become

$$\begin{aligned}
\rho\frac{d^2\xi_1}{dt^2}&=-\frac{\partial X_z}{\partial x}-\frac{\partial X_y}{\partial y}=c_{11}^*\frac{\partial x_z}{\partial x}+c_{12}^*\frac{\partial y_y}{\partial x}\\
&\quad+c_{66}^E\frac{\partial x_y}{\partial y}-e_{36}\frac{\partial E_z}{\partial y},\\
\rho\frac{d^2\xi_2}{dt^2}&=-\frac{\partial Y_z}{\partial x}-\frac{\partial Y_y}{\partial y}=c_{66}^E\frac{\partial x_y}{\partial x}+c_{12}^*\frac{\partial x_z}{\partial y}\\
&\quad+c_{11}^*\frac{\partial y_y}{\partial y}-e_{36}\frac{\partial E_z}{\partial x},
\end{aligned} \tag{35}$$

where $\xi_1$ and $\xi_2$ are the displacements along $X$ and $Y$ at any point. Since the plating is an equipotential surface $\partial E_z/\partial x=\partial E_z/\partial y=0$. Also by the definition of the strains

$$x_z=\frac{\partial\xi_1}{\partial x};\quad y_y=\frac{\partial\xi_2}{\partial y};\quad x_y=\frac{\partial\xi_1}{\partial y}+\frac{\partial\xi_2}{\partial x}. \tag{36}$$

Hence for simple harmonic motion, Eqs. (35) become

$$\begin{aligned}
&c_{11}^*\frac{\partial^2\xi_1}{\partial x^2}+c_{12}^*\frac{\partial^2\xi_2}{\partial x\partial y}\\
&\quad+c_{66}^E\left[\frac{\partial^2\xi_1}{\partial y^2}+\frac{\partial^2\xi_2}{\partial x\partial y}\right]+\omega^2\rho\xi_1=0,\\
&c_{66}^E\left[\frac{\partial^2\xi_1}{\partial x\partial y}+\frac{\partial^2\xi_2}{\partial x^2}\right]+c_{12}^*\frac{\partial^2\xi_1}{\partial x\partial y}\\
&\quad+c_{11}^*\frac{\partial^2\xi_2}{\partial y^2}+\omega^2\rho\xi_2=0.
\end{aligned} \tag{37}$$

We wish to show that when the crystal is very long in the $X$ direction compared to its width in the $Y$ direction, the shearing resonant frequency will be controlled by the $c_{66}^E$ elastic constant.

To show this let

$$\xi_1 = A \sin hy; \quad \xi_2 = 0. \tag{38}$$

This satisfies Eq. (37) provided that

$$h = \omega(\rho/c_{66}^E)^{\frac{1}{2}} = \omega/v, \tag{39}$$

where $v$ is the velocity of propagation of a shear wave. The $X_x$ and $Y_y$ stresses vanish identically over the crystal. To make $X_y$ vanish when $y = \pm l_w/2$ we have

$$\begin{aligned} -X_y &= c_{66}^E\left(\frac{\partial \xi_1}{\partial y} + \frac{\partial \xi_2}{\partial x}\right) - e_{36}E_z \\ &= A\omega(\rho C_{66}^E)^{\frac{1}{2}} \cos\frac{\omega y}{v} - e_{36}E_z, \\ &= 0 \quad \text{when} \quad y = \pm l_w/2. \end{aligned} \tag{40}$$

Hence

$$A = \frac{e_{36}E_z}{\omega(\rho c_{66}^E)^{\frac{1}{2}} \cos \omega l_w/2v}$$

and

$$\begin{aligned} \xi_1 &= \frac{e_{36}E_z \sin \omega y/v}{\omega(\rho c_{66}^E)^{\frac{1}{2}} \cos \omega l_w/2v}; \\ X_y &= e_{36}E_z\left[\frac{\cos \omega y/v}{\cos \omega l_w/2v} - 1\right]; \quad X_x = Y_y = 0. \end{aligned} \tag{41}$$

Hence all the boundary conditions are satisfied except for $X_y$ at $x = \pm l/2$. Here the shear stress puts in a force in the $y$ direction which when integrated over the surface becomes

$$F_y = e_{36}E_z l_w l_t\left[\frac{\tan \omega l_w/2v}{\omega l_w/2v} - 1\right] \text{ at } x = \pm\frac{l}{2}. \tag{42}$$

This is the type of force that will tend to drive an even order flexure in the bar. As the length $l$ increases with respect to the width $l_w$, it can be shown that the amplitude of the flexure motion approaches zero for a constant driving force, so that for a crystal long compared to its width, the solution given above is approached. Hence a harmonic of a shear mode for a long narrow crystal approaches this condition very closely. Such modes can therefore be used to evaluate the shear elastic constants $c_{66}^E$ and $c_{44}^E$.

The impedance of a long narrow shear vibrating crystal can be derived from the last of Eqs. (34) by integrating the charge over the surface of the crystal. Since

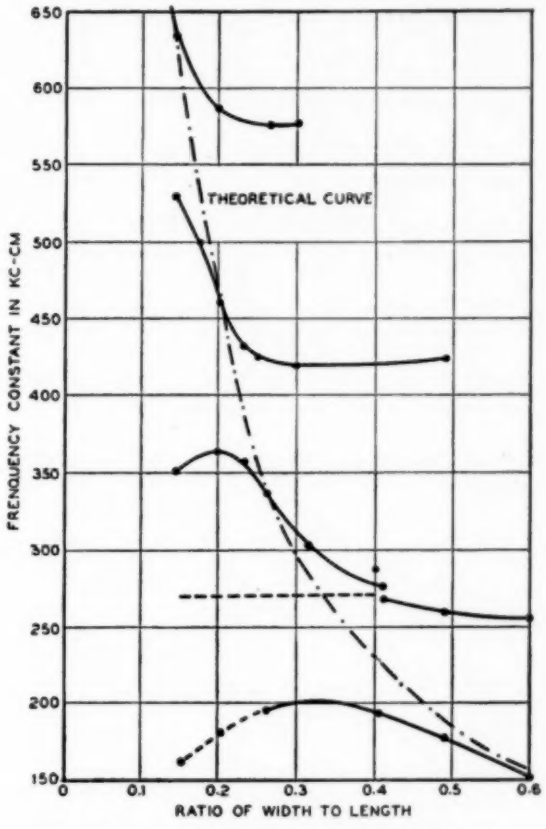


FIG. 21. Frequency spectrum of a $Z$-cut ADP crystal vibrating in shear.

$$x_y = \frac{e_{36}E_z}{c_{66}^E}\frac{\cos \omega y/v}{\cos \omega l_w/2v}, \tag{43}$$

we find

$$\begin{aligned} Q &= \int_{-l/2}^{l/2} dx \int_{-l_w/2}^{l_w/2} \sigma_x dy \\ &= E_z l l_w\left[\frac{K_3{}^C}{4\pi} + \frac{e_{36}{}^2}{c_{66}^E}\frac{\tan \omega l_w/2v}{\omega l_w/2v}\right] = \frac{i}{j\omega}. \end{aligned} \tag{44}$$

In a similar manner to that discussed for the longitudinal crystal, we can show that the resonance occurs when

$$f_R = \frac{1}{2l_w}\left(\frac{c_{66}^E}{\rho}\right)^{\frac{1}{2}} \tag{45}$$

and that the impedance of the crystal is represented by the equivalent circuit of Fig. 16, with

the constants

$$C_0=\frac{K_3{}^C l_w l}{4\pi l_t(9\times10^{11})}\text{ farads;}$$

$$C_1=\frac{8}{\pi^2}\frac{ll_w}{l_t}\left(\frac{e_{36}{}^2}{c_{66}{}^E}\right)\times\frac{1}{9\times10^{11}}\text{ farads;} \quad (46)$$

$$L_1=\frac{\rho l l_t\times9\times10^{11}}{8l_w e_{36}{}^2}\text{ henries.}$$

Hence the ratio of capacities becomes

$$\frac{C_0}{C_1}=r=\frac{\pi^2}{8}\left(\frac{K_3{}^C c_{66}{}^E}{4\pi e_{36}{}^2}\right)=\frac{\pi^2}{8}\frac{(1-k^2)}{k^2}, \quad (47)$$

where $k$ the coefficient of coupling for a shear mode is

$$k^2=\frac{4\pi e_{36}{}^2}{K_3{}^F c_{66}{}^E}=\frac{4\pi d_{36}{}^2}{K_3{}^F s_{66}{}^E}$$

and

$$K_3{}^C=K_3{}^F-4\pi d_{36}e_{36}. \quad (48)$$

When a crystal is not long compared to its width, the unbalanced forces in the $X$ direction will couple the shear mode to even order flexure modes. This is shown experimentally by Fig. 21, which shows the frequency spectrum of a $Z$-cut ADP crystal as a function of the ratio of width to length. The main modes can be identified as even order flexures coupled to the shear mode. At certain ratios of width to length the shear and flexure modes coincide and a coupled frequency curve is observed. Midway between couplings, a good agreement is obtained with the frequency calculated from (45). The smaller the ratio of width to length, the better the agreement obtained, as shown by the dotted line which shows the calculated value.

PHYSICAL REVIEW VOLUME 69, NUMBERS 5 AND 6 MARCH 1 AND 15, 1946

# Quantum Effects in the Interaction of Electrons With High Frequency Fields and the Transition to Classical Theory

LLOYD P. SMITH
*RCA Laboratories, Princeton, New Jersey*
(Received November 13, 1945)

The interaction of electrons with an electromagnetic field within a conducting enclosure is treated from the point of view of quantum mechanics. The various quantum effects to be expected with regard to energy exchanges are pointed out and it is shown how the various probabilities of energy change combine to give results in accord with classical theory for conditions where classical theory becomes appropriate. The details in the transition from quantum behavior to classical behavior are traced in a very illuminating way for two particular examples. The conditions under which quantum effects manifest themselves are given.

## INTRODUCTION

WHEN an electron interacts with an electromagnetic field which varies harmonically with time, classical electrodynamics informs us that there is a continuous transfer of energy from field to electron or *vice versa* as long as the electron is acted upon by the field. According to quantum theory, however, the energy exchange does not occur continuously. If it occurs at all, it must occur in discrete steps of one quantum each where the energy quantum is $h\nu$, $\nu$ being the frequency of the electromagnetic field and $h$ being Planck's constant. Furthermore according to quantum theory it is impossible to ascertain the exact number of successive quanta which have been exchanged during a certain interval of interaction time. It is only possible to determine what the probability is that a given number of quanta have been lost or gained by the electrons during the interaction time in question.

This would have the consequence that of a group of electrons entering the field at a given time some might not exchange any energy at all, some would exchange one quantum of energy and so on, though from a classical standpoint they should all have exchanged the same amount of energy. This effect has up to the present never been observed in circumstances where electrons have traversed a harmonically varying electromagnetic field, such as that in a resonant cavity. This is undoubtedly due to the fact that for frequencies used in the past, the quantum energy was very small and the energy spread referred to above was small compared to the kinetic energy of the electrons normally dealt with and indeed small compared to the thermal spread in energies of electrons emitted from thermionic sources. This may be inferred from the fact that when the frequency of the field is $10^6$ cycles per second, the quantum energy $h\nu$ is only $4\times10^{-9}$ electron volt.

However, for the very high frequency electromagnetic fields which can be generated today, the quantum energy is over 30,000 times as large as that mentioned above. It is possible that the time is approaching when it will be possible to witness quantum effects by direct interaction of harmonic electromagnetic fields and electrons without having the electrons bound to atoms. Be that as it may, it is important to have a clear understanding of the phenomena to be encountered in the transition region where classical electrodynamics does not suffice to describe the exchange of energy between the electron and electromagnetic field in an accurate manner.

A preliminary view of the situation raises a number of interesting questions. First, under what conditions will quantum effects manifest themselves and when must classical electrodynamics be replaced by a quantum theoretical description? Second, in classical electrodynamics, the energy transferred from field to electron has a definite relation to the time phase of the electromagnetic field while in the treatments of pure quantum theory of interaction of electrons and radiation fields, the time phase of the field is lost sight of and the exchange takes place in a purely statistical way. The question then is, how does the quantum theory contrive to establish the relation of energy exchange and the time phase

of the field in the limit when classical theory holds? Further, what are the detailed quantum processes which in aggregate lead to the classical behavior when classical theory applies?

The purpose of this paper is to trace the transition from the usual quantum theory of electron and radiation field to the classical theory and thereby provide the answers to the above questions. The various quantum processes are worked out in detail for two examples which allow one to follow the transition from quantum theory to classical theory in a very illuminating and instructive way.

## INTERACTION OF ELECTRONS AND THE ELECTROMAGNETIC FIELD

For convenience, we shall consider the interaction of electrons with oscillating electromagnetic fields which may be sustained in a perfectly conducting enclosure. It is well known that such fields can be expressed in terms of a vector potential alone when there are no charges present in the enclosed space.[1] The vector potential $\mathbf{A}$ must be a solution of the differential equations[2]

$$\nabla\cdot\nabla\mathbf{A}-\partial^2\mathbf{A}/c^2\partial t^2=0, \tag{1}$$

$$\nabla\cdot\mathbf{A}=0, \tag{2}$$

subject to the boundary condition that $\mathbf{A}\times\mathbf{n}=0$ at all points on the enclosing surface, $\mathbf{n}$ being a unit vector normal to the enclosing surface and $c$ is the velocity of light.

There are a countably infinite set of harmonic solutions $\mathbf{A}_1(r)\exp[i\omega_1 t]$, $\mathbf{A}_2(r)\exp[i\omega_2 t]$, $\cdots$ $\mathbf{A}_s(r)\exp[i\omega_s t]$, $\cdots$ which satisfy the above conditions if

$$\nabla\cdot\nabla\mathbf{A}_s(r)+\frac{\omega_s^2}{c^2}\mathbf{A}_s(r)=0. \tag{3}$$

$\mathbf{A}_s(r)$ is a function of the space coordinates alone, these coordinates being represented briefly by $r$.

The fields expressible by these particular solutions give the normal modes of oscillation of the fields. The vector potentials $\mathbf{A}_1$, $\mathbf{A}_2\cdots$ form a complete orthonormal set of vector functions[3] in terms of which any solution of Eqs. (1) and (2) satisfying the boundary conditions may be represented. Thus any field we shall have need to consider may be expressed in the form

$$\mathbf{A}(x,y,z,t)=\sum_s q_s(t)\mathbf{A}_s(x,y,z), \tag{4}$$

where $q_s(t)$ is a function of the time alone. The coefficients $q_s$ provide a coordinate system in terms of which any appropriate field can be represented. If $\mathbf{A}(x,y,z,t)$ is known then the $q$'s can be determined with the help of the orthonormal property of the $\mathbf{A}_s$'s namely

$$\int\mathbf{A}_r\cdot\mathbf{A}_s d\tau=\begin{cases}0, & r\neq s\\ 4\pi c^2, & r=s\end{cases} \tag{5}$$

where the integral is taken over the volume of the enclosure.

In order to discuss the quantum behavior of one electron which interacts with an electromagnetic field of the above type, we require the Schroedinger equation for the system composed of the electron and the radiation field. This equation may be written in the following form[4]

$$\frac{\hbar^2}{2m}\nabla^2_{x,y,z}\Psi+\sum_s\frac{\hbar^2}{2}\frac{\partial^2\Psi}{\partial q_s^2}-\frac{\omega_s^2}{2}q_s^2\Psi-\frac{\hbar}{i}\frac{\partial\Psi}{\partial t}=-\frac{e}{mc}\mathbf{A}\cdot\mathbf{p}\Psi. \tag{6}$$

The independent variables in this equation are the field variables $q_1, q_2\cdots$, etc., and the position coordinates of the electron. The first term contains the Laplace operator with respect to the coordinates of the electron only. The interaction of the electron with the field is given by the term on the right-hand side of the equation. In order to have a consistent equation, $\mathbf{A}$ should be replaced by expression (4) and $\mathbf{p}$, the momentum of the electron, should be replaced by the operator $(\hbar/i)\,\mathrm{grad}_{xyz}$. The advisability of doing this depends on the information desired from this equation and the method of solution to be adopted. However, if $\mathbf{A}$ were replaced by expression (4) and $\mathbf{p}$ by $(\hbar/i)\,\mathrm{grad}_{xyz}$, a solution of

[1] See for instance Julius A. Stratton, *Electromagnetic Theory* (McGraw-Hill Book Company, Inc., New York, 1941) page 26.

[2] E. U. Condon, J. App. Phys. **11**, 502 (1940).

[3] See for instance, W. Heitler, *The Quantum Theory of Radiation* (Clarendon Press, England), page 41.

[4] See for instance, Enrico Fermi, Rev. Mod. Phys. **4**, 94 (1932).

the equation subject to the usual conditions on $\Psi$ would furnish all the information we could know about the position of the electron and the excitation of the radiation field at any given time. Thus $\Psi\Psi^* dxdydzdq_1dq_2\cdots$ gives the probability at time $t$ that the electron will be located in the volume element $dxdydz$ and the field coordinates will have values in the volume element $dq_1dq_2\cdots$.

The conventional way of obtaining solutions of Eq. (6) is to express $\Psi$ as an expansion in the orthonormal set of functions which are solutions of Eq. (6) when the right-hand side is set equal to zero. It is well known that[5] properly behaved solutions of this equation without the interaction term can be written in the form

$$\Phi_n(xyz)\phi_{n_1}(q_1)\phi_{n_2}(q_2)\cdots\phi_{n_s}(q_s)\cdots \times\exp\left[-\frac{i}{\hbar}(E_n+\hbar\omega_1 n_1+\hbar\omega_2 n_2+\cdots\hbar\omega_s n_s+\cdots)t\right], \tag{7}$$

where $E_n$ is the energy of the electron and $\omega_s$ is the frequency of the $s$th normal mode of the radiation field and $n_1$, $n_2\cdots$ are integers giving the number of quanta in the respective modes of the field, $\Phi_n$ is a solution of the equation

$$\nabla^2\Phi_n+\frac{2m}{\hbar^2}E_n\Phi_n=0, \tag{8}$$

and $\phi_{n_s}$ is a solution of the equation

$$\frac{\partial^2\phi_{n_s}}{\partial q_s^2}+\frac{2}{\hbar^2}\left[\hbar\omega_s n_s-\frac{\omega_s^2}{2}q_s^2\right]\phi_{n_s}=0. \tag{9}$$

Thus a solution of Eq. (6) can be written in the form

$$\Psi=\sum_{n,\,n_1\cdots} a^{(t)}_{n,\,n_1n_2\cdots n_s\cdots}\Phi_n\phi_{n_1}\phi_{n_2}\cdots\phi_{n_s} \times\exp\left[-\frac{i}{\hbar}\{E_n+\hbar\omega_1 n_1+\cdots\}t\right]. \tag{10}$$

When the solution $\Psi$ is normalized so that

$$\int\Psi\Psi^* dxdydzdq_1dq_2\cdots=1, \tag{11}$$

the coefficients $a^{(t)}_{n,\,n_1n_2\cdots}$ have the following simple physical meaning: $|a^{(t)}_{n,\,n_1n_2\cdots}|^2$ is the probability that at time $t$, the electron is in a state with energy $E_n$ and the first normal mode of the radiation field has an energy corresponding to $n_1$ quanta; the second normal mode has $n_2$ quanta, etc. The above-mentioned normalization insures that

$$\sum_{n,\,n_1\cdots}|a^{(t)}_{n,\,n_1n_2\cdots}|^2=1,$$

that is, the probability of finding the system in some allowed state is unity.

For purposes of determining the probability that an exchange of energy between the radiation field and the electron takes place, a knowledge of the coefficients $a^{(t)}_{n,\,n_1\cdots}$ is sufficient as we shall presently see. If, on the other hand, we are not interested directly in the energy exchange but we are interested in the probable location of the electrons at any given time regardless of the state of the field it may be found from the solution (10). Thus if $W(x, y, z, t)dxdydz$ is the probability that at time $t$ the electron will be located in the element of volume $dxdydz$, then

$$W(x,y,z,t)dxdydz=\left\{\int\Psi\Psi^* dq_1dq_2\cdots\right\}dxdydz =\left\{\sum_{n,\,m,\,n_1n_2\cdots}a^{(t)}_{n,\,n_1\cdots}a^{*(t)}_{m,\,n_1\cdots}\Phi_n\Phi_m^*\exp\left[-\frac{i}{\hbar}(E_n-E_m)t\right]\right\}dxdydz. \tag{12}$$

It can be inferred from this formula that it is a more difficult matter to determine the probability distribution of position for the electron than to determine the probability of energy exchange.

In the immediately following sections we shall confine our attention to the exchange of energy between electron and field for various transit times.

[5] See for instance, W. Pauli, *Handbuch der Physik*, Vol. 24, part I, page 114.

## PROBABILITY OF ENERGY EXCHANGE

The usual method[6] of determining the coefficients $a^{(t)}_{n,n_1\cdots}$ is to substitute Eq. (10) into Eq. (6), after priming the $n$'s, use Eqs. (8) and (9) and multiply the result by the complex conjugate of (7) and integrate over all coordinates. This gives

$$\frac{h}{i}\dot{a}^{(t)}_{n,n_1n_2\cdots}=\frac{e}{mc}\sum_{n'n_1'\cdots}\left\{\int\Phi_n^*\phi_{n_1}^*\cdots\mathbf{A}\cdot\mathbf{p}\Phi_{n'}\phi_{n_1'}\cdots dxdydzdq_1\cdots\right\}\cdot\exp\left\{-\frac{i}{h}[E_{n'}-E_n+h\omega_1(n_1'-n_1)+\cdots]t\right\}. \quad (13)$$

If $\mathbf{A}$ be replaced by its respentation (4) in normal modes, then the integrals with respect to $q_1, q_2\cdots$ can be evaluated. From the well-known mathematical properties of the functions $\phi_{n_1}\cdots$, which lead to the selection rules for the linear simple harmonic oscillator[7] the only terms in the sum on the right-hand side of Eq. (13) which give a contribution different from zero for the $s$th normal mode are the two for which $n_1'n_2'n_s'\cdots$ equals $n_1, n_2\cdots n_s+1, n_{s+1}\cdots$ and $n_1, n_2, \cdots n_s-1, n_{s+1}\cdots$, respectively. This means that, no matter what the probability distribution of the electron is, the energy transferred in time $dt$ must either increase or decrease the field energy by *one quantum*. Thus all energy exchanges take place in steps of one quantum at a time.

If the above indicated operations are carried out, Eq. (13) becomes:

$$\frac{h}{i}\dot{a}^{(t)}_{n,n_1,\cdots}=\frac{e}{mc}\sum_{n',s}\left\{\int\Phi_n^*\mathbf{A}_s\cdot\mathbf{p}\Phi_{n'}dxdydz\right\}\exp\left[-\frac{i}{h}(E_{n'}-E_n)t\right]\cdot\left\{a^{(t)}_{n,n_1,\cdots n_s-1,\cdots}\left\{\frac{n_sh}{2\omega_s}\right\}^{\frac{1}{2}}\exp[i\omega_st]+a^{(t)}_{n,n_1,\cdots n_s+1}\left\{\frac{(n_s+1)h}{2\omega_s}\right\}^{\frac{1}{2}}\exp[-i\omega_st]\right\}. \quad (14)$$

For the treatment of a certain class of problems, this relation can be materially simplified. For the present it will be assumed that the electron's position is known with considerable accuracy so that $|\Phi_n|^2$ is different from zero over a very small region such that the quantity $(\mathbf{A}_s\cdot\mathbf{p})$ can be regarded as a very slowly varying function of position over this region. Also for simplicity we shall suppose that only one normal mode of the enclosure is excited namely the $s$th mode. Then the sum over $s$ can be removed and since $\mathbf{A}_s\cdot\mathbf{p}$ is a slowly varying function of position compared to $\Phi_n$ we may write

$$\int\Phi_n^*(\mathbf{A}_s\cdot\mathbf{p})\Phi_{n'}dxdydz\approx\langle(\mathbf{A}_s\cdot\mathbf{p})\rangle_{Av}\int\Phi_n^*\Phi_{n'}dxdydz\approx\langle(\mathbf{A}_s\cdot\mathbf{p})\rangle_{Av}\delta_{nn'}, \quad (15)$$

where $\delta_{nn'}=0$ when $n\neq n'$ and 1 when $n'=n_1$. The latter follows from the orthogonality of the functions $\Phi_n$. Consequently, it may be inferred that terms in the sum over $n'$ will be small except that for which $n'=n$ so that Eq. (14) reduces to

$$\frac{h}{i}\dot{a}^{(t)}_{n,n_s}=\frac{e}{mc}M_n\left(\frac{h}{2\omega_s}\right)^{\frac{1}{2}}\{a^{(t)}_{n,n_s-1}(n_s)^{\frac{1}{2}}\exp[i\omega_st]+a^{(t)}_{n,n_s+1}(n_s+1)^{\frac{1}{2}}\exp[-i\omega_st]\}, \quad (16)$$

where

$$M_n=\int\Phi_n^*(\mathbf{A}_s\cdot\mathbf{p})\Phi_ndxdydz. \quad (17)$$

The subscripts $n_1, n_2\cdots$ except $n_s$ have been dropped since only quanta in the $s$th mode are under consideration.

The time rate of change of the probability that $n_s$ quanta will be the $s$th normal mode at time $t$

[6] See reference 4, page 94.

[7] See for instance L. Pauling and E. Wilson, *Introduction to Quantum Mechanics* (McGraw-Hill Book Company, Inc., New York, 1935), page 82.

is given by

$$\frac{d}{dt}|a_{n,n_s}|^2=\dot{a}_{n,n_s}a^*_{n,n_s}+a_{n,n_s}\dot{a}^*_{n,n_s}$$

$$=\frac{e}{mc}\frac{iM_n}{(2\hbar\omega_s)^{\frac{1}{2}}}[a^*_{n,n_s}a_{n,n_s-1}(n_s)^{\frac{1}{2}}\exp[i\omega_s t]+a^*_{n,n_s}a_{n,n_s+1}(n_s+1)^{\frac{1}{2}}\exp[-i\omega_s t]$$

$$-\{a_{n,n_s}a^*_{n,n_s-1}(n_s)^{\frac{1}{2}}\exp[-i\omega_s t]+a_{n,n_s}a^*_{n,n_s+1}(n_s+1)^{\frac{1}{2}}\exp[i\omega_s t]\}]$$

$$=-\frac{2e}{mc}\frac{M_n}{(2\hbar\omega_s)^{\frac{1}{2}}}\text{I.P.}\{a^*_{n,n_s}a_{n,n_s-1}(n_s)^{\frac{1}{2}}\exp[i\omega_s t]+a^*_{n,n_s}a_{n,n_s+1}(n_s+1)^{\frac{1}{2}}\exp[-i\omega_s t]\},\quad(18)$$

where I.P. means "the imaginary part of." The two terms on the right can be interpreted in a very simple way. The first term gives the time rate of increase $|a_{n,n_s}|^2$ due to a transfer of one quantum from the electron to the radiation field, that is to say, the transition probability per unit time from the radiation state $n_s-1$ to $n_s$ because of interaction with the electron. The second term is the transition probability per unit time of a transition from state $n_s+1$ to $n_s$. This interpretation can be made clearer by noting the time rate of change of $|a_{n,n_s-1}|^2$. This is

$$\frac{d}{dt}|a_{n,n_s-1}|^2=-\frac{2e}{mc}\frac{M_n}{(2\hbar\omega_s)^{\frac{1}{2}}}\text{I.P.}\{a^*_{n,n_s-1}a_{n,n_s-2}(n_s-1)^{\frac{1}{2}}\exp[i\omega_s t]$$

$$+a^*_{n,n_s-1}a_{n,n_s}(n_s)^{\frac{1}{2}}\exp[-i\omega_s t]\}.\quad(19)$$

The second term in this expression is the time rate of increase in $|a_{n,n_s-1}|^2$ due to a transition from state $n_s$ to $n_s-1$. A comparison of this term with the first term on the right of (18) shows it to be identical except for the opposite sign. Thus we may conclude that the term

$$-\frac{2e}{mc}\frac{M_n}{(2\hbar\omega_s)^{\frac{1}{2}}}\text{I.P.}\,a^*_{n,n_s}a_{n,n_s-1}(n_s)^{\frac{1}{2}}\exp[i\omega_s t],\quad(20)$$

is the probability of absorption of a quantum by the field per unit time due to a transition $n_s-1$ to $n_s$ for those values of $t$ which make the above quantity positive while the negative of the above quantity is the probability of emission of a quantum by the field per unit time due to a transition $n_s$ to $n_s-1$, for values of $t$ which make it positive. Thus there is a clear demarcation in time over which absorption and emission of a quantum may occur. Consequently, in a time interval $dt$ absorption and emission will not both occur.

Since the interaction of field and electron can give rise to an absorption of a quantum by the $s$th normal mode in a number of ways, i.e., by transitions from $n_s=0$ to $n_s=1$; $n_s=1$ to $n_s=2$, etc., the total probability that the field will absorb a quantum in unit time between any two states is

$$T_{ab}=\frac{2e}{mc}\frac{M_n}{(2\hbar\omega_s)^{\frac{1}{2}}}\text{I.P.}\exp[i\omega_s t]\sum_{n_s=1}^{\infty}a^*_{n,n_s}a_{n,n_s-1}(n_s)^{\frac{1}{2}}\quad(21)$$

for values of $t$ for which $T_{ab}$ is positive. The above sum can be evaluated approximately by assuming that there are a reasonably large number of quanta in the field of the enclosure on the average. If we call this average number $n_0$, the probability $|a_{n,n_s}|^2$ that at time $t$ the radiation field will be in the state $n_s$ may be assumed to vary with $n_s$ as indicated in Fig. 1. The $(n_s)^{\frac{1}{2}}$ is also shown in the figure. Since $(n_s)^{\frac{1}{2}}$ is slowly varying, we shall assume that it varies but little

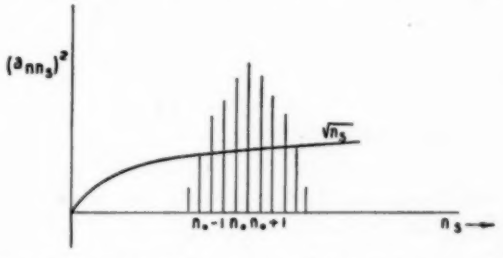


FIG. 1. The probability that at time $t$, $n_s$ quanta will be in the $s$th normal mode when the average number of quanta in this mode is $n_0$.

and is equal to $(n_0)^{\frac{1}{2}}$ over those values of $n_s$ for which the $a_{n,n_s}$ in the above sum contribute anything. Under these circumstances we may remove $(n_s)^{\frac{1}{2}}$ from the sum and write

$$\sum_{n_s=1}^{\infty} a^*_{n,n_s} a_{n,n_s-1}(n_s)^{\frac{1}{2}} \approx (n_0)^{\frac{1}{2}} \sum_{n_s=1}^{\infty} a^*_{n,n_s} a_{n,n_s-1}.$$

If we also make the assumption that $a_{n,n_s}$ is not too different from its neighbor $a_{n,n_s-1}$ in absolute value and phase, then we should obtain a good approximation[8] to the above sum by writing

$$\sum_{n_s} a^*_{n,n_s} a_{n,n_s-1} = \sum_{n_s} a^*_{n,n_s} a_{n,n_s} = 1. \quad (22)$$

A separate study of the effect of neglecting the phases of the coefficients has not been made. The final results appear to warrant the above approximation. On making use of the above approximation in (21) the absorption probability per unit time becomes

$$T_{ab} = -\frac{2e}{mc}\frac{M_n(n_0)^{\frac{1}{2}}}{(2\hbar\omega_s)^{\frac{1}{2}}} \sin \omega_s t \quad \text{for values of } t \text{ making } T_{ab}>0$$
$$= 0 \quad \text{for all other } t. \quad (23)$$

The total probability per unit time for an emission of one quantum can be arrived at in the same way and is

$$T_{em} = \frac{2e}{mc}\frac{M_n(n_0)^{\frac{1}{2}}}{(2\hbar\omega_s)^{\frac{1}{2}}} \sin \omega_s t \quad \text{for values of } t \text{ making } T_{em}>0$$
$$= 0 \quad \text{for all other } t. \quad (24)$$

To complete the treatment of energy exchange between the electron and field it is necessary to compute the probability that the field will absorb or emit a given number of quanta during the interval of time in which the field and electron interact. Since it has been shown that absorption and emission do not overlap in time, we may first consider an interval of time for which absorption occurs, i.e., $T_{ab}>0$ and determine the probability $p_j^a$ that $j$ quanta will be absorbed during this interval. Since only absorption can occur in this interval and it must proceed in steps of one quantum, the only way that $p_j^a$ can change with time is for a transition to occur so that in time $dt$ the number of quanta in the field must increase from $j-1$ to $j$ or increase from $j$ to $j+1$. This situation is expressed by the equation

$$dp_j^a/dt = T_{ab}p_{j-1} - T_{ab}p_j. \quad (25)$$

The solution of this equation can be facilitated by letting

$$s_a = \int_{t_1}^{t} T_{ab}dt \quad \text{for } t\text{'s such that } T_{ab}>0. \quad (26)$$

Then

$$dp_j^a/ds_a = p_{j-1}{}^a - p_j.$$

It is well known that a solution of this equation subject to the condition that

$$\sum_{j=0}^{\infty} p_j^a = 1$$

is

$$p_j^a = \frac{s_a{}^j \exp(-s_a)}{j!}. \quad (27)$$

In a similar way we may calculate the probability $p_j^e$ that $j$ quanta have been emitted by the field during a time interval for which $T_{em}>0$. This probability is

$$p_j^e = \frac{s_e{}^j \exp(-s_e)}{j!}, \quad (28)$$

where

$$s_e = \int_{t_2}^{t} T_{em}dt \quad \text{for } t\text{'s such that } T_{em}>0. \quad (29)$$

When the interval during which interaction occurs is such that both absorption and emission can take place, the probability that in this total interval one quantum is absorbed by a process in which $j+1$ quanta are absorbed and $j$ quanta emitted is

$$p_{j+1}(s_a)p_j(s_e).$$

Since one quantum may be absorbed in the whole interval by absorbing 2 quanta and emitting one, absorbing 3 quanta and emitting 2, etc., the total probability that one quantum will be absorbed is

$$P_1 = \sum_{j=0}^{\infty} p_{j+1}(s_a)p_j(s_e).$$

The probability that $N$ quanta will be absorbed

[8] The author is indebted to H. A. Bethe for suggesting this type of approximation which removes the necessity of determining the individual probability coefficients.

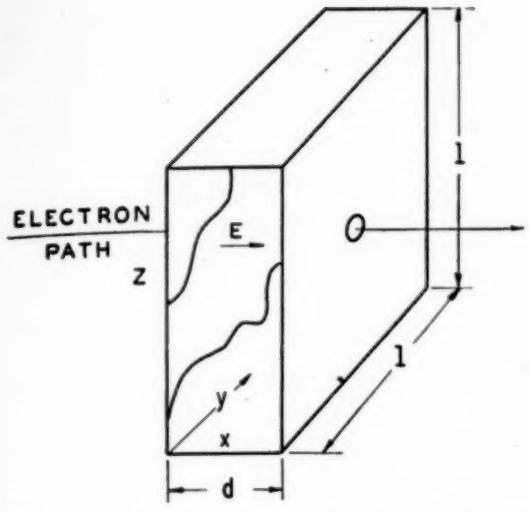


FIG. 2. Sketch of the cavity containing the radiation field.

in the interaction interval is obviously

$$P_N=\sum_{j=0}^{\infty} p_{j+N}(s_a)p_j(s_e). \tag{30}$$

We may follow a similar procedure and derive the probability $P_{-N}$ that the field will lose $N$ quanta to the electron during one transit. This is

$$P_{-N}=\sum_{j=0}^{\infty} p_j(s_a)p_{N+j}(s_e). \tag{31}$$

It is possible to express the above sums by well-known functions. To do this the expressions (27) and (28) are used in formula (30). Then

$$P_N=\sum_{j=0}^{\infty}\frac{s_a{}^{j+N}\exp(-s_a)}{(j+N)!}\cdot\frac{s_e{}^j\exp(-s_e)}{j!}$$

$$=\exp(-s_a-s_e)\sum_{j=0}^{\infty}\frac{s_a{}^{j+N}s_e{}^j}{(j+N)!j!}.$$

If we recall that the series expansion for the Bessel's function is

$$J_N(x)=\sum_{j=0}^{\infty}\frac{(x/2)^{2j+N}(-1)^j}{(j+N)!j!},$$

then by writing

$$\frac{x}{2}=i(s_as_e)^{\frac{1}{2}},$$

we have

$$\sum_{j=0}^{\infty}\frac{s_a{}^{j+N}s_e{}^j}{(j+N)!j!}=i^{-N}\left(\frac{s_a}{s_e}\right)^{N/2}J_N[i2(s_as_e)^{\frac{1}{2}}].$$

Using this formula, we may write both formulae (30) and (31) as

$$P_N=\exp(-s_a-s_e)\left(\frac{s_a}{s_e}\right)^{N/2}i^{-N}J_N[i2(s_as_e)^{\frac{1}{2}}] \tag{32}$$

which holds for both positive and negative integer values of $N$.

This formula together with (26) and (29) enables us to compute the probability that $N$ quanta will have been transferred from electron to field or *vice versa* during the time of interaction between field and electron.

The value of the mathematical expectation for the total energy exchange $W_q$, between electron and field during the complete interaction time will be

$$\langle W_q\rangle=\hbar\omega_s\sum_{N=-\infty}^{\infty}NP_N. \tag{33}$$

This series can be summed with the help of the generating function for the Bessel's function. Using the value of $P_N$ from (32) and denoting $1/i(s_a/s_e)^{\frac{1}{2}}$ by $\xi$ and $i2(s_as_e)^{\frac{1}{2}}$ by $z$, the above formula becomes

$$\frac{\langle W_q\rangle}{\hbar\omega_s}=\exp(-s_a-s_e)\sum_{N=-\infty}^{+\infty}N\xi^NJ_N(z). \tag{34}$$

The generating function for the Bessel's function yields

$$\exp\left[\frac{z}{2}\left(\xi-\frac{1}{\xi}\right)\right]=\sum_{N=-\infty}^{+\infty}\xi^NJ_N(z).$$

In order to obtain the sum in (34) we need only differentiate the above equation with respect to $\xi$. Thus

$$\frac{d}{d\xi}\exp\left[\frac{z}{2}\left(\xi-\frac{1}{\xi}\right)\right]=\frac{1}{\xi}\sum_{N=-\infty}^{+\infty}N\xi^NJ_N(z),$$

or

$$\sum_{N=-\infty}^{+\infty}N\xi^NJ_N(z)=\frac{z}{2}\left(\xi+\frac{1}{\xi}\right)\exp\left[\frac{z}{2}\left(\xi-\frac{1}{\xi}\right)\right]. \tag{35}$$

When the value of the above series is placed in Eq. (34) and $\xi$ and $z$ replaced by their definitions in terms of $s_a$ and $s_e$ we obtain the following exceedingly simple result for $\langle W_q\rangle$, namely

$$\langle W_q\rangle=(s_a-s_e)\hbar\omega_s. \tag{36}$$

In a later discussion of some special examples we shall need to compute the standard deviation

of the expected energy $\langle W_q \rangle$. By definition this is just the square root of the mathematical expectation of

$$(W_q - \langle W_q \rangle)^2$$

which will be denoted by

$$\langle (W_q - \langle W_q \rangle)^2 \rangle.$$

It is well known[9] that

$$\langle (W_q - \langle W_q \rangle)^2 \rangle = \langle W_q^2 \rangle - \langle W_q \rangle^2. \tag{37}$$

Then since

$$\langle W_q^2 \rangle = (\hbar\omega_s)^2 \sum_{N=-\infty}^{+\infty} N^2 P_N, \tag{38}$$

we require the evaluation of the series

$$\sum_{N=-\infty}^{+\infty} N^2 \xi^N J_N(z)$$

which can be done by differentiating Eq. (35) once with respect to $\xi$ and multiplying by $\xi$. When the result is substituted in (38) and $\xi$ and $z$ replaced by their definitions in terms of $s_a$ and $s_e$ as was done before, we obtain

$$\langle W_q^2 \rangle = \{(s_a - s_e)^2 + (s_a + s_e)\}(\hbar\omega_s)^2. \tag{39}$$

From (36), (37), and (39) the standard deviation is

$$D = \langle (W_q - \langle W_q \rangle)^2 \rangle^{\frac{1}{2}} = \hbar\omega_s (s_a + s_e)^{\frac{1}{2}}. \tag{40}$$

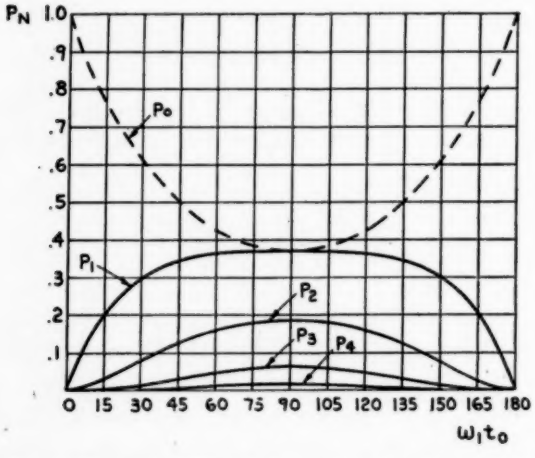


FIG. 3. The probability of absorption of various numbers of quanta as a function of the entrance phase of the electron for the short transit-time case and $\epsilon = 1$. The emission probabilities $P_0$, $P_{-1}$, etc., are given by the above curves shifted to the phase interval (180°–360°).

[9] J. V. Uspensky, *Introduction to Mathematical Probability* (McGraw-Hill Book Company, Inc., New York), p. 172.

The ratio of the deviation to the mean expected energy exchange is of interest and turns out to be

$$\frac{D}{\langle W_q \rangle} = \frac{(s_a + s_e)^{\frac{1}{2}}}{s_a - s_e}. \tag{41}$$

We are now in a position to apply the results of the general theory developed above to some particular examples.

## PARTICULAR EXAMPLES

As an example for detailed consideration, we shall consider the interaction of an electron with the lowest frequency normal mode in a perfectly conducting rectangular box of dimensions $l, l$, and $d$ as shown in Fig. 2. The normal mode we shall consider is that which has the electric field in the $x$ direction only. This will be the lowest frequency mode of the box if $d < l$. The vector potential for this mode will be

$$A_x(y, z, t) = \frac{cE_0}{\omega_1} \cos \omega_1 t \sin \frac{\pi y}{l} \sin \frac{\pi z}{l}, \tag{42}$$

where $E_0$ is the amplitude of the oscillating electric field when $y = l/2$ and $z = l/2$.

We shall assume that the electron passes through the cavity in the $x$ direction, i.e., in a direction parallel to the electric field with constant velocity $v$. Although actually $v$ will not be constant because of energy transferred to the field, we may take $v$ to be constant if $v$ is large compared to the change in velocity since this change in velocity would lead to a perturbation of the second order.

From a classical standpoint, the rate at which energy is transferred from electron to the field is given by

$$\frac{dW_c}{dt} = -evE = -evE_0 \sin \frac{\pi y}{l} \sin \frac{\pi z}{l} \sin \omega_1 t.$$

It should be noted that a specific time phase has been chosen for the vector potential (42) of the field. This has been done for the following reason. In the quantum theory treatment, the time dependence of the transition probability per unit time $T_{ab}$ given by the expression (23) is independent of the time phase of the vector potential. Consequently, the correlation of the quantum energy exchange and the classical exchange as a function of the time phase of the

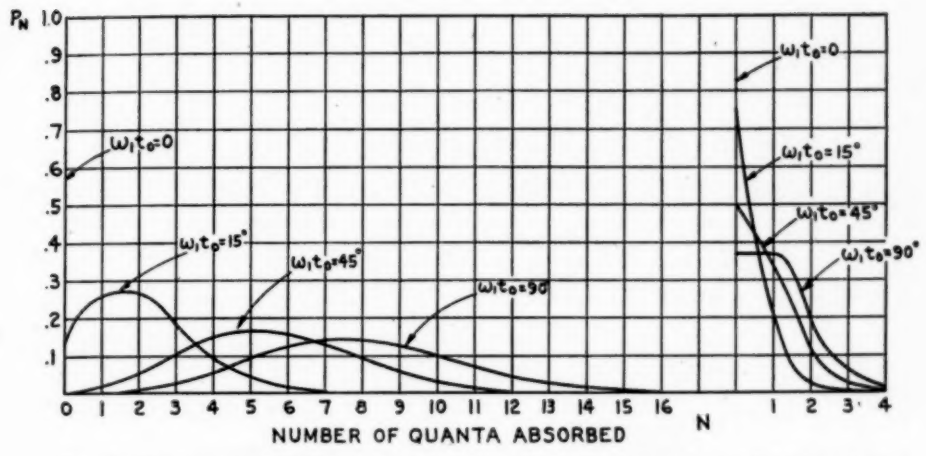


FIG. 4. The energy distribution of emerging electrons entering the cavity at various phases for the short transit-time case. The curves on the right show the probable number of quanta lost by the electrons for the case $\epsilon=1$. The curves on the left give the same information for the case $\epsilon=8$.

field in the transition region where quantum and classical theory should overlap will not automatically occur. In order to secure such a correlation or to compare the phases of the transition probability per unit time with the time rate of change of energy computed classically, it is simplest to arrange the phase of the field so that initially at $t=0$ the rate of change of energy will be zero in both theories, i.e., $dW_c/dt=T_{ab}=0$ at $t=0$. This correlation is established when $\cos\omega_1 t$ is used in the vector potential of the field.

The total energy transferred from electron to field as computed classically for an electron entering the cavity at time $t_0$ and leaving at time $t_0+\tau$ is obtained by integrating the above equation. Thus

$$W_c=-e\int_{t_0}^{t_0+\tau} vE_0\sin\frac{\pi y}{l}\sin\frac{\pi z}{l}\sin\omega_1 t\,dt$$

$$=-\frac{|e|vE_0}{\omega_1}\sin\frac{\pi y}{l}\sin\frac{\pi z}{l}[\cos\omega_1(t_0+\tau)-\cos\omega_1 t_0]. \quad (43)$$

In order to begin the quantum theory calculations, it is necessary to compute $M_n$ from formula (17) which is

$$M_n=\int\Phi_n^*(\mathbf{A}_s\cdot\mathbf{p})\phi_n dxdydz.$$

It must be remembered that in this formula $\mathbf{A}_s$ is the space distribution of the normal mode of the field and is to be normalized to $4\pi c^2$. Thus

$$(\mathbf{A}_s\cdot\mathbf{p})=A_{1z}p_z=mv\frac{4(\pi c)^{\frac{1}{2}}}{(l^2d)^{\frac{1}{2}}}\sin\frac{\pi y}{l}\sin\frac{\pi z}{l}. \quad (44)$$

Thus

$$M_n=+\frac{mv4(\pi c)^{\frac{1}{2}}}{(l^2d)^{\frac{1}{2}}}\int_{\substack{\text{over volume}\\ \text{of cavity}}}\Phi_n^*\sin\frac{\pi y}{l}\sin\frac{\pi z}{l}\Phi_n dxdydz.$$

If the electron's position at time $t_0$ is known with considerable accuracy then $\Phi_n^*\Phi_n$ will be different from zero over an extremely small region, i.e., small compared to regions over which $\mathbf{A}_1$ varies appreciably. For this case we write

$$\int\Phi_n^*\sin\frac{\pi y}{l}\sin\frac{\pi z}{l}\Phi_n dxdydz$$

$$\approx\sin\frac{\pi y}{l}\sin\frac{\pi z}{l}\int\Phi_n^*\Phi_n dxdydz$$

$$\approx\sin\frac{\pi y}{l}\sin\frac{\pi z}{l}.$$

Consequently

$$M_n=\frac{4(\pi c)^{\frac{1}{2}}}{(l^2d)^{\frac{1}{2}}}mv\sin\frac{\pi y}{l}\sin\frac{\pi z}{l}. \quad (45)$$

In order to obtain the transition probabilities per unit time as given by formulae (23) and (24), we require the average number of quanta $n_0$ in the first normal mode field in the cavity. This may be found by equating the average quantum energy $n_0\hbar\omega_1$ to the total classical

energy in the field. Thus

$$n_0\hbar\omega_1=\int\frac{E^2+H^2}{8\pi}dxdydz=\frac{l^2dE_0^2}{32\pi},$$

or

$$n_0=E_0^2l^2d/32\pi\hbar\omega_1. \tag{46}$$

The transition probabilities (23) and (24) then become

$$\begin{aligned} T_{ab}&=+\frac{|e|vE_0}{\hbar\omega_1}\sin\frac{\pi y}{l}\sin\frac{\pi z}{l}\sin\omega_1 t \\ &\qquad 0\le\omega_1 t\le\pi \\ &=0 \qquad \pi<\omega_1 t\le 2\pi \\ T_{em}&=0 \qquad 0<\omega_1 t\le\pi \end{aligned} \tag{47}$$

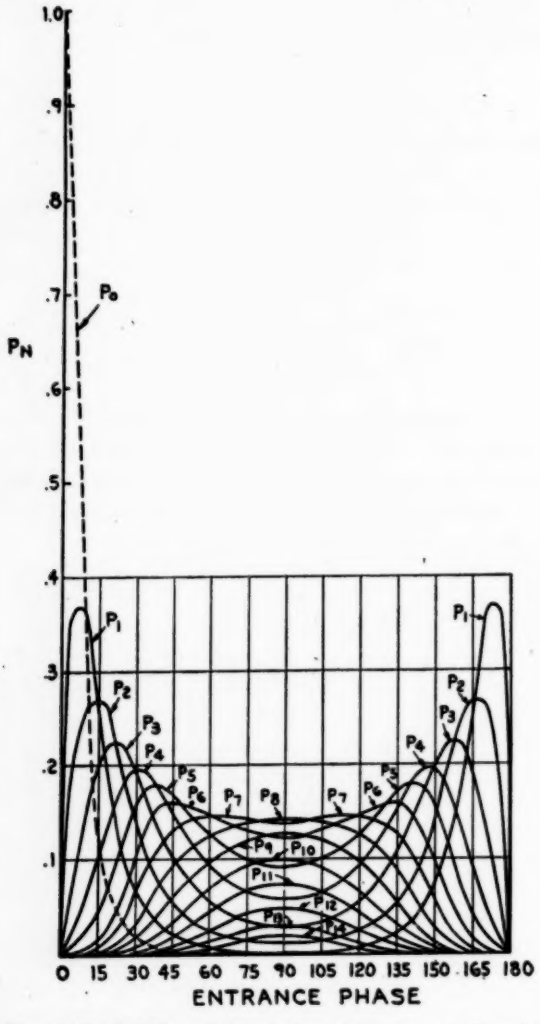


FIG. 5. Probability of absorption of quanta as a function of entrance phase of the electron for the short transit-time case and $\epsilon=8$. The probability of emission is found by displacing the above curves to the phase interval (180°–360°).

$$T_{em}=-\frac{|e|vE_0}{\hbar\omega_1}\sin\frac{\pi y}{l}\sin\frac{\pi z}{l}\sin\omega_1 t \qquad \pi\le\omega_1 t\le 2\pi \tag{48}$$

where the electronic charge $e$ has been replaced by $-|e|$.

The total probability that a given number of quanta will be emitted or absorbed will be calculated for two cases, namely the case where an electron traverses the box in a time $\tau$ very short compared to the period of the oscillating field and the case when $\tau$ is equal to a half period.

### Case I. Short Transit Time

The first step is to calculate the quantities $s_a$ and $s_e$ from Eqs. (26) and (29). The time of entrance of the electron into the cavity will be designated by $t_0$ and the transit time by $\Delta\tau\ll 2\pi/\omega_1$. From (26) and (47)

$$\begin{aligned} s_a&=\int_{t_0}^{t_0+\Delta\tau}\frac{|e|vE_0}{\hbar\omega_1}\sin\frac{\pi y}{l}\sin\frac{\pi z}{l}\sin\omega_1 t\,dt \\ &\qquad 0\le\omega_1 t_0\le\pi \\ &\approx\frac{|e|E_0v\Delta\tau}{\hbar\omega_1}\sin\frac{\pi y}{l}\sin\frac{\pi z}{l}\sin\omega_1 t_0. \end{aligned} \tag{49}$$

Since $v\Delta\tau=d$, then

$$\begin{aligned} s_a&=\epsilon\sin\omega_1 t_0 \qquad 0\le\omega_1 t_0\le\pi \\ &=0 \qquad\qquad\quad \pi<\omega_1 t_0<2\pi \end{aligned} \tag{50}$$

where

$$\epsilon=\frac{|e|E_0d}{\hbar\omega_1}\sin\frac{\pi y}{l}\sin\frac{\pi z}{l}. \tag{51}$$

A comparison of this with the expression (43) for the classical energy transferred shows that the numerator of (51) is the maximum energy that could be transferred from electron to field when computed classically so that $\epsilon$ denotes the maximum number of quanta that could be transferred on a classical basis.

In a similar way, we find that

$$\begin{aligned} s_e&=0 \qquad\qquad 0<\omega_1 t_0<\pi, \\ &=-\epsilon\sin\omega_1 t_0 \qquad \pi\le\omega_1 t_0\le 2\pi. \end{aligned} \tag{52}$$

On substituting these values of $s_a$ and $s_e$ in formula (32), we have

$$\begin{aligned} P_N&=\exp(-\epsilon\sin\omega_1 t_0)\frac{(\epsilon\sin\omega_1 t_0)^N}{N!} \\ &\qquad 0\le\omega_1 t_0\le\pi, \\ &=0 \qquad\qquad \pi<\omega_1 t_0<2\pi. \end{aligned} \tag{53}$$

Similarly, the probability that $N$ quanta will be emitted is

$$P_N=0 \qquad 0<\omega_1 t_0<\pi,$$
$$=\exp(\epsilon\sin\omega_1 t_0)\frac{(-\epsilon\sin\omega_1 t_0)^N}{N!} \qquad (54)$$
$$\pi\leq\omega_1 t_0\leq 2\pi.$$

These probabilities for absorption and emission of a given number of quanta for a transit of an electron are shown in Fig. 3, as a function of the entrance time $t_0$ for the case $\epsilon=1$. This is a case where one would expect quantum effects to manifest themselves because the maximum classical energy transferred from electron to field is equal to the energy of one quantum. An examination of the probability curves given in Fig. 3, shows one of the most important quantum effects, namely, that no matter at what time the electron transit takes place there is considerable probability that the electron will neither gain nor lose energy. This means that if a beam of electrons traversed the cavity a considerable part of the current would not be affected by the field. As will also be evident from the above-mentioned curves, of those electrons whose energy does change, the change is most likely to be by one quantum.

It follows also that if a number of electrons enter the cavity at time $t_0\neq 0$, the electrons leaving will not all have the same velocity but will have several discrete velocities corresponding to the number of quanta gained or lost. At time $t_0=0$, there is no energy distribution of the electrons leaving since no electrons gain or lose any quanta. The energy distribution of the electrons leaving the cavity is shown in Fig. 4 for four different entrance times. The spread in energies or the width of the energy distribution is greatest at $\omega_1 t_0=\pi/2$. If one were to consider electron bunching, this energy spread would be of some importance.

When the field is large enough so that a number of quanta could be absorbed on a classical basis, i.e., when $\epsilon\gg 1$, there are a variety of possibilities for the absorption of quanta. The various probabilities $P_N$ for absorption of $N$ quanta for $\epsilon=8$ are shown in Fig. 5. As is evident from the curves shown, there is considerable probability that any number of quanta up to the order of 16 may be absorbed depending on the time of entrance of the electron. In this case there is an appreciable correlation of the probability absorption of various quanta with the classical energy absorbed. For instance at $\omega_1 t_0=0$ when classically no energy would be absorbed $P_0=1$ and $P_1=P_2=\cdots=0$. For a somewhat later time, when a small amount of energy is absorbed on a classical basis, the probability of absorbing one quantum is largest. As time goes on until $\omega_1 t_0=\pi/2$, it becomes more and more probable that a larger number of quanta will be absorbed while the probability of absorbing a small number decreases.

The expected total energy transfer from elec-

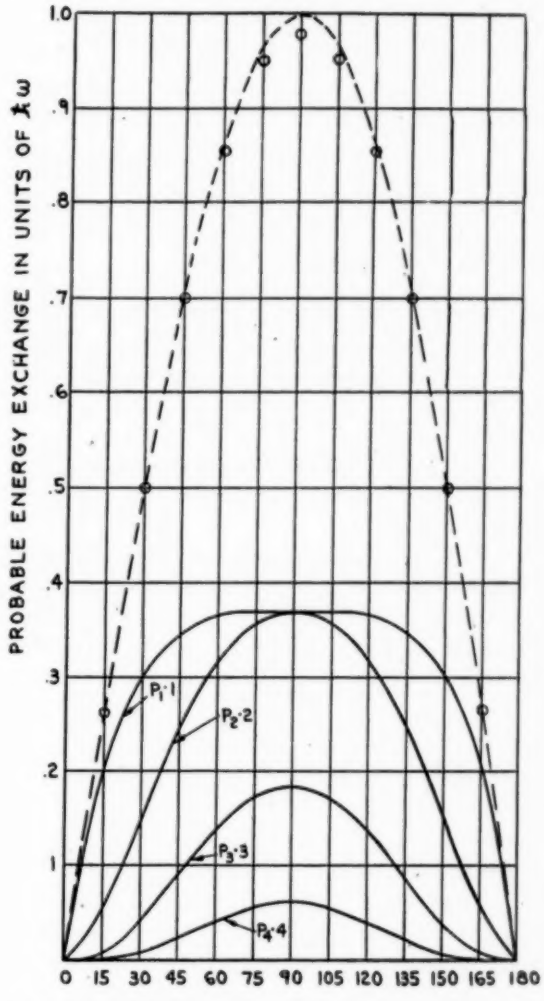


FIG. 6. Probable energy absorbed as a function of entrance phase for the short transit-time case and $\epsilon=1$. The dotted curve shows the classical energy absorption.

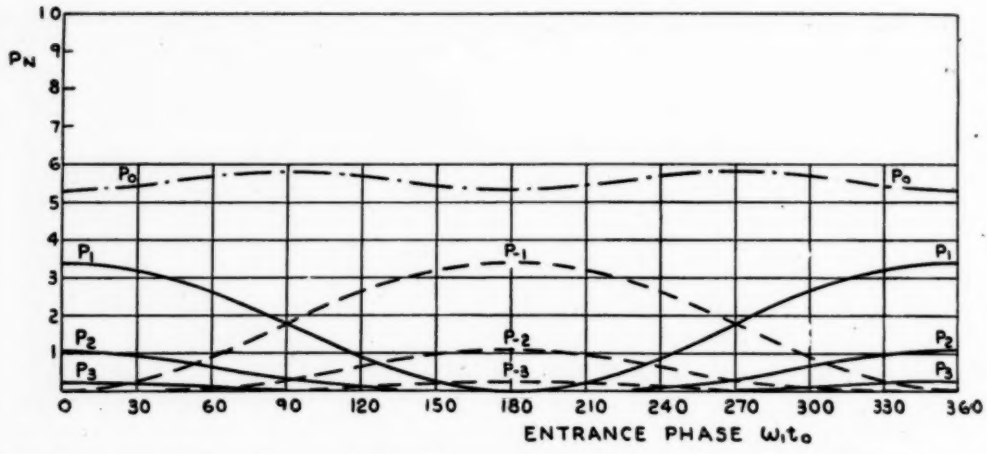


FIG. 7. The probability of absorption (solid curves) and emission (dashed curves) of quanta as a function of entrance phase of the electron for a transit time of one-half period and $\epsilon=1$.

trons to field and *vice versa* by all classes of electrons is given by formula (36). For the range of entrance phases such that $0=\omega_1 t_0=\pi$, we find on combining (50), (51), and (36) that

$$\langle W_q\rangle=\hbar\omega_1\epsilon\sin\omega_1 t_0. \tag{55}$$

A similar computation for the range $\pi\leq\omega_1 t_0\leq 2\pi$ would yield the same result hence the above formula holds for the entire range of entrance phases. A comparison of this result with the energy $W_c$ absorbed classically computed from (43) shows that $W_c=\langle W_q\rangle$. Consequently, the expected energy transfer is just that which would be found on the basis of classical theory. The correlation of energy exchange with the time phase of the field is thus established.

Since the curves in Fig. 5 show that there is a considerable probability for any of a number of quanta being absorbed, the distribution in energy of the emergent electrons is considerable for some entrance times. The energy distribution of emergent electrons for this case is also shown in Fig. 4, for electrons entering the cavity at several different times. Those entering at $\omega_1 t_0=0$ do not gain or lose any quanta so there is no distribution of emergent energies; all electrons have the same energy. A number of electrons entering at a later time will have a distribution of energies on emergence. The range of quanta over which there is appreciable probability of absorption or simply the "width" of the distribution increases as the entrance time is increased until $\omega_1 t_0=\pi/2$ and then decreases to zero again at $\omega_1 t_0=\pi$. Of a group of electrons entering the cavity at $\omega_1 t_0=\pi/2$, their emergent energies can differ by about 16 quanta. This exhibits the interesting quantum effect that an electron may lose considerably more energy than it could from classical theory.

A measure of the "half-width" of the energy distribution can be had by calculating the deviation for this case from formulae (40) and (50). Thus

$$D=[(W_q-\langle W_q\rangle)^2]^{\frac{1}{2}}=\hbar\omega_1(\epsilon\sin\omega_1 t_0)^{\frac{1}{2}}. \tag{56}$$

It is seen that the deviation from the mean or classical energy increases as the classical energy exchange increases. However, a more important quantity from the standpoint of measurement is the ratio of this deviation to the expected or

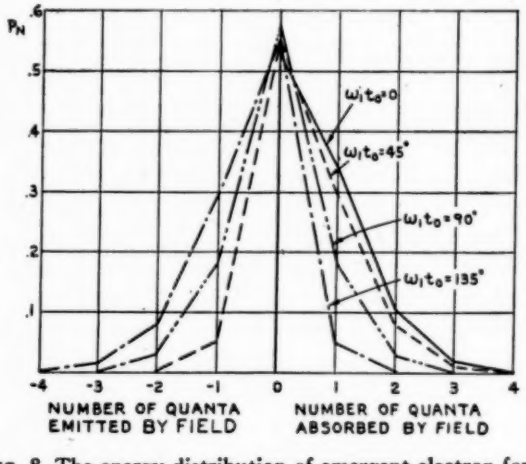


FIG. 8. The energy distribution of emergent electron for a transit time of one-half period and $\epsilon=1$.

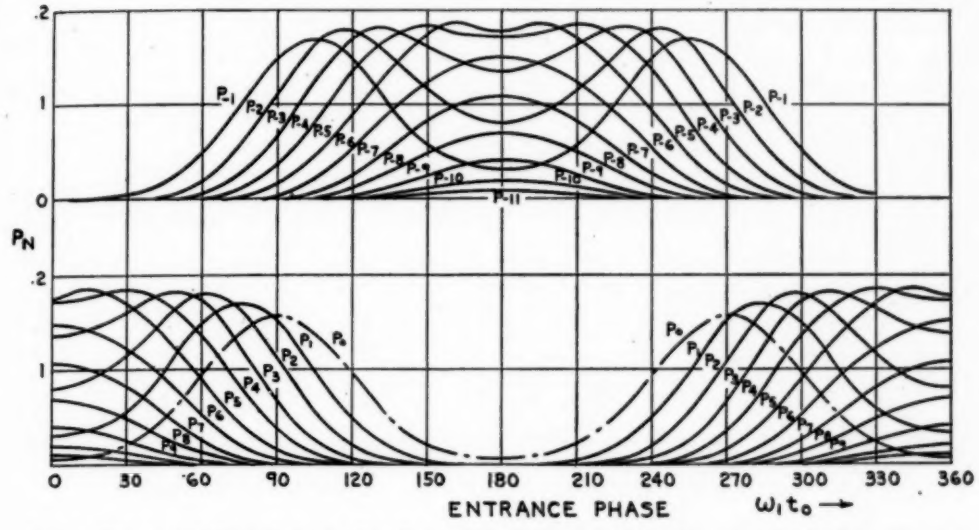


FIG. 9. The probability of absorption (lower curves) and emission (upper curves) of quanta as a function of electron entrance phase for a transit time of one-half period and $\epsilon=8$.

classical energy exchange. From (41) this is

$$\frac{D}{\langle W_q \rangle}=\frac{1}{(\epsilon \sin \omega_1 t)^{\frac{1}{2}}}. \tag{57}$$

Consequently except for $\omega_1 t \approx 0$ or $n\pi$, the deviation in the energy exchange becomes a small fraction of the classical energy when the classical energy exchange corresponds to a large number of quanta.

The probable energy transfer for each group of electrons is shown as a function of entrance time $t_0$ in Fig. 6 for $\epsilon=1$. For this case, the electrons which transfer one quantum contribute the largest part of the energy, but the electrons which transfer 2 and 3 quanta contribute a significant fraction of the energy especially at $\omega_1 t_0=\pi/2$ where the largest energy transfer takes place classically. Again we see the evidence of quantum effects in the fact that a considerable number of electrons suffer a gain or loss of energy larger than would be possible on the basis of classical theory. The dashed curve in Fig. 6 is the classical energy absorbed by the field in units of $\hbar\omega_1$, the circled points give the mathematically expected energy

$$\sum_{N=1}^{4} P_N N$$

in units of $\hbar\omega_1$. It is quite evident that the expected energy is almost exactly the classical energy even when only absorption of not more than 4 quanta per transit are taken into account.

### Case II. Transit Time a Half Period

In the next few paragraphs, a larger transit time case will be considered. From a classical point of view, it is then possible that the field first absorbs energy and later loses energy during one transit. Therefore, from a quantum theory point of view, we could expect that electrons beginning their transit at a given time would have the possibility of either gaining or losing energy as a result of the complete transit. This is just what is found to be the case.

For the consideration of the case in which the electron interacts with the field for a half period it is only necessary to calculate $s_a$ and $s_e$ for this situation. The required modification of formula (49) is obviously

$$\begin{aligned} s_a &= +\int_{t_0}^{\pi/\omega_1} \frac{|e|vE_0}{\hbar\omega_1} \sin\frac{\pi y}{l} \sin\frac{\pi z}{l} \sin \omega_1 t dt \\ &= +\frac{\epsilon}{\pi}(1+\cos \omega_1 t_0) \qquad 0 \leq \omega t_0 \leq \pi. \end{aligned} \tag{58}$$

Similarly

$$\begin{aligned} s_e &= -\int_{\pi/\omega_1}^{t_0+\pi/\omega_1} \frac{|e|vE_0}{\hbar\omega_1} \sin\frac{\pi y}{l} \sin\frac{\pi z}{l} \sin \omega_1 t dt \\ &= -\frac{\epsilon}{\pi}(1-\cos \omega_1 t_0) \qquad 0 \leq \omega t_0 \leq \pi. \end{aligned} \tag{59}$$

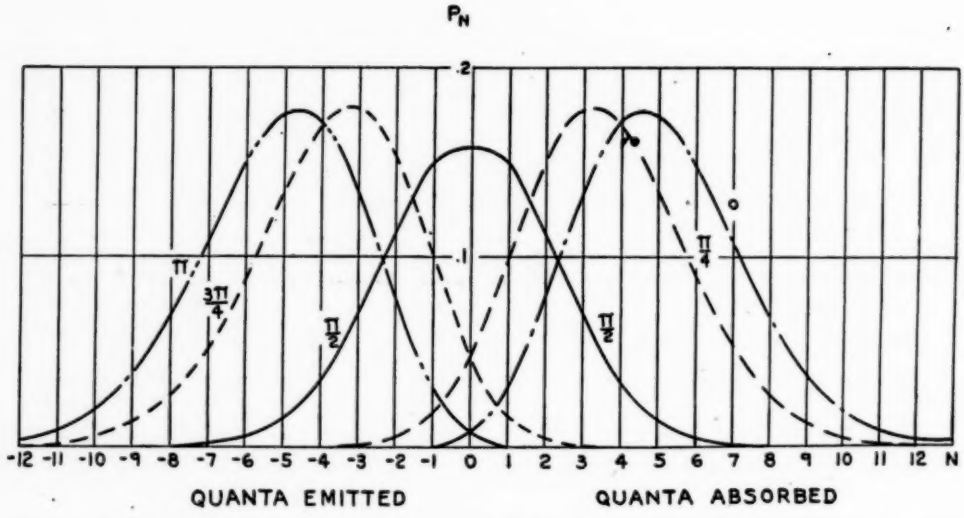


FIG. 10. Energy distribution of emerging electrons for various entrance phases for a transit time of one-half period and $\epsilon=8$.

These same formulae are obtained in the region $\pi\leq\omega_1 t_0\leq 2\pi$ so that they hold for all values of $t_0$. Substituting the above values of $s_a$ and $s_e$ in the expression (32) for $P_{\pm N}$, we have

$$P_{\pm N}=\exp\left[-\frac{2\epsilon}{\pi}\right]\{\cot\omega_1 t_{0/2}\}^{\pm N} i^{-|N|} \times J_{|N|}\left(\frac{2i\epsilon}{\pi}\sin\omega_1 t_0\right). \quad (60)$$

It may readily be shown that

$$P_N(\omega_1 t_0)=P_{-N}(\omega_1 t_0+\pi), \quad (61)$$

and

$$P_N(\omega_1 t_0+\pi)=P_{-N}(\omega_1 t_0). \quad (62)$$

Consequently, it is only necessary to calculate $P_N$ and $P_{-N}$ for the range $0\leq\omega_1 t_0\leq\pi$.

The above probabilities are shown in Fig. 7 for the case $\epsilon=1$. It is to be noted that no matter at what phase a group of electrons enter the cavity about one-half of them will emerge without having suffered any change in energy. This is inferred from the probability curve $P_0$ shown in the dot and dash curve. The solid curves give the probability of absorption of the indicated number of quanta by the field. The dashed curves give the probability of emission. Contrasting this case with the short transit time case we find for all entrance phases except $\omega_1 t_0=0$ and $\pi$ a certain probability for emission as well as absorption. This is to be expected because both processes may occur at various times during transit while in the short transit time case either absorption or emission occurred but not both.

From formulae (43) and (51), it follows that the classical energy absorbed by the field is

$$W_c=\hbar\omega_1\frac{2\epsilon}{\pi}\cos\omega_1 t_0. \quad (63)$$

Consequently, the electron which enters at $\omega_1 t_0=0$ transfers the greatest amount of energy to the field and indeed the probabilities for absorption of 1, 2, $\cdots$ quanta have their maxima at $\omega_1 t_0=0$. At $\omega_1 t_0=\pi/2$ there is no energy exchange from a classical point of view. An inspection of the curves shows that for this entrance phase the probability of absorption and emission of quanta by the field are just equal so that it is just as likely that an electron lose a given number of quanta as gain this number so that the expected energy transfer is zero at this entrance phase which of course agrees with the classical energy exchange.

The energy distributions of emerging electrons for the transit angle $\pi$ and $\epsilon=1$ are shown in Fig. 8. The solid line connects the values of probability that the electron has lost (field absorbed) the number of quanta indicated on the axis of abscissa for an electron entering the cavity at $\omega_1 t_0=0$. The field only absorbs energy from these electrons so that the distribution "curve" is one sided. The assymmetry becomes less as the entrance phase increases to $\omega_1 t_0=\pi/2$

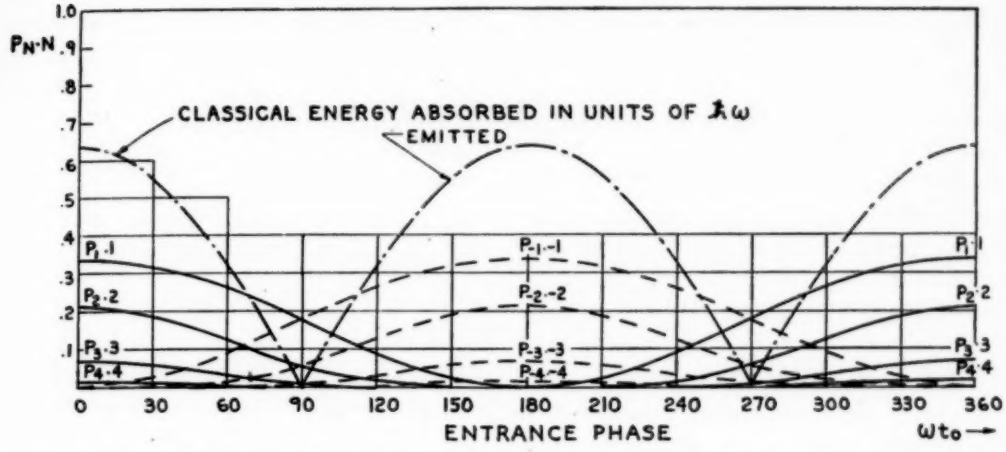


FIG. 11. The probable energy exchange as a function of electron entrance phase for a transit time of one-half period and $\epsilon=1$.

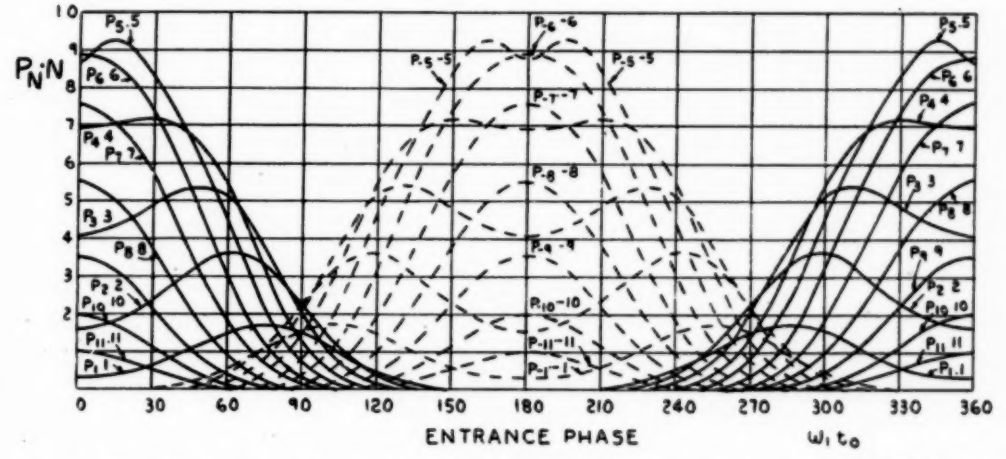


FIG. 12. The probable energy exchange as a function of electron entrance phase for a transit time of one-half period and $\epsilon=8$.

where it is symmetrical (just as many electrons lose as gain energy). As the entrance phase increases still further the curves become assymmetrical in the opposite sense. The width of the distribution is of the order of four quanta. The deviation for the transit angle $\pi$ is given by formula (64).

The probability curves for absorption and emission for $\epsilon=8$ are shown in Fig. 9. The first thing to be noticed is that the probability that no quanta will be absorbed or emitted is very much less than for $\epsilon=1$ and is really only appreciable at $\omega_1 t_0=\pi/2$ where no energy exchange could take place classically. One finds also that the probability of absorption of one quanta has its maximum at $\omega_1 t_0$ somewhat less than $\pi/2$ and the probability that an emission takes place has its maximum at $\omega_1 t_0$ somewhat larger than $\pi/2$. These curves show clearly how it is that the classical behavior is approached as $\epsilon$ becomes large.

The energy distributions for the emerging electrons for various entrance phases are shown in Fig. 10. The "width" of the distribution is about the same for all entrance phases. This is indicated analytically by the deviation which in this case is found by combining formulae (40), (58), and (59). Thus

$$D=\hbar\omega_1(2\epsilon/\pi)^{\frac{1}{2}}. \tag{64}$$

Consequently for the transit angle $\pi$, the deviation and thus the "half-width" of the energy

distribution of emergent electrons is independent of the entrance phase of the electrons.

Figures 11 and 12 show the probable energy exchange as a function of entrance phase for the two cases $\epsilon=1$ and $\epsilon=8$. An examination of these curves indicates the quantum effects already referred to and in addition show the detailed mechanism of the absorption and emission of quanta which in aggregate provide us with an understanding of the transition from pronounced quantum effects for $\epsilon$ small to a classical behavior when $\epsilon$ is large.

The expected energy transfer $\langle W_q \rangle$ for this case can be computed with the help of formulae (36), (58), and (59) and comes out to be

$$\langle W_q \rangle = \hbar\omega_1 \frac{2\epsilon}{\pi} \cos \omega_1 t_0. \tag{65}$$

A comparison of this result with expression (64) shows that $\langle W_q \rangle = W_c$ so that the expected energy is exactly the energy which would be obtained classically.

The ratio of the deviation to the expected energy is

$$\frac{D}{\langle W_q \rangle} = \frac{1}{[(2\epsilon/\pi) \cos \omega_1 t_0]^{\frac{1}{2}}}. \tag{66}$$

As in the case of short transit time the deviation becomes small compared to the expected energy transfer for large $\epsilon$ except of course for the case when no energy exchange takes place classically.

**ACKNOWLEDGMENT**

The author is indebted to Professor H. A. Bethe for many helpful discussions during the early stages of this work.

PHYSICAL REVIEW VOLUME 69, NUMBERS 5 AND 6 MARCH 1 AND 15, 1946

# Classical Theory of the Point Electron*

MARIO SCHÖNBERG
*University of São Paulo, São Paulo, Brazil*
(Received November 6, 1945)

The difficulties of the classical theory of the electron are examined and methods to eliminate them are given. It is shown that the whole theory can be derived from a division of the total field created by a point charge in two parts, one which reacts on the generating particle and accounts for the emission of radiation, another which does not react on the praticle but acts on other particles. There are several types of motions of the particles depending on the kind of field they generate, fields which are always solutions of Maxwell's equations. Only three types of motions are, apparently, physically interesting: (*a*) motions with positive or negative kinetic energy in which the particles radiate, and (*b*) radiationless motions analogous to the stationary motions of quantum theory. It is shown that the field picture of Faraday and Maxwell must be revised because not all the electric actions between particles can be considered as arising from their inferaction with a field. The whole theory of the particles and the field can be derived from an action principle and boundary conditions for the equations of motion of the particles and the field.

## INTRODUCTION

1. THE classical theory of the point electron presents serious difficulties arising from the divergences of the field on the particle's world line: (*a*) The energy of the field diverges and (*b*) the force acting on the particle is infinite, if it is taken as the Lorentz force corresponding to the total field at the particle's position.

The divergence of the force is perhaps the worst difficulty. Dirac[1] has found a method to overcome this difficulty and to justify the equations of motion which were obtained approximately from the Lorentz theory by neglecting divergent terms and the terms which depend on the particle's inner structure. Following Dirac's work, Pryce[2] has shown how it is possible to get a finite energy of the electromagnetic field. However, these theories have some unsatisfactory features. First, they introduce infinite energies of unknown nature in order to cancel out the divergencies of the electromagnetic ones. Second, they do not lead to unique equations of motion and stress-tensors. The second inconvenience is connected with the first one, because the lack of unicity is a consequence of the indeterminateness of the non-electromagnetic energies and momenta.

Later, Dirac[3] worked out the theory in a more elegant way by introducing the so-called λ-process which has been already used by Wentzel.[4] The λ-process enabled Dirac to build a Hamiltonian formalism. This method has the inconvenience of being of an entirely formal nature, and it seems impossible to base on it a satisfactory quantum theory.

However, there is a very simple method, suggested by electrostatics, that has not been worked out until now and which leads to a very simple classical theory and can also be used in quantum theory.[5] The divergencies of the total field on the electron's world line are due only to the divergence of the electron's own field. A similar divergence occurs already in electrostatics but it does not lead to any difficulties. Let us consider the static field created by $n$ point charges $Q_i$; the force acting on $Q_i$ is

$$\mathbf{F}_i = -\sum_{j\neq i} \frac{e_i e_j}{r_{ij}^3} \mathbf{r}_{ij}, \qquad (1)$$

the summation being carried over all the other particles; $\mathbf{r}_{ij}$ is the position vector of $Q_j$ in relation to $Q_i$, and $r_{ij}$ is the distance between $Q_i$ and $Q_j$.

* This paper is a reduced and somewhat generalized form of a more extensive paper sent to *The Physical Review* in March of 1945 which will appear in the *Sum. Bras. Math.*

[1] P. A. M. Dirac, Proc. Roy. Soc. **A167**, 148 (1938).

[2] M. H. L. Pryce, Proc. Roy. Soc. **A168**, 389 (1938).

[3] P. A. M. Dirac, Ann. de l'Inst. H. Poincaré **9**, 13 (1939); Proc. Roy. Soc. **A180**, 1 (1942).

[4] G. Wentzel, Zeits. f. Physik **86**, 479, 635 (1933); **87**, 726 (1934).

[5] M. Schönberg, Phys. Rev. **67**, 122 (1945) and **67**, 193 (1945).

The energy $W$ of the field is

$$W=\tfrac{1}{2}\sum_i\sum_{j\neq i}\frac{e_ie_j}{r_{ij}}. \qquad (2)$$

Frenkel[6] made an attempt to extend this method to the general dynamical case by assuming that there is no self-force. But it is easily seen that it is not possible to get the Larmor loss without introducing a self-force. This was already shown by Synge's work.[7] We must look for some invariant way of splitting the particle's field in two parts: one which reacts on it and accounts for the Larmor loss; another which does not act on the generating particle, though influencing the motion of the other particles. Such a division of the field was already proposed by Leite Lopes and Schönberg.[8] It will be the basic assumption of this paper.

**2.** Besides the divergence difficulties there are others of a different nature, related to the stability of motions of electric particles. It has been assumed that there is no classical possibility of stable accelerated motions of charged particles because of the radiation losses; the existence of stationary motions would be characteristic of quantum mechanics. However, Fokker[9] has shown a long time ago that it is possible to develop a classical theory of the motion of a system of charged particles in which there are no radiation losses, provided it is assumed that the force between two particles is half-retarded and half-advanced. Fokker's theory did not include the possibility of radiative processes and therefore was not duly considered, until recently, when Wheeler tried to use it as the starting point of a general theory of the dynamics of charged particles. It turns out that Fokker's interaction between two charged particles is precisely that part of their interaction which is due to the fields called attached fields by Leite Lopes and Schönberg,[8] the part of a particle's field which does not react on it.

Fokker's theory leads to satisfactory results when applied to the motion of a particle in an external field and presumably also in the case of the motion of a system of particles which corresponds to the stationary motions of quantum mechanics. On the other hand Eliezer[10] has shown that the Lorentz-Dirac equations of motion do not give always satisfactory results when applied to the motion of systems of particles as well as to the motion of a particle in an external field. We shall see that it is possible to formulate a consistent set of principles from which result both the Lorentz-Dirac equations and the Fokker equations, the type of equations of motion depending on the type of motion, without giving up Maxwell's equations for the field which are always satisfied. Though the field created by a particle is always a solution of the Maxwell equations, their behavior at the boundary is not always the same. The nature of the boundary conditions imposed on the solution of the field equations determines the type of the equations of motion of the particles.

The same general principles which conciliate the Lorentz-Dirac equations with Fokker's equations lead also to a satisfactory theory of motions with negative kinetic energy. It is generally assumed that the investigation of such motions belongs to quantum theory, but this point of view is not quite satisfactory because the existence of negative kinetic energies is not a quantum effect. If we try to develop a classical theory of such states of motion, there are considerable difficulties arising from the impossibility of "hiding" such states by means of the Pauli principle, as it was done by Dirac in his theory of the positron. However, it turns out that the equations of motion of a particle with negative kinetic energy are the same as those of a particle with opposite charge and positive kinetic energy, even taking in account the reaction of radiation, provided it is assumed that particles with negative kinetic energies generate advanced fields in non-stationary states of motion. The fact of generating advanced fields gives to these particles properties similar to those of holes, because the advanced fields result from the superposition of converging spherical waves, so that the particles which generate such fields behave as sinks of energy.

[6] J. Frenkel, Zeits. f. Physik **32**, 518 (1925).
[7] J. L. Synge, Proc. Roy. Soc. **A177**, 118 (1940).
[8] J. L. Lopes and M. Schönberg, Phys. Rev. **67**, 122 (1945).
[9] A. D. Fokker, Zeits. f. Physik **58**, 386 (1929).
[10] J. Eliezer, Proc. Camb. Phil. Soc. **39**, 173 (1943).

## PART I. NON-STATIONARY MOTIONS

### General Definitions

**3.** We shall consider only charged point particles without electric or magnetic moments. Since the magnetic moment of the electron is a quantum effect our theory will be applicable to electrons. The motions of a system of charged particles in which there is radiation of energy will be called non-stationary motions, those in which there is no radiation of energy will be called stationary motions.

We shall assume that any particle has only two kinds of momentum: the kinetic one $G^\mu{}_{\text{kin}}$ and the electromagnetic one $G^\mu{}_{\text{el}}$

$$G^\mu{}_{\text{kin}} = mc\frac{dx^\mu}{ds}; \tag{3}$$

however, in general we will not have

$$G^\mu{}_{\text{el}} = \frac{e}{c}A^\mu{}_{\text{act}}; \tag{4}$$

$m$ is the rest mass of the particle, $e$ its electric charge, and $A^\mu{}_{\text{act}}$ the potentials of the field which acts on the particle. If we allow $ds$ to take both positive and negative values, we shall have both positive and negative kinetic energies, the sign of the kinetic energy being the same of $ds$

$$ds = \epsilon(dx^\mu dx_\mu)^{\frac{1}{2}}, \quad \epsilon = \pm 1. \tag{5}$$

We shall call attached field of a point particle half the sum of its retarded and advanced fields.

In our tensor notation the metric tensor $g^{\mu\nu}$ has the components

$$g^{00} = 1, \quad g^{11} = g^{22} = g^{33} = -1,$$
$$g^{01} = g^{02} = g^{03} = g^{12} = g^{13} = g^{23} = 0.$$

The field tensor $F^{\mu\nu}$ is taken in such a way that

$$F_{01} = E_x, \quad F_{02} = E_y, \quad F_{03} = E_z,$$
$$F_{32} = H_x, \quad F_{13} = H_y, \quad F_{21} = H_z,$$

**E** and **H** being the electric and magnetic vectors. The field $F_{\mu\nu}$ is given in terms of the potential by the relation:

$$F_{\mu\nu} = \partial A_\nu/\partial x^\mu - \partial A_\mu/\partial x^\nu,$$
$$F^{\mu\nu}{}_{\text{at}} = \tfrac{1}{2}(F^{\mu\nu}{}_{\text{ret}} + F^{\mu\nu}{}_{\text{adv}}). \tag{6}$$

$F^{\mu\nu}$ is a field tensor and $A^\mu$ the corresponding potential. Taking in account the expressions of the advanced and retarded potentials due to Dirac[1]

$$A^\mu{}_{\text{ret}}(z) = 2e\int_{-\infty}^{s'} \frac{dx^\mu}{ds}\delta(\{x^\mu - z^\mu\}\{x_\mu - z_\mu\})\epsilon ds, \tag{7}$$

$$A^\mu{}_{\text{adv}}(z) = 2e\int_{s'}^{+\infty} \frac{dx^\mu}{ds}\delta(\{x^\mu - z^\mu\}\{x_\mu - z_\mu\})\epsilon ds. \tag{8}$$

we get

$$A^\mu{}_{\text{at}}(z) = e\int_{-\infty}^{+\infty} \frac{dx^\mu}{ds}\delta(\{x^\mu - z^\mu\}\{x_\mu - z_\mu\})\epsilon ds. \tag{9}$$

$\delta$ is Dirac's symbolic function, $s'$ is the value of $s$ corresponding to a point on the particle's world line such that

$$\{x^\mu(s') - z^\mu\}\{x_\mu(s') - z_\mu\} < 0. \tag{10}$$

Equation (9) shows that the attached field does not change when the sign of the elementary interval $ds$ is changed.

We shall call radiated field of a point particle the difference between the total field created by the particle and its attached field:

$$F^{\mu\nu}{}_{\text{rad}} = F^{\mu\nu}{}_{\text{part}} - F^{\mu\nu}{}_{\text{at}}. \tag{11}$$

### The Equations of Motion

**4.** Our theory of the non-stationary motions of a charged particle will be derived from two basic postulates:

I) $$F^{\mu\nu}{}_{\text{act}} = F^{\mu\nu}{}_{\text{ext}} + F^{\mu\nu}{}_{\text{rad}}, \tag{12}$$

II) $$F^{\mu\nu}{}_{\text{rad}} = \frac{\epsilon}{2}(F^{\mu\nu}{}_{\text{ret}} - F^{\mu\nu}{}_{\text{adv}}). \tag{13}$$

$F^{\mu\nu}{}_{\text{ext}}$ is the tensor of the external field.

It results from Eq. (13) that, in a non-stationary motion with positive kinetic energy, a particle generates a retarded field and, in a non-stationary motion with negative kinetic energy, it generates an advanced field:

$$F^{\mu\nu}{}_{\text{part}} = \left.\begin{array}{l} F^{\mu\nu}{}_{\text{ret}} \text{ when } \epsilon > 0 \\ F^{\mu\nu}{}_{\text{adv}} \text{ when } \epsilon < 0 \end{array}\right\}. \tag{14}$$

Dirac[1] has found that, on the world line of a particle, the difference between its retarded and advanced fields is given by the formula:

$$F^{\mu\nu}{}_{\text{ret}} - F^{\mu\nu}{}_{\text{adv}} = \frac{4}{3}e\left(\frac{d^2x^\mu}{ds^2}\frac{dx^\nu}{ds} - \frac{d^2x^\nu}{ds^2}\frac{dx^\mu}{ds}\right). \tag{15}$$

Therefore on the particle's world line

$$F^{\mu\nu}{}_{\text{rad}}=\tfrac{2}{3}\epsilon e\left(\frac{d^3x^\mu}{ds^3}\frac{dx^\nu}{ds}-\frac{d^3x^\nu}{ds^3}\frac{dx^\mu}{ds}\right). \tag{16}$$

But $F^{\mu\nu}{}_{\text{rad}}$ is the part of the particle's field which reacts on it and, so, the self-force is

$$K^\mu{}_{\text{self}}=\frac{e}{c}F^{\mu\nu}{}_{\text{rad}}\frac{dx_\nu}{ds}. \tag{17}$$

Taking in account Eq. (16), it is easily seen that

$$K^\mu{}_{\text{self}}=\frac{2}{3}\frac{e^2}{c}\epsilon\left(\frac{d^3x^\mu}{ds^3}+\frac{dx^\mu}{ds}\frac{d^2x_\nu}{ds^2}\frac{d^2x^\nu}{ds^2}\right). \tag{18}$$

Equation (13) shows that the radiated field of a particle in non-stationary motion is a solution of the Maxwell equations corresponding to a field of pure waves; Eq. (11) shows that both $F^{\mu\nu}{}_{\text{part}}$ and $F^{\mu\nu}{}_{\text{at}}$ are solutions of the Maxwell equations which correspond to the current due to the particle.

**5.** The equations of motion of the particle are

$$mc\frac{d^2x^\mu}{ds^2}=\frac{e}{c}F^{\mu\nu}{}_{\text{act}}\frac{dx_\nu}{ds}. \tag{19}$$

Taking in account the expression (18) of the self-force Eq. (19) becomes

$$\frac{d}{ds}\left(mc\frac{dx^\mu}{ds}-\frac{2}{3}\frac{e^2}{c}\epsilon\frac{d^2x^\mu}{ds^2}\right)-\frac{2}{3}\frac{e^2}{c}\epsilon\frac{dx^\mu}{ds}\frac{d^2x_\nu}{ds^2}\frac{d^2x^\nu}{ds^2}=\frac{e}{c}F^{\mu\nu}{}_{\text{ext}}\frac{dx_\nu}{ds}. \tag{20}$$

Hence when $\epsilon=1$, Eq. (19) coincides with the Lorentz-Dirac equations. The electromagnetic momentum of the particle is

$$G^\mu{}_{\text{el}}=\frac{e}{c}A^\mu{}_{\text{ext}}-\frac{2}{3}\frac{\epsilon e^2}{c}\frac{d^2x^\mu}{ds^2}=\frac{e}{c}A^\mu{}_{\text{ext}}+G^\mu{}_{\text{ac}}, \tag{21}$$

$$G^\mu{}_{\text{ac}}=-\frac{2}{3}\frac{\epsilon e^2}{c}\frac{d^2x^\mu}{ds^2}. \tag{22}$$

$G^\mu{}_{\text{ac}}$ is the four vector of the acceleration momentum, introduced by Schott[11] in the case of positive kinetic energies. We see that $G^\mu{}_{\text{ac}}$ is the part of the electromagnetic momentum of the particle due to its radiated field.

The third term in the left-hand side of the equation of motion (20) corresponds to the Larmor loss when $\epsilon=1$. In the case of a negative kinetic energy this term corresponds to a Larmor "gain," but it leads to a damping of the particle's motion because, in order to stop a particle with negative kinetic energy, it is necessary to supply it with positive energy.

Equation (20) does not change if we change simultaneously the signs of both the charge $e$ and the interval $ds$. Hence:

*A particle with charge e has the same equations of motion as a particle with charge $-e$ and opposite kinetic momentum $-G^\mu{}_{\text{kin}}$.*

The preceding theorem explains the reason why it is necessary to assume that a particle in a state of negative kinetic energy generates an advanced field: otherwise it would not move as a particle with positive kinetic energy and opposite charge. It is important to keep in mind that, though the particle with negative kinetic energy moves as if it had positive kinetic energy and opposite charge, it generates a field corresponding to the real sign of its charge.

## Proper Time in Motions with Negative Kinetic Energy

**6.** The basic postulates I and II can be expressed in a more elegant form by introducing a generalized conception of the flow of proper time.

In relativistic theories the time appears in two different forms: (*a*) as one of the coordinates in the four-dimensional universe; (*b*) as the proper time of the particles, measured by the length of the arcs described on their world lines. Of course the real signification of time must be attached to the length of arc described on the world line. This is seen clearly in general relativity because, in a curved universe, it is not possible to choose the coordinates in such a way that the differentials $dx^0$ along the world lines of the particles coincide always with the elementary intervals $ds$.

The usual ideas about the flow of time impose the choice of a preferred orientation of the world lines of the particles, in such a way that

$$dx^0/ds>0. \tag{23}$$

There is no strong argument against the assumption that there are two possible orientations of

[11] G. A. Schott, Phil. Mag. **29**, 49 (1915).

the world lines of the particles, corresponding to two different types of motion: motions with positive kinetic energy, with $dx^0/ds>0$, and motions with negative kinetic energy, with $dx^0/ds<0$. Thus, our purely mathematical convention (5) would correspond to the two possible orientations of the particles world lines.

Each observer chooses the coordinate $\chi^0$ according to its proper time flow and, thus, the particles whose proper times do not flow in the same direction as the observer's time appear as having negative kinetic energies. Now it becomes intuitive why particles with negative kinetic energy generate advanced fields:

*The field generated by a particle in non-stationary motion is always a retarded field for an observer whose proper time flows in the same sense as the particle's proper time.*

This proposition can be verified easily by observing that a change of sign of $ds$ in Eq. (8) transforms the advanced potentials of a particle with charge $e$ into the retarded potentials of a particle with the same charge, moving on the same world line.

Now the apparent asymmetry of the treatment of the states with positive and negative kinetic energies disappears. We may formulate postulate II as:

*The radiated field of a particle is half the difference between its retarded and advanced fields measured by an observer whose time flows in the same direction as the particle's proper time.*

From the preceding considerations it results that the direction of time flow for a charged particle in non-stationary motion is always such that there is an emission of energy for an observer attached to the particle, when there are no incoming external waves. It is not necessary to introduce statistical quantities such as the entropy in order to define the direction of time flow for an observer, the radiation of electromagnetic waves already selects a direction of time flow.

### Equations of Motion for Systems of Particles

**7.** The postulates I and II allow us to write the equations of motion of a system of particles. The field $F^{\mu\nu}{}_{i,\,\mathrm{act}}$ which acts on the $i$th particle is the sum of the total fields $F^{\mu\nu}{}_{j,\,\mathrm{part}}$ due to the other particles, of the external field $F_{\mathrm{ext}}{}^{\mu\nu}$ in which the system moves and of the particle's radiated field $F^{\mu\nu}{}_{i,\,\mathrm{rad}}$

$$F^{\mu\nu}{}_{i,\,\mathrm{act}}=\sum_{j\neq i}F^{\mu\nu}{}_{j,\,\mathrm{part}}+F^{\mu\nu}{}_{\mathrm{ext}}+F^{\mu\nu}{}_{i,\,\mathrm{rad}}, \quad (24)$$

because the fields $F^{\mu\nu}{}_{j,\,\mathrm{part}}$ are external fields for the $i$th particle. Therefore the equations of motion of the system are

$$m_i c\frac{d^2x_i^\mu}{ds_i^2}=\frac{e_i}{c}\left(\sum_{j\neq i}F^{\mu\nu}{}_{j,\,\mathrm{part}}+F^{\mu\nu}{}_{\mathrm{ext}}+F^{\mu\nu}{}_{i,\,\mathrm{rad}}\right)\frac{dx_{i,\nu}}{ds_i}. \quad (25)$$

Formula (24) leads to an expression of the force $K_i^\mu$ which generalizes the electrostatic formula (1)

$$K_i^\mu=\frac{e_i}{c}\left(\sum_{j\neq i}F^{\mu\nu}{}_{j,\,\mathrm{part}}+F^{\mu\nu}{}_{\mathrm{ext}}\right)+\frac{2}{3}\frac{\epsilon_i e_i^2}{c}\times\left(\frac{d^3x_i^\mu}{ds_i^3}+\frac{dx_i^\mu}{ds_i}\frac{d^2x_{i,\nu}}{ds_i^2}\frac{d^2x_i^\nu}{ds_i^2}\right). \quad (26)$$

It is convenient to define the radiation field of a system as the sum of the radiated fields of its particles

$$F^{\mu\nu}{}_{\mathrm{rad}}=\sum_i F^{\mu\nu}{}_{i,\,\mathrm{rad}}. \quad (27)$$

The radiative losses of a system are due to the action of $F^{\mu\nu}{}_{\mathrm{rad}}$ on the particles of the system, as we shall see later.

## PART II. STATIONARY MOTIONS

**8.** Postulate I is a generalization of the law of inertia which is presumably valid for any linear field theory, provided we replace the tensor $F^{\mu\nu}{}_{\mathrm{act}}$ by the adequate quantities of the considered field. It corresponds to the physical idea that the radiated field gets detached from the particle and behaves as an external field, so that the self-force arising from it has really the character of an external action.

Postulate II can be easily generalized. The natural condition we must impose on a radiated field is that it be a solution of the field equations corresponding to a wave field. In the electromagnetic case this condition is satisfied if we take

(IIa) $$F^{\mu\nu}{}_{\mathrm{rad}}=\frac{\eta}{2}(F^{\mu\nu}{}_{\mathrm{ret}}-F^{\mu\nu}{}_{\mathrm{adv}}), \quad (28)$$

$\eta$ being an arbitrary constant. The non-stationary motions correspond to $\eta=\epsilon$. Let us examine what results by assuming that

(IIb) $$\eta=0. \tag{29}$$

From Eqs. (12), (28), and (29) it results that

$$F^{\mu\nu}{}_{\text{act}}=F^{\mu\nu}{}_{\text{ext}}. \tag{30}$$

Taking into account the definition (11) of the radiated field we get

$$F^{\mu\nu}{}_{\text{part}}=F^{\mu\nu}{}_{\text{at}}. \tag{31}$$

Therefore condition II b corresponds to a vanishing self-force and to a total field created by the particle equal to the attached field. This is an acceptable value of $F^{\mu\nu}{}_{\text{part}}$ because it is a solution of the Maxwell equations corresponding to the charge and current generated by the particle (any value of $\eta$ would give an $F^{\mu\nu}{}_{\text{part}}$ which satisfies this Maxwell system). Since there is no self-force, there is no radiative damping of the particle's motion and, presumably, no emission of radiation. The value (31) of $F^{\mu\nu}{}_{\text{part}}$ is precisely the value of the Fokker theory[9] in which there are no radiation losses.

Postulate II b characterizes the stationary motions. Since there is now no self-force the equations of motion are

$$mc\frac{d^2x^\mu}{ds^2}=\frac{e}{c}F^{\mu\nu}{}_{\text{ext}}\frac{dx_\nu}{ds}. \tag{32}$$

It is very remarkable that the order of the equations of motion of a charged particle is not always the same: in non-stationary motions the equations are of the third order but they are of the second order in stationary motions. This is a consequence of the fact that the third-order derivatives are introduced by Schott's acceleration momentum $G^\mu{}_{\text{ac}}$ which does not exist in stationary motions.

Let us consider now a system of particles in stationary motion. It is easily seen that

$$F^{\mu\nu}{}_{i,\text{act}}=\sum_{j\neq i}F^{\mu\nu}{}_{j,\text{part}}+F^{\mu\nu}{}_{\text{ext}}=\sum_{j\neq i}F^{\mu\nu}{}_{j,\text{at}}+F^{\mu\nu}{}_{\text{ext}}. \tag{33}$$

Therefore the equations of motion are

$$m_ic\frac{d^2x_i^\mu}{ds_i^2}=\frac{e_i}{c}\left(\sum_{j\neq i}F^{\mu\nu}{}_{j,\text{at}}+F^{\mu\nu}{}_{\text{ext}}\right)\frac{dx_{i,\nu}}{ds_i}. \tag{34}$$

The most interesting type of stationary motion is that of a system free from external actions. This is the type originally considered by Fokker,[9] it is a relativistic generalization of the $n$-body problem of Newtonian mechanics.

## Conservation of Energy, Momentum, and Angular Momentum

**9.** The total momentum of the $i$th particle of an isolated system in stationary motion is

$$G_i^\mu=m_ic\frac{dx_i^\mu}{ds_i}+\frac{e_i}{c}\sum_{j\neq i}A^\mu{}_{j,\text{at}}. \tag{35}$$

Taking into account the expressions of the fields in terms of the potentials, the equations of motion can be written in the following form

$$\frac{dG_i^\mu}{ds_i}=\frac{e_i}{c}\sum_{j\neq i}\frac{\partial A^\nu{}_{j,\text{at}}}{\partial x_{i,\mu}}\frac{dx_{i,\nu}}{ds_i}. \tag{36}$$

The rate of variation of the total momentum of the system, for an observer in a Lorentz frame of reference whose time is $t$, is in general not nil

$$\frac{d}{dt}\sum_i G_i^\mu=\sum_i\left(\frac{dG_i^\mu}{ds_i}\frac{ds_i}{dt}\right)_{x^0=ct}\neq 0, \tag{37}$$

but its time integral vanishes

$$\int_{-\infty}^{+\infty}\frac{d}{dt}\sum_i G_i^\mu dt=\sum_i\int_{-\infty}^{+\infty}\frac{dG_i^\mu}{ds_i}ds_i=0. \tag{38}$$

Equation (38) may be considered as the law of conservation of energy and momentum in stationary motions. It shows that there is no permanent loss of energy and momentum by radiative processes. Equation (38) is a consequence of the relativistic generalization of the principle of action and reaction:

$$e_i\int_{-\infty}^{+\infty}\frac{\partial A^\nu{}_{j,\text{at}}}{\partial x_{i,\mu}}\frac{dx_{i,\nu}}{ds_i}ds_i=-e_j\int_{-\infty}^{+\infty}\frac{\partial A^\nu{}_{i,\text{at}}}{\partial x_{j,\mu}}\frac{dx_{j,\nu}}{ds_j}ds_j. \tag{39}$$

The principle of action and reaction (39) is valid even in non-stationary motions, because it results immediately from the expression (9) of the attached potentials of a particle.

The total angular momentum of the spinless

particles which we consider is

$$M_i^{\mu\nu}=x_i^{\mu}G_i^{\nu}-x_i^{\nu}G_i^{\mu}. \tag{40}$$

There is a law of average conservation of $\sum_i M_i^{\mu\nu}$ in stationary motions of isolated systems

$$\sum_i \int_{-\infty}^{+\infty} \frac{dM_i^{\mu\nu}}{ds_i} ds_i = 0. \tag{41}$$

Equation (41) can be easily derived from Eqs. (36) by taking into account the expression (9) of the attached potentials of a particle.

### Some Stationary Motions of a Particle

**10.** The simplest stationary motion is that of an isolated particle. It results from the equations of motion that it is a uniform rectilinear motion. Dirac[1] has shown that the Lorentz-Dirac equation for a free particle has two types of solutions: the uniform rectilinear and the self-accelerated motions. We can get rid of the self-accelerated motions by assuming as relativistic law of inertia that: *The motion of an isolated point charge is stationary.*

Another very simple motion of a particle is its stationary motion in a Coulomb field. In this case Eqs. (32) are the same studied by Sommerfeld in the old theory of the atom. So we see that the orbits of the old quantum theory correspond to classical stationary motions; the quantization rules of Bohr and Sommerfeld select those orbits which correspond to the quantum stationary motions.

Eliezer[10] has found difficulties in the application of the Lorentz-Dirac equations to the theory of the electromagnetic Kepler problem and to the electromagnetic two-body problem. These difficulties disappear if we treat those motions as stationary motions. As we have already indicated, there is an essential difference between stationary and non-stationary motions due to the acceleration energy. In stationary motions there is no acceleration energy, which behaves as an invisible source of energy and accounts for the self-accelerated motions and other physically meaningless situations. So, for instance, in the self-accelerated motions of a free particle the acceleration energy tends to $-\infty$ when time tends to $\infty$ and, thus, allows the kinetic energy to increase indefinitely, supplying at the same time the radiated energy. It is necessary, in the cases in which the Lorentz-Dirac equations are valid, to introduce suitable time boundary conditions in order to avoid the difficulties due to the acceleration energy. This was already done by Dirac[1] in the case of a particle which receives a light pulse. We will discuss later these time boundary conditions in a general form. In Eliezer's analysis the initial conditions in the recessive motion of the electron are taken in such a way that this motion is of the self-accelerated type; the decrease of the acceleration energy allows the particles to get apart with steadily increasing relative velocity. The time boundary condition that we introduce in Section 18 excludes such motions.

**11.** Synge[7] has discussed the electromagnetic two-body problem, assuming that each particle generates a retarded field which acts on the others, but not on itself. He found that, with these assumptions, there are no stable circular orbits, though the rates of shrinking of the radii are small. He found also an emission of radiation at a rate much smaller than the Larmor rate. The considerations we developed in Part I show that the basic assumptions of Synge's theory are not entirely satisfactory, because they exclude the action of the radiated part of the field of a particle on it, but not on the other particles. It can be seen that the small emission of radiation and the correlated shrinkage of the radii of the circular orbits are precisely due to the interactions between each of the particles and the radiated field of the other. If it is assumed, as we did in our theory of the stationary motions, that the two particles do not generate radiated fields then there will be permanent circular orbits. (See Appendix I.)

It is noteworthy that, even in Synge's theory, there are permanent circular orbits when one of the particles has infinite mass. In this case there are no radiation losses because the radiated field of the heavy particle vanishes and, thus, there are no dissipative forces acting on the light particle. This shows that there is a radiative loss due to the action of the radiated field of one particle on the other.

## PART III

## Electromagnetic Fields Generated by Point Particles

**12.** In Parts I and II we have shown how it is possible to derive unique equations of motion for charged point particles, avoiding the difficulties due to infinite self-forces. The whole theory of the equations of motion was built on two basic postulates

$$\text{(I)} \qquad F^{\mu\nu}{}_{\text{act}} = F^{\mu\nu}{}_{\text{ext}} + F^{\mu\nu}{}_{\text{rad}}, \tag{42}$$

$$\text{(II)} \qquad F^{\mu\nu}{}_{\text{rad}} = \frac{\eta}{2}(F^{\mu\nu}{}_{\text{ret}} - F^{\mu\nu}{}_{\text{adv}}).$$

We considered three types of motions characterized by the values $-1$, 0, and 1 of the parameter $\eta$. These three types include all the known motions of electric point particles, but the theory of the equations of motion can be developed for any value of $\eta$. In any case there is a self-force $K^{\mu}{}_{\text{self}}$

$$K^{\mu}{}_{\text{self}} = \frac{e}{c} F^{\mu\nu}{}_{\text{rad}} \frac{dx_\nu}{ds} = \frac{2}{3}\frac{e^2}{c}\eta\left(\frac{d^3x^\mu}{ds^3} + \frac{dx^\mu}{ds}\frac{d^2x_\nu}{ds^2}\frac{d^2x^\nu}{ds^2}\right), \tag{43}$$

and the corresponding equations of motion are

$$mc\frac{d^2x^\mu}{ds^2} - \frac{2}{3}\frac{e^2}{c}\eta\left(\frac{d^3x^\mu}{ds^3} + \frac{dx^\mu}{ds}\frac{d^2x_\nu}{ds^2}\frac{d^2x^\nu}{ds^2}\right) = \frac{e}{c} F^{\mu\nu}{}_{\text{ext}} \frac{dx_\nu}{ds}. \tag{44}$$

The total field generated by the particle $F^{\mu\nu}{}_{\text{part}}$ is

$$F^{\mu\nu}{}_{\text{part}} = F^{\mu\nu}{}_{\text{at}} + F^{\mu\nu}{}_{\text{rad}} = \frac{1+\eta}{2} F^{\mu\nu}{}_{\text{ret}} + \frac{1-\eta}{2} F^{\mu\nu}{}_{\text{adv}}, \tag{45}$$

and satisfies the Maxwell equations

$$\frac{\partial F^{\mu\nu}{}_{\text{part}}}{\partial x^\nu} = -4\pi\frac{e}{c}\frac{dx^\mu}{dt}\delta(x^1 - x^1(t))\delta(x^2 - x^2(t))$$
$$\frac{\partial F^{\mu\nu}{}_{\text{part}}}{\partial x^\lambda} + \frac{\partial F^{\lambda\mu}{}_{\text{part}}}{\partial x^\nu} + \frac{\partial F^{\nu\lambda}{}_{\text{part}}}{\partial x^\mu} = 0. \tag{46}$$

Until now we have not investigated whether there is conservation of energy and momentum of the system field+particles. In order to investigate this point let us introduce the stress tensor of the field $T_\nu{}^\mu$

$$4\pi T_\nu{}^\mu = F^{\mu\rho}{}_{\text{tot}} F_{\text{tot},\,\rho\nu} + \tfrac{1}{4}\delta_\nu{}^\mu (F^{\rho\sigma}{}_{\text{tot}} F_{\text{tot},\,\rho\sigma}) - \textstyle\sum_i [F^{\mu\rho}{}_{i,\,\text{at}} F_{i,\,\text{at};\,\rho\nu} + \tfrac{1}{4}\delta_\nu{}^\mu (F^{\rho\sigma}{}_{i,\,\text{at}} F_{i,\,\text{at};\,\rho\sigma})]. \tag{47}$$

$F^{\mu\nu}{}_{\text{tot}}$ is the total field created by the particles plus the field of the incoming external waves $F^{\mu\nu}{}_{\text{wav}}$

$$F^{\mu\nu}{}_{\text{tot}} = \textstyle\sum_i F^{\mu\nu}{}_{i,\,\text{part}} + F^{\mu\nu}{}_{\text{wav}}. \tag{48}$$

Our choice of the stress tensor is justified, because there is a conservation equation

$$\frac{\partial T^{\mu\nu}}{\partial x^\nu} = -\sum_i \frac{e_i}{c} F^{\mu\rho}{}_{i,\,\text{act}} \frac{dx_{i,\,\rho}}{dt} \delta(x^1 - x_i^1) \times \delta(x^2 - x_i^2)\delta(x^3 - x_i^3). \tag{49}$$

We may write, instead of (47),

$$4\pi T_\nu{}^\mu = (F^{\mu\rho}{}_{\text{wav}} + \textstyle\sum_i F^{\mu\rho}{}_{i,\,\text{rad}})(F_{\text{tot};\,\rho\nu} + \sum_j F_{j,\,\text{at};\,\rho\nu}) + \tfrac{1}{4}\delta_\nu{}^\mu (F^{\rho\sigma}{}_{\text{wav}} + \textstyle\sum_i F^{\rho\sigma}{}_{i,\,\text{rad}})(F_{\text{tot};\,\rho\sigma} + \sum_j F_{j,\,\text{at};\,\rho\sigma}) + \sum_i \sum_{j\neq i} (F^{\mu\rho}{}_{i,\,\text{at}} F_{j,\,\text{at};\,\rho\nu} + \tfrac{1}{4}\delta_\nu{}^\mu F^{\rho\sigma}{}_{i,\,\text{at}} F_{j,\,\text{at};\,\rho\sigma}). \tag{50}$$

Equation (50) shows that $T^{\mu\nu}$ diverges only as $r^{-2}$ at the particles' positions, because the radiated fields are finite and the attached fields diverge as $r^{-2}$ at the positions of the corresponding particles. Therefore, the space integrals of the components of the stress tensor over any region are finite and they are not differences of infinite quantities, as it might appear from Eq. (47).

The momentum of the field is $G^{\mu}{}_{\text{field}}$

$$G^{\mu}{}_{\text{field}} = \int T^{0\mu} d\tau. \tag{51}$$

The components of $G^{\mu}{}_{\text{field}}$ are finite; thus we have been able to get a finite energy and finite momenta for the field, without introducing unknown quantities of non-electromagnetic nature and without taking differences of infinite quantities.

**13.** The momentum $G^{\mu}{}_{\text{field}}$ has a remarkable property: it is a four vector. Let us represent by $G^{\mu}{}_{f}(V)$ the momentum of the field contained in a volume $V$ of space. If we take as volume $V$ the entire space minus $n$ small spheres of radii $\alpha$ with centers at the point particles, we shall have

at any point of $V$

$$\frac{\partial T^{\mu\nu}}{\partial x^\mu}=0. \tag{52}$$

According to a well-known theorem, it results from (52) that the $G^\mu{}_f(V)$ are the components of a four vector. If we make $\alpha$ tend to zero, the $G^\mu{}_f(V)$ will go over continuously into the $G^\mu{}_{\text{field}}$ because the components of the stress tensor diverge only as $r^{-2}$ at the particles' positions. Therefore the $G^\mu{}_{\text{field}}$ are the components of a four vector.

It is noteworthy that we have been able to obtain a four vector of momentum for the field without excluding the Coulomb forces, but only the self-forces due to the attached fields. It is well known that the classical objection against the theories which consider the mass as being of electromagnetic origin was based on the non-vectorial nature of the field's momentum $G^\mu{}_{\text{field}}$. But this objection disappears when we take for the field's stress tensor the expression (47). However, our theory does not lead, at least in a straightforward way, to an electromagnetic theory of the mass. So, for instance, the energy of the field created by a particle in a free stationary motion is *nihil.*

### The Poynting Vector

**14.** The components $P^\alpha$ of the Poynting vector of the field, in which there are $n$ point particles, are

$$P^\alpha=cT^{0\alpha}. \tag{53}$$

Hence

$$\mathbf{P}=\frac{c}{4\pi}[\mathbf{E}_{\text{tot}}\times\mathbf{H}_{\text{tot}}]-\frac{c}{4\pi}\sum_i[\mathbf{E}_{i,\text{at}}\times\mathbf{H}_{i,\text{at}}]. \tag{54}$$

From Eq. (49) it follows that

$$\frac{d}{dt}G^0{}_{\text{field}}=-\lim_{S\to\infty}\int_S(\mathbf{P}\cdot\mathbf{n})dS - \sum_i\frac{e_i}{c}F^{0\nu}{}_{i,\text{act}}\frac{dx_{i,\nu}}{dt}. \tag{55}$$

$\mathbf{n}$ is the unit vector on the outer normal of $S$. The surface integral in the right-hand side of Eq. (55) does not vanish automatically when $S\to\infty$ because, in general, the electromagnetic field varies inversely with the distance in the wave zone, so that the Poynting vector varies as the square of the inverse of the distance to the point which we take as origin of the coordinates. In order to make the surface integral tend to zero, we must impose suitable boundary conditions to the motion of the charged particles. We shall examine later these conditions.

In order to investigate the behavior of the field at the boundary it is convenient to replace the retarded and advanced fields by their parts which vary inversely with the distance. We have:[12]

$$\mathbf{E}_{\text{ret}}=-\frac{1}{c}\frac{\partial}{\partial t}\mathbf{A}^{\text{tr}}{}_{\text{ret}},\qquad \mathbf{H}_{\text{ret}}=[\mathbf{u}\times\mathbf{E}_{\text{ret}}],$$
$$\mathbf{E}_{\text{adv}}=-\frac{1}{c}\frac{\partial}{\partial t}\mathbf{A}^{\text{tr}}{}_{\text{adv}},\qquad \mathbf{H}_{\text{adv}}=[\mathbf{E}_{\text{adv}}\times\mathbf{u}]. \tag{56}$$

$\mathbf{u}$ is the unit vector in the direction of the position vector of the point in which the fields are computed, relatively to the origin of the coordinates. This origin is taken as a fixed point, inside the charge distribution. $\mathbf{A}^{\text{tr}}{}_{\text{ret}}$ and $\mathbf{A}^{\text{tr}}{}_{\text{adv}}$ are the transversal parts of the retarded and advanced vector potentials (we call transversal components those perpendicular to $\mathbf{u}$ and radial those parallel to $\mathbf{u}$). In the wave zone we may take for the transversal components of the retarded and advanced potentials of the field generated by the current density $c\mathbf{J}$ the following values:

$$\mathbf{A}^{\text{tr}}{}_{\text{ret}}=\frac{1}{R}\int\mathbf{J}^{\text{tr}}(x'^\alpha,\ x^0-R-u_\alpha x'^\alpha)dx'^1dx'^2dx'^3,$$
$$\mathbf{A}^{\text{tr}}{}_{\text{adv}}=\frac{1}{R}\int\mathbf{J}^{\text{tr}}(x'^\alpha,\ x^0+R+u_\alpha x'^\alpha)dx'^1dx'^2dx'^3. \tag{57}$$

$R$ is the distance between the origin of the coordinates and the point in the wave zone where the potentials are computed. $x^0$ corresponds to the time: $x^0=ct$.

It results from formulae (56) that the Poynting vector of a field, in which there are no other waves besides those of the radiated parts of the particles, is

$$\mathbf{P}=\frac{c}{16\pi}[(1+\eta)^2(\textstyle\sum_i\mathbf{E}_{i,\text{ret}})^2 - (1-\eta)^2(\textstyle\sum_i\mathbf{E}_{i,\text{adv}})^2]\mathbf{u} - \frac{c}{16\pi}\textstyle\sum_i(\mathbf{E}^2_{i,\text{ret}}-\mathbf{E}^2_{i,\text{adv}})\mathbf{u}. \tag{58}$$

[12] W. Pauli, *Handbuch der Physik* (1933), XXIV/1, p. 203.

It can be seen that (see Appendix II):

$$\int_{-\infty}^{+\infty}(\sum_i \mathbf{E}_{i,\,\mathrm{ret}})^2 dt=\int_{-\infty}^{+\infty}(\sum_i \mathbf{E}_{i,\,\mathrm{adv}})^2 dt,$$
$$\int_{-\infty}^{+\infty}\mathbf{E}^2_{i,\,\mathrm{ret}}dt=\int_{-\infty}^{+\infty}\mathbf{E}^2_{i,\,\mathrm{adv}}dt. \tag{59}$$

Hence, we have:

$$\int_{-\infty}^{+\infty}\mathbf{P}dt=\frac{c}{4\pi}\eta\mathbf{u}\int_{-\infty}^{+\infty}(\sum_i \mathbf{E}_{i,\,\mathrm{ret}})^2 dt$$
$$=\frac{c}{4\pi}\eta\mathbf{u}\int_{-\infty}^{+\infty}(\sum_i \mathbf{E}_{i,\,\mathrm{adv}})^2 dt. \tag{60}$$

Equation (60) shows that there is a radiation loss when $\eta>0$, a gain when $\eta<0$, and an average conservation of energy in stationary motions since $\eta=0$.

### The Stress Tensor of the Radiation Field

**15.** Equation (50) shows that the stress tensor of the total field is the sum of two parts: a part which contains the radiated fields of the particles and a part which does not contain these fields. We shall call the first prat stress tensor of the radiation field and denote it by $T^{\mu\nu}{}_{\mathrm{rad}}$

$$4\pi T^{\mu}{}_{\mathrm{rad};\,\nu}=(F^{\mu\rho}{}_{\mathrm{wav}}+\sum_i F^{\mu\rho}{}_{i,\,\mathrm{rad}})\times(F_{\mathrm{tot};\,\rho\nu}+\sum_j F_{j,\,\mathrm{at};\,\rho\nu})+\tfrac{1}{4}\delta_\nu{}^\mu(F^{\rho\sigma}{}_{\mathrm{wav}}+\sum_i F^{\rho\sigma}{}_{i,\,\mathrm{rad}})\times(F_{\mathrm{tot};\,\rho\sigma}+\sum_j F_{j,\,\mathrm{at};\,\rho\sigma}). \tag{61}$$

We shall call the second part stress tensor of the interior actions and denote it by $T^{\mu\nu}{}_{\mathrm{int}}$

$$4\pi T^{\mu}{}_{\mathrm{int};\,\nu}=\sum_i\sum_{j\neq i}(F^{\mu\rho}{}_{i,\,\mathrm{at}}F_{j,\,\mathrm{at};\,\rho\nu}+\tfrac{1}{4}\delta_\nu{}^\mu F^{\rho\sigma}{}_{i,\,\mathrm{at}}F_{j,\,\mathrm{at};\,\rho\sigma}). \tag{62}$$

Equation (49) can be split in two:

$$\frac{\partial T^{\mu\nu}{}_{\mathrm{rad}}}{\partial x^\nu}=-\sum_i\frac{e_i}{c}(F^{\mu\rho}{}_{\mathrm{wav}}+\sum_j F^{\mu\rho}{}_{j,\,\mathrm{rad}})\frac{dx_{i,\,\rho}}{dt}\times\delta(x^1-x_i{}^1)\delta(x^2-x_i{}^2)\delta(x^3-x_i{}^3), \tag{63}$$

$$\frac{\partial T^{\mu\nu}{}_{\mathrm{int}}}{\partial x^\nu}=-\sum_i\frac{e_i}{c}\left(\sum_{j\neq i}F^{\mu\rho}{}_{j,\,\mathrm{at}}\right)\frac{dx_{i,\,\rho}}{dt}\times\delta(x^1-x_i{}^1)\delta(x^2-x_i{}^2)\delta(x^3-x_i{}^3). \tag{64}$$

We may define a Poynting vector for the radiation field and a Poynting vector for the interior actions:

$$\mathbf{P}_{\mathrm{rad}}=\frac{c}{4\pi}[\mathbf{E}_{\mathrm{tot}}\times\mathbf{H}_{\mathrm{tot}}]-\frac{c}{4\pi}[(\sum_i \mathbf{E}_{i,\,\mathrm{at}})\times(\sum_j \mathbf{H}_{j,\,\mathrm{at}})], \tag{65}$$

$$\mathbf{P}_{\mathrm{int}}=\frac{c}{4\pi}[(\sum_i \mathbf{E}_{i,\,\mathrm{at}})\times(\sum_j \mathbf{H}_{j,\,\mathrm{at}})]-\frac{c}{4\pi}\sum_i[\mathbf{E}_{i,\,\mathrm{at}}\times\mathbf{H}_{i,\,\mathrm{at}}]. \tag{66}$$

Taking in account Eqs. (59), we get easily, in the wave zone:

$$\int_{-\infty}^{+\infty}\mathbf{P}_{\mathrm{rad}}dt=\int_{-\infty}^{+\infty}\mathbf{P}dt, \tag{67}$$

$$\int_{-\infty}^{+\infty}\mathbf{P}_{\mathrm{int}}dt=0. \tag{68}$$

Equation (68) shows the conservative character of the actions due to the attached fields: in the average they do not lead to any energy loss. The radiation losses are entirely due to the action of the radiation field on the particles, as it results from Eq. (67). Not only the particle's own radiated field, but also the radiated fields of the other particles and the field of the traveling waves lead to radiative losses of energy.

### The Actions at a Distance

**16.** We cannot consider the interior actions to be due to a field, because the interior force which acts on each particle is due to the attached fields of all the others, so that there is no single field which accounts for all the interior forces.

The interior actions of a system are the actions at a distance of the Tetrode[13] theory; they are also the same forces considered by Fokker[9] and Wheeler. These actions at a distance are a generalization of the forces of the old electrostatical theory: it can be seen that the space integral of $T^{00}{}_{\mathrm{int}}$ coincides with the electrostatical energy $W$ of Eq. (2), in the case of charges at rest. Since we have now relativistic actions at a distance, we can understand why they do depend on the motions of the particles at different times: they are actions at a distance both in space and time. These interior forces do not lead to any

[13] H. Tetrode, Zeits. f. Physik **10**, 317 (1922).

loss of energy, momentum, or angular momentum as we have seen in the analysis of the stationary motions; we also got the same result from the analysis of the field.

In the same way as the interior forces, the total forces acting on the particles actually do not arise from any field, because for each particle we have a different $F^{\mu\nu}{}_{i,\,\mathrm{act}}$. This is the main point of the theory of charged point particles:

*In order to exclude infinite self forces we must introduce for each particle a different acting field so that we can no longer say that the total forces acting on all the particles arise from the existence of a single field, as it happens in the Faraday-Maxwell theory.*

Our theory of the point particles may be considered as a synthesis of the Faraday-Maxwell theory of actions through a field with the Tetrode conception of relativistic actions at a distance. The total radiation field is, indeed, a field in the Faraday-Maxwell sense and it accounts for the propagation of the electromagnetic waves. But, besides the field forces, there are also actions at a distance which are due to the attached fields of the particles and which do not correspond to any wave propagation. The circumstance that the attached fields are half-retarded and half-advanced shows precisely that they are not propagated, because they are symmetrical in relation to both directions of time flow.

The difference between the actions at a distance and the actions through the field becomes sharper in quantum theory: the radiation field is quantized but the actions at a distance remain unquantized. Presumably the difficulties which appear in the quantum theory of the interaction of point particles with fields are all due to the physically inacceptable identification of the actions at a distance with actions through the field. In particular, the nuclear forces should be considered as actions at a distance of non-electromagnetic nature.

## PART IV

## Boundary Conditions

**17.** The various types of motions of the particles are characterized by the kind of radiated field they create. The radiated field is a solution of the Maxwell equations with no current density which can be characterized by convenient boundary conditions. We may also characterize the motions by means of the $F^{\mu\nu}{}_{i,\,\mathrm{part}}$, which are solutions of the Maxwell equations corresponding to the current density generated by the particle, determined by suitable boundary conditions. Therefore, our whole theory is contained in the Eqs. (69)

$$m_i c\frac{d^2x_i^\mu}{ds_i^2}=\frac{e_i}{c}(F^{\mu\nu}{}_{\mathrm{ext}}+\sum_j F^{\mu\nu}{}_{j,\,\mathrm{part}} - F^{\mu\nu}{}_{i,\,\mathrm{act}})\frac{dx_{i,\nu}}{ds_i}, \quad (69a)$$

$$\frac{\partial^2 A^\mu{}_{i,\,\mathrm{part}}}{\partial x^\rho \partial x_\rho}=4\pi\frac{e_i}{c}\frac{dx_i^\mu}{dt}\delta(x^1-x_i^1) \times\delta(x^2-x_i^2)\delta(x^3-x_i^3), \quad (69b)$$

together with the boundary conditions for the $A^\mu{}_{i,\,\mathrm{part}}$.

### Boundary Conditions for the $A^\mu{}_{i,\,\mathrm{part}}$

It can be seen that the boundary condition for $A^\mu{}_{i,\,\mathrm{part}}$ is

$$(1+\eta_i)\lim_{r\to\infty} r\left(\frac{\partial}{\partial r}+\frac{1}{c}\frac{\partial}{\partial t}\right)A^\mu{}_{i,\,\mathrm{part}}\left(\mathbf{r}, t-\frac{r}{c}\right) = -(1-\eta_i)\lim_{r\to\infty} r\left(\frac{\partial}{\partial r}-\frac{1}{c}\frac{\partial}{\partial t}\right) \times A^\mu{}_{i,\,\mathrm{part}}\left(\mathbf{r}, t+\frac{r}{c}\right). \quad (70)$$

The boundary condition (70) results immediately from the well-known formulae

$$A^\mu(\mathbf{r}, t)=\int_V \frac{J^\mu(\mathbf{r}, t-r/c)}{r}d\mathbf{r} -\frac{1}{4\pi}\int_S \frac{1}{r}\frac{\partial A^\mu(\mathbf{r}, t-r/c)}{\partial n}dS +\frac{1}{4\pi}\int_S\left[A^\mu\left(\mathbf{r}, t-\frac{r}{c}\right)\frac{\partial(1/r)}{\partial n} +\frac{1}{cr}\frac{\partial A^\mu(\mathbf{r}, t-r/c)}{\partial t}\right]dS, \quad (71a)$$

$$A^\mu(\mathbf{r},t)=\int_V \frac{J^\mu(\mathbf{r},t+r/c)}{r}d\mathbf{r}$$
$$-\frac{1}{4\pi}\int_S \frac{1}{r}\frac{\partial A^\mu(\mathbf{r},t+r/c)}{\partial n}dS$$
$$+\frac{1}{4\pi}\int_S \left[A^\mu\left(\mathbf{r},t+\frac{r}{c}\right)\frac{\partial(1/r)}{\partial n}\right.$$
$$\left.-\frac{1}{cr}\frac{\partial A^\mu(\mathbf{r},t+r/c)}{\partial t}\right]dS, \quad (71b)$$

which give two alternative expressions of any solution $A^\mu$ of the d'Alembert equations

$$\frac{\partial^2 A^\mu}{\partial x^\rho \partial x_\rho}=4\pi J^\mu. \quad (72)$$

$\mathbf{r}$ is the position vector of the point where the potentials are computed; $V$ is a region of space limited by the closed surface $S$; $n$ is the inner normal of $S$.

Until now we have considered only systems in which all the particles have the same value of $\eta$; Eq. (70) corresponds to the most general case in which each particle has its own $\eta_i$.

**18.** Excepting the stationary motions in which the equations of motion are of the second order, the equations of motion are in general of the third order. Therefore, it is no more sufficient to give the initial positions and velocities of the particles in order to determine their motions, as it happens in non-relativistic dynamics. Dirac[1] has shown, in a particular case, that it is possible to determine completely the motion of a particle by giving its initial position and velocity and imposing a time boundary condition for $t=\infty$. This time boundary condition was introduced in order to avoid motions with indefinitely increasing self-accelerations of the particle. Since the self-accelerations are due to the possibility of an indefinite decrease of the acceleration energy, we can generalize Dirac's time boundary condition in the following way:

(III) "The acceleration energy and momentum of the particles of a system cannot decrease or increase indefinitely when $t$ tends to $\pm\infty$, if the particles are not accelerated indefinitely by exterior forces."

It follows from this condition that, in general, the acceleration of the particles of an isolated system must tend to zero when $t$ tends to $\pm\infty$, if the motion of the system is not stationary. Indeed, the rate of momentum loss by the $i$th particle of a system is

$$\frac{2}{3}\frac{e_i^2}{\eta_i c}\frac{dx_i^\mu}{ds_i}\frac{d^2x_i^\rho}{ds_i^2}\frac{d^2x_{i,\rho}}{ds_i^2}$$

so, if its acceleration does not tend to zero when $t$ tends to $\pm\infty$, the total amount of radiated energy will be infinite and, since there is conservation of energy, this can only happen if the acceleration energy diverges, if we exclude an initial divergence of the kinetic energy. There is also the possibility of an infinite radiation of energy with a collapse of the system which liberates an infinite amount of potential energy, without an indefinite acceleration of the particles. The boundary condition III does not impose any restriction at all to the behavior of the systems in stationary motion, because in such motions there is no acceleration momentum, since $\eta_i=0$.

The boundary condition III is of a more restrictive kind than the condition introduced by Dirac, because it restricts the behavior both for $t=\infty$ and $t=-\infty$. However, in the particular case considered by Dirac it is satisfied automatically for $t=-\infty$. It is necessary to restrict the behavior at both time boundaries in order to have a vanishing flux of energy at the space boundary of the field: it is easily seen that the Poynting vector of the field created by the particles vanishes at infinity if the accelerations of the particles vanish for $t=\pm\infty$. Therefore, Eq. (55) becomes

$$\frac{d}{dt}G^0{}_{\text{field}}=-\frac{1}{c}\sum_i e_i F^{0\nu}{}_{i,\text{act}}\frac{dx_{i,\nu}}{dt}, \quad (73)$$

and shows that there is conservation of the energy of the system particles plus field. So we see that the *time boundary conditions for the motion of the particles are necessary in order to insure the conservation of energy, in motions which are not stationary*. In stationary motions the conservation of energy is automatically insured by the nature of the interior actions, so that it is not necessary to introduce time boundary conditions.

The time boundary condition III is compatible only with two kinds of behavior of the particles

for $t=+\infty$: ($a$) uniform rectilinear motions of the particles infinitely separated, or ($b$) a collapsed configuration of a part of the system with the other particles infinitely separated with uniform rectilinear motions.

## PART V. THE ACTION PRINCIPLE

**19.** The equations of motion of the field and the particles can be derived from an action principle

$$\delta I=0, \tag{74}$$

$$I=-\sum_i m_i c\int_{-\infty}^{+\infty} ds_i-\sum_i \frac{e_i}{c}\int_{-\infty}^{+\infty} A^{\mu}{}_{\text{rad}}\frac{dx_{i,\mu}}{ds_i}ds_i$$

$$-\tfrac{1}{2}\sum_i\sum_{j\neq i}\frac{e_ie_j}{c}\int\int_{-\infty}^{+\infty}\frac{dx_i^{\mu}}{ds_i}\frac{dx_{j,\mu}}{ds_j}$$

$$\times\delta(\{\mathbf{x}_i^{\rho}-\mathbf{x}_j^{\rho}\}\{\mathbf{x}_{i,\rho}-\mathbf{x}_{j,\rho}\})ds_ids_j$$

$$-\frac{1}{16\pi c}\int(F^{\rho\sigma}{}_{\text{tot}}+\textstyle\sum_i F^{\rho\sigma}{}_{i,\text{at}})F_{\text{rad},\rho\sigma}$$

$$\times dx^0dx^1dx^2dx^3. \tag{75}$$

$F^{\rho\sigma}{}_{\text{rad}}$ denotes the total radiation field

$$F^{\rho\sigma}{}_{\text{rad}}=F^{\rho\sigma}{}_{\text{wav}}+\textstyle\sum_i F^{\rho\sigma}{}_{i,\text{rad}}. \tag{76}$$

In the action principle (74) we variate the coordinates of the particles $x_i^{\mu}$ and the potentials $A^{\mu}{}_{\text{rad}}$ of the total radiation field, the Euler equations are

$$m_ic\frac{d^2x_i^{\mu}}{ds_i^2}=\frac{e_i}{c}\left(F^{\mu\nu}{}_{\text{rad}}+\sum_{j\neq i}F^{\mu\nu}{}_{j,\text{at}}\right)\frac{dx_{i,\nu}}{ds_i}, \tag{77}$$

$$\frac{\partial^2A^{\nu}{}_{\text{rad}}}{\partial x^{\mu}\partial x_{\mu}}=0, \tag{78}$$

provided we introduce the supplementary conditions

$$\frac{dx_i^{\mu}}{ds_i}\frac{dx_{i,\mu}}{ds_i}=1, \tag{79}$$

$$\frac{\partial A^{\mu}{}_{\text{rad}}}{\partial x^{\mu}}=0. \tag{80}$$

In the action principle (74) we consider the $A^{\mu}{}_{i,\text{at}}$ as functionals of the coordinates of the particles, taken as functions of the respective $s$, defined by Eq. (9). It is worthwhile to observe that even if we variate separately the $A^{\mu}{}_{i,\text{rad}}$ we get only the Eqs. (78). However, Eqs. (78) and (80) can always be satisfied by assuming that

$$\frac{\partial^2A^{\nu}{}_{i,\text{rad}}}{\partial x^{\mu}\partial x_{\mu}}=0,\quad \frac{\partial^2A^{\nu}{}_{\text{wav}}}{\partial x^{\mu}\partial x_{\mu}}=0,$$
$$\frac{\partial A^{\mu}{}_{i,\text{rad}}}{\partial x^{\mu}}=0,\quad \frac{\partial A^{\mu}{}_{\text{wav}}}{\partial x^{\mu}}=0. \tag{81}$$

**22.** We can get an action principle for the system of the particles, from (74), by neglecting the last integral in the right-hand side of (75):

$$\delta L=0, \tag{82}$$

$$L=-\sum_i m_ic\int_{-\infty}^{+\infty}ds_i-\sum_i\frac{e_i}{c}\int_{-\infty}^{+\infty}A^{\mu}{}_{\text{rad}}\frac{dx_{i,\mu}}{ds_i}ds_i$$

$$-\tfrac{1}{2}\sum_i\sum_{j\neq i}\frac{e_ie_j}{c}\int\int_{-\infty}^{+\infty}\frac{dx_i^{\mu}}{ds_i}\frac{dx_{j,\mu}}{ds_j}\delta(\{\mathbf{x}_i^{\rho}-\mathbf{x}_j^{\rho}\}$$
$$\{\mathbf{x}_{i,\rho}-\mathbf{x}_{j,\rho}\})ds_ids_j. \tag{83}$$

The action principle (82) coincides with the action principle of Tetrode[13] and Fokker[9] when

$$\eta_i=0\quad(i=1,2,\cdots n), \tag{84}$$

and with Dirac's[1] action principle when

$$\eta_i=1\quad(i=1,2,\cdots n). \tag{85}$$

## APPENDIX I

### Circular Orbits of Two Particles

Let us consider two charged particles describing concentrical circular orbits in a plane, in such a way that the line joining both particles passes at each moment through the center of the circular orbits. It is easily seen that the electric field of each particle, at the position occupied by the other, is directed along the radius of the orbit and the magnetic field is perpendicular to the orbits' plane. Therefore, each particle will be attracted to the center of the orbits by a constant radial force, in case both have opposite signs and are, at each moment, at different sides in relation to the center. We must see whether it is possible to determine the radii $R_1$ and $R_2$ of the two orbits and the circular frequency $\omega$ of the two circular motions in such a way that the equations of stationary motion of the two particles be satisfied. Since the forces acting on both particles are radial, we must consider only two

equations:

$$\frac{m_i}{\alpha_i}R_i\omega^2=e_i\left[E_{j,\mathrm{at}}+\frac{\omega}{c}R_iH_{j,\mathrm{at}}\right], \tag{86}$$

$$\alpha_i=\left[1-\frac{\omega^2}{c^2}R_i^2\right]^{\frac{1}{2}}. \tag{87}$$

$E_{j,\mathrm{at}}$ and $H_{j,\mathrm{at}}$ are, respectively, the moduli of $\mathbf{E}_{j,\mathrm{at}}$ and $\mathbf{H}_{j,\mathrm{at}}$. For each value of $\omega$ we have a system of two equations for the radii $R_1$ and $R_2$. It is evident from the circular symmetry of the forces that there must be circular orbits, though the equations are not simple enough to allow a direct solution.

If we take two particles describing circular orbits and assume that the retarded field of each one acts on the other, though not on itself, the circular symmetry of the forces disappears, because there are now tangential forces due to the action of the radiated fields of each particle on the other. These tangentials forces, which spoil the radial symmetry, produce a damping of the motions and a shrinkage of the radii. Assuming that the interaction between the particles is due to their attached fields, we get rid of the tangential forces, because the tangential forces due to the advanced fields cancel those due to the retarded fields.

## APPENDIX II

Let us represent $\mathbf{J}$ by a Fourier integral

$$\mathbf{J}=\int_{-\infty}^{+\infty}\mathbf{J}(k)e^{-ickt}dk. \tag{88}$$

Taking in account formulae (57), we get the Fourier integrals of the transversal components of $\mathbf{A}_{\mathrm{ret}}$ and $\mathbf{A}_{\mathrm{adv}}$ in the wave zone

$$\mathbf{A}^{\mathrm{tr}}{}_{\mathrm{ret}}=\frac{1}{R}\int_{-\infty}^{+\infty}\mathbf{J}^{\mathrm{tr}}(k)\exp\left[-ik(ct-R-u_\alpha x'^\alpha)\right]\times dkdx'^1dx'^2dx'^3, \tag{89}$$

$$\mathbf{A}^{\mathrm{tr}}{}_{\mathrm{adv}}=\frac{1}{R}\int_{-\infty}^{+\infty}\mathbf{J}^{\mathrm{tr}}(k)\exp\left[-ik(ct+R+u_\alpha x'^\alpha\right]\times dkdx'^1dx'^2dx'^3. \tag{90}$$

Therefore, we have, in the wave zone

$$\mathbf{E}_{\mathrm{ret}}=\frac{i}{R}\int_{-\infty}^{+\infty}\mathbf{J}^{\mathrm{tr}}(k)k\exp\left[-ik(ct-R-u_\alpha x'^\alpha)\right]\times dkdx'^1dx'^2dx'^3, \tag{91}$$

$$\mathbf{E}_{\mathrm{adv}}=\frac{i}{R}\int_{-\infty}^{+\infty}\mathbf{J}^{\mathrm{tr}}(k)k\exp\left[-ik(ct+R+u_\alpha x'^\alpha)\right]\times dkdx'^1dx'^2dx'^3. \tag{92}$$

It is well known that the time integral of the square of a quantity $M$ represented by the Fourier integral

$$M=\int_{-\infty}^{+\infty}e^{-ickt}\mathfrak{M}(k)dk, \tag{93}$$

is given by the formula

$$\int_{-\infty}^{+\infty}M^2dt=\frac{2\pi}{c}\int_{-\infty}^{\infty}\mathfrak{M}(k)\mathfrak{M}(-k)dk. \tag{94}$$

Taking in account this formula and the Fourier integrals of $\mathbf{E}_{\mathrm{ret}}$ and $\mathbf{E}_{\mathrm{adv}}$ in the wave zone, we see that

$$\int_{-\infty}^{+\infty}\mathbf{E}^2{}_{\mathrm{ret}}dt=\int_{-\infty}^{+\infty}\mathbf{E}^2{}_{\mathrm{adv}}dt. \tag{95}$$

Formulae (59) are special cases of this general relation.

PHYSICAL REVIEW VOLUME 69, NUMBERS 5 AND 6 MARCH 1 AND 15, 1946

# A Classical Theory of Electromagnetism and Gravitation

## (I) Special Theory

H. C. CORBEN
*Department of Physics, University of Melbourne, Melbourne, Australia*

(Received August 12, 1945)

By extending the Maxwell-Lorentz equations to five dimensions, it is shown that one is led to a simple unified theory of gravitational and electromagnetic phenomena. The generalized expressions for the force density and the work done per unit volume per unit time contain terms which correspond, respectively, to the effects of electric, magnetic, and gravitational fields. If it be assumed that no changes of physical quantities occur in the direction of the extra dimension so introduced, a special relativity theory of gravito-electromagnetic fields arises. Within this theory gravitational waves are propagated with the velocity of light, gravitational potential is invariant for Lorentz transformations, and gravitational force acts on the rest mass of a particle. The conservation laws of charge, momentum, and energy are shown to hold, but the last two yield a generalized Poynting vector, and a generalized expression for the energy density, both of which contain terms which depend on the gravitational field strengths. The finite velocity of propagation of gravitational waves leads at once to the result that an accelerated mass emits energy in the form of such waves. On the classical theory the radiation emitted by an electron has thus associated with it a small longitudinal gravitational component. Gravitational forces are shown to lead to a self-energy for an accelerated mass, and the classical radius of a mass $m$, corresponding to the classical radius of a charge, is $Gm/c^2$, where $G$ is the gravitational constant.

### A. INTRODUCTION

WHILE the general theory of relativity has had phenomenal success in describing certain well-known effects associated with gravitational interaction and even with the path of a ray of light in a gravitational field, it has not been possible to obtain a thoroughly satisfactory unified theory of gravitational and electromagnetic phenomena. Most attempts to obtain such a theory have assumed the form of generalizing the equations of the general theory of relativity, so that they incorporate terms which may be identified with electromagnetic potentials and charge and current distributions. Indeed, it is not yet certain that the five-dimensional unified theory of Einstein and Mayer[1] will not lead to an explanation of such fundamental quantum theoretical results as the uncertainty principle itself. On the other hand, the very complexity of these developments makes it difficult to see how they could lead eventually to a general relativistic quantum theory. Although the gravitational forces on elementary particles are extremely small compared with their electromagnetic interactions, one might hope that such a generalized theory would resolve some of the difficulties inherent in the present special relativistic form of quantum mechanics.

In order to develop such a theory, it seems of interest to return to the simple classical electrodynamics and look for a set of equations which yield simultaneously a relativistically covariant theory of gravitational and electromagnetic phenomena. Instead of welding electrodynamics to the relatively complicated gravitational theory of general relativity, we attempt to weld gravitational theory to the elementary electrodynamics of Maxwell and Lorentz.

It is difficult at this stage to appeal to the results of experiment for a clue to the proposed synthesis, for no experimental evidence is available concerning either the velocity of gravitational waves in a vacuum or the force on a fast-moving body in a gravitational field. The theory developed in the following pages gives definite answers to these questions. It is shown that relative to a given observer gravitational potentials are propagated in a certain region with the same velocity that light moving in that region appears to be propagated relative to that ob-

[1] A. Einstein and Mayer, Berl. Ber. 130 (1932).

server. In particular, within the dynamics of the special theory of relativity, gravitational potentials are propagated with the universally constant velocity $c$. Secondly, it is shown that gravitational attraction acts only on the rest density of a body; i.e., that relative to a certain observer the gravitational force per unit volume exerted on a body moving with constant velocity is independent of that velocity. The force density itself relative to different observers moving with respect to each other with constant velocities is different, but for such observers the gravitational potential is invariant. The total force on a body is, therefore, proportional to the relativistically increased mass. Should it be possible to disprove any of these results experimentally, it would follow that the theory as developed here is invalid, but it must be admitted that the difficulties involved in such an experimental test are almost insuperable. A high speed particle moving under the gravitational field of the earth would have sufficiently constant velocity for a test to be applied directly. On the present theory it would drop a distance $l^2g/2v^2$ in traveling a distance $l$. On the only apparent alternative hypothesis that the gravitational field acts on the rest mass, it would drop a distance $l^2g/2v^2\cdot[1-(v^2/c^2)]^{\frac{1}{2}}$.

Another result predicted by the theory is that an accelerated mass moving in a vacuum emits energy which at large distances assumes the form of longitudinal gravitational waves which have maximum intensity in the direction of the acceleration. Again it would be difficult to verify this result experimentally, as the energy involved is small.

The theory, as developed in the present paper by direct generalization of the Maxwell-Lorentz equations for a vacuum, has the advantage, in addition to its extreme simplicity, that it may be readily extended to the passage of gravito-electromagnetic waves through a material medium. The macroscopic theory which so arises yields some interesting results, some of which may be verified experimentally, concerning the passage of gravitational waves through such a medium.

### B. GENERAL EQUATIONS

For regions of space occupied only by charge and current distributions, the Maxwell-Lorentz equations expressed in tensor form,

$$\frac{\partial f_{\nu\sigma}}{\partial x_\mu}+\frac{\partial f_{\sigma\mu}}{\partial x_\nu}+\frac{\partial f_{\mu\nu}}{\partial x_\sigma}=0,$$

$$\frac{\partial f_{\mu\nu}}{\partial x_\nu}=4\pi\gamma_\mu, \tag{1}$$

$$k_\mu=f_{\mu\nu}\gamma_\nu \quad (\mu,\nu,\sigma=1,2,3,4),$$

give a very satisfactory system of Lorentz invariant equations for the determination of either the electromagnetic field produced by a given charge distribution or the behavior of a charged body in such a field. The well-known relations

$$f_{\mu\nu}=\frac{\partial A_\nu}{\partial x_\mu}-\frac{\partial A_\mu}{\partial x_\nu} \tag{2}$$

coupled with the identifications

$$H_x=f_{23}, \quad H_y=f_{31}, \quad H_z=f_{12},$$

$$iE_x=f_{41}, \quad iE_y=f_{42}, \quad iE_z=f_{43},$$

$$(A_1,A_2,A_3)=\mathbf{A}, \quad A_4=i\varphi,$$

$$(j_1,j_2,j_3)=\mathbf{j}=i/c=\rho\mathbf{v}/c, \quad j_4=+i\rho,$$

$$(k_1,k_2,k_3)=\mathbf{k}, \quad ck_4=+iW,$$

lead immediately to the classical equations connecting the electric and magnetic fields $(\mathbf{E},\mathbf{H})$, the charge and current densities $(\rho,\mathbf{i})$, the force density $\mathbf{k}$, and the work $W$ done on the charge by the field per unit volume and per unit time.

Gravitational forces do not appear in these equations, and in elementary classical theory it is usual to treat problems involving such forces separately, while noting that much of the analysis of general potential theory is common to the problems of gravitation, electricity, and magnetism. In order to develop a set of equations leading at once to a description of both gravitational and electromagnetic phenomena, we simply take the usual Eq. (1) but allow the suffixes $\mu$, $\nu$, $\sigma$ to assume the values 1 up to 5 instead of merely 1, 2, 3, 4.[2] We introduce thereby the new quantities $f_{15}$, $f_{25}$, $f_{35}$, $f_{45}$, $x_5$, $k_5$, and $i_4$. Defining a vector $\mathbf{F}$ and three scalars $\theta$, $\sigma_0$, $\mathfrak{W}$ by the equations

$$\mathbf{F}=(f_{15},f_{25},f_{35}),$$

$$i\theta=f_{45}, \quad \sigma_0=j_5, \quad \mathfrak{W}=-ck_5, \tag{3}$$

[2] T. Kaluza, Sitz. Preuss. Akad. Wiss. 966 (1921).

and writing $x_5 = ct'$, we have,

$$\nabla \cdot \mathbf{H} = 0, \quad c\nabla \times \mathbf{E} + \partial \mathbf{H}/c\partial t = 0, \tag{4}$$

$$\nabla \times \mathbf{H} - \partial \mathbf{E}/c\partial t + \partial \mathbf{F}/c\partial t' = 4\pi\rho\mathbf{v}/c, \tag{5}$$

$$\nabla \cdot \mathbf{E} + \partial\theta/c\partial t' = 4\pi\rho, \tag{6}$$

$$\nabla \cdot \mathbf{F} + \partial\theta/c\partial t = -4\pi\sigma_0, \tag{7}$$

$$\nabla\theta + \partial \mathbf{F}/c\partial t - \partial \mathbf{E}/c\partial t' = 0, \tag{8}$$

$$c\nabla \times \mathbf{F} + \partial \mathbf{H}/c\partial t' = 0, \tag{9}$$

$$\mathbf{k} = \rho\mathbf{E} + \rho/c(\mathbf{v} \times \mathbf{H}) + \sigma_0\mathbf{F}, \tag{10}$$

$$W = -ick_4 = \rho(\mathbf{v} \cdot \mathbf{E}) + c\sigma_0\theta, \tag{11}$$

$$\mathfrak{W} = -ck_5 = \rho(\mathbf{v} \cdot \mathbf{F}) - c\rho\theta. \tag{12}$$

Equations (10) and (11) may be immediately interpreted as yielding formulae for the total force density and work per unit volume per unit time if we identify $\sigma_0$ with the mass density, $\mathbf{F}$ with the gravitational field strength, and $c\theta$ with the rate at which gravitational forces do work on unit mass. From the definitions (3) of $\mathbf{F}$ and $\theta$ we have, writing $A_5 = -\Omega$,

$$\mathbf{F} = -\nabla\Omega - \partial \mathbf{A}/c\partial t', \quad \theta = \partial\Omega/c\partial t - \partial\varphi/c\partial t', \tag{13}$$

so that if derivatives with respect to the variable $t'$ yield zero, $\Omega$ is the usual gravitational potential. We further note that if $\partial/\partial t' \equiv 0$, Eqs. (5) and (6), coupled with the unaltered Eqs. (4) are identical with Maxwell's equations, Eq. (9) merely states that $\mathbf{F}$ may be written as a gradient, (8) is an identity, and (7) reduces to the wave equation

$$\nabla^2\Omega - \partial^2\Omega/c^2\partial t^2 = 4\pi\sigma_0. \tag{14}$$

Equation (14) reduces to Poisson's equation for static fields, but leads also to the result that for non-static fields gravitational potential is propagated in a vacuum with the velocity of light. Further, since $\sigma_0 = j_5$, and $j_5$ is unaffected by ordinary Lorentz transformations of the coordinates $x_1, x_2, x_3, x_4$, we see that $\sigma_0$ is an invariant for such transformations, and thus corresponds to the rest density of matter at different points of space-time. It also appears that since $\Omega = -A_5$, $\Omega$ also is invariant for ordinary Lorentz transformations, being, like $\sigma_0$, a pseudoscalar. Finally, from Eq. (12) we have, again if $\partial/\partial t' \equiv 0$,

$$\mathfrak{W} = -\rho(\mathbf{v} \cdot \nabla\Omega + \partial\Omega/\partial t) = -\rho\frac{d\Omega}{dt}, \tag{15}$$

where the differentiation is taken along the path of a moving particle. This quantity, as yet undefined, is invariant for Lorentz transformations. Equation (15) suggests that under certain circumstances a gravitational field may do work even on the electric charges in the field. If $\mathfrak{W} = 0$, either the charge density is zero, or along the path of the particle $\Omega$ is constant.

Hence we see that formally Eqs. (4) to (12) yield at once the equations of electromagnetism and gravitation, provided that we assume that the partial derivatives of all physical quantities with respect to the extra variable $t'$ vanish. This assumption leads to what we shall call the special theory of gravito-electrodynamics. On the other hand, the equations are completely symmetrical with respect to the five coordinates $x_1, x_2, x_3, ict, ct'$, and it is natural to investigate the theory which arises if all five of these coordinates are treated on an equal footing. At present, however, our chief interest is in the special theory, but in places we retain the terms involving derivatives with respect to the extra time $t'$ in order to show the symmetrical roles played by $t'$ and $t$. We cannot expect to see a physical significance which may be attached to $t'$ within the framework of the special theory, since as then nothing changes with $t'$ it has *no* physical significance. As we have no evidence apart from observations with a telescope that the special theory does not describe the behavior of macroscopic bodies exactly, it is not surprising that our minds have no conception of a second dimension of time, or a fourth of space.

If now we retain the terms involving $\partial/\partial t'$, substitution of (13) into (8) and (9) yields the identities

$$\frac{\partial}{\partial t'}(\mathbf{E} + \nabla\varphi + \partial \mathbf{A}/c\partial t) = 0, \qquad \frac{\partial}{\partial t'}(\mathbf{H} - \operatorname{curl} \mathbf{A}) = 0. \tag{16}$$

and Eq. (7) becomes

$$\nabla^2\Omega - \partial^2\Omega/c^2\partial t^2 = 4\pi\sigma_0 - c\frac{\partial}{\partial t'}(\nabla \cdot \mathbf{A} + \partial\phi/c\partial t) \tag{7'}$$

which reduces to the wave Eq. (14) provided

that the Lorentz condition

$$\nabla\cdot\mathbf{A}+\partial\phi/c\partial t=0 \tag{17}$$

is assumed to hold. We note, however, that Eq. (17) is not invariant for general rotations of the five-dimensional continuum. The extension of (17) which appears naturally is

$$\frac{\partial A_\nu}{\partial x_\nu}\equiv\nabla\cdot\mathbf{A}+\partial\phi/c\partial t-\partial\Omega/c\partial t'=0. \tag{18}$$

Indeed the equation

$$\frac{\partial^2}{\partial x_\mu\partial x_\mu}\frac{\partial A_\nu}{\partial x_\nu}=0$$

is deducible from (1) and (2) as for four dimensions. If we add (18) to our general equations, we have from (7′)

$$\nabla^2\Omega-\partial^2\Omega/c^2\partial t^2+\partial^2\Omega/c^2\partial t'^2=4\pi\sigma_0, \tag{19}$$

together with

$$\nabla^2\mathbf{A}-\partial^2\mathbf{A}/c^2\partial t^2+\partial^2\mathbf{A}/c^2\partial t'^2=-4\pi\rho\mathbf{v}/c, \tag{20}$$

$$\nabla^2\varphi-\partial^2\phi/c^2\partial t^2+\partial^2\phi/c^2\partial t'^2=-4\pi\rho. \tag{21}$$

Even if the terms involving $\partial/\partial t'$ be different from zero it may be seen from these equations that electromagnetic and gravitational waves at the same point are propagated with respect to a given observer with the same velocity.

Equations (19) to (21) may be written

$$\frac{\partial^2}{\partial x_\nu\partial x_\nu}A_\mu=\square A_\mu=-4\pi j_\mu, \tag{22}$$

where

$$\text{pent}\equiv\square\equiv\frac{\partial^2}{\partial x^2}+\frac{\partial^2}{\partial y^2}+\frac{\partial^2}{\partial z^2}-\frac{1}{c^2}\frac{\partial^2}{\partial t^2}+\frac{1}{c^2}\frac{\partial^2}{\partial t'^2}. \tag{23}$$

Returning to Eqs. (10) and (11), we see that $\mathbf{F}$, $\theta$, may be defined as gravitational field strengths, by analogy with the electromagnetic field strengths $\mathbf{E}$, $\mathbf{H}$. In general they are related to the potentials, $\mathbf{A}$, $\varphi$, $\Omega$ by Eqs. (13) and only when the derivatives $\partial\mathbf{A}/\partial t'$, $\partial\varphi/\partial t'$ are negligible are $\mathbf{F}$ and $\theta$ expressible in terms of the second scalar potential function $\Omega$, which then becomes naturally identifiable with the gravitational potential. We shall, therefore, call $\Omega$ the gravitational potential even though the gravitational field strengths are not in general derivable from it alone.

The field strengths $\mathbf{E}$, $\mathbf{H}$, $\mathbf{F}$, $\theta$ are invariant for transformations of $\mathbf{A}$, $\varphi$, $\Omega$ of the form

$$\begin{aligned}&\mathbf{A}\rightarrow\mathbf{A}+\nabla\chi,\\ &\varphi\rightarrow\varphi-\partial\chi/c\partial t,\\ &\Omega\rightarrow\Omega-\partial\chi/c\partial t',\end{aligned} \tag{24}$$

where $\chi$ is any solution of the equation

$$\text{pent}\ \chi=0.$$

In particular, if $\Omega$ is not transformed as well as $\mathbf{A}$ and $\varphi$, $\mathbf{F}$ and $\theta$ are not invariant for the transformation. We are thus led to a generalized conception of gauge invariance which of course reduces to the usual form for the special theory.

For Lorentz transformations of the coordinate system, the quantities $(\mathbf{F}, i\theta)$ clearly behave as a four-vector, and in particular for the rotation

$$x_1'=\frac{x_1-vt}{(1-\beta^2)^{\frac{1}{2}}},\quad x_4'=\frac{x_4-ivx_1/c}{(1-\beta^2)^{\frac{1}{2}}},$$

we have

$$\begin{aligned}&F_x'=\frac{F_x+v\theta/c}{(1-\beta^2)^{\frac{1}{2}}},\\ &\theta'=\frac{\theta+vF_x/c}{(1-\beta^2)^{\frac{1}{2}}},\\ &F_y'=F_y,\quad F_z'=F_z.\end{aligned} \tag{25}$$

As would be expected, such transformations do not mix up the gravitational field strengths with $\mathbf{E}$ and $\mathbf{H}$, although it is clear that a similar rotation involving $x_5$ would do so.

### C. THE CONSERVATION OF CHARGE, ENERGY, AND MOMENTUM

The conservation law which arises directly from the general equations is

$$\nabla\cdot\rho\mathbf{v}+\partial\rho/\partial t+\partial\sigma_0/\partial t'=0, \tag{26}$$

which reduces to the usual statement of charge conservation provided that partial derivatives with respect to $t'$ vanish. If relative to a particular observer this latter condition is not satisfied, the law of conservation of charge no longer holds strictly, but is replaced by a more general law indicating that mass and charge are

interchangeable. A similar result appears in various unified field theories.[3]

Defining the kinetic energy density $\mathfrak{J}$ of the material by

$$\partial\mathfrak{J}/\partial x_\mu = -k_\mu, \tag{27}$$

we may write

$$\nabla\mathfrak{J} = -\mathbf{k}, \quad \partial\mathfrak{J}/\partial t = W, \quad \partial\mathfrak{J}/\partial t' = \mathfrak{W}. \tag{27'}$$

From (10)–(12)

$$\mathbf{k}\cdot\mathbf{v} = W + \sigma_0\mathfrak{W}/\rho,$$

so that if dashed quantities are again zero

$$W = \mathbf{k}\cdot\mathbf{v}, \tag{28}$$

and, from (15), the theory then applies strictly to a charged particle only when $\Omega$ is constant along its path.

In general, the total force $\mathbf{K}$ acting on the material within a certain volume, and the rate of change of the kinetic energy $T$ of the material are given by

$$\mathbf{K} = \int \mathbf{k}\,d\tau, \quad \frac{\partial T}{\partial t} = \int W\,d\tau. \tag{29}$$

Only if (28) holds may this last equation be written

$$\partial T/\partial t = \int \mathbf{k}\cdot\mathbf{v}\,d\tau.$$

If $\mathbf{p} = m\mathbf{v}$ be the mechanical momentum of the material in a certain volume, Eqs. (29) yield

$$\partial\mathbf{p}/\partial t = \int d\tau[\rho\mathbf{E} + (\rho/c)(\mathbf{v}\times\mathbf{H}) + \sigma_0\mathbf{F}],$$

$$\partial T/\partial t = \int d\tau[\rho\mathbf{v}\cdot\mathbf{E} + c\sigma_0\theta].$$

From Eqs. (4) to (9) these may be written

$$\partial\mathbf{p}/\partial t = -1/4\pi c(\partial/\partial t)\int d\tau(\mathbf{E}\times\mathbf{H} + \theta\mathbf{F}) + 1/4\pi c(\partial/\partial t')\int d\tau(\mathbf{F}\times\mathbf{H} + \theta\mathbf{E})$$
$$+ 1/4\pi\int d\tau(\mathbf{E}\,\mathrm{div}\,\mathbf{E} - \mathbf{F}\,\mathrm{div}\,\mathbf{F} - \theta\,\mathrm{grad}\,\theta - \mathbf{E}\times\mathrm{curl}\,\mathbf{E} - \mathbf{H}\times\mathrm{curl}\,\mathbf{H} + \mathbf{F}\times\mathrm{curl}\,\mathbf{F}), \tag{30}$$

$$\partial T/\partial t = -1/8\pi(\partial/\partial t)\int d\tau(E^2 + H^2 + F^2 + \theta^2) + 1/4\pi(\partial/\partial t')\int d\tau(\mathbf{E}\cdot\mathbf{F})$$
$$+ c/4\pi\int d\tau(\mathbf{E}\cdot\mathrm{curl}\,\mathbf{H} - \mathbf{H}\cdot\mathrm{curl}\,\mathbf{E} - \mathbf{F}\cdot\nabla\theta - \theta\nabla\cdot\mathbf{F}). \tag{31}$$

These formulae suggest that we write

$$1/4\pi\int d\tau(\mathbf{E}\times\mathbf{H} + \theta\mathbf{F}) = \int \mathbf{g}\,d\tau = \mathbf{G} \tag{32}$$

and

$$1/8\pi\int d\tau(E^2 + H^2 + F^2 + \theta^2) = \int u\,d\tau = U \tag{33}$$

as the momentum and energy of the fields within a certain volume. We are thus led to a generalized Poynting vector

$$\mathbf{S} = c\mathbf{g} = c/4\pi(\mathbf{E}\times\mathbf{H} + \theta\mathbf{F}) \tag{34}$$

and to the result that the energy per unit volume of a gravitoelectromagnetic field is

$$u = 1/8\pi(E^2 + H^2 + F^2 + \theta^2).$$

It is of interest to note that if we were to replace $\mathbf{F}$, $\theta$, and $\sigma_0$ by $\mathbf{i}$ times these quantities throughout, the energy density would not assume this positive definite form. Just as in electromagnetic theory the energy density is positive definite only for the theory for which like charges repel each other, so the present theory requires for positive $u$ that masses attract each other.

The energy of gravitational waves within a volume may thus be written for the special theory[4]

$$1/8\pi\int d\tau[(\nabla\Omega)^2 + (\partial\Omega/c\partial t)^2]. \tag{35}$$

[3] A. Einstein and P. Bergmann, Ann. Math. 39, 683 (1938).

[4] For infinitesimal irrotational motion in a homogeneous isotropic fluid of density $\sigma$, the expression (35) becomes

$$\tfrac{1}{2}\sigma\int d\tau[(\nabla\Phi)^2 + \dot{\Phi}^2/v^2],$$

where $\Phi$ is the velocity potential and $v$ the velocity of sound in the fluid. This is the well-known expression for the energy of a sound wave.

Transforming the last term in (31) to an integral over the surface surrounding the volume, we have

$$\partial(T+U)/\partial t = -\oint \mathbf{S}\cdot\mathbf{n}d\sigma + 1/4\pi(\partial/\partial t')\int \mathbf{E}\cdot\mathbf{F}d\tau, \quad (31')$$

with $\mathbf{S}$ defined by (34), and for the special theory this leads to the law of energy conservation. If we define a generalized tension tensor

$$4\pi T_{xx} = \tfrac{1}{2}[E_x^2 - E_y^2 - E_z^2 + H_x^2 - H_y^2 - H_z^2 - F_x^2 + F_y^2 + F_z^2 - \theta^2], \quad (36)$$

$$4\pi T_{xy} = 4\pi T_{yx} = E_xE_y + H_xH_y - F_xF_y, \text{ etc.},$$

then

$$\operatorname{div}_x \mathbf{T} = \frac{\partial T_{xx}}{\partial x} + \frac{\partial T_{xy}}{\partial y} + \frac{\partial T_{xz}}{\partial z}$$

$$= 1/4\pi\Big[E_x \operatorname{div}\mathbf{E} + H_x \operatorname{div}\mathbf{H} - F_x \operatorname{div}\mathbf{F} - \theta\frac{\partial\theta}{\partial x} - (\mathbf{E}\times\operatorname{curl}\mathbf{E})_x - (\mathbf{H}\times\operatorname{curl}\mathbf{H})_x + (\mathbf{F}\times\operatorname{curl}\mathbf{F})_x\Big],$$

so that

$$c(\partial p_x/\partial t)_x + (\partial G_x/\partial t)_x = c\oint T_{xn}d\sigma + 1/4\pi(\partial/\partial t')\times\int(\mathbf{F}\times\mathbf{H}+\theta\mathbf{E})_x d\tau, \quad (30')$$

reducing to the law of conservation of momentum in the case $(\partial/\partial t')\equiv 0$. If we define

$$1/4\pi\int(\mathbf{E}\cdot\mathbf{F})d\tau = \int v d\tau = V, \quad (37)$$

$$1/4\pi\int(\mathbf{F}\times\mathbf{H}+\theta\mathbf{E})d\tau = \int \mathbf{g}^* d\tau = 1/c\int \mathbf{S}^* d\tau = \mathbf{G}^*, \quad (38)$$

Eqs. (31′) and (30′) become

$$\partial(T+U)/\partial t - \partial V/\partial t' = -\oint \mathbf{S}\cdot\mathbf{n}d\sigma, \quad (39)$$

$$c(\partial \mathbf{p}_x/\partial t)_x + (\partial \mathbf{G}_x/\partial t)_x - \partial \mathbf{G}_x^*/\partial t' = c\oint T_{xn}d\sigma. \quad (40)$$

In addition to these generalized conservation laws we now have another which involves terms each of which depend on both the electromagnetic and gravitational field strengths. From the third of equations (27′) we may write

$$\frac{\partial T}{\partial t'} \equiv T' = \int \mathfrak{W} d\tau = \int \rho(\mathbf{v}\cdot\mathbf{F} - c\theta)d\tau, \quad \text{by (12)}$$

or

$$\partial(T-U^*)/\partial t' + \partial V/\partial t = -\oint \mathbf{S}^*\cdot\mathbf{n}d\sigma, \quad (41)$$

where

$$\mathbf{U}^* = (1/8\pi)\int(E^2 - H^2 + F^2 - \theta^2)d\tau = \int u^* d\tau. \quad (42)$$

This equation is completely analogous to (39) and in the general theory the two equations play exactly equivalent roles.

In the special theory, which is our chief interest here, (41) becomes

$$\partial V/\partial t = -\oint (\mathbf{S}^*\cdot\mathbf{n})d\sigma, \quad (41')$$

which is of the form of an energy-conservation law and suggests that we may define

$$v = (1/4\pi)(\mathbf{E}\cdot\mathbf{F}) \quad (43)$$

as an extra energy density in regions of space at which both the electric and gravitational field strengths are non-zero, and

$$\mathbf{S}^* = (c/4\pi)(\mathbf{F}\times\mathbf{H} + \theta\mathbf{E}) \quad (44)$$

as another vector, similar to the generalized Poynting vector (34), representing the flow of this extra energy.

Combining (39) and (41) for the special theory, we have

$$\partial T/\partial t + \partial U/\partial t + \alpha\partial V/\partial t = -\oint (\mathbf{S} + \alpha\mathbf{S}^*)\cdot\mathbf{n}d\sigma.$$

As $\alpha$ is a completely arbitrary quantity, the

actual energy density then loses its physical significance. The meaning of this appears more clearly when we investigate the general theory. However, the energy density is made definite if at all points $v=0$, i.e., $\mathbf{E}\cdot\mathbf{F}=0$, and hence $\mathbf{F}$ is at right angles to the plane containing $\mathbf{E}$ and $\mathbf{H}$. The special theory therefore holds strictly only if this condition is satisfied. Of course for electrons the expression $v=(1/4\pi)\mathbf{E}\cdot\mathbf{F}$, if not identically zero, is completely negligible compared with $u$.

As in pure electromagnetic theory, we may write, from Eqs. (1)

$$k_\mu=(1/4\pi)f_{\mu\nu}\frac{\partial f_{\nu\sigma}}{\partial x_\sigma} \tag{45}$$

and define a symmetrical tensor

$$T_{\mu\nu}=(1/4\pi)(f_{\mu\sigma}f_{\sigma\nu}+\tfrac{1}{4}\delta_{\mu\nu}f_{\sigma\tau}f_{\sigma\tau}). \tag{46}$$

Then

$$k_\mu=\frac{\partial T_{\mu\nu}}{\partial x_\nu}=-\frac{\partial \mathfrak{F}}{\partial x_\mu}, \quad \text{by (27)}, \tag{47}$$

and

$$T_{\mu\nu}=\begin{vmatrix} T_{xx} & T_{xy} & T_{xz} & -iS_x/c & S_x^*/c \\ T_{yx} & T_{yy} & T_{yz} & -iS_y/c & S_y^*/c \\ T_{zx} & T_{zy} & T_{zz} & -iS_z/c & S_z^*/c \\ -iS_x/c & -iS_y/c & -iS_z/c & u & iv \\ S_x^*/c & S_y^*/c & S_z^*/c & iv & -u^* \end{vmatrix}, \tag{48}$$

with the components $T_{xx}$, etc., defined by (36).

In the absence of a gravitational field, the fifth row and column, with the exception of $T_{55}$, vanish, and the other elements of the tensor reduce to the ordinary Maxwell tension tensor. Equation (47) is of course identical with the conservation laws (39)–(41).

From (47) we may obtain formulae for the momentum and energy of a particle by integrating over an invariant region of the continuum. For the special theory, a 4-dimensional section of the 5-space is invariant, and we obtain

$$\int k_x d\tau dt=\int K_x dt=p_x, \qquad \int k_4 d\tau dt=iT/c. \tag{49}$$

Thus as in pure electromagnetic theory the momentum $p$ and $i/c$ times the kinetic energy $T$ of a particle form a four-vector, and $m_0^2c^4=T^2-c^2p^2$.

### D. THE FIELDS OF A POINT CHARGE-MASS

In what follows we shall restrict ourselves to the special theory, for which derivatives with respect to $t'$ are zero. Just as the Wiechert potentials

$$\varphi(P,t)=\left.\frac{e}{r+\mathbf{v}\cdot\mathbf{r}/c}\right|_{t-r/c}, \qquad A(P,t)=\left.\frac{e\mathbf{v}/c}{r+\mathbf{v}\cdot\mathbf{r}/c}\right|_{t-r/c}$$

give the electromagnetic potentials at a point $P$ at time $t$ due to a point charge at $P'(PP'=\mathbf{r})$ moving with velocity, $\mathbf{v}$, so one easily obtains

$$\Omega(P,t)=\left.\frac{-m}{r+\mathbf{v}\cdot\mathbf{r}/c}\right|_{t-r/c} \tag{50}$$

for the gravitational potential due to a particle of rest-mass $m$. Then since

$$\mathbf{F}=-\text{grad }\Omega, \quad c\theta=\partial\Omega/\partial t,$$

the gravitational field strengths caused by the particle are given by

$$\frac{\mathbf{F}}{m}=\frac{-1}{s^2}\text{grad } s, \quad \frac{c\theta}{m}=\frac{1}{s^2}\frac{\partial s}{\partial t}, \tag{51}$$

where $s=r+\mathbf{v}\cdot\mathbf{r}/c$. Hence

$$\frac{\mathbf{F}}{m}=\frac{\mathbf{r}}{s^3}\left(1-\frac{v^2}{c^2}-\frac{\mathbf{r}\cdot(\partial\mathbf{v}/\partial t)}{c^2}\right)+\frac{\mathbf{v}}{cs^2}, \qquad \frac{\theta}{m}=-\frac{r}{s^3}\left(1-\frac{v^2}{c^2}-\frac{\mathbf{r}\cdot(\partial\mathbf{v}/\partial t)}{c^2}\right)+\frac{1}{s^2}=\frac{1}{rs}-\frac{\mathbf{F}\cdot\mathbf{r}}{rm}. \tag{52}$$

Thus the vector $\mathbf{F}$ has components in the directions of $\mathbf{r}$ and $\mathbf{v}$, and both $\mathbf{F}$ and $\theta$ contain terms involving $\mathbf{v}$ which behave like $1/r$ for large $r$. We are therefore led to the result that on the classical theory an accelerated mass emits gravitational waves in the same way that an accelerated charge emits electromagnetic waves.

For $\mathbf{v}=0$, Eqs. (52) become

$$F=m\mathbf{r}/r^3, \quad \theta=0,$$

corresponding to a static gravitational potential

$$\Omega=-m/r$$

due to a fixed mass $m$, as the direction of $\mathbf{r}$ is towards the mass.

From (52) it follows that

$$\partial\mathfrak{I}/\partial t'=\mathfrak{W}=\rho(\mathbf{v}\cdot\mathbf{F}-c\theta)=\frac{-\rho m}{s^2c}(\mathbf{r}\cdot(\partial\mathbf{v}/\partial t)).$$

This derivative with respect to $t'$ is therefore zero only if there be no charges present in the field, or if the acceleration of the point-mass is zero or at right angles to the vector $\mathbf{r}$.

If all of these conditions are violated, we may expect contradictions which may be resolved only within the framework of the more general theory in which variations with $t'$ are permitted.

We now consider a system of point masses, and investigate the nature of the radiation they may emit. As in electromagnetic theory we may define a Hertzian vector

$$\mathbf{Z}(T)=\sum_k m_k\mathbf{x}_k(t_k'),$$

where $m_k$ is the rest-mass of the $k$th particle and $\mathbf{x}_k(t_k')$ the position vector of the $k$th particle relative to a center $Q$ at time $t_k'$. At large distances from a particle, the gravitational field strengths (52) due to the particle are

$$\mathbf{F}=-m\frac{\mathbf{r}}{s^3c^2}(\mathbf{r}\cdot(\partial\mathbf{v}/\partial t)), \quad \theta=\frac{mr}{s^3c^2}(\mathbf{r}\cdot(\partial\mathbf{v}/\partial t)),$$

so that if $PQ=\mathbf{R}$, the field strengths at $P$ at time $t$ due to the system of particles are

$$\mathbf{F}=\frac{-1}{R^3c^2}\mathbf{R}(\mathbf{R}\cdot(\partial^2\mathbf{Z}/\partial t^2)^2)\Big|_{t-R/c}, \qquad \theta=\frac{1}{R^2c^2}(\mathbf{R}\cdot(\partial^2\mathbf{Z}/\partial t^2)^2)\Big|_{t-R/c}. \tag{53}$$

The energy flow per unit time through the area $R^2d\omega$ is then $\mathbf{S}R^2d\omega=c/4\pi(\mathbf{E}\times\mathbf{H}+\mathbf{F}\theta)R^2d\omega$ which becomes, for uncharged point masses

$$\frac{-d\omega}{4\pi c^3}\frac{\mathbf{R}}{R}(\partial^2\mathbf{Z}/\partial t^2)^2\cos^2\phi, \tag{54}$$

where $\phi$ is the angle between the direction of $\mathbf{Z}$ and the vector $\mathbf{R}$, denoting the direction of observation. The energy flow is therefore a maximum in the direction of $\mathbf{Z}$. The total energy radiated per unit time is

$$S=\frac{1}{3}\frac{(\partial^2\mathbf{Z}/\partial t^2)^2}{c^3}. \tag{55}$$

For a harmonic oscillator with rest mass $m_0$, frequency $\nu/2\pi$, amplitude $a$, the time average of this expression is

$$\bar{S}=\frac{1}{6}\frac{m_0^2}{c^3}\nu^4a^2. \tag{56}$$

It is clear from the form of $\mathbf{S}$ (Eq. (34)) that a pure gravitational wave is longitudinal, the vector $\mathbf{F}$ being always parallel to $\mathbf{S}$. The radiation emitted by an accelerated electron in a vaccum normally referred to as electromagnetic waves has associated with it an oscillating gravitational field in the direction of propagation. Since at large distances from the electron such a field is at right angles to both $\mathbf{E}$ and $\mathbf{H}$, it follows from (42) that $v=0$ and from (34) that the flow of energy remains at right angles to the electric and magnetic field strengths. Since the gravitational forces between electrons are extremely small relative to their electrostatic interaction, this effect is completely negligible. For a macroscopic body, however, the result (56) may become measurable.

We have been using throughout units in terms of which charge and mass are of the same dimensions. Given a unit of time (e.g., the second) one could naturally construct a unit of distance (e.g., the light-second) and hence a natural unit of mass as that which placed unit distance from a like mass receives unit acceleration. A natural unit of charge is then such that two particles of unit mass and unit charge if placed at relative rest would remain so.

If, however, we express electric charge in electrostatic units, the corresponding unit of mass is $G^{-\frac{1}{2}}$ gram, where $G$ is the gravitational constant $=6.659\times10^{-8}$ c.g.s. unit. We may call this quantity the electrostatic unit of mass. If $m_0$ be expressed in grams, Eq. (56) becomes

$$\bar{S}=\frac{Gm_0^2\nu^4a^2}{6c^3}\ \text{ergs/sec.}$$

For $m_0=100$ g, $a=10$ cm, $\nu=10$, $\bar{S}=10^{-15}$ erg/sec.

Similarly, for the motion of the earth around the sun, $S=10^{13}$ ergs/sec. Even at this rate it would take $10^{20}$ years for the earth to spiral into the sun.

### E. GRAVITATIONAL SELF-ENERGY

It has been shown that even for a mass as large as the earth the energy of the radiation emitted in virtue of its acceleration is small compared with the energy of its motion. As for electromagnetism the radiation reaction is thus generally small compared with other forces acting on a body. Following the usual classical treatment of radiation reaction,[5] we have, for a mass moving with velocity $\mathbf{v}(v\ll c)$

$$\mathbf{K}+\mathbf{K}_s=m(\partial\mathbf{v}/\partial t),$$

where $\mathbf{K}$ denotes the external force and $\mathbf{K}_s$ the self-force. Hence if at times $t_1$, $t_2$ the state of motion of the mass is the same, we have from (55)

$$\int_{t_1}^{t_2}(\mathbf{K}_s\cdot\mathbf{v})dt=-\frac{1}{3}\frac{m^2}{c^3}\int_{t_1}^{t_2}(\partial\mathbf{v}/\partial t)^2dt.$$

Thus we may write

$$\mathbf{K}_s=\frac{G}{3}\frac{m^2}{c^3}\partial^2\mathbf{v}/\partial t^2, \tag{57}$$

if $m$ is now expressed in grams.

For a harmonic oscillator of natural frequency $\nu_0/2\pi$, expression (57) is small compared with the elastic force if $Gm\nu_0\ll c^3$, or

$$\lambda=\frac{2\pi c}{\nu_0}\gg\frac{Gm}{c^2}=R_0\ \text{say.} \tag{58}$$

Thus corresponding to any mass there is a characteristic length, which may be called the classical radius of the mass. The expression of masses in terms of length units is of course well-known in astrophysics, Eq. (58) simply defining the gravitational mass.

For two bodies of mass $m$, $\epsilon m$ rotating in circles about their center of mass under the influence of their mutual gravitational attraction, the ratios of the reactive forces to the gravitational force become, from (58),

$$\left(\frac{v}{c}\right)^3(1+\epsilon)^2 \quad\text{and}\quad \left(\frac{v}{c}\right)^3\epsilon(1+\epsilon)^2,$$

respectively, where $v$ is the velocity of the mass $m$. Gravitational radiation damping is therefore generally small. Even for a body moving around the sun in an orbit of radius $10^6$ km, the ratio for the consequent motion of the sun is of the order $10^{-9}$. The possibility arises, however, of connecting the radiation reaction with tidal friction, since the gravitational waves emitted by one body do work on another body by producing elastic deformations recognized as tides.

The self-force may be also evaluated by direct calculation of the force which is exerted on a moving mass by the gravitational field produced by the mass. We, therefore, consider a rigid, spherically symmetrical distribution of matter of mass $m$ momentarily at rest at the time $t$. From Eqs. (52), the gravitational field strengths produced by an element $dm$ of mass at a point distant $-\mathbf{r}$ from it are

$$d\mathbf{F}_s(t)=dm\left[\frac{\mathbf{r}}{s^3}\left\{1-\frac{v^2(t')}{c^2}-\frac{\mathbf{r}\cdot\mathbf{v}(t')}{c^2}\right\}+\frac{\mathbf{v}(t')}{cs^2}\right], \tag{59}$$

$$d\theta_s(t)=\frac{dm}{rs}-\frac{\mathbf{r}\cdot d\mathbf{F}_s(t)}{r}, \tag{60}$$

where

$$s=r+(\mathbf{r}\cdot\mathbf{v}(t'))/c,\quad \mathbf{v}(t)=0,\quad t'=t-r/c.$$

As for the electromagnetic case, we assume that

$$R_0^*(\partial^2\mathbf{v}/\partial t^2)\ll(\partial\mathbf{v}/\partial t)c,$$

where $R_0^*$ is of the order of the radius of the spherical mass. We may then approximate to

[5] W. Heitler, *The Quantum Theory of Radiation* (Oxford, 1936), Chap. I, paragraph 3.

(59)

$$d\mathbf{F}_s(t)=dm\left[\frac{\mathbf{r}}{r^3}+\frac{2\mathbf{r}(\mathbf{r}\cdot(\partial\mathbf{v}/\partial t))}{r^3c^2}-\frac{\mathbf{r}(\mathbf{r}\cdot(\partial^2\mathbf{v}/\partial t^2))}{2r^2c^3}-\frac{(\partial\mathbf{v}/\partial t)}{rc^2}+\frac{(\partial^2\mathbf{v}/\partial t^2)}{2c^3}\right], \quad (61)$$

so that on averaging over the mass distribution

$$\langle d\mathbf{F}_s(t)\rangle_{Av}=dm\left[-\frac{(\partial\mathbf{v}/\partial t)}{3rc^2}+\frac{(\partial^2\mathbf{v}/\partial t^2)}{3c^3}\right]. \quad (62)$$

Hence, finally, the self-force becomes

$$\mathbf{K}'=\mathbf{K}_{0m}+\mathbf{K}_{sm},$$

where

$$\mathbf{K}_{0m}=-\frac{1}{3}\frac{\partial\mathbf{v}/\partial t}{c^2}\mu_{0m}, \quad (63)$$

$$\mathbf{K}_{sm}=-\frac{1}{3}\frac{Gm^2}{c^3}\partial^2\mathbf{v}/\partial t^2, \quad (64)$$

$$\mu_{0m}=\frac{G}{2}\int\frac{dmdm'}{r}=\frac{Gm^2}{R_0^*}, \quad (65)$$

and the masses are now expressed in grams. Equation (64) is of course identical with (57). If, again following electromagnetic theory, we put $R_0=R_0^*$,[6] we obtain from (58) and (65)

$$\mu_{0m}=mc^2. \quad (66)$$

If we combine the self-force (63) with the self-force of an electric charge

$$\mathbf{K}_{0e}=-\frac{2}{3}\frac{\partial\mathbf{v}/\partial t}{c^2}\mu_{0e}=-\frac{2}{3}m(\partial\mathbf{v}/\partial t),$$

we obtain

$$\mathbf{K}_{0m}+\mathbf{K}_{0e}=-m(\partial\mathbf{v}/\partial t). \quad (67)$$

For a charged particle the total self-force is therefore given by (67), and even if the mass of the particle be extremely small the contribution from $K_{0m}$ is always of the same order of magnitude as that from $K_{0e}$.

The special relativistic theory of gravitational interaction developed here therefore enables us to calculate the total retarding force exerted on an accelerated charged particle by the gravito-electromagnetic field which it produces. It is possible that if complete account be taken of these forces, some of the difficulties inherent in the classical (and hence the quantum) theory of radiation may be resolved.

The above equations form the natural generalization of the Lorentz electron theory to include gravitational as well as electromagnetic interactions. It is clear that the whole of classical electrodynamics could be similarly generalized. In particular, the macroscopic theory of isotropic dielectrics leads on generalization to a theory of the passage of gravitational waves through matter. It is found that the velocity of the longitudinal gravitational wave emitted by an oscillating body is greatly reduced by the presence of matter, and the energy emitted per second greatly increased, and that such a wave becomes the ordinary longitudinal wave recognized as sound. The phenomena of light and sound thus appear as different aspects of the one fundamental phenomenon.

Details of the macroscopic theory and of the general theory in five dimensions will be published later.

[6] If we set $R=R_0$ in (58), and denote by $\rho$ the density of the spherical mass, we have

$$R_0^{*2}=3c^2/4\pi G\rho.$$

This is closely analogous to the well-known relation between radius and density for an Einstein universe.

# Letters to the Editor

*PROMPT publication of brief reports of important discoveries in physics may be secured by addressing them to this department. The closing date for this department is the third of the month. Because of the late closing date for the section no proof can be shown to authors. The Board of Editors does not hold itself responsible for the opinions expressed by the correspondents. Communications should not in general exceed 600 words in length.*

## Neutron Yields from the Photo- and Electro-Disintegration of Beryllium

MARCELLUS L. WIEDENBECK*
*Department of Physics, University of Notre Dame, Notre Dame, Indiana*
February 19, 1946

BY using electrons and x-rays produced with a Van de Graaff generator, the neutron yield from the disintegration of beryllium has been studied. It was of particular interest to investigate this process since it occurs at a lower energy (1.63 Mev)[1-3] than any other $\gamma-n$ process. As such, the electrostatic generator may be conveniently used to produce a moderately strong source of neutrons. Although the cross section for disintegration by x-rays is low, one can obtain appreciable intensities by using large quantities of beryllium in the region of the target.

In these experiments the neutrons were slowed down in a large cylinder of paraffin and detected with a rhodium cylinder counter and by foils of indium. The paraffin and detectors were calibrated by placing a 100-millicurie radon-beryllium source at the point normally occupied by the beryllium sample. The yield curve for $x$-ray disintegration is shown in Fig. 1. As seen, with an electron accelerating potential of 3.2 Mev and with a beam current of 100 microamperes, the yield is 26 curies equivalent per gram of beryllium. Two hundred grams of powdered beryllium can be used with an efficiency of about 20 percent and as such the yield can be made equivalent to $10^3$ curies. The curve indicates the great advantage gained in working at higher voltages with this process.

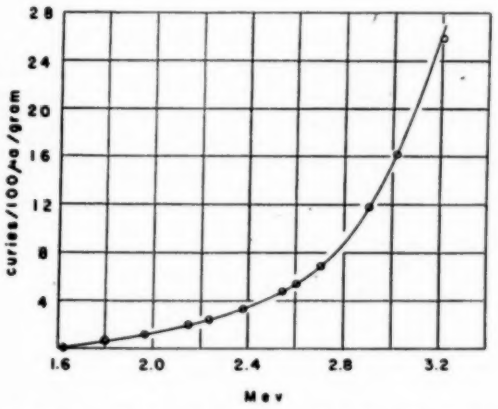


FIG. 1. Neutron yield from the distintegration of beryllium by x-rays. By using 200 grams of beryllium the yield can be increased to $10^3$ curies equivalent.

Figure 2 indicates the neutron yield when the electron

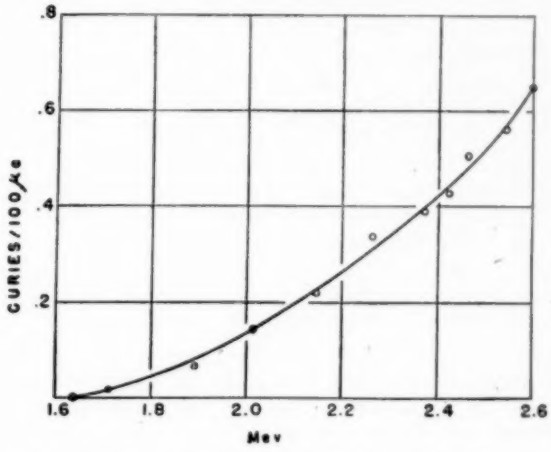


FIG. 2. Neutron yield from the disintegration of beryllium by electrons.

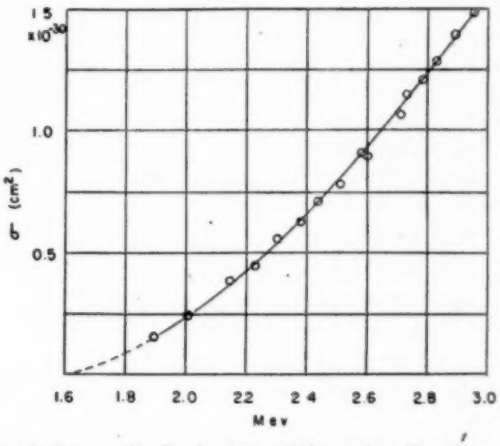


FIG. 3. Cross section for the electro-disintegration of beryllium.

beam of 100 microamperes strikes a thick beryllium target. This is due almost entirely to the electro-disintegration of beryllium. This was shown by placing a second piece of beryllium directly behind the one which stopped the electron. With the second piece in position practically no increase in yield was observed. The efficiency of the electro-disintegration process is very low.

The cross section for the electro-disintegration process was found by determining the yield from a thin sample (12 mg/cm²) of beryllium bombarded with electrons. This is shown in Fig. 3. At 2.5 Mev the cross section is $8\times10^{-31}$ cm² and the variation is quite uniform with voltage. The value of the cross section at 1.73 Mev ($\sim1\times10^{-31}$ cm²) is in good agreement with the early determination by Collins, Waldman, and Guth.[2]

* Now at the University of Michigan.
[1] J. Chadwick and M. Goldhaber, Proc. Roy. Soc. 151, 479 (1935).
[2] G. B. Collins, B. Waldman, and E. Guth, Phys. Rev. 56, 876 (1939).
[3] M. L. Wiedenbeck, Phys. Rev. 67, 54 (1945).

## Neutron Scattering in Ortho- and Parahydrogen and the Range of Nuclear Forces*

C. S. Wu, L. J. Rainwater, W. W. Havens, Jr., and J. R. Dunning
*Department of Physics, Columbia University, New York, New York*
February 15, 1946

USING the results of Alvarez and Pitzer[1] on the neutron scattering cross section of ortho- and parahydrogen [$\sigma_{para}=(5.2\pm0.6)\times10^{-24}$ cm$^2$ and $\sigma_{ortho}=(100\pm3)\times10^{-24}$ cm$^2$]. Schwinger[2] has calculated the range of the neutron proton forces and found this to be either zero or $8\times10^{-13}$ cm. Both of these values are theoretically unreasonable. Schwinger also showed that the value of the neutron scattering cross section of the free proton calculated from these values was incompatible with the experimental value.

We wish to point out that, if a reasonable range of the neutron proton force is assumed to be $2.8\times10^{-13}$ cm$^2$ and the more recently measured value of $21\times10^{-24}$ cm$^2$ [3] is taken for the neutron scattering cross section of the free proton, the calculated value of the cross section of parahydrogen is not very different from that measured by Alvarez. However, the measured value of the scattering cross section of orthohydrogen cannot be reconciled with the calculated value.

In contemplating a repetition of the experiments of Alvarez and Pitzer with the Columbia University neutron velocity spectrometer the theoretically exprected cross sections were calculated. The two equations derived by Schwinger[2] for the scattering cross section of ortho- and parahydrogen under Alvarez's experimental conditions were used. These equations are:

$$\sigma_{para}=\sigma_{0\to0}=6.473(3a_1+a_0)^2$$
$$\sigma_{ortho}=\sigma_{1\to1}+\sigma_{1\to0}=6.291[(3a_1+a_0)^2+2(a_1-a_0)^2]+1.447(a_1-a_0)^2,$$

where $a_0$ and $a_1$ are the singlet and triplet scattering amplitudes which are related to the corresponding cross sections by $\sigma_0=4\pi a_0^2$ and $\sigma_1=4\pi a_1^2$. The slow neutron cross section of the free proton can also be expressed in terms of $a_1$ and $a_0$ by

$$\sigma_{fp}=\pi[3a_1^2+a_0^2]=\tfrac{1}{4}\pi[(3a_1+a_0)^2+3(a_1-a_0)^2].$$

The value of $a_1$ can be expressed in terms of the energy of the triplet state (which is accurately known) and the range of the nuclear forces. The corresponding $a_0$ can be obtained from the equation for the cross section of the free proton. Recently the value of the cross section of the free proton was remeasured using the Columbia University neutron velocity spectrometer and found to be $(21\pm1)\times10^{-24}$ cm$^2$ which is in good agreement with the value obtained by Hanstein.[3]

The variation of the calculated cross section of both ortho- and parahydrogen with the range of the neutron proton forces is shown in Fig. 1 for three different values of the scattering cross section of the free proton which constitute the outside limit of error on the measurement of this value. If the value of the para scattering cross section obtained by Alvarez is used, the range of the nuclear forces will be $(1.7\pm0.8)\times10^{-13}$ cm from the curves which is not unreasonable.

From the point of view of remeasuring the values of ortho- and parahydrogen scattering cross section it is of interest to use the generally accepted value of the range of the nuclear forces as $2.8\times10^{-13}$ cm$^2$ and find the expected value of the ortho- and parascattering cross sections. Using the scattering cross section of the free proton as $21\times10^{-24}$ cm$^2$, the expected values are $\sigma_{para}=3.4\times10^{-24}$ cm$^2$ and $\sigma_{ortho}=125\times10^{-24}$ cm$^2$.

It does not seem unreasonable that the value obtained by Alvarez for the cross section of orthohydrogen is too low or that the value obtained for parahydrogen is too high. It seems quite possible that in the measurement of the ortho cross section the ratio of the para- and orthohydrogen in the cell was no longer that of normal hydrogen which is 1 to 3, respectively. At these extremely low temperatures the walls of the container might act as a catalyst for conversion of ortho- to parahydrogen. Also special precautions might not have been taken to insure the normal composition of the gas before it was introduced into the cell.

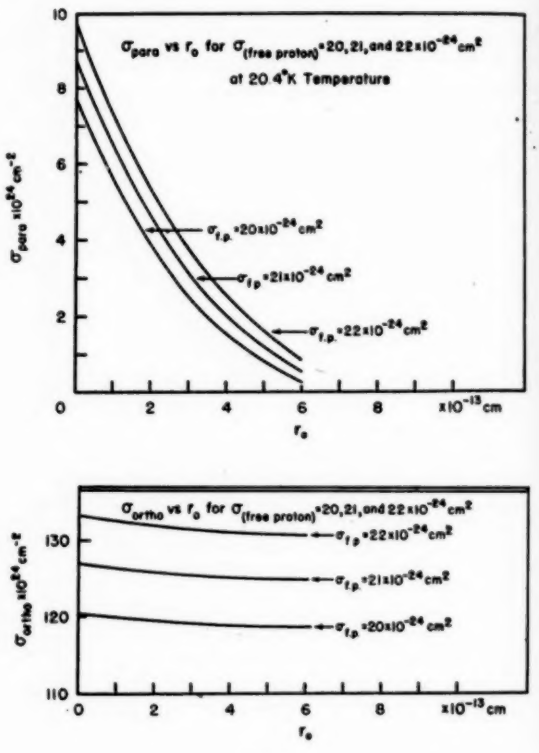


FIG. 1.

An extremely small increase in the amount of orthohydrogen in the measurement of the parahydrogen cross section would account for the larger measured value of the cross section than the calculated value. Any improvement in the experimental technique in the performance of this

experiment should tend to lower the measured value of the para cross section slightly and should increase the measured value of the ortho cross section considerably.

* Publication assisted by the Ernest Kempton Adams Fund for Physical Research of Columbia University, New York, New York.
[1] L. W. Alvarez and K. S. Pitzer, Phys. Rev. 55, 596 (1939); Phys. Rev. 58, 1003 (1940).
[2] J. Schwinger, Phys. Rev. 58, 1004 (1940).
[3] H. B. Hanstein, Phys. Rev. 59, 489 (1941).

## On the Abundance of Nuclei in the Universe

C. LATTES AND G. WATAGHIN
*Department of Physics, University of São Paulo, Brasil*
February 11, 1946

THE correlation between the abundance of variqus nuclei in the universe and their mass defects, pointed out by several authors, gives us the first indication on the thermodynamical character of processes which determined the actual distribution of the isotopes. C. F. v. Weizsaecker,[1] S. Chandrasekhar and L. Heinrich[2] studied the problem and found by different methods the required temperature (with results of the expected order of magnitude: $kT\sim10^6$ ev), but some disagreements between theoretical and observed abundances remained unexplained. The purpose of the present remark is to point out the advantages and the limitations of a statistical method, suggested some years ago by one of us,[3] and to give results of some preliminary calculations which may help to decide whether the nuclei were formed in a nearly thermal equilibrium state of matter of high temperature and density.

Obviously, if $kT\sim10^6$ ev, many nuclear processes: as excitation of higher energy-states and higher spins, photo-effect, neutron evaporation and capture, $\beta$-processes and fission, become essential. Thus a non-negligible fraction of nuclei will not react in their normal states, and that is the chief reason of the difficulties of the Weizsaecker's method. Mesons production at this temperature can be neglected.

In view of the importance of $\beta$-processes under the conditions of our problem, it will be necessary to introduce explicitly the neutrinos into the statistics. Let $N_s$, $n_{es}$, $n_{ps}$, $n_{ns}$, $n_{as}$, $n_{ZAs}$ be the numbers (per cm$^3$) of photons, electrons, positrons, neutrinos and antineutrinos and nuclei of charge $Z$ and mass-number $A$, which belong to the momentum interval $p_s$, $p_s+dp_s$. We assume the validity of the laws of conservation of charge

$$(\Sigma_s[n_{ps}-n_{es}+Zn_{ZAs}]=\text{const.}),$$

of energy, of the total number of nucleons

$$(\Sigma An_{ZAs}=\text{const.})$$

and of

$$\Sigma_s[n_{ps}-n_{as}-n_{es}+n_{ns}]=\text{const.}$$

or

$$\Sigma_s[n_{ps}-n_{es}+n_{as}-n_{ns}+Zn_{ZAs}-(A-Z)n_{ZAs}]=\text{const.} \quad (1)$$

We obtain in the usual way the formula for $n_{ZAs}$ already published[3] with a somewhat different meaning of the parameter $\alpha$, because of (1). Integrating $n_{ZAs}$ in the momentum space (summing with respect to $s$), one can show that the term $\pm1$ can be neglected and one obtains, with a good approximation the following value for the abundance

$$n_{ZAs}=1.735\times10^{35}\times(2\zeta+1)\times\left[\frac{kT}{mc^2}\times\frac{E_{ZA}}{M_Hc^2}\right]^{\frac{1}{2}}\times\exp\left[-\alpha Z+\gamma A-\frac{E_{ZA}}{kT}\right]. \quad (2)$$

Here $E_{ZA}$ is the total energy of a nucleus at rest in the reference system of the centrum of gravity of the assembly

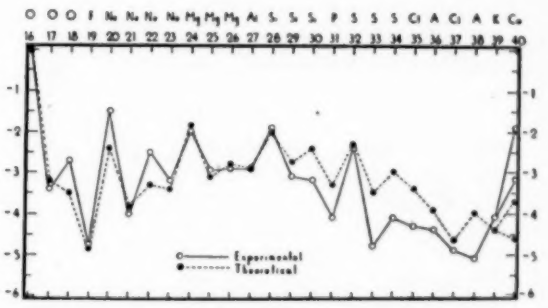
O O O F Na Ne Na Mg Mg Mg Al Si S S P S S S Cl A Cl A K Ca
16 17 18 19 20 21 22 23 24 25 26 27 28 29 30 31 32 33 34 35 36 37 38 39 40
-1 -2 -3 -4 -5 -6
Experimental
Theoretical

FIG. 1. Comparison of present theory with measured abundances.

(including the excitation-energy acquired in an inelastic collision). In the present preliminary survey, we shall substitute $E_{ZA}$ with $M_{ZA}c^2$ where $M_{ZA}$ is the rest mass of the nucleus in the fundamental state. In this way we obtain:

$$\log\frac{n_{ZA}}{n_{Z'A'}}\cong\log\frac{2\zeta+1}{2\zeta'+1}+\frac{3}{2}\log\frac{M_{ZA}}{M_{Z'A'}}+D\times(A-A')-B(M_{ZA}-M_{Z'A'})-\alpha(Z-Z'). \quad (3)$$

Here the parameter values

$$\alpha=\alpha\log e;\quad B=(c^2/kT)\log e;\quad D=\gamma\log e$$

can be determined from 3 values of $\log(n_{ZA}/n_{Z'A'})$ known experimentally. Because of the uncertainty of the experimental data and of the limitations of the suggested method, we have chosen by trial approximated values of these parameters and we obtained as a preliminary result the theoretical abundances (for between 8 and 20) indicated in Fig. 1, with: $\alpha=0.1$, $D=525$, $D-B=-0.85$.

We have not considered the excited states and the higher spin states. We have not taken into account the changes in the relative abundance subsequent to the equilibrium and due to the radioactivity, photo-effect, evaporation, and fission processes at temperatures below the equilibrium when the main nuclear reactions are already slowed or stopped. The general satisfactory accord between the theoretical and observed abundances, shown in Fig. 1, leads us to the conclusion that nuclei were formed under conditions not far from the conditions of a thermal equilibrium. Further results and a detailed account of the calculations will be published elsewhere.

[1] C. F. v. Weizsaecker, Physik. Zeits. 39, 633 (1938).
[2] S. Chandrasekhar and L. Heinrich, Astrophys. J. 95, 288 (1942).
[3] G. Wataghin, Comptes rendus 203, 909, (1935); Phys. Rev. 66, 149 (1944).

## A Device Producing Ion Beams Homogeneous as to Mass and Energy

JØRGEN KOCH
*Institute for Theoretical Physics, University of Copenhagen, Denmark*
February 9, 1946

IN the production of beams of one definite kind of ions, as, e.g., in many experiments within nuclear physics or in apparatuses for collecting isotopes, a mass-spectrographic analyzer is often used which consists of a homogeneous, magnetic deflecting field only. In order to focus the separated ion beams on a target or on the slit of a collector, it is necessary to keep both the magnetic field and the accelerating potential extremely constant. The former may generally be done by using accumulators for running the magnet. With a high accelerating potential the stabilization of the high tension generator, however, may be rather inconvenient, and in many cases may be replaced by the device described below, which has been used in connection with the construction of a mass spectrograph for the collection of small samples of pure isotopes.[1,2]

The principle of the method is shown in Fig. 1. The ions are accelerated with a potential of about 70 kv in the space between the low voltage capillary ion source $I$ and the earthed cylinder $C_1$. The ions paths are collimated by means of an electrostatic retardation lens consisting of the cylinders $C_1$, $C_2$, and $C_3$. The ion beam now passes through a small deflecting condenser, one plate of which is earthed. The other plate is connected to a potential $E$ which is proportional to the fluctuation of the average accelerating potential $V$: $E=E_0\Delta V$. If the accelerating potential is exactly $V(\Delta V=0)$, the beam will not be deflected, but will enter the magnetic field at $b$, after which it continues along a circular path with a radius of curvature $\rho$ to $b'$ and from there rectilinearly to the slit of the collector at $F$. If the accelerating potential increases by $\Delta V$, the ion beam will be slightly deflected by passing the condenser and enter the magnetic field at $a$, from where it continues along a circular path with a somewhat longer radius than before to $a'$, and from there tangentially in the direction of focus $F$. For negative values of $\Delta V$ the ion beam will be deflected in the direction of $c$, but after passing the magnetic field it will again arrive at focus $F$.

The deflecting potential is produced as follows. The high tension generator (H. T.) is connected with a resistance $R$ of $70M\Omega$ (which is also used to determine the potential of the electrostatic lens $V_1$) in series with a much smaller resistance $r$ of $140k\Omega$. If the switch $A$ is on, the current in $r$ may be compensated for a definite accelerating potential $V$ by adjustment of the potentiometer $P$. If now the accelerating potential fluctuates by $\Delta V$, fluctuations of $r/2R\cdot\Delta V$ will appear on the resistance $r$ $(=r')$. By adjustment of the slider $S$ fluctuations of suitable size may be led to the d.c. linear amplifier, with a constant amplification factor of about 1400, and herefrom to the plate of the deflecting condenser. The battery $B_g$ determines the grid bias of the first valve, while $B_a$ compensates the d.c. anode potential of the output valve.

After emerging from the deflecting condenser the beam may be taken as radiating from a virtual source $G$, the angle of deflection being proportional to $\Delta V$. The potential $E(=E_0\Delta V)$ necessary to focus the ion beam coming from $G$ at a point $F$ on the median beam after deflection in a magnetic prism with the central angle $\vartheta$ is obtained from the expression

$$E_0=\frac{d}{l}\cdot\frac{1+n\sin\vartheta-\cos\vartheta}{(1-\eta\xi)\sin\vartheta+(\eta+\xi)\cos\vartheta},$$

where $\xi=g/\rho$, $\eta=f/\rho$ (see Fig. 1) and $l/d$ is the ratio between the length of the condenser plates and their mutual distance. In the investigations made with the mass spectrograph of the Institute the following experimental conditions were used: $\rho=80$ cm, $\vartheta=\pi/2$, $\xi=0.38$, $\eta=1$, and $l/d=3.2$, hence $E_0\approx1$. In spite of the fact that the high tension generator (conventional voltage doubling circuit) was connected directly to the tension of the city mains, no displacements of the lines of the mass spectrum were observed. This result corresponds to a stabilization of the accelerating potential of about $1:10^4$. It should be added that the method described also compensates for the ripple of the accelerating potential and even for much faster fluctuations, which may originate from sudden changes of the working conditions of the accelerating tube.

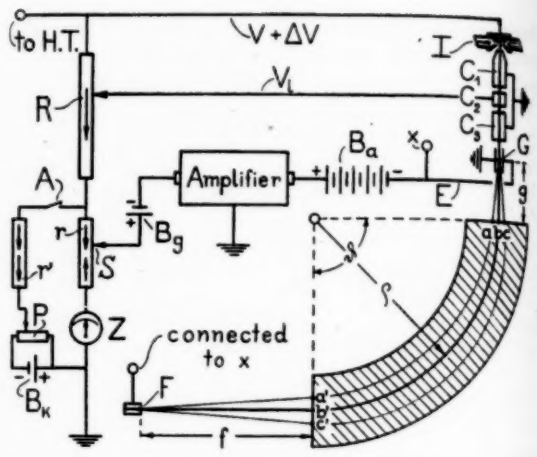


FIG. 1. Diagram of mass-spectrographic analyzer.

The ions of course hit the target or the collector with different energies $V+\Delta V$. By mounting these electrodes isolatedly and connecting them to the output potential of the amplifier $E=\Delta V(E_0=1)$ it is, however, possible to make the ions always arrive with the same energy $V$. This principle may be of importance in experiments within nuclear physics (e.g., investigations on resonance curves) with or without the employment of magnetic analysis of the ion beam.

An account containing the detailed discussion of the focusing method here mentioned, and a description of the apparatuses pertaining to it, will soon be published in *Det Kongelig Danske Videnskabernes Selskabs Mathematisk-fysiske Meddelelsker*. Finally I wish to express my cordial thanks to Professor Niels Bohr for the active interest he has taken in the questions discussed above.

[1] J. Koch, Diss., Copenhagen (Publ. by Thaning & Appel, 1942).
[2] J. Koch and B. Bendt-Nielsen, Det Kgl. Danske Vid. Sels. Mat.-fys. Medd. 21, 8 (1944).

## Mass Measurement with a Single Field Mass Spectrometer

EDWARD P. NEY AND ALFRED K. MANN
*Rouss Physical Laboratory, University of Virginia, Charlottesville, Virginia*
February 11, 1946

IN the past, accurate mass measurements have been accomplished with "double focusing" mass spectrographs.[1-3] This method allows high precision, but requires that the measurements be made from a photographic plate which has previously been exposed in a vacuum to the ion beams.

If a single field mass spectrometer were capable of the requisite resolving power, then the accelerating potentials necessary to focus ions of different $m/e$ should be inversely proportional to the masses of the ions from the familiar equation,

$$m/e = 4.8 \times (10)^{-5} r^2 H^2 / V,$$

providing $H$ is held constant. No record of the application of a single field mass spectrometer to this problem could be found in the literature.

An improved Nier-type, 60-degree mass spectrometer has been used in this manner to measure the doublet separation of $H^{1+}{}_2 - He^{4++}$. The mass spectrum of hydrogen and helium in the vicinity of mass 2 is shown in Fig. 1 to

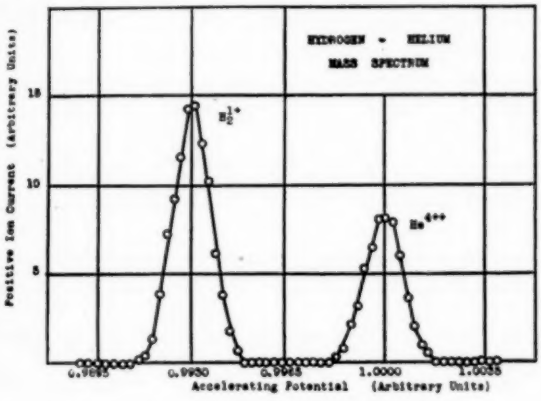


FIG. 1. The mass spectrum of hydrogen and helium in the vicinity of mass 2.

demonstrate the resolving power obtained. Voltages proportional to the accelerating voltages at which the $H^{1+}{}_2$ and $He^{4++}$ ions were focused were measured with a Rubicon high precision type B potentiometer.

If R designates the ratio of the voltage corresponding to $H^{1+}{}_2$ to the voltage corresponding to $He^{4++}$, it can be shown that the mass ratio, $He^4/H^1{}_1$, is equal to $4R$ to within several parts in a million. An average of 56 measurements gives the value $3.97163 \pm 0.00005$ for the helium hydrogen mass ratio, where the error is the probable error in the measurement. Aston originally measured 3.97126 for this ratio,[4] but later revised this to 3.97166.[5] The agreement between the result reported here and Aston's value is well within the accuracy of our voltage measurement. This agreement with Aston's value is significant because it indicates that mass measurements can be made with a Nier type spectrometer providing the resolving power is sufficiently high. In the Nier type instrument it is customary to use an auxiliary magnetic field across the ion source in order to increase the intensity. It should be stated, however, that this magnetic field cannot be presented when mass measurements are made.

It is hoped that with some redesign of the ion source and with improved voltage measurements, greater precision can be obtained in future experiments.

The authors wish to acknowledge their indebtedness to Professors J. W. Beams, L. B. Snoddy, and A. O. C. Nier.

[1] F. W. Aston, *Mass Spectra and Isotopes* (Edward Arnold and Company, England, 1933).
[2] K. T. Bainbridge and E. B. Jordan, Phys. Rev. **50**, 282 (1936).
[3] K. T. Bainbridge, Phys. Rev. **40**, 130 (1932).
[4] F. W. Aston, Proc. Roy. Soc. **A115**, 487 (1927).
[5] F. W. Aston, Nature **137**, 357 (1936).

## Influence of Intercrystalline Forces on Beta-Ray Absorption

HENRI D. RATHGEBER
*University of Melbourne, Australia*
January 9, 1946

IT has been reported that a considerable difference between the absorption of beta-rays by cold-rolled and that by annealed aluminium has been found.[1] These measurements have been repeated with the following apparatus. The beta-rays emitted by a rad $D$+rad $E$ source (0.3-cm diameter) obtained by anodic deposition of radiolead, are counted at a distance of 8 cm in coincidence Geiger counters with an effective aperture of 0.6-cm diameter and a total window thickness (bubble window+Al-foil) of about 0.1 g/cm². A mechanical counter preceded by a scale of eight registers the counts. The area of the absorber is limited to 0.7-cm diameter by a brass aperture plate which is at a distance of 2.5 cm from the source. The absorbers were cut two at a time from the same aluminium foil; one was used in the cold-rolled state while the other was annealed in vacuum at 350°C for 5 hours. (Table I.)

The differences in intensity of not more than 2 percent do not exceed the standard error sufficiently to be significant. It was, therefore, decided to check these results

TABLE I.

| Absorption | Intensity of beta-rays Number per minute | |
|---|---|---|
| (1) Al 0.038 cm thick $0.102 \pm 0.0005$ g cm$^{-2}$ cold-rolled | $573.6 \pm 5.6$ | |
| (2) Al same, annealed | $562.4 \pm 5.6$ | |
| Difference | $+11.2 \pm 8.0 =$ | $2.0 \pm 1.4\%$ |
| (3) Al 0.051 cm thick $0.136 \pm 0.0005$ g cm$^{-2}$ cold-rolled | $303.2 \pm 3.2$ | |
| (4) Al same, annealed | $308.8 \pm 3.2$ | |
| Difference | $-5.6 \pm 5.6 =$ | $-1.8 \pm 1.8\%$ |
| Average | | $0.1 \pm 1.6\%$ |

TABLE II.

| Scattering | Intensity of beta-rays Number per minute |
|---|---|
| (1) Al 0.19 cm thick cold-rolled | 63.2±0.6 |
| (2) Al 0.3 cm thick macrocrystalline | 62.7±0.6 |
| Difference | 0.5±0.8 = 0.8±1.3% |

by a scattering experiment. The beta-ray source and the aluminum scatterers were placed in such a way that the rays were deflected on the average by 90°. The scattering by a cold-rolled specimen was compared with that of a strain-free specimen consisting of a few very large crystals (about 1 cm). Identical surfaces were obtained by etching with dilute HCl shortly before the measurements. The difference in thickness of the scatterers is of no influence because the thinnest one is thicker than the range of the beta-rays. (Table II.)

The condition of the absorbers and scatterers was checked by x-ray back reflection photographs which confirmed that the intended states of deformation and recrystallization had been obtained in the cold-rolled and annealed specimens. The macrocrystalline scatterer gave the Laue diagram of an undeformed single crystal.

It is to be concluded from these experiments that the state of deformation in aluminum has no measurable effect (less than 1 percent) either on absorption or on scattering of beta-rays of such an energy that they are still able to penetrate matter of a surface density of 0.1 g/cm$^{-2}$ after the absorption or the scattering.

[1] G. Winchester, Phys. Rev. **68**, 100 (1945).

## Mass of the Neutron

KUAN-HAN SUN*
*c/o Universal Trading Corporation, 630 Fifth Avenue, New York, New York*
February 14, 1946

THE commonly accepted value for the mass of the neutron is that by Bethe[1] who deduced a value 1.00893±0.00005 from the binding energy of the deuteron (2.17±0.04 Mev), the mass spectroscopic difference of $H_2^1$ and $D^2$ (0.00153±0.00004 mass units) and the isotopic mass of hydrogen (1.00813±0.00002 mass units). The mass difference of $H_2^1$ and $D^2$ and the isotopic mass of hydrogen have since been revised by Mattauch[2] are adopted by Aston[3] in his recent book. These values are 0.001539 ±0.0000021 and 1.008130±0.0000064 mass units, respectively. Modifying Bethe's deduction with these new figures and using the relationship: 1 Mass Unit = 931.4 Mev derived from constants given by Birge[4], the new mass of the neutron becomes 1.00892±0.00004 mass units.

* On leave of absence from Kodak Research Laboratories, Rochester, New York.
[1] H. A. Bethe, Phys. Rev. **53**, 314 (1938).
[2] J. Mattauch, Phys. Rev. **57**, 1155 (1940).
[3] F. W. Aston, *Mass Spectra and Isotopes* (Longmans, Green and Company, New York, 1942), second edition, p. 116.
[4] R. T. Birge, Rev. Mod. Phys. **13**, 233 (1941).

## On the Intensity Distribution Among the Rotational Lines of AlO

FRANCINE P. COHEUR AND PIERRE M. COHEUR
*Department of Astrophysics, University of Liège, Belgium*
February 8, 1946

H. BRINKMAN* has found that the rotational intensity distribution in the AlO bands emitted by an electric arc between carbon electrodes loaded with $Al_2O_3$ does not depend upon the current intensity or the distance between the electrodes; the corresponding temperature is 4000°±300°, while the temperature obtained from the rotational intensity distribution of the CN bands emitted by the same arc is of the order of 6500°. Brinkman explains this result by stating that the AlO bands are emitted in the cool peripheric regions of the arc. It may seem strange that no temperature gradient is found between the 6500° zone (core of the arc, emitting the CN bands) and the 4000° zone (periphery of the arc, emitting the AlO bands).

In the course of a systematic investigation of the rotational intensity distribution in the AlO bands we have obtained a rotational temperature $T \leqq 4000°$ in all the following cases of emission:

(a) explosion of thin wires of aluminum;
(b) arc between electrodes of hydronalium (alloy of aluminum and magnesium), for all currents from 3 up to 15 amp;
(c) condensed spark between electrodes of hydronalium;
(d) arc between electrodes of carbon loaded with grains of aluminum, burning in oxygen at a pressure of one atmosphere; temperature obtained $T = 4225 \pm 200$;
(e) same arc burning in air, i.e., oxygen pressure = 0.2 atmos.; $T = 4210 \pm 300$;
(f) same arc in vacuum, i.e., oxygen pressure, about 0.002 atmos.; $T = 4275 \pm 300$;
(g) arc between electrodes of carbon, loaded with $Al_2O_3$, burning in air; $T = 4175 \pm 225$;
(h) same arc, electrodes loaded with $AlCl_3$; $T = 3877 \pm 250$;
(i) same arc, electrodes loaded with $Al_2(SO_4)_3$, $T = 3950 \pm 300$.

The constancy of the rotational temperature obtained in such a wide variety of sources would seem to indicate that such a "temperature" does not give a real picture of the source, but may instead characterize a specific molecule. One may wonder whether the constant value of 4000° results from the mechanism of formation of AlO molecules from Al and O atoms, or whether 4000° is simply an optimum temperature for the formation and emission of AlO molecules.

In order to decide between these alternatives, sources have been investigated in which the temperature at all points could be expected to be lower than 4000°. First an oxyacetylemic flame was studied in which aluminum powder was dropped producing "explosions": the temperature obtained was still of the same order ($T = 4250 \pm 275$). But when using a flame, poor in oxygen, in which a flow of nitrogen containing aluminum powder was introduced, we found a definitely lower temperature, $T = 3050 \pm 250$.

This last result eliminates the first hypothesis suggested. It thus seems that we should consider $T \leqq 4000°$ as an optimum temperature for AlO emission. In sources presenting regions hotter than 4000° the AlO molecules subsist only in the relatively cool regions around 4000°; in such a case the rotational intensity distributions among AlO lines is not related to the highest temperature in the source. However, in sources cooler than 4000°, the AlO

intensity distribution may possibly provide the actual temperature of the source.

At any rate great care should be exercised in applying the rotational intensity distribution of lines of AlO and possibly of other molecules to the determination of temperatures in most types of sources.

* "Optische Studie van de Electrische Lichtboog," Thesis, Utrecht, 1937.

## Superconductivity and Magnetic Energy between Currents

WILLIAM BAND
*Yenching University, Peiping, China*
January 23, 1946

FRENKEL'S supposition[1] that classical magnetic attraction between currents might cause electrons to "freeze" into a collective assembly at sufficiently low temperatures, which would be superfluid in its interaction with the atom lattice was disproved by Bethe and Fröhlich.[2] Frenkel's assumption essentially amounted to supposing that the potential energy

$$\sum_{ij} e^2 u_i u_j / r_{ij} \tag{1}$$

would of itself ensure that at the transition temperature the velocities $u_i = u_j = u$ the same for all electrons.

Instead, let (1) be simplified by considering any sample electron and smooth out the effect of all the other electrons by writing

$$\Sigma_j e u_j / r_{ij} = \gamma I, \quad \text{all } i, \tag{2}$$

so that the total interaction energy becomes

$$\Sigma_i \gamma e u_i I. \tag{3}$$

The contribution from an electron with speed $u$ in the direction of the current $I$ is then

$$\gamma e u I \quad \text{per cm of its path} \tag{4}$$

or

$$\gamma e u^2 \tau I \tag{5}$$

between collisions, where $\tau$ is the time of relaxation.

This energy, proportional to the total current $I$, now ensures the possibility of spontaneous current without e.m.f. in a manner analogous with the way in which Stoner's spin exchange energy, proportional to magnetization, ensures spontaneous magnetization without magnetizing field.

Thus, from Boltzmann's equation in the form

$$(f - f_0)/\tau = (e\epsilon u \pm e\gamma u^2 I)\partial f/\partial E, \tag{6}$$

it is easy to show that

$$I = \epsilon/(R - \gamma\bar{u}), \tag{7}$$

where $R$ is the ideal resistance, $\bar{u}$ the Fermi velocity.

When the normal temperature dependence of $R$ carries it down to the value of $\gamma\bar{u}$ it is clear that the effective resistance will vanish. The value of $\gamma$ required to account for actual data is of the order

$$10^{-12} \text{ cm}^{-3} \text{ sec.}^2$$

For normal current densities, this gives roughly $10^{-15}$ erg for the magnetic energy of an electron over its time of relaxation.

[1] J. Frenkel, Phys. Rev. 43, 907 (1933).
[2] H. Bethe and H. Fröhlich, Zeits. f. Physik 85, 389 (1933).

## Diamagnetism and Superconductivity

WILLIAM BAND
*Yenching University, Peiping, China*
January 23, 1946

LET the magnetic energy between electron currents in a conductor be assumed such that the mean contribution per electron is proportional to the product of the total current within a defined range and the speed of the electron in the direction of the total current: then the ideal resistance of a conductor can be neutralized at sufficiently low temperatures.[1]

Let the surface of the conductor, and internal surfaces of discontinuity if sufficiently marked, be regarded as sites for two-dimensional resonance states in equilibrium with the ordinary three-dimensional resonance states in the metal. Then the superconducting transition occurs when, at the critical temperature, the neutralization of the ideal resistance of these surfaces by-passes the residual resistance of the body of the metal.

At the same critical temperature, statistical equilibrium ensures that exactly the right number of electrons enter the surface states to give the whole metal an ideal diamagnetic susceptibility. These equilibrium conditions are disturbed by a magnetic field, and the transition temperature is shown to depend on the magnetic field in the observed manner.[2]

The "intermediate state" is explained as one in which the number of electrons in the superconducting surface states is constrained by a non-uniform resultant magnetic field to remain at an intermediate value which is inadequate to produce ideal diamagnetism.

The theory is statistically, and, therefore, thermodynamically, satisfactory, but the model needs a more rigorous justification by quantum mechanics for its basic assumptions.

[1] W. Band, "Superconductivity and magnetic energy between currents," Phys. Rev. 69, 241 (1946).
[2] Article under same title as this letter appearing shortly in Proc. Camb. Phil. Soc.

## The Albedo of Thermal Neutrons

MARIO AGENO
*Roma—Istituto di fisica della Università—Centro di fisica nucleare del C.N.R., Rome, Italy*
January 1, 1946

ARLEY has shown[1] that the scattering process of slow neutrons in paraffin can be represented by a scattering probability in the solid angle sen $\vartheta\, d\vartheta d\varphi$ equal to:

$$(d\varphi/4\pi)(1 + a\cos\vartheta)\sin\vartheta d\vartheta,$$

where $\vartheta$ is the angle between neutron velocities before and after the collision and $a \approx 0.4$. As G. C. Wick pointed out,[2]

it may be of some interest to see how the expression:[3]

$$\alpha=\rho(\infty)/\rho(0)=(N+1)^{\frac{1}{2}}+1 \qquad (1)$$

of the ratio of neutron densities on the border and inside a paraffin half-space, must be changed in order to take into account Arley's results. ($N=\sigma_s/\sigma_a$ is the ratio of scattering and absorption cross sections and $\alpha$ is connected with the albedo $\beta$ by the expression: $\alpha=2/(1-\beta)$.)

The diffusion equation (unidimensional) is then:

$$u\frac{\partial}{\partial x}f(x,u)+f(x,u)=\frac{\sigma}{2}\int_{-1}^{+1}f(x,v)dv + \frac{\sigma a}{2}u\int_{-1}^{+1}vf(x,v)dv+q(x), \qquad (2)$$

where ($a$) $u=\cos\vartheta$ is the $x$ component of neutron velocity, which we assume to remain constant, ($b$) the mean free path is assumed equal to one, and ($c$) $\sigma=\sigma_s/(\sigma_a+\sigma_s)=N/(N+1)$. $q(x)$ is a term representing the production of slow neutrons.

We can solve (2) with the same approximation method employed by Wick[2] in the case $a=0$, which consists in substituting Eq. (2) with a set of linear differential equations:

$$u_i\frac{\partial}{\partial x}f(x,u_i)+f(x,u_i)=\frac{\sigma}{2}\sum_{-n}^{+n}p_kf(x,u_k) + \frac{\sigma a}{2}u_i\sum_{-n}^{+n}p_ku_kf(x,u_k)+q(x), \qquad (i=-n,\,-n+1,\,\cdots -1,\,+1,\,\cdots n)$$

where the $u_i$ and $p_i$ are so chosen as to make:

$$\sum_{-n}^{+n}p_kf(x,u_k)\approx\int_{-1}^{+1}f(x,v)dv, \qquad \sum_{-n}^{+n}p_ku_kf(x,u_k)\approx\int_{-1}^{+1}vf(x,v)dv.$$

In order to calculate the ratio $\rho(\infty)/\rho(0)$, we must assume Eq. (2) to be valid for: $0<x<+\infty$, and put: $q(x)=$const., with the boundary conditions:

$f(0,u)=0$ if: $0<u\leq 1$, $f(x,u)$ bounded as $x\to+\infty$.

The solution is:

$$f(x,u_i)=\frac{q}{1-\sigma}+\Sigma_rL_r\frac{1+\dfrac{(1-\sigma)a}{k_r}}{1-k_ru_i}e^{-k_rx}$$

and:

$$\frac{\rho(\infty)}{\rho(0)}=\left\{1+\frac{1-\sigma}{q\sigma}\Sigma_rL_r\right\}^{-1}. \qquad (3)$$

The $k_r$ are the $2n$ significant solutions of:

$$1=\frac{\sigma}{2}\frac{k^2+a(1-\sigma)}{k^2+a\sigma(1-\sigma)}\Sigma_j\frac{p_j}{1-ku_j},$$

and the $L_r$ are to be determined by the boundary conditions. Here we can avoid troublesome calculations by introducing the polynomials:

$$P(u)=\prod_1^n{}_s(u-u_s) \qquad R(u)=\prod_1^n{}_s(1-k_su),$$

and we can write (3) in the more convenient form:

$$\frac{\rho(\infty)}{\rho(0)}=(-1)^n\frac{2u_1u_2\cdots u_n}{(1-\sigma)Z}-\frac{\sigma}{1-\sigma} \qquad Z=\sum_1^n{}_ip_i\frac{P(-u_i)}{R(-u_i)}.$$

Wick has shown that in the case $a=0$ a very good approximation is attained assuming as $u_i$ the roots of the sixth Legendre polynomial. With the same assumption we find now:

$$\alpha=\frac{\rho(\infty)}{\rho(0)}=(N)^{\frac{1}{2}}\left\{0.577(3-a)^{\frac{1}{2}}+(1+0.073a)\frac{1}{(N)^{\frac{1}{2}}} +(0.866-0.118a+0.039a^2)(3-a)^{-\frac{1}{2}}\frac{1}{N}+\cdots\right\}.$$

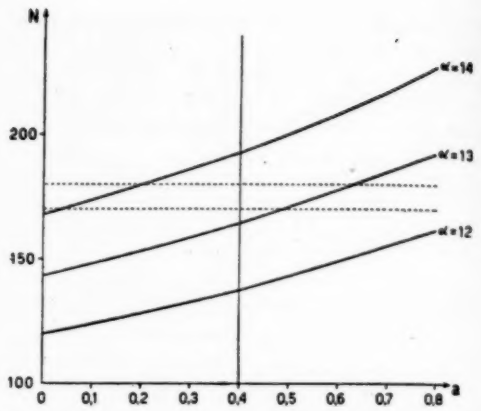


FIG. 1. Average number of free path covered by a thermal neutron, as a function of the anisotropy of the scattering by bounded protons, for several values of the albedo coefficient $\alpha$.

In Fig. 1, $N$ is plotted as a function of $a$ for different values of $\alpha$. The vertical straight line at $a=0.4$ represents Arley's value. Cross-section measurements[4] give for $N$ a value $170\div180$, which falls between the two dotted lines of Fig. 1. From the graph one would expect a value of $\alpha\sim13.5$. The well-known experimental data are not accurate enough to confirm Arley's result.

More detailed calculations will appear in *Il nuovo Cimento*.

[1] N. Arley, Kgl. Danske Vid. Sels. Math.-Fys. Medd **16**, 1 (1938).
[2] G. C. Wick, Zeits. f. Physik **121**, 702 (1943). See also: G. Placzek, Phys. Rev. **60**, 166 (1941).
[3] E. A. Schuchard and E. A. Uehling, Phys. Rev. **58**, 611 (1940).
[4] Goldhaber and Briggs, Proc. Roy. Soc. **A162**, 127 (1937); C. P. Baker and R. F. Bacher, Phys. Rev. **59**, 332 (1941); H. Carroll, Phys. Rev. **60**, 702 (1941); J. H. Manley, L. J. Haworth and E. A. Luebke, Phys. Rev. **61**, 152 (1942).

## The Heat of Vaporization of Helium II Below 1.5°K

J. E. HAGGENMACHER
*Commonwealth Color and Chemical Company, Brooklyn, New York*
February 12, 1946

THE behavior of saturated fluids, when reported on rectangular $p$, $v$, $T$ coordinates, is confined to the line of saturation and may be represented by the equation[1]

$$p=\frac{RT}{v+B}-\frac{A}{T(v+B)^3}, \qquad (1)$$

where $p$, $v$, $T$, are, respectively, the pressure, the volume per mole, and the temperature of the fluid under saturated conditions. $A$ and $B$ are constants, and $R$ is the universal gas constant.

Denoting the roots of the quadratic Eq. (1) by $v_g$ and $v_l$,

TABLE I. $L$ (g-cal./mole) Comparison of results of present theory with those of Bleaney and Simon.

| Temp. °K | Bleaney Simon | Eq. (7) |
|---|---|---|
| 1.4 | — | 20.49 |
| 1.2 | — | 19.98 |
| 1.0 | 19.18 | 19.13 |
| 0.8 | 18.21 | 18.21 |
| 0.6 | 17.22 | 17.24 |
| 0.4 | 16.23 | 16.24 |
| 0.2 | 15.24 | 15.25 |
| 0.1 | 14.75 | 14.75 |
| 0.01 | 14.31 | 14.31 |
| 0.00 | 14.26 | 14.257 |

which, respectively, are the vapor volume and the liquid volume of the saturated fluid, we get for the difference of the roots

$$v_g - v_l = \left[\left(\frac{RT}{2p}\right)^2 - \frac{A}{pT}\right]^{\frac{1}{2}}. \tag{2}$$

The constant $A$ is evaluated from Eq. (2), noting that at the critical point, $v_g - v_l = 0$.

Thus

$$A = R^2 T_c^3 / 4 p_c.$$

Subscripts $c$ indicate critical values.

Then

$$v_g - v_l = \frac{R}{p}\left(T^2 - \frac{Dp}{T}\right)^{\frac{1}{2}} \quad \text{where} \quad D = \frac{T_c^3}{p_c}. \tag{3}$$

From the Clapeyron-Clausius equation,

$$L = dp/dT(v_g - v_l),$$

and Eq. (3) we obtain for the heat of vaporization, per mole

$$L = R\frac{dp}{dT}\frac{T}{p}\left(T^2 - \frac{Dp}{T}\right)^{\frac{1}{2}}. \tag{4}$$

The vapor pressure of saturated helium II, below 1.5°K, is given by the expression[2]

$$\log p_{\text{atmos}} = -\frac{3.117}{T} + 2.5 \log T - 0.6848. \tag{5}$$

Then

$$\frac{dp}{dT} = \left(\frac{7.1775}{T} + 2.5\right)\frac{p}{T}. \tag{6}$$

Taking $p$ in atmos., $T$ in °K, ice point = 273.16°K, $p_c = 2.261$ atmos., $T_c = 5.25$°K, $R = 0.08206$, and 1 liter-atmos. = 24.206 g-cal.; we obtain for Eq. (4)

$$L = \left(\frac{14.257}{T} + 4.9659\right)\left(T^2 - \frac{Dp}{T}\right)^{\frac{1}{2}}. \tag{7}$$

Below 0.6°K, since $T \gg Dp/T$, Eq. (7) reduces to

$$L = 14.257 + 4.966T. \tag{8}$$

Bleaney and Simon[3] have calculated the heat of vaporization of helium, up to 1°K, from entropy considerations. Their values and the figures given by Eq. (7) are compared in Table I.

[1] J. E. Haggenmacher, J. Am. Chem. Soc. 66, 313 (1944).
[2] Burton, Smith, and Wilhelm, *Phenomena at the Temperature of Liquid Helium* (Reinhold Publishing Corporation, New York, 1940), p. 69.
[3] Bleaney and Simon, Trans. Faraday Soc. 35, 1205 (1939).

## Bose-Einstein Condensation of Trapped Electron Pairs. Phase Separation and Superconductivity of Metal-Ammonia Solutions

RICHARD A. OGG, JR.
*Department of Chemistry, Stanford University, California*
March 2, 1946

WITH the invaluable assistance of Drs. Claudio Alvarez-Tostado and William Perkins, the previously reported[1] studies of the behavior resulting from rapid freezing of very dilute solutions of alkali metals in liquid ammonia have been extended (in the case of sodium solutions) over the entire concentration range, up to the saturation point. Sufficiently rapid cooling to temperatures in the range from −90°C to −180°C resulted in the production of apparently homogeneous deep-blue solid solutions, of bronze-like luster when extremely concentrated. All of the solid samples proved to be good electrical conductors, although shrinkage and cracking frequently caused erratic measurements. No abnormal resistance change accompanying solidification was observed, except for solutions in the concentration range (of the order of one molar) characterized by the remarkable phenomenon of separation into two dilute liquid phases[2] at sufficiently low temperatures. Extremely rapid freezing of such solutions (initially at −33°C, i.e., above the upper consolute temperature) caused a relatively enormous decrease of measured resistance. In a representative case, the resistance of the liquid sample at −33°C was some 10,000 ohms, while that of the solid at −95°C was only 16 ohms. Variation of conditions suggested that even such small residual resistances might be due to "end effects" and faulty contact with the platinum electrodes. That the solutions in this special concentration range actually became superconducting was demonstrated by adaptation of the classical Kammerlingh Onnes "ring experiment." Thin-walled glass cells having the shape of an annular disk were filled with the proper solution at −33°C and then rapidly plunged into a vessel of liquid air between the poles of an electromagnet (field strength some 1500 gauss). After removal from the magnetic field, the existence of persistent currents was shown by tests with a sensitive magnetometer. Numerous control experiments obviated any other possible explanation. The magnetometer tests were conducted at −180°C, but intervening warming of the ring samples to much higher temperatures did not destroy the persistent currents. In all probability such solid solutions remain superconducting up to the melting point, i.e., to absolute temperatures of the order of 180 to 190 degrees.

The probable explanation of the above phenomena is to be found in the behavior of trapped electron pairs, recently demonstrated[3] to be a stable constituent of fairly dilute metal-ammonia solutions. In the concentration range characterized by liquid-liquid phase separation, experimental studies[4] show the solute to be diamagnetic at temperatures just above the consolute point. This suggests the electron constituent to be almost exclusively in the trapped electron pair configuration. Because of their

zero angular momentum, such pairs must obey Bose-Einstein statistics. If the effective mass does not exceed twice the electron mass by an extremely large factor, then the calculated degeneration temperature[5] at the concentrations in question is relatively high—of the order of a few hundred degrees absolute. It is postulated that the liquid-liquid phase separation which occurs on slow cooling (upper consolute temperature 232°K) is the device adopted by the systems to avoid the Bose-Einstein condensation, with its unfavorable free energy change. In the more dilute phase the electron constituent is still predominantly the trapped pair, but at a concentration low enough to raise the degeneracy temperature to just above the prevailing temperature. In the more concentrated phase, the trapped electron pairs have become unstable because of the greater interionic forces, and one has essentially a liquid metal, the trapped single electrons being below the Fermi-Dirac degeneration temperature. The small, temperature independent paramagnetism[4] of very concentrated solutions would appear to support this latter model.

By sufficiently rapid cooling, it appears that the liquid-liquid phase separation is prevented, and that the system becomes frozen and hence metastable in the "forbidden" concentration region, which is thus characterized by the Bose-Einstein condensation of trapped electron pairs. From the discussion of London,[5] apparently such a state must display the phenomenon of electrical superconductivity, in agreement with the above experimental observations.

The extension of the above model to explain previously observed superconductivity is apparent, and is the more plausible in view of the essentially only quasi-metallic character of the large number of alloys and compounds which display the phenomenon.[6]

[1] R. A. Ogg, Jr., J. Chem. Phys. 13, 533 (1945).
[2] For literature references, see W. C. Johnson and A. W. Meyer, Chem. Rev. 8, 273 (1931).
[3] R. A. Ogg, Jr., J. Chem. Phys. 14, 114 (1946).
[4] E. Huster, Ann. d. Physik [5], 33, 477 (1938); S. Freed and N. Sugarman, J. Chem. Phys. 11, 354 (1943).
[5] F. London, Phys. Rev. 54, 947 (1938).
[6] H. G. Smith and J. V. Wilhelm, Rev. Mod. Phys. 7, 237 (1935).

## Concerning Some New Methods of Acceleration of Relativistic Particles

V. VEKSLER
*Lebedev Physical Institute of the Academy of Sciences, Moscow, U.S.S.R.*
February 16, 1946

IN two papers[1,2] appearing in 1944 under the above title the author of the present letter pointed out two new principles of acceleration of relativistic particles which generalize the resonance method.

New possibilities for the resonance acceleration of particles in a constant magnetic field are described in the first of these papers, and the possibility of resonance acceleration in magnetic fields which increase with time is also noted.

This latter case is specially examined in the second paper. It is shown that phase stability automatically sets in if the time variation of the field is sufficiently small; relation between the amplitude of the variable electric fields and the rate of variation of the magnetic field is established.

It is also pointed out that the radiation losses in such acceleration do not violate phasing mechanism. Finally in a detailed paper[3] an accelerator of heavy particles based on a variation in frequency is analyzed.

Thus the foregoing papers cover completely the contents of the note by McMillan[4] in which no reference is made to my investigations.

Construction of a 30-Mev accelerator with varying magnetic field is now nearing completion at the Physical Institute of the Academy of Sciences, U.S.S.R.

[1] V. Veksler, Comptes Rendus (Doklady), Acad. Sci. U.S.S.R. 43, No. 8, 444 IX (1944) (communicated April 25, 1944).
[2] V. Veksler, Comptes Rendus (Doklady), Acad. Sci. U.S.S.R. 44, No. 9, 393 (1944) (communicated July 19, 1944).
[3] V. Veksler, J. Phys. (U.S.S.R.) 9, No. 3, 153 (1945) (received March 1, 1945).
[4] E. McMillan, Phys. Rev. 68, 143 (1945).

## Erratum: A Method for Measuring Effective Contact e.m.f. between a Metal and a Semi-Conductor

W. E. STEPHENS, B. SERIN, AND W. E. MYERHOF
*Randal Morgan Laboratory of Physics, University of Pennsylvania Philadelphia, Pennsylvania*
[Phys. Rev. 69, 42 (1946)]

UNFORTUNATELY Fig. 1 which should have appeared with the above Letter to the Editor was omitted. It is reproduced here.

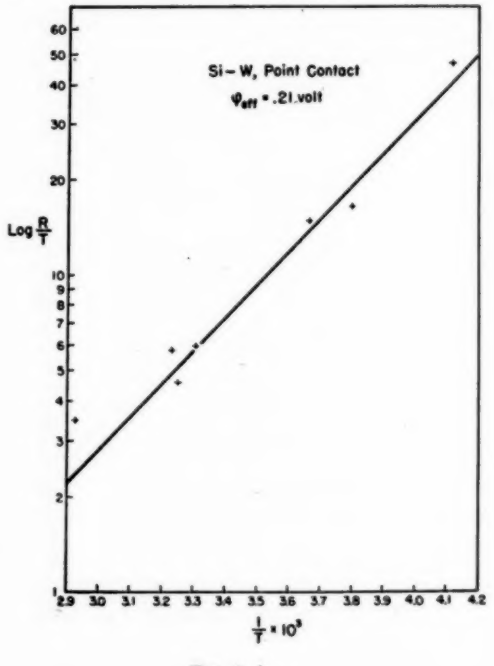


FIG. 1

## Spectrum of High Frequency Discharge in Air in Relation to Active Nitrogen

N. R. TAWDE AND G. K. MEHTA
*Royal Institute of Science, University of Bombay, Bombay, India*
February 16, 1946

HAYES, Winans, and Culp[1] have recently reported some interesting observations on the effect of the excitation frequency on the spectra of gaseous discharges. The spectrum of commercial argon-filled bulbs at lower frequencies (50 c) mainly consisted of the violet second positive bands of nitrogen, and at higher frequencies (10 mc) the first positive bands were found with high intensity giving the discharge an orange color. This effect could not be noticed in tubes containing pure nitrogen. Similar results[2] were obtained in these laboratories while working with high frequency discharge in air at frequencies ranging from 5 to 15 mc. The relative changes in intensities of the two band systems of nitrogen which are responsible for the change in color of the discharge could be obtained by changing any one of the three parameters, i.e., the pressure, frequency, and voltage of excitation. This clearly shows that the intensity changes are the consequences of the change in velocity of the exciting electrons with change in any discharge parameter. The quantitative spectroscopic study of these intensity changes in air has been done by Asundi and J. Singh[3] where they have also observed a relative intensity change in the two band systems of nitrogen with the change in excitation frequency. According to Brasefield's[4] simplified picture of the h.f. discharge, an increase in the excitation frequency will result in a decrease in the electron velocity which will facilitate the production of spectra requiring smaller excitation energy, i.e., the first positive band system. A detailed study of the variations of the electron velocities with the other parameters of the discharge is in progress in these laboratories and the results will be communicated soon.

The absence of the phenomenon of change of intensity with the change in the frequency of excitation in pure nitrogen can be explained by the results of Tawde and Patankar[5] derived from altogether independent spectral study. They have investigated the rôle of impurities particularly of the rare gases like argon in the spectra of nitrogen by quantitative intensity measurements. Their study is confined to the comparison of the intensity distribution in the nitrogen molecular spectra obtained from (1) discharge in air and (2) in pure nitrogen, under identical conditions. It was found that the nitrogen spectra in air, i.e., the first positive and the second positive band systems are very much susceptible to relative changes in intensities as compared to those in pure nitrogen. This may be attributed to the production of active nitrogen under the influence of argon, the major rare gas constituent of air. The exact role played by foreign gases is still a matter in dispute, but in the light of the observations in the h.f. discharge and the results of Tawde and Patankar,[5] it appears that the foreign gas acts in such a way as to accelerate the formation of excited molecules or to retard the rapid reversion of active nitrogen. This may be taken as an evidence for the possible presence of active nitrogen in the h.f. discharge in air.

[1] K. J. Hayes, J. G. Winans, and W. Culp, Phys. Rev. **68**, 98 (1945).
[2] N. R. Tawde and G. K. Mehta, Proc. Ind. Acad. (to be published).
[3] Asundi and J. Singh, Proc. Ind. Acad. Sci. **22**, 60 (1945).
[4] C. J. Brasefield, Phys. Rev. **35**, 92 (1930).
[5] N. R. Tawde and V. S. Patankar, Phil. Mag. **35**, 616 (1944).

# Proceedings of the American Physical Society

## 1945 Annual Meeting at New York, January 24–26, 1946

THE 270th meeting of the American Physical Society, being the 1945 Annual Meeting, was held at Columbia University in New York City on Thursday, Friday, and Saturday, January 24–26, 1946, in conjunction with a meeting of the American Association of Physics Teachers. This was a meeting of unforeseen and unprecedented size, outranking by far in attendance the most populous of the Washington meetings of old. Of 1293 who registered, 911 gave themselves as members of the American Physical Society, and an undetermined fraction of the rest were members of both the Society and the Association. The halls of the scientific sessions were often overfilled and sometimes crowded to such an extent that many would-be listeners were excluded; one session was repeated in its entirety, also an event without precedent. All the available rooms of the capacious Mens' Faculty Club were bespoken for the dinner, yet a third of those who applied had to be turned away. This plethora of visitors, welcome sign as it is that the restrictions of the war are largely past, is a source of foreboding for the meetings of the future, and augurs a change in their character not altogether agreeable. The unexpected burdens were nobly borne by the Local Committee, composed of H. W. Farwell, W. W. Havens, J. E. Nafe, and B. A. Wooten, and ably assisted by Miss Margaret Griffin and other members of the staff of the American Institute of Physics.

President Harvey Fletcher gave his Retiring Presidential Address, and P. E. Klopsteg delivered the fifth Richtmyer Memorial Lecture of the AAPT. H. A. Bethe and A. H. Compton were joined by James T. Shotwell of the Carnegie Endowment for International Peace in a symposium "Nuclear Energy" ranging from the scientific to the national and international aspects of this timely topic. M. H. Trytten and E. U. Condon spoke on "Physics in National Affairs" under the auspices of the AAPT. Invited papers were given by Gleb Wataghin and by Marcel Schein, G. S. Klaiber, A. J. Hartzler, and D. C. Baldwin, the last four composing the group under the title "Nuclear Transformations Produced by High Energy X-Rays" which, describing as it did a break-through into a new field of experimental physics, was justly honored by an encore to accommodate the many people who could not force their way into the largest hall of the Pupin Laboratories. The Division of Electron and Ion Optics had ten invited papers, the Division of High Polymer Physics had twenty-six. The titles of all these speeches will be found below. Fifty-two ten-minute papers were contributed; the abstracts follow.

At the Business Meeting of the Society, the election of the following officers was disclosed by the report of the tellers: President, E. U. Condon; Vice President, L. A. DuBridge; Secretary, K. K. Darrow; Treasurer, G. B. Pegram; Councillors, J. A. Bearden and G. E. Uhlenbeck (term 1946–1949); Members of the Board of Editors, E. C. Konopinski, H. H. Nielsen, E. C. Pollard (term 1946–1948). J. T. Tate has resumed the Editorship after leave of absence for war work. J. W. Buchta, to whose able management of its journals during the war years the Society has great reason to be thankful, becomes Assistant Editor. L. P. Smith becomes Chairman of the Division of Electron and Ion Optics, J. B. Fisk succeeds him as Vice-Chairman. J. R. Pierce is re-elected as Secretary-Treasurer, A. J. Dempster remains on the Executive Committee and A. O. Nier enters upon it. H. A. Robinson becomes Chairman and S. L. Gerhard Vice-Chairman of the Division of High Polymer Physics; W. J. Lyons continues as Secretary and L. A. Wood as Treasurer; R. B. Barnes, W. F. Busse, and J. H. Dillon remain on the Executive Committee.

The dinner of the Society and of the Association was held on the Friday evening at the Mens' Faculty Club, and those whose places were in the main dining room heard short addresses by Harvey Fletcher, E. U. Condon, and R. C. Gibbs before the early adjournment customary at the New York dinners.

The Council, meeting on January 24, elected four candidates to Fellowship and one hundred and seventy-eight to Membership; their names are appended.

*Elected to Fellowship:*

H. L. Andrews, Louis Goldstein, E. J. Schremp, and Samuel Silver.

*Elected to Membership:*

Turner Alfrey, Jr., Harold V. Argo, William A. Arnold, Martin J. Arvin, Sidney Austin, Peter Axel, Hans George Baerwald, Paul H. Baldwin, Ralph B. Baldwin, Ferdinand P. Beer, Persa Raymond Bell, Jr., Floyd Mitchell Bennett, Jr., Paula Berger, Bernard Berkowitz, Seymour Bernstein, Howard W. Boehmer, Robert W. Bogle, Lowell M. Bollinger, Ralph Bown, Henry G. Brewer, Jr., Wesley E. Brittin, Bernard B. Brody, Harold Brown, Cornelius P. Browne, Walter V. Burg, Elias Burnstein, Blendin L. Burton, L. W. Butler, Kenneth M. Case, Geoffrey F. Chew, S. M. Christian, Melville Clark, Jr., J. Reid Clement, Solly G. Cohen, Norman Clark Colby, Eugene F. Coleman, Paul Dare Coleman, John W. Cook, L. E. Copeland, Clifton Bernard Cosby, Prescott D. Crout, Westley Farnsworth Curtis, Perry W. Davison, William Dashifsky, David B. Davis, W. Bruce Dayton, P. J. G. deVos, Laura Diehl, Robert E. Dillon, Carl E. Drumheller, Murray Ellis, B. G. Farley, William C. Farmer, Daniel B. Feer, Frederick W. Fenning, Lester M. Field, Francis George Firth, Robert C. Fletcher, Samuel N. Foner, Earl W. Ford, Victor Hugo Fraenckel, George K. Fraenkel, Katherine L. Franck, Sherman Frankel, Wolfgang Franzen, George D. Freier, David L. Fry, Chester R. Fultz, F. J. Gaffney, Irving G. Geib, Kenneth D. George, David Gilbarg, Norman Goldstein, Serge Golian, William Edwin Gordon, Elizabeth R. Graves, Richard F. Greene, Wm. G. Griffin, Jr., James E. Hacke, Raymond M. Hainer, Jay M. Hansen, Walter J. Haring, Charles W. Harris, Hiram E. Hart, John C. Hart, Paul L. Hartman, Donald E. Hartvigsen, Emmi Hauser, Fred Brown Haynes, H. M. Herreman, Erna M. J. Herrey, Claude Richard Hocott, Herman W. Hoerlin, G. Robert Hoke, Jean E. Hoopes, John J. Hopkins, Maynard H. Hunt, Irvien B. Irving, Herman Jarrell, Wilbur Kaye, Chris P. Keim, Walter H. Kohl, Walter S. Koski, Ernst Henry Krause, Norman M. Kroll, Thomas Samuel Kuhn, Dhirendra Nath Kundu, Jack Hershel Lepoff, Werner Leszynski, Seymour A. Lippmann, John A. Lockwood, Lawrence W. Lockwood, John F. Marshall, Lucien Martelli, Albert E. Martin, Jr., Harry Mason, R. L. McCarthy, Robert A. McConnell, James S. McCorkle, Walter C. McCrone, John Joseph Gerald McCue, Brunson S. McCutchen, John McElhinney, John C. Mead, Alfred W. Meyer, John A. Miskel, Joseph Frederick Mullaney, Harold Peter Myers, Joseph Alfred Neuendorffer, Leonard William Niedrach, H. Nordsieck, William C. Parkinson, Robert Erle Payne, George D. M. Peeler, Frederick T. Peirce, Robert T. Phelps, Eric Pickup, John L. Powell, Rene J. Prestwood, George T. Rado, John Rehner, Jr., T. Doman Roberts, Charles Vernon Robinson, J. Robert Rogers, Herbert Ruderfer, Donovan J. Salley, Fred H. Schmidt, Roderic M. Scott, Elwood F. Seasholtz, Montford W. Smith, Louis D. Smullin, Wilmer H. Souder, Robert Franz Stamm, Rudolph Max Sternheimer, John Willard Stout Jr., Martin Jay Swetnick, Benjamin Tannenbaum, John Torrence Tate, Jr., Robert H. Thayer, Hsue-shen Tsien, Anne Axon Unger, B. H. Van Horne, Thomas B. Van Poole, Jr., John J. Wagner, Robert Lee Walker, William Edward Waller, John Bernard Warren, Wallace Waterfall, Nelson Wax, Robert T. Webber, J. Weber, David V. P. Williams, R. B. Windsor, Jules I. Wittebort, Paul F. Yergin, Elmer L. Younker, James Henry Young, and Luke Chia-Liu Yuan.

Reports reaching the office of the Society indicate that we have lost through death since the previous meeting the following Fellows and Members: Harry Bateman (F, California Institute of Technology); A. A. Bacon (retired); A. E. Flowers (deLaval Company); Walker Kincaid (Georgia Institute of Technology); H. N. McCoy (F, retired); L. M. Potts, (F, retired).

KARL K. DARROW, *Secretary*
American Physical Society
Columbia University
New York 27, New York

## Retiring Presidential Address of the American Physical Society

**"The Pitch, Loudness and Quality of Musical Tones." (Demonstration Lecture introducing the new Tone-Synthesizer.)** HARVEY FLETCHER, *Bell Telephone Laboratories.*

## Fifth Richtmyer Memorial Lecture of the American Association of Physics Teachers

**"Technological Research in the University."** P. E. KLOPSTEG, *Northwestern University Technological Institute.*

### Nuclear Energy

**Scientific Aspects.** H. A. BETHE, *Cornell University.* (30 min.)

**Social Implications.** A. H. COMPTON, *Washington University.* (30 min.)

**International Implications.** JAMES T. SHOTWELL, *Carnegie Endowment for International Peace.*

### Invited paper

**Statistical Mechanics at High Temperatures and Showers of Penetrating Particles.** GLEB WATAGHIN, *University of São Paulo.*

### Nuclear Transformations Produced by High Energy X-Rays

**Artificial Production of Mesons by X-Rays from a 100-Mev Induction Accelerator.** MARCEL SCHEIN, *General Electric Company and University of Chicago.*

**Ionization-Chamber and Cloud-Chamber Studies of Nuclear Processes Induced by High Energy X-Rays.** G. S. KLAIBER, *General Electric Company.*

**Cloud-Chamber Studies of Artificially-Produced Particles of Intermediate Mass.** A. J. HARTZLER, *General Electric Company.*

**New Types of Photo-Nuclear Reaction.** D. C. BALDWIN, *General Electric Company.*

## *Division of Electron and Ion Optics*

### Symposium on Oxide Coated Cathodes

**Recent Published Work on Oxide Coated Cathodes.** J. P. BLEWETT, *General Electric Company.*

**The Experimental Basis for Present Theories of the Oxide Coated Cathode.** G. E. MOORE, *Bell Telephone Laboratories.*

**Some Chemical Studies of Oxide Coated Cathodes.** L. A. WOOTEN, *Bell Telephone Laboratories.*

**The Pulsed Properties of Oxide Coated Cathodes.** E. A. COOMES, *University of Notre Dame.*

**Studies of the Interface of Oxide Coated Cathodes.** A. FINEMAN, *Radiation Laboratory, Massachusetts Institute of Technology.*

**The Study of Oxide Coated Cathodes by X-Ray Diffraction Methods.** A. S. EISENSTEIN, *Radiation Laboratory, Massachusetts Institute of Technology.*

**Effect of Composition of Coating of Oxide Coated Cathodes.** E. G. WIDELL, *Radio Corporation of America.*

**Poisoning Troubles and Their Cures in Vacuum Tubes.** B. R. CORSON, *Hytron Corporation.*

**Cataphoretic Coating of Emissive Material.** J. CARDELL, *Raytheon Manufacturing Company.*

**Sparking of Oxide Coated Cathodes in Inert Gases.** J. W. MCNALL, *Westinghouse Electric Corporation.*

## *Division of High-Polymer Physics*

**Thermal Diffusion of Polymers.** P. DEBYE, *Cornell University.*

**X-Ray Diffraction by Potassium Laurate Solutions (A Contribution to the Mechanism of Emulsion Polymerization).** E. W. HUGHES, *Shell Development Company.*

**The Use of Color and Fluorescence Indicators for Studying the Constitution of Glasses.** W. A. WEYL, *Glass Science, Inc., State College, Pennsylvania.*

**The Mechanical Properties of Fibers.** HENRY EYRING AND GEORGE HALSEY, *Textile Research Institute Laboratories, Princeton, New Jersey.*

**Stress-Relaxation of Compressed Cork.** S. L. DART AND EUGENE GUTH, *University of Notre Dame.*

**The Formation of Ionized Water Films on Dielectrics under Conditions of High Humidity.** ROBERT W. FIELD, *General Radio Company.*

**The Molecular Structure of Some Polyuronides as Revealed by X-Ray Diffraction Studies.** K. J. PALMER, *Western Regional Research Laboratory.*

**Statistics of Cross Linked Polymers.** WALTER H. STOCKMAYER, *Massachusetts Institute of Technology.*

**Thermal Polymerization of Drying Oils.** H. E. ADAMS AND P. O. POWERS, *Armstrong Cork Company.*

**Some Thermodynamic Properties of Slightly Cross-Linked Gels.** R. F. BOYER AND R. S. SPENCER, *The Dow Chemical Company.*

**The Determination of Polymer-Liquid Interaction by Swelling Measurements.** PAUL DOTY AND HELEN S. ZABLE, *Polytechnic Institute of Brooklyn.*

**Electrostatic and Tensile Properties of Rubber and GR-S at Elevated Temperatures.** R. S. HAVENHILL, H. C. O'BRIEN AND J. J. RANKIN, *St. Joseph Lead Company.*

**Significance of the Stress-Temperature Relationships for Rubber.** PAUL E. WACK, R. L. ANTHONY AND EUGENE GUTH, *University of Notre Dame.*

**The Theory of Permanent Set at Elevated Temperatures in Natural and Synthetic Rubber Vulcanizates.** R. D. ANDREWS, E. E. HANSON AND A. V. TOBOLSKY, *Princeton University and Firestone Tire and Rubber Company.*

**The Crystallization of Unvulcanized Rubber at Different Temperatures.** LAWRENCE A. WOOD AND NORMAN BEKKEDAHL, *National Bureau of Standards.*

**Tackiness of GR-S and Other Elastomers.** W. F. BUSSE, J. M. LAMBERT, AND R. B. VERDERY, *General Aniline and Film Corporation.*

**Stress-Time-Temperature Relations in Polysulfide Rubbers.** M. D. STERN AND A. V. TOBOLSKY, *Princeton University.*

**Application of Infra-Red Methods in the Structural Examination of Synthetic Rubber.** J. E. FIELD, D. E. WOODFORD, AND S. D. GEHMAN, *The Goodyear Tire and Rubber Company.*

**Viscometric Investigation of Dimethyl Siloxane Polymers.** ARTHUR J. BARRY, *Dow-Corning Corporation.*

**Some Fundamental Relationships between Intrinsic Viscosity, Diffusion and Sedimentation Constants, and Thermodynamic Properties of High Polymer Solutions.** ROBERT SIMHA, *National Bureau of Standards.*

**Thin Section Methods for the Electron Microscopic Examination of Cured Polymers.** H. C. O'BRIEN, *St. Joseph Lead Company.*

**Attachment for Obtaining Angular Distribution of Scattered Light from Measurements with a Ninety-Degree Turbidimeter.** J. N. WILSON, *Shell Development Company.*

**A Photoelectric Light Scattering Instrument and a Differential Refractometer for Measuring Molecular Weights.** P. P. DEBYE, *General Aniline and Film Corporation.*

**Thermal Expansion and Second-Order Transition Effects in High Polymers. III. Time Effects.** R. S. SPENCER AND R. F. BOYER, *The Dow Chemical Company.*

**A New Approach to the Theory of Relaxing Polymeric Media.** M. S. GREEN AND A. V. TOBOLSKY, *Princeton University.*

**Application of Molecular Distribution Methods to the Statistical Mechanisms of High Polymer Solutions.** BRUNO H. ZIMM, *Polytechnic Institute of Brooklyn.*

## *Symposium of the AAPT*

## Physics and the Nation

**Physicists in National Affairs.** M. H. TRYTTEN, *Office of Scientific Personnel.*
**Federal Support of Science.** E. U. CONDON, *National Bureau of Standards.*

## ABSTRACTS OF CONTRIBUTED PAPERS

**A1. A Solution of the Equation for the Propagation of Waves of Finite Amplitude in One Dimension.** JOHN M. RICHARDSON AND WILLIAM SHOCKLEY, *Bell Telephone Laboratories, Inc.*—The one-dimensional motion of a volume of gas initially at a uniform pressure $p_0$ and density $\rho_0$ is given by

$$\frac{\partial^2 x}{\partial t^2}-\frac{\gamma p_0}{\rho_0}\left(\frac{\partial x}{\partial x_0}\right)^{-\gamma-1}\frac{\partial^2 x}{\partial x_0^2}=0,$$

when vanishing thermal conductivity and the adiabatic law $p=p_0(\rho/\rho_0)^\gamma$ are assumed and $x$, $p$, and $\rho$ are at time $t$ the position, pressure, and density, respectively, of an element of gas initially at $x_0$. In case the initial conditions possess no characteristic length, one can show that the solution must be of the form $x=tf(x_0/t)$. With this form of the solution the equation of motion splits into two factors, one giving a non-trivial solution, and the other, a trivial solution corresponding to gas of uniform dilatation moving with constant velocity. These solutions can be fitted together to satisfy the initial and boundary conditions occurring in several situations, among which are the special cases of (1), an initially uniform gas expanding into a vacuum, and (2), an initially uniform gas expanding into another initially uniform gas of lower pressure.

**A2. Diabatic, Rotational Flow in Two Dimensions.** BRUCE L. HICKS, *Aircraft Engine Research Laboratory.*—The equations recently developed for three-dimensional diabatic flow[1] have been studied in the case of uniplanar flow. If the (variable) limiting velocity is $V_l$ and the velocity field is represented by $\bar{w}=\bar{V}/V_l$, potential, stream, and vorticity functions can be introduced through the equations $(1-w^2)^{1/\gamma-1}\bar{w}=\nabla\varphi+\nabla\times\bar{k}\psi$ and $\omega=|\nabla\times\bar{w}|=L_1(\varphi)+L_2(\psi)$ where $L_1$ and $L_2$ are quasi-linear partial differential operators of the second order. Then $\partial\psi/\partial s=\partial\varphi/\partial n$ where $\partial/\partial s$ and $\partial/\partial n$ denote spatial differentiation parallel and perpendicular to the streamlines. If the heat source function is $Q$, then the equation of continuity requires that $\nabla^2\varphi=qf(w)$ where $q=Q/V_l^3$. The equation of motion reduces to a relation between $w,\omega,q$ and their $s$ and $n$ derivatives. If $q=0$, Crocco's equation[2] $(\partial/\partial s)(\omega/p)=0$ is obtained. If $\omega=0$, $(\partial/\partial n)(Q/V_lT)=0$. For $w\ll1$ (the case of "incompressible" flow), the symmetrical equations $\nabla^2\varphi=q$, $\nabla^2\psi=-\omega$, $2\omega q+w((\partial\omega/\partial s)-(\partial q/\partial n))=0$ are found. The third of these equations restricts considerably the variation of $\omega$ and $q$. Thus where $((\partial\omega/\partial s)-(\partial q/\partial n))$ is finite and continuous in the flow, $(\omega q)$ is of the same order as $w$.

[1] B. Hicks, Pasadena meeting of the American Physical Society, Jan. 12, 1946.
[2] L. Crocco, Z. a. M. M. 17, 1 (1937).

**A3. Elastic Waves in Bars.** J. HOWARD MCMILLEN,* *Princeton University.*—A method for measuring the velocity and propagation of elastic waves in bars was found. A bar, partially immersed in water, was struck and the waves within the bar were conveyed to the water as acoustic waves. These were recorded by means of spark shadowgrams. A fast and a slow wave was observed. Their velocities relative to the velocity of sound in water were measured by making use of the angle between the water wave and the bar. The fast wave was a dilation wave traveling with a velocity characteristic of a longitudinal wave in an infinite medium; this velocity is larger than the one associated with the stationary vibrations within the bar. The dilation wave velocities in cold rolled steel and yellow brass were $5994\pm34$ and 4252 meters per second, respectively. These velocities agreed within 2.5 percent and 4 percent with the calculated velocities when R. W. Vose's values for the elastic constants were used. The slow wave velocities were $2959\pm79$ and 1978 meters per second, respectively. These velocities were 8 percent and 11 percent lower than the calculated transverse wave velocity and 4.5 percent and 6 percent lower than the calculated Raleigh wave velocity. Dilation waves in Tennessee marble were also observed; they had a velocity of 6345 meters per second.

* Work done under contract with the Office of Scientific Research and Development.

**A4. Measured Values of Ultrasonic Absorption and Velocity in Liquid Mixtures.** F. H. WILLIS, *Bell Telephone Laboratories.*—G. W. Willard[1] reported an absorption peak at an intermediate concentration of a mixture of acetone and water, measured at a single frequency of about 10 mc. Professor K. F. Herzfeld[2] showed on theoretical grounds that this increased absorption could hardly be attributed to the unmixing effect of the acoustic wave—the observed increase in $\alpha/\nu^2$ was enormously greater. The writer has measured this mixture and others at four frequencies in the range 3.8 to 19.2 mc, using the Debye-Sears-Lucas-Biquard optical method with a differential photoelectric cell indicator. In the mixtures investigated $\alpha/\nu^2$ was found to be independent of frequency within the accuracy of the method, and there was no measurable dispersion of acoustic velocity. An absorption peak at intermediate concentrations not shifting with frequency was found in mixtures of acetone and water, and of ethyl alcohol and water, but not in mixtures of acetone and ethyl alcohol and of glycerol and water. The observed absorptions, except in the case of glycerol, were considerably greater than can be accounted for classically by viscosity and heat conduction alone. The absorption peaks await theoretical explanation. The work was done at New York University.

[1] G. W. Willard, J. Acous. Soc. Am. 12, 438 (1941).
[2] K. F. Herzfeld, J. Chem. Phys. 9, 513 (1941).

**A5. Studies in Friction I. "Solid" *versus* "Polar" Boundary Films.** M. EUGENE MERCHANT, *The Cincinnati Milling Machine Company.*—A study has been made of frictional phenomena under boundary lubrication conditions employing a type of apparatus which is designed to promote pronounced "stick-slip" sliding motion, of the type described by Bowden and Leben.[1] It has been found that the effect produced by adding a non-polar but chemically "active" organic compound, such as carbon tetrachloride, to a purified mineral oil is strikingly different from

that produced by adding a strongly polar compound such as oleic acid. The true kinetic friction value obtained with the pure mineral oil when applied to iron surfaces is unchanged by the addition of carbon tetrachloride, while the static friction value decreases linearly with increasing mole fraction of carbon tetrachloride. On the other hand, when oleic acid is added to the pure mineral oil both the kinetic and the static friction coefficients drop precipitously with minor additions, then much more slowly as concentration is increased. The durability of the boundary films produced by these two types of lubricant is also very different. The above behavior can be explained by a consideration of the method of formation and nature of the surface films produced by these two different classes of materials.

[1] F. P. Bowden and L. Leben, Proc. Roy. Soc. A169, 371–391 (1939).

**A6. A Rapidly Acting Vacuum Valve.** D. D'EUSTACHIO, *Bliley Electric Company.*—A cam operated vacuum valve is described. Construction details are given. It has been designed for use in small dynamic vacuum systems and has the following characteristics. The volume added to the side of the system that is periodically exposed to atmospheric pressure is reduced to a few cubic centimeters. The area of rubber exposed to the vacuum system is small. When the valve is open it acts as a baffle for the diffusion pumps, thus eliminating the need for additional baffles. The impedance is no greater than that of a good baffle. The valve is extremely rapid in action, requiring but a fraction of a second from the fully closed to the fully open position. The valve was designed for operation on a small system capable of going from atmospheric pressure to less than $10^{-4}$ mm in 30 seconds, and has been successfully used on such a system.

**A7. Optical Analysis of the Structure of Supersonic Inhomogeneous Air-Jets.*** J. WINCKLER, C. C. VAN VOORHIS, AND R. LADENBURG, *Princeton University.*—The air stream expanding from a reservoir under high pressure through an orifice into the atmosphere flows at supersonic speed and forms various shock configurations. Studies of such air-jets at various pressures in the reservoir have been made by interferometric technique supplemented by shadowgrams (see the following paper). The measured densities and derived values of shock strength, etc., are in satisfactory agreement with those calculated from the conventional theory. The structure of the jets is revealed by computing the streamlines and Mach lines. Some anomalous phenomena occurring when a needle was inserted into the shock region have been studied.

* This work was done in whole under Contract No. OEMsr-260 between Princeton University and the Office of Scientific Research and Development, which assumes no responsibility for the accuracy of the statements contained herein.

**A8. Interferometric Study of Gas Flow around Various Objects in a Free Supersonic Homogenous Air-Jet.*** R. LADENBURG, C. C. VAN VOORHIS, AND J. WINCKLER, *Princeton University.*—The gas flow in a free homogenous air-jet escaping with supersonic speed from a high pressure tank through a conventional Laval nozzle has been studied with the help of a Mach interferometer. The density (2.20 mg/cm$^3$) and Mach number (1.70) in the jet, computed from the observed shift of the interference fringes with respect to their position without the jet were constant over a region large enough to study the airflow about various objects inserted into the jet. Cones of 10°, 30°, and 45° semi-apex angle and a sphere of $\frac{9}{32}$" diameter have been examined. Since the jet is axially symmetric and the light passes perpendicularly through the axis of the jet, the radial density distribution can be obtained from the fringe shifts by the use of the Abel integral equation. From the density distribution one can compute easily the pressure, temperature, and velocity everywhere, including the discontinuous change of pressure, etc., in a shock front. The agreement of the results with the conventional theory of compressible fluids, especially with the theory of Taylor-Maccoll of the gas flow around conical objects, is satisfactory.

* The work was done in Palmer Physical Laboratory under the sponsorship of the Navy Department, Bureau of Ordnance.

**A9. An Electromagnet for Non-Magnetic Substances.** WILLIAM VAIL LOVELL, *Sanford, Florida.*—The alternating current electromagnet described is effective on armatures of non-magnetic conducting substances, being able to attract objects from an appreciable distance. In addition to attracting magnetic material, the device attracts and holds diverse objects such as: a silver coin, an aluminum cup, a roll of copper wire, etc. The operation depends on well-known phenomena of attraction and repulsion between conductors carrying current. In the simplest form an alternating flux field induces currents of substantially like phase in a fixed member (called the attractor) and in a conducting object adjacent to the attractor. The zone of attraction is roughly a cone having its base in the surface of the structure and its apex in the axis extended. A non-magnetic conducting object situated so that the principal induced currents lie within this zone is attracted, otherwise it is repelled. In one form characterized by relatively short coils and conductive, rather than inductive, energization of the attractor element, there is a region of attraction between inner and outer zones of repulsion. Curves are given showing how the boundaries of the zones are determined.

**A10. Further Observations on the Helical Movement of Matter in Sunlight.** FELIX EHRENHAFT, *New York City.*—Photomicrographs in sunlight show that droplets of liquids and particles of light reflecting and heat conducting substances as Ag, Cu, Au, and light absorbing matter as *C* move in helical paths with regularly spaced turns towards the source of light—light negative—or away from it—light positive, simultaneously in the same portion of the beam (longitudinal photophoresis).[1] Further, a movement of matter normal to the beam already noted by the author and Whytlaw-Gray (transversal photophoresis), is seen from the photographs to follow helical paths with regularly spaced turns. In one example a particle 2 to $3\times10^{-4}$ cm radius makes about 56 turns per second each with a diameter of about $3\times10^{-3}$ cm. It is thus seen that light can

exert not only repulsion, but also attraction and torsion on matter free to move with six degrees of freedom. Forces heretofore postulated cannot account for these movements, nor do these movements violate the principle of entropy. Bartoli and Boltzmann suggested the hypothesis of light pressure in discussing the perpetuum mobile of the second kind envisioned by Eddi. Boltzmann attributed to his calculations a provisional character only, and stated that a contradiction to the second law of thermodynamics could be avoided by another hypothesis in agreement with Bartoli.[2] Droplets of an aqueous solution of chlorophyll are all attracted by the sunlight (attractive force about $10^{-7}$ dyne, gravitational force about $10^{-10}$ dyne). Droplets of distilled water under the same conditions relatively unaffected by the light. Other examples of organic solutions will be cited.

[1] F. Ehrenhaft, Ann. d. Physik 56, 103 (1918); Ann. de physique 13, 171 (1940); J. Frank. Inst. 233, 235 (1942); Science 101, 676 (1945).
[2] D. A. Goldhammer, Arch. Neerl. de Sci. [2] 5, 468 (1900).

**A11. Motion of Electrolytes in Magnetic Field.** C. E. SWARTZ AND W. VAN DER GRINTEN, *University of Rochester.*—Further investigations have been made of the motion of electrolytes in contact with metal in a magnetic field. It was shown a year ago[1] that the motion was due to current flow in the solution caused by potential differences which could be measured. The source of these potential differences is now proved to be simply voltaic cells set up at different parts of the same piece of metal. The phenomenon is only an unusual variation of those already discovered in the investigation of electro-chemical corrosion. Application of a "ferroxyl indicator"[2] shows regions of anodes and cathodes which confirm the readings taken with probes and potentiometer and also predict the observed liquid movement in the magnetic field.

[1] C. E. Swartz, Phys. Rev. 67, 201 (March, 1945).
[2] Walker, Cederholm, and Bent, J. Am. Chem. Soc. 29, 1256 (1907)

**A12. An X-Ray Method for Measuring the Thickness of Thin Crystalline Films.** A. EISENSTEIN, *Massachusetts Institute of Technology.**—When x-rays are scattered from a thin crystalline surface film overlying a crystalline base material, diffraction lines are observed from both components.[1,2] Equations are developed for the general case of (1) a flat sample, and (2) a cylindrical sample expressing the ratio of line intensities from the two materials as a function of film thickness. A usable range of $10^{-6}$ cm to $5\times10^{-2}$ cm is indicated. Experimental confirmation is found in the range $10^{-4}$ cm to $6\times10^{-3}$ cm.

* This paper is based on work done for the Office of Scientific Research and Development under Contract OEMsr-262. It is separated from similar contributed papers at the author's wish to avoid coincidence in time with the Division of Electron and Ion Optics.
[1] G. L. Clark, G. Pish, and L. E. Weeg, J. App. Phys. 15, 193 (1944).
[2] R. B. Gray, Bull. Am. Phys. Soc. 20, No. 5 (1945).

**B1. On the Inelastic Photo-Effect of the Deuteron.** J. M. JAUCH, *Princeton University.*—An experiment is proposed which would allow a decision between the two competing meson theories of nuclear forces, the weak[1] and the strong[2] coupling theories. The strong coupling variety predicts the existence of excited states of the nucleons with different spin and charge values. According to the latest calculations the first excited state of the nucleon would have an excitation energy of approximately $\epsilon=45$ Mev.[3] For $\gamma$-rays with an energy larger than $\epsilon+2.17$ Mev an inelastic photo-effect of the deuteron is possible where one of the ejected particles is in the lowest excited state. An order of magnitude calculation with perturbation theory neglecting the tensor force shows that the ratio of the inelastic to the elastic cross section goes through a maximum value near 90 Mev where it reaches about 0.07. This seems therefore to be an effect which could be observed with the experimental methods now available. In the weak coupling case no such states exist and an experimental distinction between the two theories could thus be reached.

[1] W. Pauli, Phys. Rev. 64, 332 (1943).
[2] G. Wentzel, Helv. Phys. Acta 13, 269 (1940); J. R. Oppenheimer and J. Schwinger, Phys. Rev. 60, 150 (1941).
[3] G. Wentzel, Helv. Phys. Acta 18, 430 (1945).

**B2. High Energy Neutron-Proton Scattering and the Meson Theory of Nuclear Forces with a Strong Coupling.** J. LEITE LOPES, *Princeton University.*—We investigated the anisotropy of the scattering of 14-Mev neutrons by protons in the symmetrical Møller-Rosenfeld theory with a strong coupling. In the second Born's approximation, the virtual excited states (isobars) of the nucleons decrease the ratio $R$ of the differential cross sections in the backward and perpendicular directions (in the center of mass system), and $R$ decreases with the isobar energy. However, $R$ is still larger than 1 and our results suggest the possibility that the combined effects of the virtual isobars and the tensor force might give a forward scattering in agreement with Amaldi's experiments.[1] We also evaluated the cross section of the inelastic scattering of 100–200-Mev neutrons by protons with production of isobars, in the Møller-Rosenfeld, pseudoscalar and Schwinger theories (in first Born's approximation). The total cross section is $\sim10^{-26}$ cm$^2$ and its ratio to the elastic cross section $\sim0.03$, for 100-Mev neutrons; the isobar energy assumed was 45 Mev. An experiment to detect the isobars would be crucial for a decision between the assumptions of the weak coupling and the strong coupling theories.

[1] G. Wentzel, Helv. Phys. Acta 18, 430 (1945).

**B3. The Energy Distribution and Number of Cosmic-Ray Neutrons in the Free Atmosphere.** S. A. KORFF AND B. HAMERMESH, *New York University.*—A balloon flight to determine the energy distribution and the number of neutrons produced by the cosmic radiation in the free atmosphere was carried. It was found that, in agreement with theoretical prediction,[1] there are practically no thermal neutrons in the free atmosphere, in contrast to the fact that near the surface of the ground, most of the neutrons are known to be thermal. The number, and the rate of production of the neutrons, increases rapidly with elevation, in good agreement with previous measurements.

[1] H. A. Bethe, S. A. Korff, and G. Placzek, Phys. Rev. 57, 573 (1940).

**B4. The Transition Effect for Large Cosmic-Ray Bursts in Iron.** R. E. LAPP, *The University of Chicago.*—Integral size-frequency distribution curves for cosmic-ray bursts larger than 100 particles were obtained with a spherical ionization chamber shielded by 1.25, 12, and 35 cm of iron. All three curves conform to the same inverse exponential power law having an exponent $=2.0\pm.2$. With the aid of G-M counter coincidence sets, the simultaneous occurrence of bursts and extensive atmospheric showers was determined for the three thicknesses of iron. For 1.25 cm of iron, it was found that 85 percent of the bursts were coincident with extensive atmospheric showers, while for 12 cm of iron 20 percent were coincident, and for 35 cm only 5 percent of the total bursts were observed to be simultaneous with atmospheric showers. Consideration of these results definitely indicates that at the maximum in the transition curve (about 12 cm of iron) 45 percent of the bursts are produced by narrow air showers or extremely high energy single electrons and 35 percent originate from mesotronic interactions (bremsstrahlung and knock-on processes). Based on these results, a discussion is given about the origin of large bursts under various thicknesses of material at higher altitudes.

**B5. Absorption of Slow Mesotrons in Lead, Iron, Aluminium, and Water.** H. P. KOENIG, *Laval University* (Introduced by F. Rasetti).—The absorption of slow mesotrons in lead, iron, aluminium, and water was measured by means of counters arranged in anticoincidence. The statistical error in the percentage of mesotrons stopped by the absorbing layers was less than 3 percent in all cases. This accuracy was made possible by the high efficiency (about 99 percent) of the anticoincidence group of counters. The values obtained for the relative absorptions in the different substances were compared with those calculated from the theory of energy losses by collision. As is well known, the theory predicts a lesser absorption in heavier elements for a given superficial mass. The uncorrected experimental values, however, gave an apparent discrepancy with the theory, especially in the case of lead. By taking into account the effect of scattering, which is of particular importance in heavy elements, the experimental data were brought into excellent agreement with the theory for lead, iron, and aluminium. For water, no reliable theoretical value could be calculated.

**B6. Correction of G-M Counter Data II.** J. D. KURBATOV AND G. K. GROETZINGER, *The Ohio State University.*—An expression has been derived for the correction of experimentally obtained G-M counter data which allows one to determine the number of counts lost due to the finite recovery time of the counter.[1] Experiments with a counter using a Neher-Harper circuit were performed to develop an experimental method for determining the correction of G-M data. Thin samples of $P^{32}$ as $Na_2HPO_4$ of identical geometry and known relative intensity of electron emission were prepared which allowed us to vary in steps between 10 and 50,000 per second the number of electrons entering the counter and producing at least one ion pair. A curve will be shown which gives the correction directly up to a certain intensity after which the counting rate becomes independent of the intensity of the source. Comparison of these results with the theoretical correction[1] allows a determination of the recovery time as a function of the counting rate. For one arrangement the recovery time decreased from 7.4 to $5.0\times10^{-4}$ second as the number of electrons entering the counter increased from 400 to 2500 per second.

[1] J. D. Kurbatov and H. B. Mann, Phys. Rev. 68, 40 (1945).

**B7. Upper Limit of the Number of Low Energy Neutrons from a Ra-α-Be Source.** A. A. YALOW,* R. S. YALOW,* AND M. GOLDHABER, *University of Illinois.*—A method has been developed to ascertain the upper limit for the fraction of the neutrons from a given source which are below a given energy, for which a comparison source exists. The relative number of neutrons from a Ra-α-Be and from a Ra-γ-Be source which are slowed to thermal energies by transmission through or reflection from thin layers of paraffin was determined as a function of the paraffin thickness. The neutrons were detected in a boron-lined proportional counter, shielded by cadmium from all C neutrons except those produced in the paraffin. The number of these neutrons was determined from the difference in counting rate which resulted when cadmium was interposed between the paraffin layer and the counter. When reduced to the same number of incident fast neutrons, the initial slope of the growth curves of the C neutrons is at least 10 times larger for Ra-γ-Be neutrons than for Ra-α-Be neutrons. It is therefore concluded that not more than 10 percent of the neutrons from the latter source have an energy as low as the mean energy of the photo-neutrons from the Ra-γ-Be source.

* Now at Federal Telecommunications Laboratories, New York.

**B8. Radioactive Isotopes of Mo and Ma.** J. E. EDWARDS AND M. L. POOL, *Ohio State University.*—A $4.2\pm.1$-day masurium activity has been produced by bombardment of Mo with deuterons or protons and by bombardment of Cb with alpha-particles. The production of this activity by proton bombardment of Mo has been reported.[1] The activity can now be definitely assigned to $Ma^{98}$ by the reactions Cb$(\alpha, n)$, Mo$(p, n)$, and Mo$(d, n)$. The isotope emits a 0.92-Mev γ-ray and also Mo x-rays as identified with a curved crystal spectrograph showing decay by $K$-capture. The 67-hour Mo activity, produced previously by Mo bombardment,[2] has been produced by the reaction Zr$(\alpha, n)$ which assigns this β-emitter to $Mo^{99}$. Spectrograph photographs show Ma x-rays associated with this activity confirming earlier identification of the radiation.[2] X-ray photographs of a long period (64 days) Ma activity resulting from deuteron bombardment of Mo show x-rays characteristic of Mo and Ma of about the same intensity. A photograph taken 110 days after bombardment shows the Mo $K\alpha$ line to be slightly stronger than the Ma $K\alpha$ line. A later photograph shows a decrease in the relative intensity of the Mo $K\alpha$ line.

[1] D. Ewing, T. Perry, and R. McCreary, Phys. Rev. 55, 1136 (1939).
[2] G. T. Seaborg and E. Segrè, Phys. Rev. 55, 808 (1939).

**B9. Low Energy Alpha-Ray Spectra and Mechanism of Alpha-Decay.** W. Y. CHANG, *Princeton University.*—The same method as used for studying the low energy groups of alpha-particles from Po* was employed to investigate the alpha-particles from radium. A line at 4.615 Mev identifiable with Rosenblum's and five previously unknown lines in a region 0.5 to 0.9 Mev below the main line were found; their intensities are respectively about 2500, and between 110 and 60, if the intensity of the main line is set as 100,000. As in the Po case, if the particle groups do actually come from the nucleus as all performed experiments have indicated so, the ordinary alpha-decay theory is also in the present case in serious disagreement with the experiments, for the theoretical intensity varies with energy much more rapidly than the observed one. A mechanism other than a simple penetration through the statical potential barrier may therefore be needed. It may be reasonable to assume tentatively that the out-coming particle, while about completely leaving the nucleus, may interact strongly with the rest of the nucleus and consequently impart a certain portion of its kinetic energy to the latter, which may then become the energy of oscillation of the residual nucleus. Hence, at a given emission probability, the observed kinetic energy should be smaller than would be expected from the theory. In other words, the intensity would then appear greater for the observed energy, as can be seen from the Geiger-Nuttall curves. This may generally explain the experimental facts.

* W. Y. Chang, Phys. Rev. 67, 267 (1945); details to be published soon.

**B10. A Slow Neutron Velocity Spectrometer.** L. J. HAWORTH[1] AND F. N. GILLETTE,[2] *University of Illinois.*—This apparatus, designed and constructed in 1941, employs a "time of flight" method for the study of those neutrons of a continuous distribution which have energies lying in particular small intervals. Ten such intervals may be covered simultaneously. The deflection modulated deuteron beam of the Illinois linear accelerator,[3] falling briefly on a target of heavy water ice, produces a short burst of fast neutrons. Paraffin around the target slows the neutrons almost to thermal equilibrium before escape. The neutrons are subsequently detected by a $BF_3$ chamber placed either 1.25 or 2.5 meters from the source. The resulting pulses are registered on one of ten counters which are made sensitive in consecutive time intervals of arbitrary length. The time interval covered by the entire group can be shifted at will with respect to the beam modulated pulse. Strength of the source limited the study to neutrons of energy between .004 and 1.0 electron volt. Certain experimental results obtained with the apparatus are described in the following paper.

[1] Now at Massachusetts Institute of Technology, Radiation Laboratory, Cambridge, Massachusetts.
[2] Now at General Precision Laboratory, New York.
[3] Manley, Haworth, and Luebke, Rev. Sci. Inst. 12, 587 (1941).

**B11. Experiments with a Slow Neutron Velocity Spectrometer.**[1] J. H. MANLEY, F. B. BERGER,[2] AND F. N. GILLETTE,[2] *University of Illinois.*—Using the apparatus described in the previous abstract the relative numbers of thermal neutrons arriving at the detector in consecutive time intervals from paraffin sources at 300°K, 200°K, and at 135°K were measured. The colder the source the greater is the relative abundance of the slower neutrons. The velocity distribution curve for 300°K was obtained by analyzing the data taking into account the resolution of the apparatus and the strength of the source as a function of time and velocity. The best maxwellian fit is that for 400°K. By determining the time distribution of neutrons at the detector with and without an absorber in the beam, the total cross section of mercury and of manganese as a function of the neutron velocity was measured. For neutrons in the energy range from 0.004 electron volt to 1 ev the capture cross section for both these elements varies inversely as the neutron velocity. For mercury, $\sigma = (1180/v) \times 10^{-24}$ cm², where $v$ is in km/sec. For manganese the constant is 24.7.

[1] This work was done in 1941 and early 1942.
[2] Now at General Precision Laboratory, New York.

**C1. On an Inequality of Quantum Hydrodynamics.** F. LONDON, *Duke University.*—It can be shown that the commutation rules of the components of the hydrodynamical mass current density operators $\mathbf{j}(R)$ and $\mathbf{j}(S)$ at the points $R$ and $S$[1]

$$[\mathbf{j}(R)\times\mathbf{j}(S)]+[\mathbf{j}(S)\times\mathbf{j}(R)] = -\frac{h}{2\pi i}\delta(R-S)\left(\operatorname{curl}\mathbf{j}(R)+2\mathfrak{n}(R)\frac{e}{c}H(R)\right)$$

($n$ = particle density, $H$ = magnetic field strength) correspond to an inequality for the *total* kinetic energy

$$U_{\text{total}} \geqslant \frac{h}{4\pi m}\left|\operatorname{curl} j+\frac{ne}{c}H\right|.$$

On the other hand available data about low temperature transfer processes (superconductivity and liquid helium II) indicate that these processes might be restricted by an inequality for the *hydrodynamical* kinetic energy

$$U_{\text{hydrodynamic}} < \frac{h}{4\pi m}|\operatorname{curl} j|.$$

[1] F. London, Rev. Mod. Phys. 17, 310 (1945).

**C2. Statistical Hypotheses in Stellar Dynamics.** HERBERT JEHLE, *Université de Bruxelles and Harvard University.*—A stellar system like our galaxy is composed of a variety of different statistically independent elements (stars, multiple stars, clusters). Their motion is mainly determined by the smooth field of force produced by the smoothed-out stellar system. In order to discuss micro-aspects of the streaming field of the elements, and to find out what additional forces arise from encounters between neighboring elements, we have first of all to introduce a statistical hypothesis about the density of elements in the six dimensional Boltzmann phase space: we assume that statistically independent elements cannot be crowded into phase space more closely than with an expected value of one element per volume $\sigma^3$, $\sigma$ being a constant characteristic for the system. This is plausible because too great densities in position space, without large mean square deviations of velocities, give cause to aggregation of formerly inde-

pendent clusters or stars into larger units. Given local values of mean square deviation of velocity $\Delta v_x$, our assumption indicates a minimum probable distance between elements. As we cannot expect a stellar system to be flattened into a disk narrower than this minimum distance, we get a minimum relation $\Delta x_3 \Delta v_3 \geqq \sigma/4\pi$.

**C3. Relativistic Transformation of Current and Charge Densities.** BORIS PODOLSKY, *University of Cincinnati.*—The components of $\rho\mathbf{v}/c$ and $i\rho$ must transform as components of a four-vector, so that if measured in one coordinate system they are known in all coordinate systems. On the other hand any operational definition of $\rho(\mathbf{r}, t)$ must take account of the positions of particles, that of $s$th particle being $\mathbf{r}_s(t)$, at the same time $t$. Upon performing the Lorentz transformation these will be $\mathbf{r}_s'(t_s')$ and $t_s'$, since the transformed time will be different for each particle. Another observer, in measuring $\rho'$, would use $\mathbf{r}_s'(t')$ and $t'$, $t'$ being the same for all particles. As particles are in motion $\mathbf{r}_s'(t_s') \neq \mathbf{r}_s'(t')$, and there appears to be no necessary relation between $\rho(\mathbf{r}, t)$ and $\rho'(\mathbf{r}', t')$, operationally defined in each coordinate system. It turns out, however, that if in each coordinate system the charge density is defined by $\rho(\mathbf{r}, t) = \Sigma e_s \delta(\mathbf{r} - \mathbf{r}_s(t))$, then relativistic equations of transformation hold.

**C4. A Generalization of Nyquist's Thermal Noise Theorem.** E. J. SCHREMP, *Massachusetts Institute of Technology.*—Nyquist's thermal noise theorem[1] may be stated in the following form: If $y(\nu) = g(\nu) + jb(\nu)$ is the admittance, at the frequency $\nu$, of any 2-terminal linear passive network in thermal equilibrium at an absolute temperature $T$, then there exists in parallel with $y(\nu)$ a constant current generator of thermal noise, whose mean square in the frequency interval $d\nu$ at the frequency $\nu$ is given by[2]

$$\langle i(\nu) i(-\nu) \rangle_{Av} d\nu = 2kTg(\nu)d\nu, \qquad (1)$$

where $k$ is Boltzmann's constant. The present generalization of Nyquist's theorem yields, for any $M$-terminal linear passive network in thermal equilibrium, infinitely many equivalent representations in the sense of the companion theorem.[3] Thus, it is shown that in every such representation the internodal thermal noise currents $i_{mn}(r, a; \nu)$ are mutually incoherent and satisfy the invariant relations

$$\langle i_{mn}(r, a; \nu) i_{mn}(r, a; -\nu) \rangle_{Av} d\nu = 2kTg_{mn}(r, a; \nu)d\nu, \qquad (2)$$

provided the generating parameter $a$ obeys the constraint

$$a(-\nu)[a(\nu) - 1]y_{rr}(\nu) + a(\nu)[a(-\nu) - 1]y_{rr}(-\nu) = 0. \qquad (3)$$

This theorem is similarly expressible on the loop basis.

[1] H. Nyquist, Phys. Rev. 32, 110 (1928).
[2] In this formula the factor $2kT$ may be replaced by the more usual factor $4kT$, if the noise contributions at the frequencies $+\nu$ and $-\nu$ are combined.
[3] Cf. abstract number SP1.

**C5. Normal Modes in the Theory of Wave Guides.** GLENN M. ROE, *University of Minnesota.*—In the usual development of the theory of electromagnetic wave guides[1, 2] it is assumed that the field can be expressed in terms of an infinite set of normal modes, each of which satisfies the wave equation and the proper boundary conditions. This assumption is valid for perfectly conducting boundaries, or for boundaries characterized by an impedance, but not for actual bounding media having zero or finite conductivities. In the latter case there can exist at most a finite number of modes satisfying both the continuity conditions at the interfaces and the boundary conditions at infinity. Furthermore, such modes are not orthogonal. The exact solution, in which the Green's function is given by a contour integral, can be manipulated to yield residues having the form of normal modes and an additional correction term given by loop integrals about one or more branch points. This correction term is important only for conductivities approaching zero.

[1] Carson, Mead, and Schelkunoff, Bell Sys. Tech. J. (April, 1936).
[2] J. A. Stratton, *Electromagnetic Theory* (McGraw-Hill Book Company, Inc., New York, 1941).

**C6. On the Design of a Cavity of a Linear Electron Accelerator.** E. S. AKELEY, *Purdue University.*—Consider a resonating cavity formed by planes $x = 0$, $x = \pi$ and surface of revolution $y(x)$ connecting planes. Assume electromagnetic field expressible as sum of finite number of $TM_{01}$ modes, each characterized by its phase velocity $v$ on axis. Only mode imparting energy to electron is $v = c$. Differential equation for $y(x)$ is $E_x dx + E_y dy = 0$. The analytic character of $y(x)$ in neighborhood of $x = 0$ is easily determined. This point is a singular point of the differential equation and may be a nodal point. The types of possible $y(x)$ are discussed in terms of the roots $E_x$ and $E_y$ and their common roots which are the singular points of the differential equation. The following cases have been or are being investigated: (1) modes $v = c$ and $v = c/2n+1$. The case $n = 1$ appears most favorable as regards energy dissipation. (2) modes $c$, $c/3$, $c/5$. A perturbation computation indicates a lower dissipation of energy with weak $c/5$ than with other two modes only. (3) $c$, $c/2$, $c/3$. (4) $c$, $2c$. Cases (3) and (4) give unsymmetrical and alternating cavities which may produce a more favorable separation of modes for the whole accelerator than is obtained in cases (1) and (2).

**C7. Propagation of Radiation in a Medium with Random Inhomogeneities.** PETER G. BERGMANN, *Columbia University.*—When radiative energy is propagated through a material medium over any considerable distance, it is frequently found that the signal picked up at some fixed point is subject to random fluctuations. This effect is present even when reflections from bounding surfaces are eliminated. The fluctuation is, therefore, believed to be caused, at least in part, by the random inhomogeneities of the medium itself. A theory has been developed which, on the basis of ray optics, leads to quantitative relations between the statistical fluctuations of the index of refraction of the medium and the fluctuations of the radiative field, provided the latter do not become too large. It is found that the r.m.s. fluctuation of the optical path length between two fixed points increases with the square root of the distance, while the r.m.s. intensity fluctuation for a fixed path of transmission increases with the $\frac{3}{2}$th power.

Similarly, relations can be derived for the deviation of a transmission path from a straight line and for the correlation of field intensities at two distant points.

**C8. The Mean Free Paths of Cesium Atoms in Helium, Nitrogen, and Cesium Vapor.** I. ESTERMANN, S. N. FONER, AND O. STERN, *Carnegie Institute of Technology.*—The mean free paths of cesium atoms in helium, nitrogen, and cesium vapor were measured with a molecular beam apparatus permitting the measurement of scattering deflections of about 5 seconds of arc. Using the free fall of the beam atoms, the variation of the mean free path with the velocity of the beam atoms could be determined directly. This variation was found to be in agreement with the equations calculated on the basis of classical theory treating the atoms as elastic spheres. The sums of the effective atomic radii found are $12.0\times10^{-8}$ cm for Cs-He, $17.2\times10^{-8}$ cm for Cs-$N_2$, and $27.3\times10^{-8}$ cm for Cs-Cs collisions. These values correspond to mean free paths of 2.1 meters in He 2.2 meters in $N_2$, and 1.36 meters in Cs-vapor of $10^{-6}$ mm Hg pressure for cesium atoms corresponding to the maximum intensity of the gravity deflection curve.

**C9. Maximum Rate of Multiplication of Unicellular Organisms.** ALLEN L. KING, *Dartmouth College.*—When spherical unicellular organisms multiply by the fission process, the rate depends upon several physical factors. A kinetic treatment of the problem yields a maximum rate of $1.735\alpha\bar{c}V_0N^2/a$, where $\bar{c}$ represents the average speed of certain molecules, such as those of oxygen or a vitamin, which limit the multiplication process, and $\alpha$ represents that fraction of such molecules striking the cell surface which become part of the cell. $V_0$ represents the volume and $a$ the radius of a single daughter cell immediately after fission and $N$ represents the number of cells per unit volume when the rate of multiplication is a maximum.

**R1. Ambiguities in X-Ray and Electron Diffraction Analysis.** A. L. PATTERSON, *Bryn Mawr College.*—In a previous report[1] it has been shown that, in many cases, there are two or more non-congruent arrangements of atom positions in a crystal lattice which have the same vector distance set, i.e., which give the same x-ray diffraction pattern. This result is now extended to include non-congruent finite arrangements of points which have the same vector distance set even when all distances are distinct. A discussion is also given of the many finite arrangements of points which have the same scalar distance set and a comment is made on the effect of this result on the interpretation of electron diffraction data. It is pointed out with the aid of examples that weighting of atomic positions and of related distances does not necessarily remove the ambiguity, and that consequently the method used by Robertson and others for the investigation of isomorphous series will not always resolve an ambiguity.

[1] A. L. Patterson, Phys. Rev. 65, 195 (1944).

**R2. The Orientation of Single Crystals by the Use of Two Simultaneous Bragg Reflections.** I. FANKUCHEN, *Polytechnic Institute of Brooklyn.*—In connection with the problem of orienting quartz crystals for cutting into piezoelectric elements, a simple and accurate method was devised which depends on setting up a crystal so that two strong Bragg reflections of one incident beam occur simultaneously. The method was suggested by some experiments designed to observe Renninger's[1] forbidden reflections. In Renninger's experiments, one of the two planes in a position to reflect has zero intensity while for orienting purposes, it is convenient to use two strong reflections. The crystal is adjusted so that one of the planes is perpendicular to an axis of rotation and the x-ray beam is set to make the Bragg angle with this set of planes. Rotation, therefore, does not change the constancy of this reflection when the crystal is properly adjusted. Many other reflections occur during a complete rotation and by properly choosing a second reflection, the crystal is not only fixed in orientation but for quartz the "sense of cut" is also determined at the same time.

[1] Renninger, Zeits. f. Krist. 97, 107 (1937).

**R3. The Breaking up of Single Crystals of Quartz.** D. D'EUSTACHIO AND S. B. BRODY, *Bliley Electric Company.*—Quartz wafers prepared by etching from wafers 75 to 100 microns thick, are found no longer to be single crystals when they become thinner than 25 microns. The break-up is shown by a series of Laue photographs of progressively thinner crystals taken in the following way. A suitably prepared crystal is set in and nearly parallel to a well-collimated x-ray beam. The "spots" from thick crystals are broad, uniformly illuminated areas. As the crystal becomes thinner the intensity distribution becomes less uniform. The pictures of the thinnest crystals show many sharp dark lines against a faint general background. These dark lines become broader and the background increases in intensity when the crystal is bent. The entire crystal appears to be changed. The authors believe that the change from single crystal to the polycrystalline state is initiated by the formation of surface layers in the manner previously described.[1] If this is so, the effect should be time dependent. No method for preparing thin wafers that is fast enough to permit this to be verified has yet been found.

[1] D. D'Eustachio and S. B. Brody, J. Opt. Soc. Am. 35, 544 (1945).

**R4. X-Ray Microradiographic Study of Strains in Crystals.** C. M. LUCHT, M. MANN, AND R. SMOLUCHOWSKI, *General Electric Company.*—In previous x-ray microradiographic study of compounds and diffraction effects in various metals and alloys* a selective transmission within single grains was observed. Certain grains appear as having a "mottled" pattern which depends upon orientation of the grain. This phenomenon was further studied and interpreted as due to a diffraction effect in imperfect grains. By using filtered radiation and improving the experimental technique, many additional features were brought out which confirm this interpretation and provide a tool for the study of strains within single grains. This

method permits a study of strain distribution and temperature influence during annealing and cold working. Strain discontinuities at twin and grain boundaries can be observed.

* Hurd, Lucht, and Smoluchowski, Phys. Rev. 68, 100 (1945).

**R5. Forced Vibrations of Piezoelectric Crystals.** H. EKSTEIN, *Armour Research Foundation*.—The vibrations of anisotropic bodies under the influence of sinusoidally variable volume forces and boundary stresses are investigated. The displacement components are represented as sums of a system "zero order" solutions which solve approximately the free-vibration problem. By using Betti's theorem, the problem is reduced to a system of inhomogeneous linear equations which, for the free-body case, reduces to the homogeneous system derived in an earlier paper.[1] If the external forces are piezoelectric, the forces are no longer given explicitly because the electrical field distribution is known only if Maxwell's equations are solved simultaneously. However, if the pertinent piezoelectric constants are small, the field can be calculated approximately as if the crystal were not vibrating. The solutions can then be obtained by the above method. The electric reaction of the crystal upon the driving system can then be determined. As an example, forced vibrations of thin quartz plates between parallel electrodes are discussed.

[1] H. Ekstein, Phys. Rev. 66, 108 (1944).

**R6. Deuteron Bombardments of Organic Compounds.** RICHARD E. HONIG, *Massachusetts Institute of Technology*.—In order to study the chemical effects of heavy charged particles, a number of organic compounds—gases, liquids, and solids—have been bombarded with deuterons from the Massachusetts Institute of Technology cyclotron. This work, carried out under American Petroleum Institute Project 43c, included paraffins, organic acids, salts, and some complex mixtures. Gas bombardments were made at approximately atmospheric pressure in a water-cooled gas chamber (volume: 2.54 liters) provided with a two-mil copper window for the entry of the external deuteron beam. A thermocouple and a Bourdon gauge connected to a Microtorque potentiometer allowed the gas temperature and pressure to be recorded electrically at the control bench during the bombardment. Fixed volume runs as well as flow runs have been made. For the bombardment of liquids and solids, water-cooled target-holders provided with two-mil copper windows were mounted inside the gas chamber which served to collect the product gases. To prevent chemical reactions of the compounds with the metal parts, chamber and target-holders were goldplated. The efficiency of deuterons in producing particular chemical reactions has been computed in terms of the mean energy dissipated per primary molecule decomposed ("dissociation expenditure" $\Delta E/\Delta M$).

**R7. Study of Metastable Ions with the Mass Spectrometer.** J. A. HIPPLE, R. E. FOX AND E. U. CONDON,* *Westinghouse Research Laboratories*.—In the mass spectra of hydrocarbons there are peaks occurring at non-integral masses when the spectra are obtained with a mass spectrometer employing simply a magnetic analyzer. These have recently[1] been attributed to ions which dissociate spontaneously after being accelerated from the ion source into the analyzer. On the basis of this explanation the energy of each ionic fragment formed from a metastable parent may be predicted. Using an energy filter on the exit end of a mass spectrometer, a study has been made of *n*-butane, 1,3-butadiene, and ethane. In each case the energy measurements agreed with the values predicted confirming the earlier interpretation of the phenomenon. As a variation of the pressure does not affect the relative abundance of the metastable fragments as compared with the rest of the spectrum, the possibility of the phenomenon being caused by ion-molecule collisions is eliminated. Other evidence that the dissociation is spontaneous is obtained by varying the small voltage accelerating the ions out of the ion source into the ion gun. As this voltage is increased, the metastable ions reach the analyzer earlier in their lifetime and hence the peaks arising from their dissociation increase rapidly. Metastable ions have been observed in many hydrocarbons and some of these will be discussed.

* Present address National Bureau of Standards, Washington, D. C.
[1] J. A. Hipple and E. U. Condon, Phys. Rev. 68, 54 (1945).

**R8. Mechanism of the Luminescence of Solids.** FERD E. WILLIAMS, *RCA Laboratories* AND HENRY EYRING, *Princeton University*.—Equations calculated from a simple energy *versus* configuration coordinate diagram for the normal and excited states of the activator atom reproduce the complete temperature-dependence curves of luminescent efficiency of many phosphors. The configuration contours are drawn so as to provide an activated step with a small heat of activation for the luminescent process and an activated step with a large heat of activation for the radiationless recombination of the excited electron and the activator atom. This model, confirming experimental results, indicates that excitation with short wave ultraviolet light produces increased luminescent efficiency at low temperatures while excitation with long wave ultraviolet produces decreased efficiency compared to room temperature efficiency. On removal of the excitation some of the electrons exist in an excited state from which transitions to the normal state are forbidden, and some electrons have surmounted the potential hump and exist in an excited state from which transitions to the normal state are allowed. The latter electrons spontaneously drop to the normal level by a monomolecular temperature-independent process, while the former slowly surmount the barrier by strongly temperature-dependent kinetics. Such two stage decay is observed. The height of the barrier is confirmed by glow curve data.

**R9. The Infra-Red Absorption of Methane as Influenced by Foreign Gases.** NORMAN D. COGGESHALL AND ELEANOR L. SAIER, *Gulf Research & Development Company*.—The influence of foreign gases on the intensity of the infra-red

absorption of some of the light gases has been known for some time. A number of light gases among which are: CO, $CO_2$, $SO_2$, $CH_4$, etc. do not obey Beer's law of absorption in the infra-red either in a pure form or when contaminated by foreign gases. For example, when a non-absorbing gas such as hydrogen is added to a certain amount of an absorbing gas such as methane the absorption due to the latter is considerably increased. Dennison[1] has theoretically examined the shape and intensity of infra-red absorption lines and found that they are affected by the effective diameters of the molecules. Cross and Daniels[2] have studied the effect of several different gases on the absorption due to nitrous oxide and for each determined an "optical" collision diameter. The present work is an application of the same type of study to the case of methane. The shape and intensity of the absorption bands of methane have been studied as depending upon the type and partial pressure of foreign gas. Data will be shown and discussed which show large differences in the effects of different foreign gases. The data are also of practical interest in that they indicate what types of gas mixtures may be analyzed by infra-red absorption means.

[1] D. M. Dennison, Phys. Rev. 31, 503 (1928).
[2] P. C. Cross and F. Daniels, J. Chem. Phys. 2, 6 (1934).

**R10. A Method of Preparing Absorbing Surfaces for the Infra-Red.** L. N. HADLEY AND D. M. DENNISON, *University of Michigan.*—Surfaces which absorb practically 100 percent of the radiation falling within a small wave-length range have been used extensively for short radio waves. Solution of Maxwell's equations requires a perfect reflector covered with a dielectric layer of thickness $\lambda/4n$, where $n$ is the index of refraction. Upon the dielectric layer lies a thin semiconducting layer whose resistance is 377 ohms/square. We have constructed surfaces of this type for the infra-red, using evaporated films. The mirrors are made of aluminum on glass, the dielectric films of lithium fluoride, and the semiconducting films of chromium. The fundamental frequency for which the surfaces are prepared is blacked out as are all odd multiples of the fundamental. A surface with fundamental at 13.9$\mu$ shows seven bands in the visible, corresponding to the odd overtones 21 through 33. A surface with fundamental at 3.25$\mu$ shows two bands in the visible: the fifth and seventh overtones. Theoretical and experimental curves of reflectivity *versus* wave-length have been obtained. We propose to use the surfaces in infra-red spectroscopy in the manner of reststrahlen plates to eliminate the use of a foreprism, and perhaps also in the detecting system. It is also possible through reflection at oblique incidence to obtain polarized infra-red radiation.

**S1. Electrical Properties of Germanium Alloys. I. Electrical Conductivity and Hall Effect.** K. LARK-HOROVITZ, A. E. MIDDLETON, E. P. MILLER, AND I. WALERSTEIN, *Purdue University.*—Germanium samples purified by high vacuum treatment have been alloyed by adding from 0.001 percent to 1.0 percent of metallic impurities. The electrical conductivity and transverse Hall effect of these samples have been investigated over temperatures ranging from −180°C to 650°C. Plotting log $\rho$ (resistivity) and log $R$. (Hall constant) against $1/T$ shows that the resistivity at low temperatures decreases with increasing temperature, increases around room temperature and then drops sharply with a slope identical for the various samples. The Hall curves indicate electron ($N$ type) or hole ($P$ type) conduction, depending upon the type of impurity. $P$ type samples show reversal of Hall effect, and the slope at high temperatures is identical for all samples, $P$ and $N$ alike, indicating that germanium behaves at low temperatures as an impurity semiconductor, but is at high temperatures an intrinsic semiconductor with energy level separation of about 0.76 volt. Hall values show that the number of current carriers ranges from about $10^{15}$ up to $10^{19}$ per cc. The temperature behavior of mobility, determined by $R/\rho$, cannot be explained as due to lattice scattering alone, but indicates the existence of another scattering mechanism, especially at low temperatures.

**S2. Theory of Impurity Scattering in Semiconductors.** E. CONWELL AND V. F. WEISSKOPF, *University of Rochester.*—Recent experiments on Hall effect and resistivity of germanium semiconductors have shown that the simple theory of lattice scattering alone cannot explain the temperature dependence of mobilities. Another obvious source of resistance is scattering by impurity centers, such as Rutherford scattering of electrons (or holes) by a random distribution of impurity ions. Because of the large wave-length of these thermal electrons their movement can be considered as free and their scattering by the impurity ions is given by the classical expression, assuming perfectly elastic collisions and effectively infinite mass for scattering centers. Scattering of an electron by one ion is treated as approximately independent of all other ions. The resistivity due to such impurity scattering is (in ohm-cm)

$$\rho=\frac{9\times10^{11}\pi^{3/2}e^2m^{1/2}}{2^{7/2}\kappa^2(kT)^{3/2}}\ln\left(1+\frac{36\kappa^2k^2T^2d^2}{e^4}\right),$$

where $d$ is half the average distance between impurity ions and $\kappa$ the dielectric constant of the semiconductor.

**S3. Theory of Resistivity in Germanium Alloys.** K. LARK-HOROVITZ AND V. A. JOHNSON, *Purdue University.*—The temperature dependence of resistivity of germanium alloys is considered in three ranges: (1) the impurity range of low temperatures with conduction due to impurity electrons or holes, (2) the transition range with contributions from both impurity and intrinsic electrons and holes, and (3) the intrinsic range of temperatures so high that the numbers of electrons and holes are equal. Resistivity in the impurity range is the sum of resistivity due to lattice scattering (proportional to $T^{\frac{3}{2}}$) and resistivity due to impurity scattering. Mean-free-path calculations indicate that the impurity mean-free-path increases and the lattice mean-free-path decreases with rising temperature. At a given temperature the lattice mean-free-path is the same for all germanium samples, but the impurity mean-free-path varies widely with impurity content. In the transition and intrinsic ranges conductivity is the sum of conductivities due to electrons and holes; their values are based upon

Hall constant values. Combination of these two methods allows complete synthesis of the experimental results throughout the entire temperature range.

**S4. Electrical Properties of Germanium Alloys. II. Thermoelectric Power.** K. LARK-HOROVITZ, A. E. MIDDLETON, E. P. MILLER, W. W. SCANLON, AND I. WALERSTEIN, *Purdue University.*—The thermoelectric power, $Q$ of Germanium alloyed with various metallic impurities has been studied as a function of temperature from −180°C to 650°C. For this purpose thermocouples have been imbedded into the body of the semiconductors and temperature gradients of .5 to 30°C/cm have been used depending on the temperature range and the size of the sample. The thermoelectric behavior parallels $R$, the Hall effect. $R$ and $Q$ are positive for $P$ type samples at low temperatures, reversing sign at high temperatures. The thermoelectric power, $Q$ becomes zero at a temperature near but not identical with the temperature where $R$ becomes zero. In most cases $Q$ as a function of temperature rises in the low temperature range, passes through a maximum and decreases again near room temperature. The position and height of the maximum depends on the amount and type of impurity used. The temperature dependency of $Q$ for samples containing the same type of impurity in varying amounts are represented by a family of similar curves: with increasing impurity content the position of the maximum shifts to higher temperatures and lower values.

**S5. Theory of Thermoelectric Power in Germanium.** V. A. JOHNSON AND K. LARK-HOROVITZ, *Purdue University.*—Thermoelectric power $Q$ in semiconductors has been calculated under conditions of simultaneous conduction by positive and negative conductors. The low temperature form (impurity conduction only) becomes

$$Q=(\ln RT^{\frac{3}{2}}-5.32)k/e+\Delta Q,$$

where $R$ is the Hall constant in cm³/coulomb and $\Delta Q$ is a term to compensate for the dependence of mean free path on velocity. In general

$$Q=-\frac{k}{e}\left[38.121\frac{n_1c-n_2}{n_1c+n_2}-0.659\frac{n_2}{n_1c+n_2}-\frac{n_1c}{n_1c+n_2}\ln\left(\frac{n_1}{T^{\frac{3}{2}}}\right)+\frac{n_2}{n_1c+n_2}\ln\left(\frac{n_2}{T^{\frac{3}{2}}}\right)\right],$$

where $n_1$ and $n_2$ are the number of electrons and holes per cc determined from conductivity and $c$ is the ratio of electrons and hole mobility in the intrinsic range, identical for all germanimum samples. The thermoelectric power thus calculated is in agreement with experiment throughout the temperature range.

**S6. On the Flow of Binary Gas Mixtures through a Long Capillary when the Mean Free Path is Comparable to the Capillary Diameter.** A. J. DEBETHUNE AND R. D. PRESENT, *SAM Laboratories, New York, New York.*—The separation of a gas mixture by diffusion through a capillary of radius $r$ depends on the fact that the molecules have different masses $m_i$ and mean velocities $\bar{v}_i$. When the inlet pressure is so low that the mean free path $\lambda$ is much greater than $r$, the flow is diffusive and the separation factor (at zero outlet pressure) has its maximum value $(m_2/m_1)^{\frac{1}{2}}$. At high pressures ($\lambda \ll r$) no separation occurs. We have treated the intermediate case ($\lambda \approx r$) where the transfer of forward momentum from light to heavy molecules in unlike collisions equalizes the transport velocities and decreases the separation factor. As the inlet pressure rises, this effect makes the flow non-separative before it becomes viscous. Flow equations are derived by equating the momentum acquired by each component from the pressure gradient to the momentum lost to the wall plus that transferred to the other component. The viscous effects are treated as a small additive perturbation on the flow. The integrated flow equations express the separation factor as a function of the inlet and outlet pressures. The same results have been derived by another method and extended to porous media by Bosanquet, Pollard, and Present. The theory has been quantitatively verified in many experiments on the flow and separation of several gas mixtures through various porous media.

**S7. Separation of Gas-Mixtures Flowing through Porous Media.** W. A. NIERENBERG, *SAM Laboratories, New York, N. Y.*—An experiment was performed measuring the separation of $O_2$-$N_2$ mixtures flowing through porous plates made of etched alloys as a function of high side pressure. The low side pressure is 1 percent of the high side pressure and the data are extrapolated to zero low side pressure. The porous plate forms one side of a 0.015" channel down which the high pressure gas flows viscously (~50 cm Hg) and the exit flow is 0.7 percent of the entrance flow. This technique is termed the "high-cut" method and it implies the continuous increase in heavy molecular concentration in the high pressure fraction by selectively removing the lighter molecules through the plate. This proceeds logarithmically (Rayleigh's law) with the undiffused fraction of the gas. The achieved magnification factor five is an extreme apparatus limit. The plate is tapered in the direction of flow to maintain the gas velocity and minimize back diffusion. Appropriate corrections are made for diffusion losses. The mixture is 50 percent $O_2$ and 50 percent $N_2$ to afford the maximum change in mole fraction. The analysis and comparison of samples is performed by a micro-absorption unit of novel design which handles 0.6 cc to 0.04 percent accuracy. The averaged fore-pressure curve of separation agreed with the theory of the previous paper to 0.6 percent compared to 0.43 percent average scatter from the best-fitting curve over a range of separation from 100 percent to 15 percent of the maximum theoretical value. The agreement is considered excellent.

**SP1. Theorem on Equivalent Representations of an Arbitrary Linear Network.** E. J. SCHREMP, *Massachusetts Institute of Technology.**—For any $M$-terminal linear network, active or passive, this theorem yields infinitely many equivalent representations, including one $M$-node representation, together with others having $N>M$ nodes, of which $(N-M)$ are internal and generally fictitious nodes.

Thus, with each internal node $r$ the theorem associates a continuous group of equivalent representations generated by the transformation

$$i_m(r,a)=i_m-a(y_{mr}/y_{rr})i_r \qquad (m,n=1,2,\cdots,N), \quad (1a)$$

$$y_{mn}(r,a)=y_{mn}-a(y_{mr}/y_{rr})y_{rn} \qquad (r=M+1,M+2,\cdots,N), \quad (1b)$$

where, in a given $N$-node representation, $i_m$ is the net current injected at node $m$, $e_m$ is the voltage of node $m$, and $y_{mn}=\partial i_m/\partial e_n$; and where $i_m(r,a)$, $e_m$, and $y_{mn}(r,a)=\partial i_m(r,a)/\partial e_n$ are the corresponding quantities for any value of the generating parameter $a$. For all values of $a$, the nodal equations

$$i_m(r,a)-\Sigma_n y_{mn}(r,a)e_n=\Sigma_n y_{mn}(r,a)=\Sigma_n y_{nm}(r,a)=0 \quad (2)$$

are satisfied. By successive application to different internal nodes $r$, $s$, $\cdots$, the transformation (1) and its inverse will generate all equivalent representations of the given network. This theorem is similarly expressible on the loop basis.

* To be given after paper C9 if time permits.

**SP2. Transformation Theory of Hydrodynamical Equations.** HERBERT JEHLE, *Université de Bruxelles and Harvard University.**—Stellar dynamics has still to overcome mathematical difficulties involved in solving hydrodynamical equations, particularly selfconsistent fields. Hydrodynamical equations can be simplified by writing them over into a wave equation for $|\psi|\exp(iS/\bar{\sigma})$ (time dependent Schroedinger type) which can be split into two real equations:

$$0=-\Sigma\nabla_\nu\langle(|\psi|^2\nabla_\nu S)\rangle+(\partial/\partial t)\langle|\psi|^2\rangle=\Sigma\nabla_\nu(\rho v_\nu)+(\partial/\partial t)\rho,$$

$$0=-(\partial/\partial t)\langle(|\psi|^2\nabla_\mu S)\rangle+\langle|\psi|^2\rangle\nabla_\mu\bar{U}+\langle|\psi|^2\nabla_\mu(\delta U)\rangle$$
$$+\Sigma\nabla_\nu\langle\{-\tfrac{1}{4}\bar{\sigma}^2|\psi|^2\nabla_\mu\nabla_\nu\log|\psi|^2+|\psi|^2(\nabla_\mu S)(\nabla_\nu S)\}$$
$$=(\partial/\partial t)(\rho v_\mu)+\rho\nabla_\mu\bar{U}-\iiint v_\mu\nabla(f)dv_1dv_2dv_3$$
$$+\Sigma\nabla_\nu(\rho\langle v_\mu v_\nu\rangle).$$

Poissons equation determines gravitation potential $\bar{U}+\delta U$ from $|\psi|^2$; bars or $\langle\rangle$ denote averages over position space volumes containing many elements; ($\bar{\sigma}$ stands for $\sigma/2\pi$). We assume that the distribution (numbers and intensities) of excited $\psi_{nlm}$ states ($n$ is about $10^5$) corresponds statistically to the distribution (in numbers and masses) of statistically independent elements of a stellar system. This replaces the assumption about maximum phase space density and makes it impossible to observe discreteness of stationary states.

* To be given after paper C9 if time permits.

**T1. The Constant Magnetic Current and Heinrich Hertz.*** FELIX EHRENHAFT, *New York City.*—Heinrich Hertz[1] stated that with respect to unipolar induction we have to speak of the constant magnetic current with the same right as of the constant electric current, and that magnetic poles which form a continuous line and are mechanically moved in the direction of the line have an electrostatic action in the surrounding space. This action and the existence of single magnetic poles (charges) the author[2] has demonstrated in many experiments and has given photomicrographic evidence. The helical path of an iron particle with the mobility $B$ with the axis of the helix parallel to an external homogeneous magnetic field $H$ of 50 gauss has been described.[3] It can be calculated that, neglecting the velocity due to the constant longitudinal magnetic field in the beam of light, the constant horizontal velocity $w$ due to the external field of 50 gauss is about $1\times10^{-2}$ cm per second. Since the magnetic charge $q$ equals $w/BH$, it follows that $q$ is about $5\times10^{-12}$ m.s.u. That the electrostatic charge $e$ is about $4\times10^{-10}$ e.s.u. can be calculated, since $mv^2/R$ equals $evH$. Here an electrostatically charged particle rotates around $H$ with a velocity of around $10^{-1}$ cm per second, a speed clearly not sufficient to create its own magnetic field. The mass $m$, the magnetic charge $q$, and the electrostatic charge $e$ of the above particle have been determined by experiment, whereas in the theory of cathodic rays, beta-particles, etc. it was assumed that the particles carry only an electric charge, overlooking the possibility of their simultaneously carrying a magnetic charge. Thus the relationship $e/m$ is open to question.

* Read by title only.
[1] Heinrich Hertz, Wied. Ann. 23, 88 (1884).
[2] F. Ehrenhaft, Phys. Rev. 68, 102 and 105 (1945).
[3] F. Ehrenhaft, Bull. Phys. Soc., St. Louis Meeting, E7 (Dec. 1, 1945).